PERTURBATIVE CALCULATIONS FOR STANDARD MODEL PRECISION PHYSICS: HIGGS PRODUCTION AND YANG-MILLS GRADIENT FLOW

TOBIAS NEUMANN

Dissertation zur Erlangung des Grades Dr. rer. nat.
vorgelegt von Dipl.-Phys. Tobias Neumann

Theoretische Teilchenphysik
Fachbereich C
Bergische Universität Wuppertal

Juli 2015

Die Dissertation kann wie folgt zitiert werden:
urn:nbn:de:hbz:468-20151005-111240-6
[http://nbn-resolving.de/urn/resolver.pl?urn=urn%3Anbn%3Ade%3Ahbz%3A468-20151005-111240-6]

BETREUENDER PROFESSOR:
Prof. Dr. Robert Harlander

ZWEITGUTACHTER:
Prof. Dr. Michał Czakon

ORT:
Wuppertal

DATUM:
Juli 2015

KURZFASSUNG

In dieser Arbeit stellen wir Störungsrechnungen vor, die zu einem besseren Verständnis des Standardmodells führen. Nur mit solchen Rechnungen kann das Ziel erreicht werden, unerforschte und unerklärte Physik zu verstehen und zu finden.

Elektroschwache Symmetriebrechung geschieht durch einen Higgs-artigen Mechanismus und erreicht die Phase von Präzisionsmessungen. Im Rahmen dieser Arbeit verbessern wir die Zuverlässigkeit von Vorhersagen für differentielle und exklusive Wirkungsquerschnitte für den größten Higgs-Produktionskanal am Large Hadron Collider (LHC), Gluon-Fusion. Dies geschieht durch Abschätzung und Vorhersage von endlichen Topmassen-Effekten zum häufig benutzten Limes eines unendlichen schweren Top-Quarks. Weiterhin untersuchen wir die Higgs-Gluon-Kopplung in einer effektiven Theorie mit Dimension-5 und -7 Higgs-Gluon koppelnden Operatoren. Dies ermöglicht eine systematische Suche nach neuer Physik im Higgs Sektor, sowie Quantifizierung dieser.

Man glaubt, dass die Quantenchomodynamik (QCD), welche von höchster Wichtigkeit für Vorhersagen am LHC ist, die starke Wechselwirkung über alle Längenskalen beschreibt. Im QCD Gradientflow-Formalismus haben wir die erste Drei-Loop-Rechnung durchgeführt. Die betrachtete Observable ermöglicht es beispielsweise die Niederenergie-Region der QCD, welche sich auf die Gitter-Formulierung stützt, mit dem störungstheoretischen Hochenergie-Bereich zu verbinden. Insbesondere ist eine Definition einer laufenden Kopplung möglich, die es erlaubt $\alpha_s(m_Z)$ aus Niederenergie-Observablen, wie z. B. Hadron-Massen, zu gewinnen. Die Bestimmung von $\alpha_s(m_Z)$, für die wir die störungsrechnerische, mit Drei-Loop erreichbare Unsicherheit angeben, wird möglich, sobald entsprechende Daten aus einer Gitter-QCD-Rechnung verfügbar sind.

ABSTRACT

In this thesis we present perturbative calculations, leading toward a more thorough understanding of the Standard Model. Only with such calculations, the endeavor of unexplained and unexplored physics can be approached.

Electroweak symmetry breaking proceeds through a Higgs-like mechanism and enters the phase of precision measurements. In this thesis we improve the reliability of differential and exclusive cross section predictions for the largest Higgs production channel at the Large Hadron Collider (LHC), gluon fusion. This is achieved by estimating and predicting finite top-mass effects to the commonly used heavy top limit. Furthermore, we study the Higgs-gluon coupling in an effective field theory of dimension-5 and -7 Higgs-gluon coupling operators, allowing for a systematic search and quantification of new physics in the Higgs sector.

Quantum chromodynamics (QCD) is believed to describe the strong interactions over all length scales, and is of utmost importance for predictions at the LHC. In the framework of the QCD gradient flow, we present the first perturbative three loop calculation. The specific considered observable allows, for example, to bridge the low energy region of QCD, relying on the lattice formulation, to the perturbative high energy regime. In particular, a definition of a running coupling is possible, allowing an extraction of $\alpha_s(m_Z)$ from low energy observables such as hadron masses. This extraction, for which we estimate the perturbative three loop uncertainty, will be possible, once the data from lattice QCD is available.

CONTENTS

I Introductory part 1

1 Elements of the Standard Model 3
1.1 Electroweak and Higgs physics 8
1.2 Effective field theories 12
1.3 Quantum chromodynamics 15
1.4 Perturbative calculations in QCD 18

II Top mass effects in differential and exclusive Higgs production through gluon fusion 23

2 Introduction to gluon fusion 25
2.1 Gluon fusion from the beginning 26
2.2 Recent advancements 32
2.3 Mass effects in H + jet + X at (N)LO 34

3 Calculation and setup 39

4 Results and discussion 43
4.1 Input parameters and notation 43
4.2 Jet-veto at NNLO 44
4.2.1 Other approximations 48
4.3 Inclusive Higgs+jet at NLO 49
4.4 Distributions of the hardest jet at NLO 53

5 Summary 57

III Probing the Higgs-gluon coupling 59

6 Introduction to the Higgs-gluon coupling 61

7 Basis of dimension-7 operators and their implementation 63

8 Kinematical Distributions 67
8.1 Higgs+1-jet cross sections 68
8.2 Higgs+2-jet cross sections 71
8.3 Higher order suppressed terms 75

9 Conclusions 79

IV The perturbative QCD gradient flow to three loops 81

10 Introduction to perturbative gradient flow 83
10.1 Formalism 85

11 Calculation of the action density 89
11.1 Analytical calculation of flowtime integrals 91
11.2 Numerical evaluation of the perturbative series 99
11.3 Validation of the calculation 103

12 Results and discussion 107
12.1 Perturbative uncertainty of $t^2 \langle E(t) \rangle$ 108
12.2 Extraction of α_s 112
12.3 Summary and outlook 115

Appendix 117

A Documentation of the gradient flow setup 117
A.1 Generation of momentum integrals 117
A.1.1 Expansion in fundamental gauge fields 118
A.1.2 Simplifications and reductions 120
A.1.3 Integration by parts 124
A.2 Schwinger parameter representation and sector decomposition . 125
A.3 Global structure of the setup 127

B Numerical integration 131

C Normalization factors for kinematical distributions in chapter 8 133

Publications 139

Bibliography 141

LIST OF FIGURES

1.1 Projected future precision for the determination of multiplicative Higgs coupling scale factors κ_j at the LHC with integrated luminosities of 300 fb^{-1} and 3000 fb^{-1} (high-luminosity (HL)-LHC). As in ref. [57, fig. 17]. 9

1.2 Leading Feynman diagrams for the largest Higgs boson production channels at the LHC. 10

1.3 Standard model inclusive Higgs production cross sections for $m_H = 125\,\text{GeV}$ in dependence of the center of mass energy $\sqrt{s}$. As in ref. [63, fig. 2]. 10

1.4 Measured Higgs boson couplings to different fermion flavors and massive bosons fitted to the form in eq. (1.1). The red line is the SM prediction, the black dashed line the best fit with fit parameters shown on top. As in ref. [54, fig. 6]; see same place for details. 11

1.5 Standard model phase diagram in terms of Higgs and top pole masses. The dotted contour lines show the instability scale in GeV. The grey areas denote the allowed region at 1, 2, and 3σ confidence levels of the parameters. Taken from ref. [80, fig. 3]; see same place for details. 12

2.1 Feynman diagram for gluon fusion at LO. 27

2.2 Leading order inclusive Higgs+jet cross section as defined in eq. (2.2), with $p_{\text{T,H}}^{\text{cut}} = 30\,\text{GeV}$, in dependence of m_H, split by partonic initial-state channels gg, gq, $q\bar{q}$. Shown is the exact m_t dependence and the asymptotic expansion up to $1/m_t^2$. As in ref. [43, fig. 3]. 35

2.3 Differential cross section $\mathrm{d}\sigma/\mathrm{d}p_{\text{T,H}}$ at LO, split by partonic initial-state channels gg, gq and in the sum, with exact m_t dependence and truncations of the asymptotic expansion at order $1/m_t^k$, $k \in \{0,2,4,6\}$. As in ref. [43, fig. 5]. 36

2.4 K-factor for the transverse momentum distribution of the Higgs, split by partonic initial-state channels gg, gq and in the sum, with exact m_t dependence and truncations of the asymptotic expansion at order $1/m_t^k$, $k \in \{0,2,4\}$. As in ref. [115, fig. 15], see also ref. [115, fig. 10]. 37

3.1 Sample Feynman diagrams of virtual corrections for gluon fusion. 39
3.2 Sample real emission diagrams (a,b,c) and real-virtual corrections (d,e) for gluon fusion. 41
3.3 Sample double real emission diagrams for gluon fusion. 41

4.1 Higgs+0-jet cross section at NLO including terms up to $1/m_t^4$ as a function of m_H for $p_{\mathrm{T,veto}}^{\mathrm{jet}} = 30\,\mathrm{GeV}$. As in ref. [115, fig. 4]. . . . 45
4.2 Higgs+0-jet cross section at NLO including terms up to $1/m_t^4$ as a function of $p_{\mathrm{T,veto}}^{\mathrm{jet}}$. As in ref. [115, fig. 5]. 46
4.3 Higgs+0-jet cross section at NNLO including terms up to $1/m_t^4$ as a function of $p_{\mathrm{T,veto}}^{\mathrm{jet}}$. For reference, the horizontal lines indisplay the corresponding total cross sections in the asymptotic expansion. As in ref. [115, fig. 8]. 47
4.4 Higgs+0-jet cross section at NNLO including terms up to $1/m_t^4$ as a function of m_H normalized to heavy-top limit ($k = 0$) for $p_{\mathrm{T,veto}}^{\mathrm{jet}} = 30\,\mathrm{GeV}$. As in ref. [115, fig. 9]. 47
4.5 Same as fig. 4.3b, but for the approximations defined in eq. (4.3). Left/center/right plot show the approximations for κ_0,κ_1,κ_2, defined in eq. (4.3). As in ref. [115, fig. 14]. 49
4.6 Inclusive Higgs+jet cross section at LO including terms up to $1/m_t^k$ as a function of $p_{\mathrm{T,min}}^{\mathrm{jet}}$. As in ref. [115, fig. 6]. 51
4.7 Same as fig. 4.6b, but normalized to the unmatched $1/m_t^0$ cross section (dotted curve of fig. 4.6a). As in ref. [115, fig. 7]. 51
4.8 Inclusive Higgs+jet cross section at NLO including terms up to $1/m_t^k$ as a function of $p_{\mathrm{T,min}}^{\mathrm{jet}}$. As in ref. [115, fig. 10]. 52
4.9 Same as fig. 4.8a, but normalized to the unmatched $1/m_t^0$ cross section (dotted curve of fig. 4.8b). As in ref. [115, fig. 11]. 53
4.10 K-factors as defined in eq. (4.2), for the transverse momentum distribution of the hardest jet, i. e. $K_k^{\mathrm{NLO}}(p_{\mathrm{T,1}}^{\mathrm{jet}})$. As in ref. [115, fig. 12]. 54

4.11 K-factors as defined in eq. (4.2), for the rapidity distribution of the hardest jet, i. e. $K_k^{\mathrm{NLO}} \equiv K_k^{\mathrm{NLO}}(y_1^{\mathrm{jet}})$. Left-top/right-top/-left-bottom/right-bottom plot: $p_{\mathrm{T,max}}^{\mathrm{jet}}$ = 200 GeV, 400 GeV and 600 GeV, and no cut. As in ref. [115, fig. 13]. 55

8.1 Normalized Higgs transverse momentum distribution for scalar coupling operators. The normalization factors σ_{ij} are given in table C.1. 69
8.2 Normalized Higgs transverse momentum distributions for pseudoscalar coupling operators. Note that the gg channel is identical to the scalar case. σ_{ij} are given in table C.2. 69
8.3 Higgs transverse momentum distributions with SM matching coefficients resulting in a total $1/m_t^2$ suppression with respect to C_1^2. Note that in the case of the gq and summed channel the cross term $\mathcal{O}_1\mathcal{O}_5$ has been multiplied with −1. For the qq channel the cross term $\mathcal{O}_1\mathcal{O}_2$ has been multiplied with −1. 70
8.4 Normalized distributions for azimuthal angle difference of the two final state jets for scalar operators. σ_{ij} are given in table C.3. 71
8.5 Normalized distributions for azimuthal angle difference of the two final state jets for pseudoscalar operators. σ_{ij} are given in table C.4. 72
8.6 Normalized distributions for rapidity separation of the two final state jets for scalar operators. σ_{ij} are given in table C.5. 73
8.7 Normalized distributions for rapidity separation of the two final state jets for pseudoscalar operators. σ_{ij} are given in table C.6. . . 73
8.8 Normalized azimuthal angle difference distributions for scalar operators as in fig. 8.4, but restricted to events with $p_{\mathrm{T,H}} >$ 200 GeV, where $p_{\mathrm{T,H}}$ is the transverse momentum of the Higgs boson. σ_{ij} are given in table C.7. 74
8.9 Normalized rapidity separation distributions for scalar operators as in fig. 8.6, but restricted to events with $p_{\mathrm{T,H}} > 200$ GeV, where $p_{\mathrm{T,H}}$ is the transverse momentum of the Higgs boson. σ_{ij} are given in table C.8. 74
8.10 Normalized Higgs transverse momentum distributions, suppressed by $1/\Lambda^6$, for scalar coupling operators. σ_{ij} are given in table C.9. 75
8.11 Normalized Higgs transverse momentum distributions suppressed by $1/\Lambda^6$ for pseudoscalar coupling operators. σ_{ij} are given in table C.10. 76
8.12 Normalized azimuthal angle difference distributions suppressed by $1/\Lambda^6$ for scalar coupling operators. σ_{ij} are given in table C.11. 76

8.13 Normalized azimuthal angle difference distributions suppressed by $1/\Lambda^6$ for pseudoscalar coupling operators. σ_{ij} are given in table C.12. 77
8.14 Normalized rapidity separation distributions suppressed by $1/\Lambda^6$ for scalar coupling operators. σ_{ij} are given in table C.13. 77
8.15 Normalized rapidity separation distributions suppressed by $1/\Lambda^6$ for scalar coupling operators. σ_{ij} are given in table C.14. 78

12.1 $t^2 \langle E(t) \rangle$ for $N_f = 3$ as a function of μ/q_8 for various values of q_8 at leading order (LO) (black dotted), next-to-leading order (NLO) (orange dashes), next-to-NLO (NNLO) (red solid). All curves are normalized to the NNLO result at $\mu = 3q_8$. Note the different scales for each plot. 109
12.3 $t^2 \langle E(t) \rangle$ for $N_f = 3$ as a function of $\sqrt{8t}$ (in GeV^{-1}) for $\mu = 3q_8$ (lower) and $\mu = 1.15q_8$ (upper) at LO (gray), NLO (orange), and NNLO (red). 112
12.4 Upper plot: numerical value for $\alpha_s^{(5)}(m_Z)$ derived at LO (gray), NLO (orange), and NNLO (red) from a hypothetical exact value of $t^2 \langle E(t) \rangle$. Lower plot: corresponding theoretical uncertainty (see eq. (12.7)). 114

A.1 Schematic overview of the perturbative gradient flow setup. The prefix subdirectories are not shown. 130

LIST OF TABLES

12.1 Uncertainties for $t^2 \langle E(t) \rangle$ obtained by a μ variation between $1.15q_8$ and $3q_8$ following eq. (12.5) for different values of $q_8 = 1/\sqrt{8t}$. 111

C.1 Normalization factors for p_T distributions in H+1-jet production for a scalar Higgs. They are obtained by integrating the distributions of fig. 8.1 over the complete p_T interval of 30–800 GeV. . . 133
C.3 Normalization factors for $\Delta\Phi_{jj}$ distributions in H+2-jets production for a scalar Higgs. They are obtained by integrating the distributions of fig. 8.4 over the interval $\Delta\Phi_{jj} \in [0,\pi]$, with the cuts described in eq. (8.2) and (eq. (8.3)). 134
C.4 Same as table C.3, but for a pseudo-scalar Higgs (see fig. 8.5). . . 134
C.5 Normalization factors for $\Delta\eta_{jj}$ distributions in H+2-jets production for a scalar Higgs. They are obtained by integrating the distributions of fig. 8.6 over the interval $\Delta\eta_{jj} \in [0,10]$, with the cuts described in eq. (8.2). 134
C.6 Same as table C.5, but for a pseudo-scalar Higgs (see fig. 8.7). . . 135
C.7 Normalization factors for $\Delta\Phi_{jj}$ distributions in H+2-jets production for a scalar Higgs with $p_{T,H} > 200$ GeV. They are obtained by integrating the distributions of fig. 8.8 over the interval $\Delta\Phi_{jj} \in [0,\pi]$, with the cuts described in eq. (8.2) and eq. (8.3). . 135
C.8 Normalization factors for $\Delta\eta_{jj}$ distributions in H+2-jets production for a scalar Higgs with $p_{T,H} > 200$ GeV. They are obtained by integrating the distributions of fig. 8.9 over the interval $\Delta\eta_{jj} \in [0,10]$, with the cuts described in eq. (8.2). 135
C.9 Normalization factors for p_T distributions suppressed by $1/\Lambda^6$ in H+1-jet production for a scalar Higgs. They are obtained by integrating the distributions of fig. 8.10 over the complete p_T interval of 30–800 GeV. 136
C.10 Same as table C.9, but for a pseudoscalar Higgs (see fig. 8.11). . . 136
C.11 Normalization factors for $\Delta\Phi_{jj}$ distributions suppressed by $1/\Lambda^6$ in H+2-jets production for a scalar Higgs. They are obtained by integrating the distributions of fig. 8.12 over the interval $\Delta\Phi_{jj} \in [0,\pi]$, with the cuts described in eq. (8.2) and eq. (8.3). 136

C.12 Same as table C.11, but for a pseudoscalar Higgs (see fig. 8.13). . . 137
C.13 Normalization factors for $\Delta\eta_{jj}$ distributions suppressed by $1/\Lambda^6$ in H+2-jets production for a scalar Higgs. They are obtained by integrating the distributions of fig. 8.14 over the interval $\Delta\eta_{jj} \in [0,10]$, with the cuts described in eq. (8.2). 137
C.14 Same as table C.13, but for a pseudo-scalar Higgs (see fig. 8.15). . 138

ACRONYMS

Notation	Description
N^3LL	next-to-NNLL
BSM	beyond the Standard Model
CP	charge parity
DGLAP	Dokshitzer-Gribov-Lipatov-Altarelli-Parisi
EFT	effective field theory
EWSB	electroweak symmetry breaking
EW	electroweak
FKS	Frixione-Kunszt-Signer
HL	high-luminosity
HTL	heavy top limit
IBP	integration by parts
IMT	Iri-Moriguti-Takasawa
IR	infrared
LHC	Large Hadron Collider
LL	leading logarithmic
LO	leading order
MB	Mellin-Barnes
MSSM	minimal supersymmetric Standard Model
NLO	next-to-leading order
NNLO	next-to-NLO
PDF	parton distribution function
QCD	quantum chromodynamics

Notation	Description
SCET	soft-collinear effective theory
SD	sector decomposition
SM	Standard Model
UV	ultraviolet
$\overline{\text{MS}}$	modified minimal subtraction

Part I

INTRODUCTORY PART

This first part establishes the greater context in which this thesis fills a tiny gap: Standard Model phenomenology and high-energy particle physics. We begin with the features and limitations of the Standard Model and specialize to the sectors of electroweak symmetry breaking and quantum chromodynamics, which are two central topics here.

1

ELEMENTS OF THE STANDARD MODEL

Since its completion in the 60s, the unifying theory of electroweak interactions [1–3] has proven to be of extraordinary success. This relativistic quantum field theory is guided by principles of local gauge invariance and renormalizibility [4, 5]. Together with quantum chromodynamics (QCD) [6–11][1] it forms the Standard Model (SM) of elementary particle physics.[2]

Experimentally, the Standard Model found its internal completion with the discovery of the Higgs boson [17, 18]. It is the quantum excitation of the Higgs field that leads through a non-vanishing vacuum expectation value (vev) to spontaneous breaking of the electroweak (EW) symmetry and gives masses to the $W^{\pm}$ and Z gauge bosons. With over 20 free parameters, the Standard Model leaves us with the question of their origin. Not only do these parameters, but also clear evidence of new physics from astrophysical and cosmological observations, motivate us to search for extending it in a unifying way.

Among the things that the Standard Model does not at all, or not sufficiently explain are:

- Neutrino masses, observed from flavor oscillations.
- Gravity. Why is it so weak compared to the other forces? We expect that at least at energies near the Planck mass of $m_P = \sqrt{\hbar c/G} \simeq 10^{19}$ GeV, where G is the gravitational constant, gravity must be quantized.
- Dark matter, which is, up to now, only indirectly observed, for example in galaxy rotation curves.

1 See for example ref. [12] for a comprehensive review of QCD, when it counted as the established theory of strong interactions; so ref. [13] for a review of the gluon discovery from a personal perspective. Ref. [14] focuses on recent progress and the current status.

2 A recommended read on the experimental verification of the SM can be found in ref. [15]. See also the PDG-review in ref. [16].

- Insufficient CP violation to account for the matter-antimatter asymmetry since baryogenesis.
- Cosmic inflation, to explain among other things the homogeneity of the observed universe and cosmic microwave background.
- … (See for example ref. [15, 19].)

Other questions, that are more fundamental though, can be asked about the number of particle generations, the specific choice of gauge group and their representations for fields, or why electroweak symmetry is broken. Is it possible to derive the Standard Model with its immediate parameters and choices from simpler or more natural principles? What is 'more natural' then? Naturalness, by 't Hooft [20], claims that at any energy scale μ, a physical parameter, or a set of physical parameters $a_i(\mu)$ are allowed to be very small only if the replacement $a_i(\mu) = 0$ enhances the symmetry of the system.

Is the Standard Model then rather natural or unnatural? Can the introduction of a Higgs doublet, with its non-vanishing vev to spontaneously break electroweak symmetry, be considered an ad-hoc approach [21] to give masses to fundamental particles? What about the strong CP problem, or the ultraviolet (UV)-sensitivity of the Higgs mass to the Planck scale? These questions could be considered rather artificial, yet we look for physics beyond the Standard Model (BSM) guided by naturalness.

For example, it is strongly believed that the sector of electroweak symmetry breaking (EWSB) will us give clues about an extension or UV-completion of the Standard Model. Because of the unnatural Higgs mass UV-sensitivity (fine-tuning, hierarchy problem) [22–25], we conclude that it must be fixed by new physics. To solve this problem, an additional symmetry is imposed on the Higgs field that makes a mass term natural by 't Hooft's definition. Because, unlike for gauge bosons, which are protected by gauge symmetries, and fermions, which are protected by chiral symmetries, the removal of a scalar mass term does not enhance the theory's symmetry. Introducing a protecting symmetry then forbids the Higgs mass term, and subsequently a natural one is generated by softly breaking this symmetry. Multiple choices for protecting symmetries have been introduced through[1]:

1 Listing based on a presentation in the 'Fourth Annual Visiting Lectureship Series, 2014; Prof. Michael E. Peskin'; see also ref. [26].

- Supersymmetry, extending the Poincaré space-time symmetry group by transformations between fermionic and bosonic fields. This relates the Higgs field to a fermion partner field, whose mass is forbidden by a chiral symmetry [27, 28].

- Extra space dimensions, that relate the Higgs field to a vector field, whose mass is forbidden by a gauge invariance [29–31].

- Treating the Higgs boson as a (pseudo) Goldstone boson, whose mass is protected by a shift symmetry [32, 33].

- Assuming a fixed point for all couplings; scale invariance then protects the Higgs mass [34, and references therein].

Early simple models of strongly interacting electroweak sectors like Technicolor [35] have been disfavored meanwhile. New approaches treat the Higgs boson as an effective field, arising from new dynamics which become strong at some scale [36–38]. Recently, a novel idea has been proposed to solve the issue of Higgs mass naturalness: The effective Higgs mass dynamically evolves from its natural UV cutoff value in the inflationary phase of the universe to a now small value [39, 40]. This is achieved through a coupling to an axion field, whose potential serves for the Higgs mass term to cross zero, and, thus, subsequently leads to a non-vanishing Higgs vev. Naturalness is given, since the crossing of zero is the special point where electroweak symmetry enters the broken phase. This is exactly where the mass evolution stops due to barriers in the axion potential, leading to a light Higgs mass.

All approaches lessen the fine-tuning problem, but the realistic ones also increase the number of additional parameters and particles considerably. Generally, they provide explanations for problems considered above. For example, the minimal supersymmetric Standard Model (MSSM) can provide gauge coupling unification, dark matter, sources of additional CP violation, and is itself an appealing extension of the space-time symmetry. Of course, cherishing hopes and following the anthropic principle is also a possibility to 'explain' fine-tuning, but could endanger the scientific method [41, 42].

Speaking on a high level, in this thesis we performed perturbative calculations *motivated* by the following questions:

1. Is the newly found scalar particle really the SM Higgs boson? Is it completely and solely responsible for electroweak symmetry breaking? How

do we quantify the search for deviations and exclude other theories?

2. How do the detailed Higgs kinematics look like in the SM? How large are the errors of current calculations? Are we prepared to compete with increasing experimental precision at the LHC, especially at high energies, where higher order perturbative calculations face the approximation of an infinitely heavy top-quark?

3. Is QCD the right theory to describe low energy hadronic physics and high energy jet physics simultaneously? What is the size of the SU(3) coupling?

More specifically, this thesis aims to further test the Standard Model in two specific sectors. The first sector is the Higgs one. The Higgs boson is predominantly produced through gluon fusion at the LHC.[1] Perturbative calculations of this production mode have a very specific uncertainty: since the coupling of the Higgs boson to gluons, being prevalent in proton-proton collisions, is induced by a heavy quark loop, the Feynman diagrams at LO demand already a massive one-loop calculation. This would not be a problem by itself, if higher orders were small. Instead, the perturbative corrections at higher orders turned out to be significant. They are usually performed in the limit of an infinitely heavy top-quark mass, the heavy-top limit (HTL). It is thus essential to justify the HTL approximation.

A comprehensive review of gluon fusion and the associated top-mass uncertainty is given in part II chapter 2. Up to our study [43], top-mass effects were only considered in inclusive Higgs production or at LO for differential quantities. In part II of this thesis we extend our previous analysis [43], which examines finite top-mass effects at NLO in differential observables through an asymptotic expansion in $1/m_t$, to the jet-veto at NNLO and semi-inclusive quantities. We also improve our previous results by increasing the order of the asymptotic expansion.

High energies are required to probe new physics. So estimating the HTL error or predicting the size of finite mass effects are important for a precise comparison with experimental data to constrain or detect new physics. In part III we study an effective theory description of the Higgs-gluon coupling. We show that differential distributions in Higgs+1- and 2-jet production from dimension-5 and -7 Higgs-gluon coupling operators can give significant deviations from the

1 See fig. 1.2 in the next section for its LO Feynman diagram.

SM behavior. This allows one to quantify and constrain new physics specific to the Higgs-gluon coupling.

The second sector we focus on in this thesis is QCD. QCD has been well tested in the 70s and 80s through jet-physics and deep inelastic scattering, relying on the factorization theorem and asymptotic freedom/perturbativity at high energies. However, at low energies the fundamental degrees of freedom are not quarks and gluons, but, through confinement, strongly bound hadrons. Effective theories like chiral perturbation theory have been established to describe this low energy region. Through the increasing computational power, a direct integration of the discretized path integral can be performed on a space-time lattice. Of course, QCD on the lattice is not without numerical and computational problems, such that lattice QCD comprises a complete field by itself.

A difficult and thus, up to now, rather underdeveloped aspect of QCD is the connection of the low-energy sector with the high-energy sector. Recently, a new approach named gradient flow, to be introduced in part IV, was developed. It opens a new way for calculations on the lattice that reach into the perturbative regime. Additionally, perturbative calculations of observables in the gradient flow are possible and allow bridging both well tested parts of QCD. We performed the first NNLO calculation in gradient flow, corresponding to three loops. The calculational details and results are given in part IV. The observable we consider allows for a definition of the strong coupling on the lattice. By combining the lattice result with our perturbative NNLO result, $\alpha_s(m_Z)$ can be extracted with high precision. We estimate the uncertainty on $\alpha_s(m_Z)$ that can be achieved through our calculation and lattice data given at a specific gradient flow induced scale.

The three following parts of this thesis ask for some more details: Regarding Higgs physics, gluon fusion is brought into a larger context in section 1.1. In section 1.2 we cover aspects of SM effective field theory (EFT) with specifics to the Higgs sector. Section 1.3 reviews features of QCD. Some essentials on techniques in perturbative calculations used in this thesis are reviewed in section 1.4.

1.1 ELECTROWEAK AND HIGGS PHYSICS

A good candidate for the beginning of Higgs physics is the direct discovery of the $W^{\pm}$ [44, 45] and Z bosons [46–48][1], whose longitudinal components constitute three of four degrees of freedom in the complex SU(2) Higgs doublet. The direct discovery of the fourth component, the Higgs boson, has been achieved recently by the observation of a resonance with Higgs-like properties [17, 18].[2] The most significant Higgs decay channels for its discovery were $H \to \gamma\gamma$ and $H \to ZZ \to 2l^+2l^-$. Thus, missing are direct determinations of the Higgs self coupling, implying a non-vanishing vev, and the Yukawa coupling to fermions.[3] Of course, these are indirectly determined and constrained by the observed SM-like signals [58–62].

Figure 1.1 considers the precision of coupling measurements that can be achieved at the LHC with 300 fb^{-1} of data, and at the HL-LHC with 3000 fb^{-1}. By modifying SM couplings by a multiplicative factor κ_j, estimates can be done on how much data is required to limit κ_j below a certain value. The lines S1 and S2 (conservative (csv.) and optimistic (opt.)) follow from different scenarios, where S1 assumes no improvement in theory predictions, while the S2 scenarios assume a halved uncertainty for parton distribution functions (PDFs) and involved partonic cross sections. The upper part of fig. 1.1 considers limits on invisible Higgs decays. For further details we refer to ref. [57].

An important coupling is the loop induced Higgs-gluon coupling, since the predominant Higgs production mechanism at the LHC in the Standard Model is gluon fusion. Gluon fusion at LO is depicted in fig. 1.2, next to other Higgs production modes, and is mediated by a quark loop. With its large Yukawa coupling, the top-quark provides the biggest contribution to the loop, and, as such, to the Higgs-gluon coupling. Although a challenge for higher order perturbative calculations, the coupling provides a good sensitivity to additional massive particles circulating in the loop. Any simple heavy fourth generation would considerably increase the coupling. Figure 1.1 shows that this Higgs-gluon coupling is experimentally challenging and a precision of better than $\simeq 10\%$ can be reached only at the HL-LHC with improved predictions.

1 $W^{\pm}$ and Z bosons were constrained earlier, see e.g. a review in ref. [49].

2 Earlier, a Higgs boson mass of 81^{+52}_{-33} GeV has been indirectly obtained from precision measurements of electroweak parameters at LEP [50].

3 For analyses on Higgs couplings see, for example, refs. [51–57].

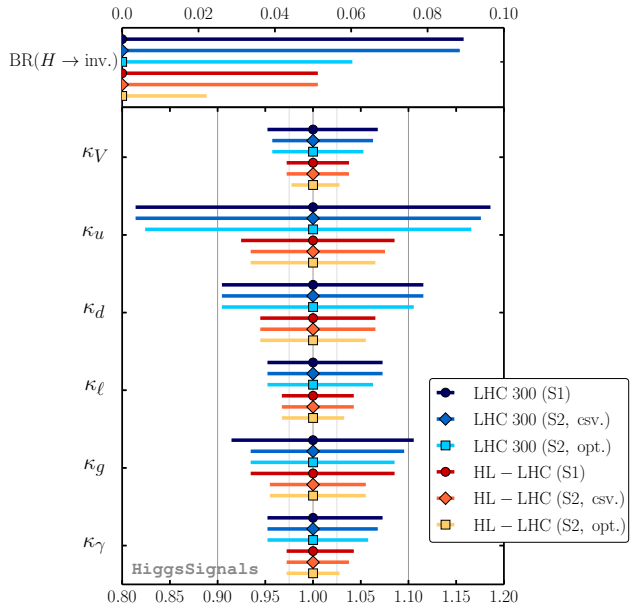

Figure 1.1: Projected future precision for the determination of multiplicative Higgs coupling scale factors κ_j at the LHC with integrated luminosities of 300 fb^{-1} and 3000 fb^{-1} (HL-LHC). As in ref. [57, fig. 17].

A comparison of the Higgs production cross section predictions for the channels shown in fig. 1.2 is given in fig. 1.3. An overview of the magnitude of the decay channels can be found in ref. [63, fig. 4].

From the Higgs signal strengths in its different decay channels, the couplings to fermions and electroweak gauge bosons can be extracted [64]. Parameterizing the couplings to fermions λ_f and to massive bosons g_V as

$$\lambda_f(M,\varepsilon) = \sqrt{2}\left(\frac{m_f}{M}\right)^{1+\varepsilon}, \quad g_V(M,\varepsilon) = 2\frac{m_V^{2(1+\varepsilon)}}{M^{1+2\varepsilon}}, \tag{1.1}$$

a fit as shown in fig. 1.4 can be obtained. The fermion masses are denoted as m_f, the gauge boson masses as m_V. The Standard Model corresponds to $\varepsilon = 0$ and $M = v = 246\,\text{GeV}$, where v is the Higgs vev.

Note that, for example, even though the coupling to the top-quark is very much as in the SM, it is only indirectly constrained. A direct measurement through a Higgs discovery in association with $t\bar{t}$ is expected for LHC Run-2, giving first direct evidence for non-zero Yukawa couplings.

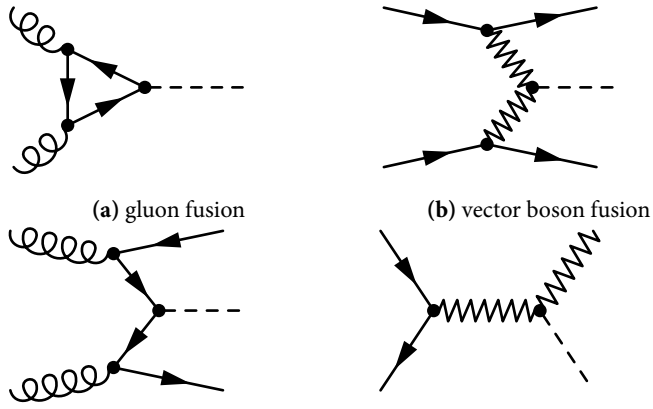

(a) gluon fusion **(b)** vector boson fusion

(c) with $t\bar{t}/b\bar{b}$-pair **(d)** Higgs strahlung

Figure 1.2: Leading Feynman diagrams for the largest Higgs boson production channels at the LHC.

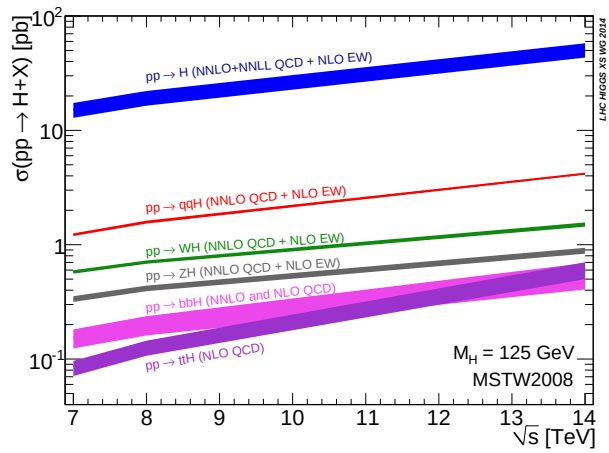

Figure 1.3: Standard model inclusive Higgs production cross sections for m_H = 125 GeV in dependence of the center of mass energy $\sqrt{s}$. As in ref. [63, fig. 2].

HIGGS OFF-SHELL EFFECTS. While the zero-width approximation works well to describe the Higgs production and decay chain, off-shell effects can become sizable in certain kinematical regions and must be cut off in such differential analyses [65–69]. They can also turn relevant if BSM physics modifies the Higgs width, and can invalidate Higgs coupling studies, which rely on the zero-width approximation. But these off-shell effects can also be used to constrain the Higgs width and couplings, as has been recently observed [70–77].

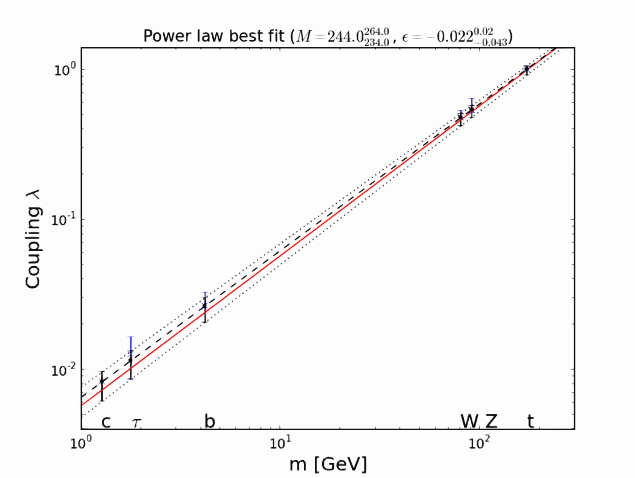

Figure 1.4: Measured Higgs boson couplings to different fermion flavors and massive bosons fitted to the form in eq. (1.1). The red line is the SM prediction, the black dashed line the best fit with fit parameters shown on top. As in ref. [54, fig. 6]; see same place for details.

VACUUM STABILITY. Assuming that the Standard Model is valid up to the Planck scale, one can calculate bounds on SM parameters, that, when evolved up to the Planck scale, lead to a Higgs potential with a minimum that lies lower than the current electroweak vacuum. This signifies an unstable or false vacuum. Close to these parameters, metastable regions exist that generate an unstable but long-lived universe. The calculation of the stability bounds depends essentially on the running of the Higgs quartic coupling $\lambda(\mu)$. For current values of m_t and m_H, upon which the running of $\lambda(\mu)$ mainly depends, $\lambda(\mu)$ runs down close to zero around the Planck scale. This also opens up scenarios where the Higgs field plays a role during cosmic inflation [78–80].

Absolute SM electroweak vacuum stability is excluded at about 2.8σ [80], where the largest uncertainty comes from m_t. It is believed that the remarkable near-criticality of the measured SM parameters, displayed in the SM phase diagram in fig. 1.5, encodes information about a more fundamental theory.

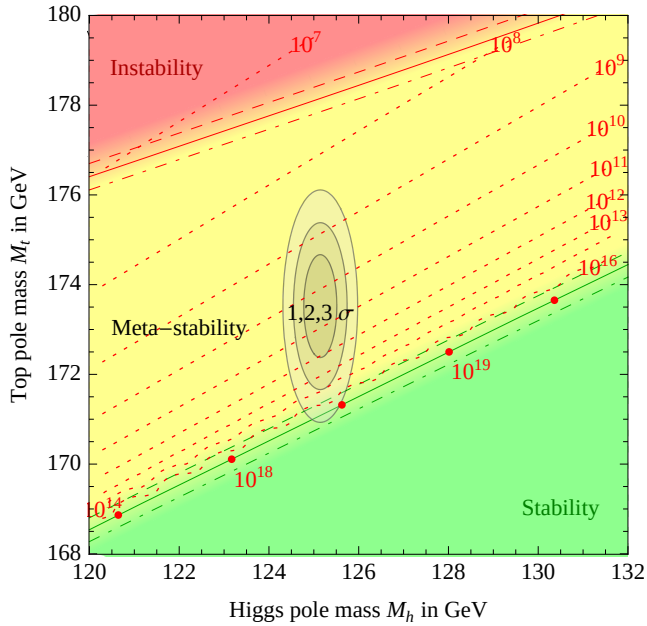

Figure 1.5: Standard model phase diagram in terms of Higgs and top pole masses. The dotted contour lines show the instability scale in GeV. The grey areas denote the allowed region at 1, 2, and 3σ confidence levels of the parameters. Taken from ref. [80, fig. 3]; see same place for details.

1.2 EFFECTIVE FIELD THEORIES

We have seen that the Higgs sector is already strongly constrained by direct and indirect coupling measurements at the LHC. Assuming that no new fundamental particles will be found soon, an era of precision measurements will begin. With precisely measured parameters, we can improve our understanding of considerations like vacuum stability, and further constrain models beyond the SM.

The constraining and quantification of physics beyond the Standard Model can be either performed in simplified ways, like fitting rescaled SM couplings to measurements [81], or by using effective field theories[1] (EFT). Since the scalar particle discovered in 2012 is SM-like, we can assume approximate validity of the SM, and augment it with higher dimensional operators $\mathcal{O}$, composed of SM

1 For an introduction to effective field theories see ref. [82], which also covers precision electroweak measurements.

fields:

$$\mathcal{L} = \mathcal{L}_{\text{SM}} + \sum_{d>4} \sum_{i} \frac{C_{i,d}}{\Lambda^{d-4}} \mathcal{O}_{i,d} \,, \tag{1.2}$$

where d is the operator mass dimension, C_i are Wilson coefficients, and Λ is a scale of new physics, where the effective field theory description breaks down. The set of operators is usually chosen by enforcing gauge invariance, validity of electroweak precision measurements, baryon or lepton-number conservation, and additional symmetries like the custodial symmetry.

Normally, EFT calculations are performed for operators of dimension-5 and -6 only: higher mass dimensions are suppressed by additional scales of Λ. Unless a mechanism renders the Wilson coefficients large, possibly proportional to Λ, the operators of larger dimension should be negligible. Under mild assumptions, the number of operators of dimension-5 and -6 for SM fields is about 60 [83, 84]. Recently, also a classification of dimension-7 operators has been done [85], adding just about 20. Also, the renormalization of all one-loop dimension-5/6 operators has been performed [86–88] lately, and was applied in one-loop analyses for Higgs couplings [89–92].[1]

Likewise, in the context of the SM itself, effective field theories turned out to be useful. For example, for energies below m_W and m_Z, the W and Z bosons can be integrated out, resulting in the Fermi theory. This allows focusing on the relevant degrees of freedom for a given problem, makes the calculation often easier, and, additionally, resums large logarithmic corrections that could spoil a perturbative calculation in the full theory. The distinct N_f-flavor schemes in QCD, with N_f different quark flavors, are also a prominent example. For the modified minimal subtraction ($\overline{\text{MS}}$) renormalization scheme, heavy degrees of freedom do not decouple by the renormalization group [104], and a ladder of N_f-flavor theories must be constructed and matched when one theory is switched at a quark threshold to the next. For low energy hadronic physics, effective theories of QCD, such as soft-collinear effective theory (SCET) or chiral perturbation theory, were constructed.

We are mainly interested in effective theories involving the Higgs boson in QCD here. Our study of the Higgs-gluon coupling in part III covers specifically dimension-5 and -7 Higgs-gluon coupling operators that can augment, modify,

1 A vast amount of tree-level studies covering Higgs couplings through effective theories have been published, of which some can be found in refs. [55, 93–103].

or replace the mainly top-quark loop induced coupling in the SM. Deviations of kinematical distributions from the SM shape show up if we perform scattering processes at high enough energies. We show how these operators can significantly deform, for example, the shape of the Higgs p_{T} spectrum toward high p_{T}. In contrast to that, our study on top-mass effects in differential gluon fusion in part II also covers those operators, but only implicitly through an asymptotic expansion in $1/m_t$. We do not perform the matching of the asymptotic expansion up to $1/m_t^4$ to the operators of dimension-5, -7 and -9 there, since we are only interested in the validity of the leading dimension-5 operator at low energies. In this context, it is sufficient for us to consider the effect of the SM matched dimension-7 and dimension-9 operators altogether, and not distinctly for each one.

Following our EFT study, a number of publications engaged in studies on higher dimensional operators in H+jet production. A general problem for inclusive quantities is that the Yukawa coupling term $-\kappa_t \frac{m_t}{v} H(\bar{t}_R t_L + \text{h.c.})$ is degenerate with $\kappa_g C_1 \frac{H}{v} G^a_{\mu\nu} G^{a,\mu\nu}$, where C_1 is obtained by integrating out the SM top-quark. Inclusive gluon fusion cross sections including both operators are functions of the sum $\kappa_g + \kappa_t$. In other words, the limit of an infinitely heavy top-quark works very well: instead of $\kappa_g = 0$, $\kappa_t = 1$ we can use the approximation $\kappa_g = 1$, $\kappa_g = 0$. Only through differential observables at high energies, the specifics of the Higgs-gluon coupling can be resolved to disentangle κ_g and κ_t.

High p_{T} jets can be used to probe for fermionic top-partners [105], or to lift the mentioned $\kappa_g + \kappa_t$ degeneracy in the SM [106]; emphasis on composite Higgs and supersymmetric models has been given in ref. [107]. Analyses taking into account decay, background and detector were presented in refs. [108, 109]. The impact of renormalization group running and mixing on such analyses is discussed in ref. [110]. Specifics to an additional second jet can be found in ref. [111]. Additionally, impact of the triple gluon operator on measurements of the Higgs-gluon coupling has been inspected [112]. Finally, our study of dimension-5 and -7 operators has been extended to NLO for $H+1$-jet production [113]. Matching of dimension-5 and -7 operators to models with heavy colored scalars and heavy fermions has been done recently [114]. Of course, a reliable SM prediction, including quark-mass effects at higher orders in the high p_{T} regime, is a necessary condition for precision studies [43, 115–118]; see also part II.

1.3 QUANTUM CHROMODYNAMICS

Quantum chromodynamics gives rise to most of the visible mass of the universe. Through dimensional transmutation, the confining scale Λ_{QCD}, setting the mass scale of the observed hadron spectrum, is generated from a classically conformal theory (in case of massless quarks). It is under active investigation if QCD is the correct theory to describe the phase diagram of nuclear matter, and, as such, allows for an explanation of cosmological phenomena. How does the transition going from the hadronic confined phase to higher densities, as in neutron stars, look like? Going toward the highest temperatures, as in the beginning of the universe, we expect QCD to describe the phase of quark gluon plasma [119]. Lastly, QCD also serves as a prototype for other strongly coupled theories that provide alternatives to the SM Higgs mechanism.

At hadron colliders, quantum chromodynamics is of paramount importance for perturbative calculations. There, often QCD dominates the dynamics, while electroweak effects are suppressed by an order of magnitude. Only through the separation into long ranged physics, modeled though parton distribution functions, and short ranged physics, modeled as hard scattering cross sections of partons, are perturbative calculations possible [120, 121]. This property, called factorization, is intuitively understood in Feynman's parton model. Subsequently, after the hard scattering, models for hadronization must be employed.

LOW ENERGIES. The confining low energy regime of QCD, with hadrons as the degrees of freedom, is traditionally described by effective field theories. A discretization of Feynman's path integral leads to the lattice formulation of QCD. Using it became feasible through Moore's law of computing power and compelling algorithmic advances [122]. For example, the recent ab initio calculation of the neutron-proton mass difference [123] and the prediction of the hadron mass spectrum [122] point out the progress that has recently been made [14]. Also in the context of flavor physics, lattice QCD turns out to be an indispensable formulation [124].

Through QCD on the lattice, we can learn how mass is generated as binding energy from the confining properties of quark and gluon fields: QCD with N massless quark flavors has an $\mathrm{SU}(N)_L \times \mathrm{SU}(N)_R \times \mathrm{U}(1)_V \times \mathrm{U}(1)_A$ symmetry. The chiral symmetry $\mathrm{SU}(N)_L \times \mathrm{SU}(N)_R$ is spontaneously broken to the diagonal isospin subgroup $\mathrm{SU}(N)_V$ through the quark/chiral-condensate $\langle \bar{\Psi}\Psi \rangle$. If one assumes that the three Goldstone bosons of this spontaneous symmetry breaking

are the pions, they should be massless. It can be shown that

$$m_\pi^2 \langle \bar{\Psi}\Psi \rangle = 0 \tag{1.3}$$

holds for massless quarks, where m_π is the pion mass [122, 125, 126]. Recent lattice calculations found a non-vanishing value of $\langle \bar{\Psi}\Psi \rangle$ [127–129], confirming through eq. (1.3) the pion as the Goldstone boson of the spontaneously broken chiral symmetry. Adding small up- and down-quark masses, breaks the symmetry explicitly and explains the small observed pion mass.

STRONG COUPLING α_s. Determining the strong coupling α_s at different scales, and evolving them to a common point for comparison, is an important test that establishes QCD as the correct fundamental theory of strong interactions on all scales. For example, an extraction of α_s from low energy inputs, such as hadron masses, provides a unique connection of the non-perturbative sector with the high-energy perturbative regime. It answers questions such as: is confinement related to the increase of α_s at low energy?

The current world average of $\alpha_s(m_Z) = 0.1185(6)$ [130] has an error of about half a percent. It limits the accuracy of all calculations involving QCD. Especially the process of Higgs production through gluon fusion, which starts at $\mathcal{O}(\alpha_s^2)$ at leading order and proceeds with large perturbative corrections at order α_s^3 and α_s^4, is sensitive to α_s. Small errors on α_s amplify and constitute a substantial uncertainty of a few percent [131–133].

But the sensitivity of observables to α_s can also be useful for its extraction from measurements. One tries to find observables that, on the one hand, can be measured with high precision, and, on the other hand, allow for precise theoretical predictions that are sensitive to QCD corrections. For example, while the hadronic decay width of the Z boson in e^+e^- collisions provides a clean experimental signal, the α_s corrections constitute only about 4% [134]. Other used observables include the hadronic branching fraction of the τ lepton, and jet rates and event shapes in $e^+ e^-$ collisions [14, 134, 135]. For proton-proton collisions, the ratio of the hadronic to leptonic branching ratios of bottomonium decays [14, 134, 135], being proportional to α_s^3, or inclusive top-pair production [136, 137] are used. In the context of PDFs, α_s used to be determined together with the parton spectrum in a global fit [133].

The most precise determinations of α_s involve calculations in lattice QCD [14, 124, 138–141]. Unlike for perturbative calculations, where an expansion in the

renormalized coupling $\alpha_s = g^2/(4\pi)$ is done, on the lattice, the bare coupling g_0^2 is an input. It is not a suitable expansion parameter, and a perturbative conversion to the $\overline{\text{MS}}$ scheme is an obstacle. If we want to extract α_s in the $\overline{\text{MS}}$ scheme at the reference scale $\mu = m_Z$, we must compute a short distance quantity on the lattice, and then build a bridge to the perturbative $\overline{\text{MS}}$ scheme. For example, this bridge can be constructed through lattice perturbation theory [142–145], where g_0^2 is replaced in favor of a renormalized g^2. Another way is to use a framework where the computed short distance quantities on the lattice in the continuum limit can be compared directly to continuum perturbation theory. A powerful framework in that category provides the Schrödinger functional [144, 146–150]. Usually the Schrödinger functional is used with a step scaling scheme [151–153], which is basically a non-perturbative finite volume renormalization, where the renormalized quantities and the gauge coupling run with the scale $\mu = 1/L$, where L is the spatial lattice size. This allows one to use modest lattice sizes, while reaching into the perturbative high energy regime.

A relatively new framework is the Yang-Mills gradient flow [154–156], to be introduced in depth in part IV. The gradient flow is described by a diffusion equation of the gauge fields that smooths the fields for an increasing auxiliary flowtime t. The smoothing property makes it attractive for lattice calculations: a high precision evaluation of quantities is possible. In fact, observables are finite for $t > 0$ due to the smearing, and only the normal UV renormalization is required at the boundary $t = 0$. The flowtime t sets a natural scale $\mu = 1/\sqrt{8t}$. Because the gradient flow has a perturbative expansion in the continuum, it is an ideal candidate to make contact between low-energy and high-energy QCD.

Among the wealth of applications discovered so far, gradient flow allows for precise lattice scale setting [154, 157, 158], a definition of the renormalized coupling [154, 159–162], and, more generally, renormalization of composite operators on the lattice [154–156, 163, 164][1]. In part IV we calculate the perturbative expansion of a specific observable, the QCD action density, in the gradient flow framework to three loops (NNLO). One interesting application is then to extract $\alpha_s(m_Z)$, using the observable as a running coupling definition and making contact with the lattice result.[2]

1 See for example refs. [165–169] for specific applications: the small flowtime expansion is used to relate local products of gradient flow operators to the continuum energy-momentum tensor.

2 For a sneak preview, see fig. 12.4 at the end of part IV.

1.4 PERTURBATIVE CALCULATIONS IN QCD

For perturbative calculations of higher order, mainly all complications arise through the appearance of infinities that require a regularization scheme, such as the commonly used dimensional regularization [170]. Accompanying it, the preferred renormalization scheme is $\overline{\text{MS}}$ [171, 172]. Although four-dimensional formulations were developed [173, 174], so far none showed a significant decrease in the required computational, algebraic or analytic effort.

Infinities are categorized by their UV or infrared (IR) origin. UV divergences are absorbed into a redefinition of the parameters by renormalization. IR divergences, on the other hand, are due to a semantic problem. The definition of the scattering matrix assumes the existence of well defined asymptotic particle states. In the presence of massless particles, the energy gap between one particle states and the multi particle continuum vanishes, leading to collinear and infrared/soft divergences, commonly both referred to as IR divergences. For QCD, the asymptotic states are, additionally, bound states of quarks and gluons.

A mechanism to handle the IR divergences consistently and well-defined must be provided, leading to *infrared safe* observables. In practice, the cross section method of Kinoshita, Lee and Nauenberg [175–178] is employed. IR divergences from virtual corrections cancel against those from degenerate initial and final states (real emission) from the phase-space integration. To regularize them in calculations, usually also the dimensional regularization is chosen [179]. In principle ε_{IR} and ε_{UV} should be chosen differently, since they require different signs to lead to convergent integrals: $D = 4 \mp 2\varepsilon_{\text{UV,IR}}$. More conveniently, $\varepsilon_{\text{IR}} = \varepsilon_{\text{UV}} \equiv \varepsilon$ is chosen, which, for example, leads to the famous vanishing scaleless integrals, where IR and UV poles are exactly equal and opposite to each other.

The IR divergences in virtual corrections and real emission contributions stem from different phase spaces, which poses a problem for higher order perturbative calculations. On the one hand, we have the regularized infrared poles from the loop integrals of the virtual corrections. On the other hand, the regularized counter-poles from the real emission only emerge after the integration over the final state phase space. By construction of a counter-term that mimics, say, the divergent behavior of the real contribution singularity, we can subtract it from the real contribution to make it finite. Then we integrate it over the singular phase space region, and add it back to the virtual contribution. Cancellations between real emission and virtual corrections lead to large logarithms of the involved scales. They must be resummed to all orders for reliable predictions.

A common approach for NLO calculations is the process independent Catani-Seymour dipole subtraction [180, 181].[1] This algorithm has been used for our NLO calculation of differential top-mass effects in gluon fusion in refs. [43, 115, 185, 186], see part II. Among other methods are phase-space slicing [187–190] and Frixione-Kunszt-Signer (FKS) subtraction [191, 192]. For NNLO cross sections, many approaches have been developed meanwhile [193–199][2], accounting for the newly occurring doubly unresolved singularities. Many of these methods were specifically developed toward differential NNLO Higgs cross sections, see chapter 2. Considering that, neglecting PDFs, exclusive observables with complicated jet functions and algorithms require a numerical evaluation, fully numerical methods [193–195, 198], where no analytic cancellation of IR poles is necessary, are particularly attractive. In the simplest case, one can use sector decomposition [209, 210], a well known approach for loop integrations, to extract the singularities from the phase-space integrals [193, 195, 210]. By combining this approach with ideas from FKS subtraction, a general subtraction method has been constructed [198].

Collinear singularities, caused by on-shell massless initial states, are handled by a renormalization of the bare PDFs.[3] Similarly to the scale $\mu \equiv \mu_R$ in UV-renormalization, this renormalization is performed at a scale μ_F, and the evolution is governed by the Dokshitzer-Gribov-Lipatov-Altarelli-Parisi (DGLAP) equations [212–215].

Let us finish this excursion on the calculation of hadronic cross sections by emphasizing that the separation of hard, high energy, and soft, confined QCD is guaranteed by factorization theorems [120, 121, 211]: For scattered hadrons A and B, the hadronic cross section can be written in terms of a convolution of parton distribution functions f and the partonic cross section $\hat{\sigma}_{ij}$ as follows:

$$\mathrm{d}\sigma^H = \sum_{i,j} \int_0^1 \mathrm{d}\xi_i \int_0^1 \mathrm{d}\xi_j \, \mathrm{d}\hat{\sigma}_{ij}(\xi_i\xi_j s, \mu_R, \mu_F) f_{i,A}(\xi_i, \mu_F) f_{j,B}(\xi_j, \mu_F) + \text{p.s.c.},$$

where the sum is over all parton flavors i, j, and ξ_i and ξ_j represent hadron momentum fractions, constituting the center of mass energy $\sqrt{s}$. 'p.s.c.' denotes corrections that are suppressed by a power of $\sqrt{s}$, when $\sqrt{s}$ is large enough.

1 See also refs. [182–184], where this approach has been used before, for specific processes.

2 Work toward a completely general and process independent formulation can be found in refs. [200–208].

3 See section 'The IR point-of-view' of ref. [211] why in the actual theory only UV divergences occur that are related by scaleless integrals to collinear IR divergences.

Loop integrations

Loop integrations form the other big part in higher order perturbative calculations, next to the aforementioned necessity for subtraction schemes in cross section due to IR divergences. They are required to calculate virtual corrections for the hard partonic cross section $\hat{\sigma}$. Modern techniques are summarized and reviewed in ref. [216]. Some of them are referred to in the following parts. The ultimate goal is to derive a Laurent expansion in the dimensional regulator ε. Before that, one usually tries to minimize the number of integrals, by solving a linear system of equations generated by integration by parts (IBP) and Lorentz invariance equations [217–219]. Among the most powerful methods to solve the integrals are Mellin-Barnes (MB) representations, differential equations and dimensional recurrence relations. The latter two rely on the IBP reduction to a set of master integrals. Of special importance in this thesis is sector decomposition [209, 210]. It is an algorithm to construct the Laurent expansion of Feynman integrals with arbitrary kinematics, and is, in its core, again a subtraction method. An implementation in a computer program is straightforward. Since we use sector decomposition (SD) implemented in FIESTA [220] for our 3-loop calculation in part IV, we shortly review this method here.

Sector decomposition decomposes a $D = 4 - 2\varepsilon \to 4$ divergent integral into sectors, such that each of them only contains singularities in a factorized form, to be explained below. Without loss of generality, we assume that the integration domain is over a hypercube, and singularities can only occur for integration variables approaching zero. Otherwise, we can apply simple transformations to fulfill this requirement. A factorized singularity in the variable x exists, if, firstly, the integrand factors into x, raised to a power depending linearly on ε, times a remainder $f(x)$. Secondly, the Taylor expansion of f about zero in x, when subtracted from $f(x)$, must render the integral finite. In this case the subtraction is done, and the expanded term with the isolated singularity in x is added back as a new integral. The latter integration over x is trivial and delivers

poles in ε. This is illustrated in the following example:

$$\begin{aligned} I &= \int_0^1 \mathrm{d}x\, x^{-1+\varepsilon} f(x) \\ &= \int_0^1 \mathrm{d}x\, x^{-1+\varepsilon}\big(f(x) - f(0)\big) + \int_0^1 \mathrm{d}x\, x^{-1+\varepsilon} f(0) \\ &= \int_0^1 \mathrm{d}x\, x^{-1+\varepsilon}\big(f(x) - f(0)\big) + \frac{1}{\varepsilon} f(0)\,. \end{aligned}$$

Note that additional integrations are unaffected and understood to be included in f. In case of multiple factorized singularities, they are resolved one by one. Both parts, the remaining integral and $f(0)$, are now finite by construction and can be expanded in ε.

In contrast to that, a simple overlapping singularity might look like

$$\iint_0^1 \mathrm{d}x\, \mathrm{d}y \left(x + y\right)^{-2+\varepsilon} \equiv \iint_0^1 \mathrm{d}x\, \mathrm{d}y\, P^{-D/2}\,.$$

Generally, the integrand consists of a complicated polynomial P, raised to the power of a linear function in D. Through a subset of variables approaching zero, P itself can vanish and singularities occur for $D \to 4$.

Recursive strategies to decompose overlapping singularities step in at this point.[1] They choose a subset $M = \{i_1, \ldots, i_k\} \subset \{1, \ldots, n\}$ of the integration variables $x_1, \ldots, x_n$, for which the integral diverges when the simultaneous limit $x_{i_1}, \ldots x_{i_k} \to 0$ is performed. The unit hypercube $0 \le x_i \le 1$ is then decomposed into k sectors S_l, $l = 1, \ldots, k$, where

$$S_l = \left\{(x_1, \ldots, x_n) \mid x_i \le x_{i_l} \forall\, i \in M\right\},$$

and the new variables are introduced as follows:

$$\begin{aligned} x_i &= x_i' \forall\, i \notin M\,, \\ x_{i_l} &= x_{i_l}'\,, \\ x_{i_r} &= x_{i_l}' x_{i_r}' \forall\, i_r \in M, r \neq l\,. \end{aligned}$$

1 We follow ref. [216], where further details and subtleties are discussed.

The integration domain in the new variables x_i' is again a hypercube for each sector, and, by construction, x_{i_l} factorizes, such that the subtraction method above can be applied. For each of the sectors, the method is applied recursively until no more subset can be chosen, that is, until a constant term (kinematic invariants) in the polynomial P appears. The leftover integrals are expanded in ε, and the coefficients in ε can be integrated numerically after setting numeric values for the kinematic invariants. The numerical evaluation of these integrals turns out to be challenging, because, through the subtractions, they contain integrable singularities, which require high precision arithmetics and/or special handling.

From the algorithm of SD we see that, in principle, arbitrarily high loop integrations can be performed. Since it can lead to plenty sectors for a single integral, non-linear transformations have been developed [221]. They transform overlapping singularities into factorized singularities – without a decomposition into different sectors. This method has not been shown to be fully algorithmic though, and instead relies on some heuristics and manual testing. Therefore, it is also unclear if with this method any Feynman integral can be transformed to a single one with only factorized singularities.

Part II

TOP MASS EFFECTS IN DIFFERENTIAL AND EXCLUSIVE HIGGS PRODUCTION THROUGH GLUON FUSION

This part is based on our publication 'Finite top-mass effects in gluon-induced Higgs production with a jet-veto at NNLO' [115], an extension of our preceding study 'Top-mass effects in differential Higgs production through gluon fusion at order α_s^4' [43]. We estimate and predict finite top mass effects through an asymptotic expansion in $1/m_t^n$ up to $n = 4$ for jet differential and inclusive Higgs+jet cross sections at NLO and the jet-vetoed cross section at NNLO. We find effects of at most a few percent for H + jet production as long as the jet p_T stays below m_t, and sub-percent effects for the jet-veto.

2

INTRODUCTION TO GLUON FUSION

Since July 2012 no publication, no summary and no introduction about the Higgs boson[1] may miss the citation of its discovery publications [17, 18]. The publications themselves are reluctant calling it the Higgs boson in the title, and prefer calling it 'a new boson of mass 125 GeV', even though the reported significances for a SM Higgs boson are about six standard deviations. Meanwhile, three years later, at the time of writing, the name Higgs boson predominates publications.

The second run of the LHC is starting, and all data available from 'Run 1' suggest no deviations from a SM Higgs behavior [58–62]. The Higgs mass m_H has been obtained to a precision of two per mill to $m_H = 125.09(24)$ GeV [228]. In the following, we will talk about the Higgs boson, even if all the work also applies to a Higgs-*like* particle, which it is in any case. Deviations can be quantified model independently by effective theories.[2]

Of course, all the experimental success would not have been possible without the necessary Standard Model Higgs predictions, while, likewise, most theorists need experiments and their accompanying analyses to justify their work. The basis of all these predictions at the LHC are cross sections. For example, the total Higgs production cross section is an important test of electroweak symmetry breaking in the Standard Model. But in order to improve the signal significance in analyses and identify detailed Higgs kinematics, Higgs candidate events are categorized for example in different p_{T} (transverse momentum), y (rapidity) or jet bins depending on the search channel, that is, depending on Higgs production and decay mode and background processes.

Since the Higgs boson discovery, three years have passed, and analyses have

1 The Higgs boson is also, more precisely, called the Brout-Englert- [222] Higgs- [223, 224] Guralnik-Hagen-Kibble [225] -boson; see also Anderson, Nambu [226, 227].

2 In the next part we will introduce an effective theory analysis of the important Higgs-gluon coupling.

fully accounted for the complete LHC Run 1 data. Sufficient significance has been reached to claim an observation alone in the channels $H \to \gamma\gamma$ [229, 230], $H \to ZZ \to 4l$ [229, 231] and $H \to W^+W^- \to l^+\nu l^-\bar{\nu}$ [232, 233]. To disentangle signal and background processes, phase space cuts are applied that enhance the signal regions. For example, in the search mode $H \to W^+W^- \to l^+\nu l^-\bar{\nu}$ the huge QCD background due to $pp \to t\bar{t}$ and $pp \to W^+W^-$ is reduced using a veto cut ($p_{\mathrm{T}}^{\mathrm{jet}} < p_{\mathrm{T,veto}}^{\mathrm{jet}} \simeq 20$–$30\,\mathrm{GeV}$) on jets [234, 235]. A good understanding of Higgs differential distributions at low p_{T} is therefore important. Three handbooks on inclusive and differential Higgs cross sections have been published [236–238], summarizing all theory effort.

The following two sections give a detailed historic overview to single Higgs production through gluon fusion in the SM from the beginning LO calculations to the latest results at the time of writing. They will point out one specific uncertainty for gluon fusion: the common use of an effective theory where the top-quark is integrated out, helping to calculate necessary higher order perturbative corrections. In this work, based on ref. [115] and extending ref. [43], we estimate finite top-mass effects through an asymptotic expansion in $1/m_t^2$ for differential H + jet cross sections at NLO and the jet-veto at NNLO. We also consider the inclusive jet cross section. For the inclusive jet cross section and jet p_{T} distributions we not just give estimates, but present improved predictions, accounting for a finite top-mass. In the next chapter we will elaborate on the calculation itself. In chapter 4 we present our results and discuss them.

2.1 GLUON FUSION FROM THE BEGINNING

In the Standard Model, for proton-proton colliders, the main production mechanism for the Higgs boson is gluon fusion. It is already at leading order a one-loop process, where two gluons couple through a quark loop to the Higgs boson, see fig. 2.1. Although all quark flavors contribute to the quark loop, the top-quark with its large Yukawa coupling is dominant. Naively, the bottom quark contribution is suppressed with respect to the top quark by a factor of m_b/m_t, a few percent. Other production channels of the Higgs boson are suppressed by at least an order of magnitude, but allow for different analyses when considering the whole scattering final state configuration. They can also be enhanced in extended models. For example, the highly PDF-suppressed tree level production of the Higgs boson via b-quarks can grow in models with two Higgs doublets, depending on the ratio of the two uncharged scalar Higgs vacuum expectation

values. We will only consider gluon fusion with a top-quark loop here.

The first studies on gluon fusion, calculating the total cross section by the one loop diagram(s) in fig. 2.1, and acknowledging it as the largest Higgs production process for pp collisions, have been performed in the seventies [239, 240] (also [241, 242]). A remarkable fact of this process is that in the limit of a very heavy quark ($m_t \to \infty$), the one-loop diagram can be approximated by an effective vertex described by $HG^a_{\mu\nu}G^{\mu\nu,a}$, where H is the scalar Higgs field and $G^{\mu\nu,a}$ is the gluon field strength tensor. In particular, this vertex is independent of the heavy quark mass, and one is then able to count the number of heavy quarks in the loop through a measurement of this process [239, 240], since each heavy quark will contribute the same amount to the total cross section. Kinematic one-jet distributions at LO were studied approximately ten years later [243, 244]. For those, as well as for the inclusive NLO cross section, initial states with quarks open up. The quark-gluon initiated channel is usually suppressed by a factor of ~ 10, while the purely quark initiated channel is at the percent level.

Radiative corrections to the total cross section were first performed in the heavy top limit [245, 246], being valid for Higgs masses and energy scales roughly less than two times the top-quark mass. The heavy top limit (HTL) effective theory is obtained from the SM by integrating out the top quark, resulting in an effective theory described by Higgs-gluon vertices [247–249]:

$$\mathcal{L}_{\text{Yuk.}} = -\frac{H}{v} m_t \overline{\Psi}_t \Psi_t \quad \rightsquigarrow \quad \mathcal{L}_{\text{eff.}} = -\frac{H}{v} C_1 G^a_{\mu\nu} G^{\mu\nu,a} \,,$$

where v is the Higgs vacuum expectation value, m_t is the top-quark mass and Ψ_t the top-quark Dirac-field. The Wilson coefficient C_1 can be obtained perturbatively through a matching procedure, and currently known to four loop precision [250–254].

The large size of the corrections (of order 100%, depending on the back then

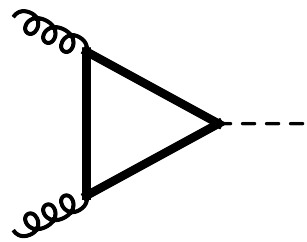

Figure 2.1: Feynman diagram for gluon fusion at LO.

unknown Higgs mass and collider energy) was emphasized, as well as the sizable renormalization scale dependence. With the numerical calculation of the NLO cross section, including a finite top quark mass [255][1], the results in the HTL were verified, confirming that the HTL works sufficiently well even for Higgs masses above the top-quark threshold: At this point in time the gluon luminosity contributed the largest uncertainty, such that even top-mass effects of less than 15% for $m_H \lesssim 700\,\text{GeV}$ were considered excellent. It also became apparent that the full NLO cross section is very well approximated by factoring out the LO one from the NLO HTL one, which means that the mass dependence of the cross section stays the same for higher order corrections:

$$\sigma^{\text{NLO}}(m_t) \simeq \frac{\sigma^{\text{LO}}(m_t)}{\sigma^{\text{LO}}(m_t \to \infty)} \sigma^{\text{NLO}}(m_t \to \infty)\,. \tag{2.1}$$

Additionally to one-jet distributions, two-jet distributions were studied at LO, first in the HTL [261, 262], then with a finite top-mass [263, 264]. It was found that the limit works well even for partonic center of mass energies $\sqrt{\hat{s}} > 2m_t$, provided that $m_H \leq m_t$ and transverse momenta $p_t \lesssim m_t$.

The reason that the HTL works so well, especially for the total cross section, is due to the large gluon luminosity at small proton momentum fractions. To leading order, the Higgs is produced without any transverse momentum through recoiling partons/jets[2], where the partonic cross section is proportional to $\delta(\hat{s} - m_H^2)$. Only at higher orders the Higgs boson can recoil against emitted QCD radiation, which is then, due to the PDFs, predominantly soft. Higher energies are PDF suppressed, and all scales remain sufficiently below the top-quark threshold $2m_t$.

Gluon fusion has two important thresholds [243]: The first one occurs for $m_H = 2m_t$, when the top-quarks, coupling to the Higgs, can become real. This is, of course, only relevant if we consider the cross section as a function of m_H. The second threshold being of relevancy, occurs for partonic center of mass energies of $\sqrt{\hat{s}} = 2m_t$, when in the NLO box graph the top-quarks can become real. This threshold can be translated into a threshold in the p_{T} distribution, depending

1 See also refs. [256, 257]; and ref. [258] for subleading terms in the HTL. Later an analytic form of the NLO cross section has been obtained [259, 260].

2 Neglecting the small intrinsic transverse momentums the partons have.

on rapidity; for $y = 0$ it is [265]:

$$p_{\mathrm{T}}^{\mathrm{th.}} = \frac{4m_t^2 - m_H^2}{4m_t}\,.$$

Note that this threshold does not exist in the heavy top limit. We can therefore expect the heavy top limit to break down in p_{T} distributions for $p_{\mathrm{T}} \gtrsim m_t$.

A peculiarity for transverse momentum spectra, including the Higgs transverse momentum distribution $\mathrm{d}\sigma/\mathrm{d}p_{\mathrm{T}}^2$, is a $1/p_{\mathrm{T}}^2$ divergence for $p_{\mathrm{T}} \to 0$ for the gluon-gluon and quark-gluon initiated channels.[1] At small p_{T}, initial-state radiation diagrams contribute soft and collinear singularities. For the p_{T}-integrated total inclusive cross section this is canceled by the virtual corrections at $p_{\mathrm{T}} = 0$, which do not affect the p_{T} distribution, though.

Furthermore, for $p_{\mathrm{T}} \to 0$, the differential cross section $\mathrm{d}\sigma/\mathrm{d}p_{\mathrm{T}}^2$ contains large logarithms $\log(m_H^2/p_{\mathrm{T}}^2)$. The convergence of the perturbative series in this region is not just determined by α_s alone, but by factors $\alpha_s \log^2(m_H^2/p_{\mathrm{T}}^2)$ close to or beyond a numerical value of one, meaning that higher order perturbative contributions are not suppressed. For these facts, it is necessary to take multiple parton emission over all orders into account, called resummation, most importantly for $p_{\mathrm{T}} \ll m_H$.[2] Resummation was originally worked out for the Drell-Yan process, and can be performed in Fourier transformed p_{T} space (b-space) [268–271] or directly in p_{T} space [272, 273]. It can also be done in the framework of SCET [274–276][3], recently applied to Higgs production [279–285]. In general, terms of the following order are generated, with $m \leq 2n - 3$ [286]:

$$\frac{1}{p_{\mathrm{T}}^2}\alpha_s^n \log^m(m_H^2/p_{\mathrm{T}}^2)\,.$$

Taking into account only the term with $m = 2n - 3$ constitutes the leading logarithmic (LL) approximation. Taking into account lower powers of logarithms to all orders in α_s constitutes next-to-LL (NLL), and so on. The fixed order part is additionally identified by the usual LO, NLO labels. For the Higgs p_{T} distribution, first resummations have been performed in the HTL [286–288] and

1 The quark-antiquark initiated channel for $H + g$ production proceeds only through an s-channel gluon, and is thus not singular at LO for $p_{\mathrm{T}} \to 0$.

2 Parton showers [266] provide an alternative semi-classical approach, often used in Monte-Carlo event generators, but are problematic to combine with higher fixed order perturbative results. For Higgs production, a comparison with resummation has been given in ref. [267].

3 For a recent introductions to resummation and SCET see ref. [277] and ref. [278].

with a finite top-mass [265] in an approximation where only the first leading logarithms have been accounted for in the LO cross section. Along that, also subleading logarithms [289, 290] and resummation for logarithms in the NLO p_T distribution have been considered [291–298]. Resummation of soft gluon radiation in the HTL was also used to estimate the NNLO corrections to the total cross section [251].

After the calculation of the one loop HTL real emission [299] and the two loop HTL virtual amplitude [300], having known the double real emission for some time [261], there is still a lot of work to end up with a hadronic cross section: all these terms in different phase spaces need to be combined, requiring for example higher order parton splitting functions. Soft-virtual approximations to the NNLO HTL cross section have been obtained [301, 302] to estimate NNLO contributions. Finally, the NNLO HTL cross section has been calculated [303–305], showing that the perturbative corrections add another $20 - 30\%$[1]. The dependence on the renormalization and factorization scales is with $15 - 20\%$ still large. Additionally, these ingredients allowed the calculation of H+jet differential distributions to NLO in the HTL, for example p_T and y distributions [308–310].[2] The Higgs+jet p_T distribution has NLO corrections of order 50–60%, with a remaining scale uncertainty of about 20%. Two-jet observables show the same magnitudes of corrections and scale uncertainties [315, 316].

Note that in ref. [303] the NNLO HTL total inclusive cross section has been obtained by expanding the partonic cross section $\hat{\sigma}$ in powers of $(1 - z)$ around the soft limit, where $z = m_H^2/\hat{s}$. After a few terms ($\mathcal{O}(10)$) the series can be truncated, being very close to the exact result. Taking just the first or second terms does not provide a satisfactory approximation.

We have reached the early beginning of the 21st century in our review. Techniques to solve integration by parts (IBP) [217] equation systems algorithmically [218, 219], Mellin-Barnes representations [317–319], differential equations [219, 320, 321] and sector decomposition [209, 210] have since then been established, and allow tackling multi-loop integrations.[3]

The gluon fusion cross section had, and still has, uncertainties of various sources, which have been surmounted and discussed in the last decade: PDF + α_s [131,

1 Reasoning for the large corrections has later been given in refs. [306, 307].

2 See also ref. [311] for an approx. beyond the HTL. Additional resummation effects have been considered in refs. [284, 312–314].

3 See for example ref. [216] for a recent and comprehensive overview.

132], perturbative truncation after NNLO, HTL (see below), electroweak effects [322–328] and (bottom-) quark mass effects [116, 257, 328–333]. Soft gluon emission can be resummed to all orders in the HTL up to next-to-NNLL (N^3LL) accuracy [334–340]. Additionally, resummation is required in certain regions of kinematic distributions. For example, the resummation of logarithmic terms for small p_T has been performed up to NNLL [279–283, 285, 341–346], also relying on the heavy top limit. Resummation becomes especially important for the jet-vetoed cross section [347–354], which has been obtained through NNLO so far [355]. Besides this, other contributions for various regions have been considered, like for example contributions away from threshold $z \ll 1$ in the HTL [356]. Paying special attention to finite top-mass effects, we can say that this uncertainty needs updated estimates to match the latest perturbative level. Specifically, the NNLO inclusive Higgs cross section needs such an estimate, as well as exclusive quantities like differential kinematic distributions in H + jet production at NLO and the jet-vetoed cross section at NNLO.

A calculation of the NNLO total cross section with a finite top-quark mass, being a three loop calculation, is even by todays means a tough project. Instead, the total cross section has been obtained [357–360] in an asymptotic expansion [361, 362] in $1/m_t^2$. Although high partonic energy $\hat{s}$ contributions to the cross section are PDF suppressed, the $1/m_t^2$ expansion breaks down at some point: The increasing negative mass-dimension in $1/m_t^k$, $k = 0,2,4,\ldots$, must be compensated with a positive mass-dimension in the numerator, among it terms like $\sqrt{\hat{s}}^k$. This problem has been solved by matching with the exact (in m_t) large $\hat{s}$ limit of the NNLO cross section [357, 363–366]. The size of these finite mass effects, when one factors out the LO mass dependence, is then less than a percent for a wide range of Higgs masses. This means that a very good approximation to higher order cross sections is obtained by taking the LO cross section, and multiplying it by K-factors in the HTL; the mass dependence is well described at LO.

Let us emphasize again that a crucial ingredient in this finite mass effects estimation was a matching to the high energy limit, since otherwise the asymptotic expansion in $1/m_t^k$ diverges quickly. We would also like to estimate mass effects in less inclusive observables. What happens if we compute these cross sections where specific kinematic regions are pronounced? As a rule of thumb, such an asymptotic expansion will only work reliably if all scales remain sufficiently below the top-quark mass m_t. Up to our publication in 2012 [43], analyses for differential quantities in $H + n - \text{jet} + X$ production, with $n = 0,1,2$, going beyond qualitative statements, have been performed only at LO [243, 244, 263, 264, 330, 331, 366], where an analytic treatment of the full top-quark mass dependence is

possible. Also, all non-inclusive NLO calculations, as well as the resummation of logarithmic terms for small p_T, the jet-vetoed cross section, and, finally, fully exclusive NNLO partonic Monte Carlo programs for Higgs production in gluon fusion [194, 197, 367, 368] rely strongly on the heavy top limit.

2.2 RECENT ADVANCEMENTS

In a previous study [43, 185, 186] we have estimated top-mass effects in differential Higgs plus jet production at NLO through asymptotic expansions in $1/m_t^2$. We find that for the differential K-factor for Higgs p_T and y distributions, the heavy-top limit is valid at the 2 – 3% level for the rapidity distribution, and for the p_T distribution as long as the transverse momentum of the Higgs remains below about 150 GeV. In the next section we will recapitulate some of these results. Our present work [115], to be presented in chapters 3 and 4, is an extension, where we additionally consider top-mass effects of the NNLO jet-veto, NLO p_T and y jet distributions, and the inclusive NLO jet cross section. By not only considering the first subleading terms of order $1/m_t^2$, as done previously [43], but also taking the $1/m_t^4$ terms into account, we can check the convergence of the asymptotic expansion more reliably.

For the jet-vetoed cross section, we find that finite top-quark effects, for realistic experimental values of the jet-veto cut $p_{\text{Tveto}}^{\text{jet}} \sim 30\,\text{GeV}$, are numerically negligible at the few per mill level. Even for jet-veto cuts up to 600 GeV they remain below two percent. The use of the effective theory for jet-vetoed cross sections is thus fully justified. For the inclusive jet cross section and kinematic jet distributions we find similar mass effects of a few percent, as previously found for the Higgs distributions [43]. Additionally, for $p_{\text{T}} \lesssim 2m_t$ in the jet p_{T} distribution and for a minimum jet p_{T} of less than $\sim 100\,\text{GeV}$ in the inclusive jet production, we can predict the exact top-mass effects, giving corrections of a few percent.

LASTLY, to finish this overview of gluon fusion in the Standard Model, we shall mention the latest important fixed order[1] results that appeared over the last few years up to just the time of writing. The N^{3}LO HTL cross section has been calculated [369] using a soft series expansion around Higgs production threshold, as previously also used for the NNLO HTL cross section calculation

1 Recent resummation results up to NNLL+NNLO HTL for the Higgs p_{T} distribution, and N^{3}LL+NNLO HTL for the total inclusive cross section have been cited in the previous section.

[357, 365]. Corrections of order 2% are much smaller than anticipated through earlier approximations, and the residual scale uncertainty is also at the few percent level. Finally, the perturbative expansion of gluon fusion in its core is under control, such that previously subleading uncertainties stand now on equal footing, among it the HTL. Accompanying, the NNLO HTL Higgs+jet cross section has been published [314, 370–373] with corrections of ~ 20% with respect to the NLO result and a remaining scale uncertainty of about 9%, being close to the remaining PDF uncertainty of order 5%.

Just as along the path toward the total NNLO cross section, many approximations beyond NNLO were performed, where the use of the heavy top limit is understood. For example, through the universality of radiative corrections due to soft emissions, higher-order logarithmic soft terms can be resummed [334, 335, 374, 375] using three loop splitting functions [376, 377]. For a full calculation of the N^3LO cross section, all contributions, from triple real radiation [378, 379] along two loop single real radiation [380–384] over one loop double real [385–388] to three loop virtual corrections [389–391] are required. Ultraviolet [392, 393] [394–397] and infrared counterterms [334, 335, 398] have also been computed to complete the calculation. These contributions are partly available only in threshold limit, or just beyond, and have been combined to provide the first two terms of the N^3LO cross section in the threshold expansion [399, 400]. Of course, further approximations have been made [401] until the 'full' result was published. As in the case for the NNLO threshold expansion, taking just the leading terms is not enough for a reasonable approximation. By taking $\mathcal{O}(10)$ terms, a close to exact result can be reproduced [357, 365, 369].

Finally, for NLO cross sections, common approaches to extract singularities from real emission contributions are phase space slicing [187, 188] and dipole subtraction [180, 182–184].Extended methods for NNLO cross sections had to be developed to account for the newly occurring doubly unresolved singularities [193, 195–199].[1] These new methods found their application in fully differential NNLO Higgs+jet production, for example.

1 See also the introductory section 1.4 for more details.

2.3 MASS EFFECTS IN H + JET + X AT (N)LO

In this section we give some initial considerations for finite top-mass effects at LO in Higgs+jet production, and recapitulate important NLO results of our previous study [43]. We remind the reader that we only consider the dominant Higgs production channel of gluon fusion, and that here, and in the following, all Yukawa-couplings, except for the top-quark, are set to zero. As for perturbative corrections, we only consider QCD corrections. At LO, the exact top-mass dependencies of the cross sections are known and can be compared to the asymptotic expansion in $1/m_t^2$.

For the following figure (2.2) we define the inclusive Higgs+jet cross section by integrating the Higgs p_{T}-differential cross section from a lower value of $p_{\mathrm{T,H}}^{\mathrm{cut}} = 30\,\mathrm{GeV}$:

$$\sigma(p_{\mathrm{T,H}} > p_{\mathrm{T,H}}^{\mathrm{cut}}) = \int\limits_{p_{\mathrm{T,H}} > p_{\mathrm{T,H}}^{\mathrm{cut}}} \mathrm{d}p_{\mathrm{T,H}} \, \frac{\mathrm{d}\sigma}{\mathrm{d}p_{\mathrm{T,H}}} \,. \tag{2.2}$$

Figure 2.2 shows this inclusive Higgs+jet cross section at LO in dependence of the Higgs mass m_H, for the initial-state partonic channels gg, gq and $q\bar{q}$. To see in how far we can expect the asymptotic expansion to work, the exact mass dependence as well as the cross sections from the expansion truncated at $1/m_t^0$ (HTL) and $1/m_t^2$ are displayed. The kink at $m_H \simeq 2m_t$ is due to the top-quark threshold in the scattering amplitude, and the expansion is clearly not able to reproduce this threshold effect. Up to $m_H \lesssim m_t$ the asymptotic expansion provides a good approximation for the gg and gq channels.

The $1/m_t^2$ expansion does not provide a convergent series for the purely quark induced channels, as was already observed for the total inclusive cross section [43, 365, 402], particularly when no matching to the exact result in the high-energy limit is applied. A reason, responsible for this, is that at LO the $q\bar{q}$ channel consists only of a single s-channel gluon diagram, while for the other partonic channels also t-type diagrams contribute.[1] Note though that the $q\bar{q}$ channel is suppressed by two orders of magnitude with respect to the gg and gq channels. For our following analyses we neglect the purely quark induced channels. Kinematical cuts could, in principle, enhance these channels and render the HTL unreliable.

1 See fig. 3.2 for examples of Feynman diagrams.

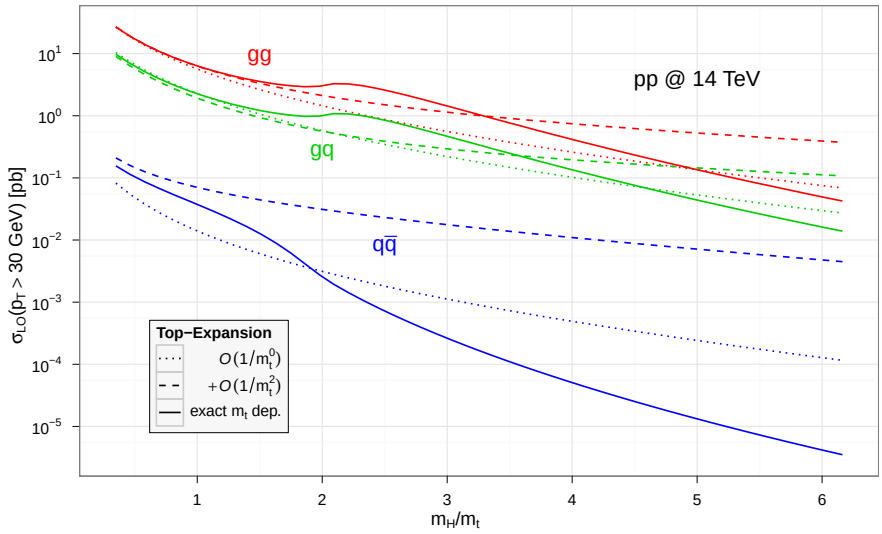

Figure 2.2: Leading order inclusive Higgs+jet cross section as defined in eq. (2.2), with $p_{\mathrm{T,H}}^{\mathrm{cut}} = 30\,\mathrm{GeV}$, in dependence of m_H, split by partonic initial-state channels gg, gq, $q\bar{q}$. Shown is the exact m_t dependence and the asymptotic expansion up to $1/m_t^2$. As in ref. [43, fig. 3].

We next consider the $p_{\mathrm{T,H}}$-differential distribution in fig. 2.3. Displayed are the dominating partonic channels gg, gq and their sum $gg + gq$ separately. Again the exact top-mass dependence and the asymptotic expansion up to $1/m_t^6$ are shown.

For the gg channel we now see the remarkable reproduction of the exact m_t dependence by the asymptotic expansion in more detail. Already the leading term (HTL) is almost indistinguishable by eye from the exact m_t curve. At some expansion order though, $1/m_t^6$ for the gg channel, it breaks down. This is due to the fact that the expansion generates expressions of higher power in $\hat{s}/m_t^2$, $p_{\mathrm{T,H}}^2/m_t^2$, etc. At some point, they become too large for their contribution at high energy to be suppressed by the PDFs. In the gq channel this divergent behavior is already visible after fewer expansion terms. Due to the dominance of the gg channel, the overall result provides satisfactory estimates of the top-mass effects below $m_t \gtrsim p_{\mathrm{T,H}}$.

Stepping up from these quantitative considerations, we shall have a look at fig. 2.4: It shows the K-factor, defined as the ratio of the NLO cross section to the LO cross section, for the Higgs p_{T} distribution, again split by initial-state partonic channels. Any common normalizations will drop out in the K-factor; it is a

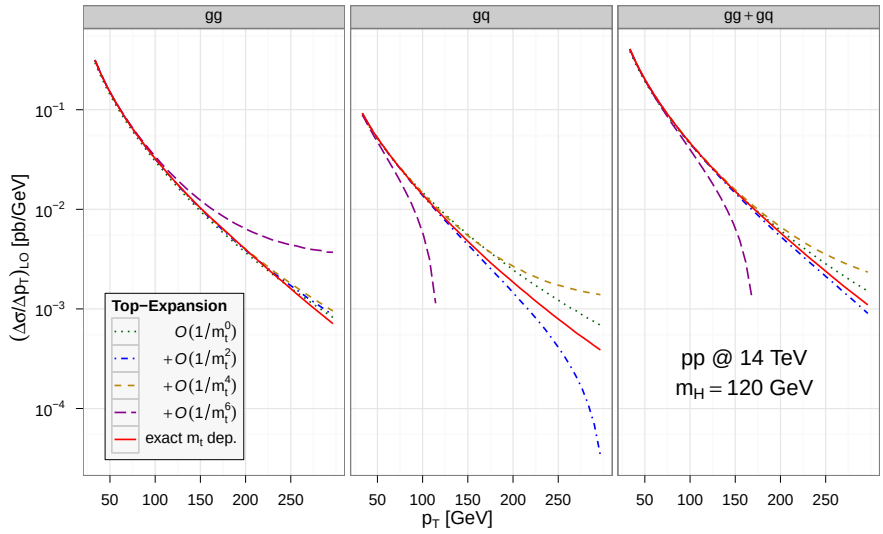

Figure 2.3: Differential cross section $\mathrm{d}\sigma/\mathrm{d}p_{\mathrm{T,H}}$ at LO, split by partonic initial-state channels gg, gq and in the sum, with exact m_t dependence and truncations of the asymptotic expansion at order $1/m_t^k$, $k \in \{0,2,4,6\}$. As in ref. [43, fig. 5].

measure for the perturbative corrections. Then, since we display the K-factor in the asymptotic expansion for different orders, from the HTL up to $1/m_t^4$, we can evaluate how well the asymptotic expansion describes the perturbative corrections.

If the higher terms in the asymptotic expansion of the K-factor do not deviate much from the leading HTL, we can claim that the differential NLO cross section is well described by taking the LO cross section with full top-mass dependence, and reweighting it by the HTL K-factor – just as for the total cross section in eq. (2.1). Finite top-mass effects can then be estimated by looking at the spread of terms beyond the HTL. If it, additionally, turns out to be well-convergent, say, $1/m_t^2$ and $1/m_t^4$ match for some region, we can claim a prediction of the mass effects.

Indeed, we observe that for $p_{\mathrm{T}} \lesssim m_t$, in all channels the asymptotic expansion is well-convergent and deviates from the HTL at most a few percent. The conclusion we draw [43] is therefore that the NLO HTL *corrections* provide an excellent approximation to the ones in full theory. The complete result is obtained by taking the full LO prediction, and reweighting it by the NLO K-factor in the HTL. We find validity at the 2 – 3% level for $p_{\mathrm{T}} \lesssim 150\,\mathrm{GeV}$ by comparing the $1/m_t^2$

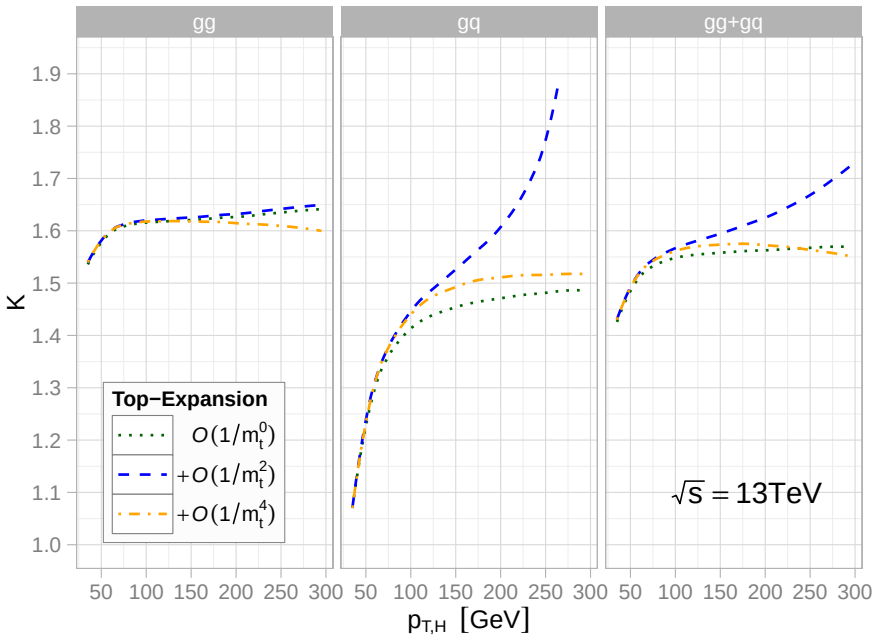

Figure 2.4: K-factor for the transverse momentum distribution of the Higgs, split by partonic initial-state channels gg, gq and in the sum, with exact m_t dependence and truncations of the asymptotic expansion at order $1/m_t^k$, $k \in \{0,2,4\}$. As in ref. [115, fig. 15], see also ref. [115, fig. 10].

and $1/m_t^0$ curves at 150 GeV.[1] Beyond $p_T \gtrsim m_t$, the curves clearly diverge, as already expected from naive estimates of the expansion range validity, and we cannot give quantitative or even qualitative estimates.

Note that there is a small region $p_T \lesssim 120\,\text{GeV}$ for which the expansion converges well. In principle, this allows us to predict the exact mass effects, and not just set an upper error bound. We consider this region too small for further consideration, since it would just give negligible sub-percent additions to the HTL. In section 4.4 we will again consider a p_T distribution, but instead of the Higgs, of the hardest jet. It will turn out that the $1/m_t^2$ and $1/m_t^4$ curves match very well, and allow us to predict mass effect additions of a few percent.

We close this section of LO considerations and previous results for Higgs dif-

1 For p_T integrated quantities, for example for the rapidity distribution, estimates of similar error size hold, see ref. [43].

ferential quantities. In the next chapter the setup/program for our extended study is summarized, stating the ingredients and methods to obtain the results. In chapter 4 we present our results of top-mass effects in the NNLO jet-veto, jet-inclusive cross sections and hardest jet differential distributions. The chapter starts with a list of all input parameters and notations. Finally, in chapter 5 we summarize.

3

CALCULATION AND SETUP

Our setup consists, firstly, of a program for H + jet production through gluon fusion at NLO QCD in an asymptotic expansion in $1/m_t^2$. It is based on our program already used in ref. [43] but with added $1/m_t^4$ terms and the anti-k_T jet-algorithm[1] [403]. Secondly, by combining it with `ggh@nnlo`[2] [303, 357, 365], which can calculate the NNLO total inclusive cross section in an $1/m_t^2$ expansion, we are able to compute the NNLO jet-vetoed (or 0-jet) cross section by subtraction:

$$\sigma_{\text{veto}}^{\text{NNLO}} \equiv \sigma_{0\text{-jet}}^{\text{NNLO}} = \sigma_{\text{tot}}^{\text{NNLO}} - \sigma_{\geq 1\text{jet}}^{\text{NLO'}}, \tag{3.1}$$

where the prime mark on the NLO jet cross section $\sigma_{\geq 1\text{jet}}^{\text{NLO'}}$ denotes a calculation with NNLO PDFs, just as for the total inclusive NNLO cross section $\sigma_{\text{tot}}^{\text{NNLO}}$. To compute the NLO jet-veto with exact top-mass dependence, we used `SusHi` [404] for the NLO total inclusive cross section.

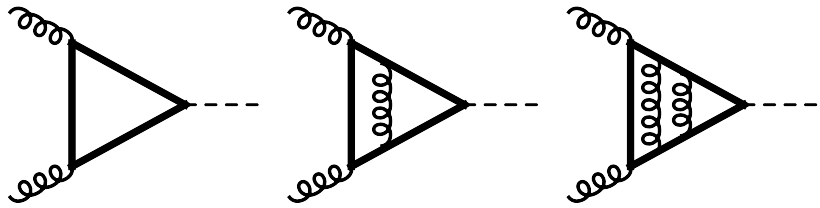

(a) Gluon fusion at leading order.

(b) An NLO virtual correction.

(c) An NNLO virtual correction.

Figure 3.1: Sample Feynman diagrams of virtual corrections for gluon fusion.

1 Since at most two jets can occur in our calculation, the anti-k_T algorithm leads to the same results as the k_T and the Cambridge-Aachen algorithm.

2 `http://particle.uni-wuppertal.de/harlander/software/ggh@nnlo/`

PARTONIC CONTRIBUTIONS. At leading order, the jet-vetoed cross section is identical to the total cross section, where only the partonic process $gg \to H$ with no final state partons contributes, as depicted in fig. 3.1a. At next-to-leading order, virtual corrections as in fig. 3.1b, as well as real emissions as in figs. 3.2a to 3.2c contribute. Additionally, for the NNLO cross section, two-loop real emission diagrams like in figs. 3.2d and 3.2e, and one-loop double emission diagrams as in fig. 3.3 are necessary. A list of all partonic subprocesses required at various loop orders for the total NNLO cross section is given below. Remember that already the LO process is loop-induced. q denotes a quark, $\bar{q}$ the same flavor anti-quark, and q' a quark with a different flavor from q. The inclusion of the charge conjugated processes goes without saying:

- $gg \to H$ to three loops (purely virtual), see fig. 3.1c,
- $gg \to gH$, $gq \to qH$, $q\bar{q} \to gH$ to two loops (real-virtual), see fig. 3.2,
- $gg \to ggH$, $gg \to q\bar{q}H$, $gq \to gqH$, $q\bar{q} \to q\bar{q}H$, as well as $q\bar{q} \to ggH$, $qq \to qqH$, $qq' \to qq'H$, $\bar{q}q' \to \bar{q}q'H$ to one loop (double real), see fig. 3.3 .

The $1/m_t$ expansion does not provide a convergent series for the purely quark induced channels [43, 365, 402], particularly when no matching to the exact result in the high-energy limit is applied. Since additionally their contribution is numerically negligible for our observables considered, we disregard them from our calculation and further considerations.

Integrals stemming from two-loop box-type diagrams, see fig. 3.2d, and three-loop triangle type, see fig. 3.1c, with massless and massive (mass m_t) internal and one massive external line (mass m_H) currently cannot be calculated with enough numerical efficiency to be combined in a complete NNLO calculation. Instead, the HTL is commonly used to reduce the loop order for all contributions by one. For a complete NLO calculation of Higgs+jet production, the purely virtual contributions to three loops are not required.

To estimate the effects of a finite top-quark mass, we use the amplitudes calculated in refs. [357, 365]. They were obtained from the full NNLO amplitudes by automatic asymptotic expansions [361, 362, 405–407], assuming that m_t is larger than all other scales in the process. This reduces occurring integrals to convolutions of simpler integrals of fewer scales and/or lower number of loops; see ref. [365, fig. 1] for an actual diagrammatic example. We combined these contributions to a numerical program for fully differential NLO H+jet cross

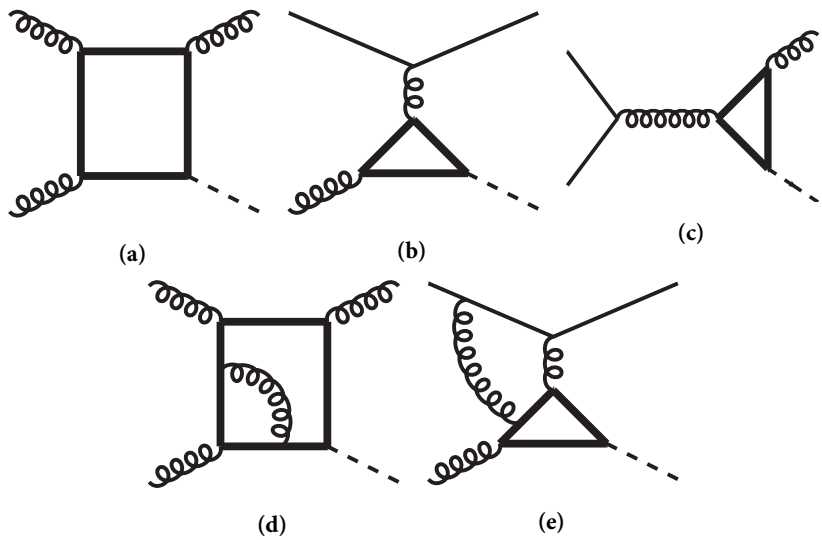

Figure 3.2: Sample real emission diagrams (a,b,c) and real-virtual corrections (d,e) for gluon fusion.

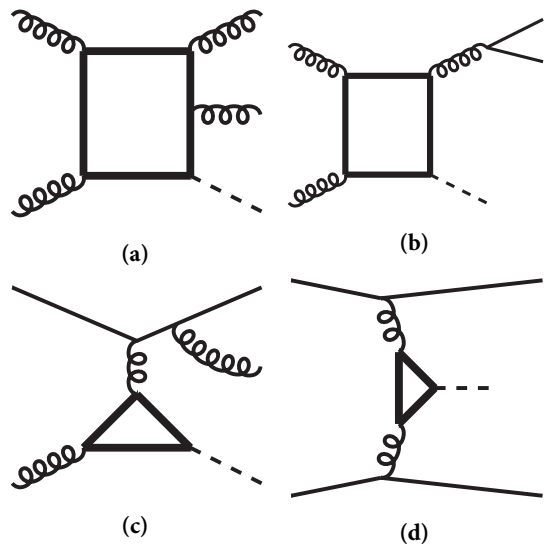

Figure 3.3: Sample double real emission diagrams for gluon fusion.

sections using Catani-Seymour dipole subtraction terms [180]. It includes the subleading terms $1/m_t^2$ and $1/m_t^4$ to the leading HTL terms. Renormalization has been performed in the $\overline{\text{MS}}$ scheme for α_s, and in the on-shell scheme for the top-quark mass and the gluon field.

To validate the correctness of our setup and results, we have performed a number of checks:

- The amplitudes for the $1/m_t^n$ terms have been checked previously by the agreement of the inclusive cross section between ref. [357] and ref. [358].
- The Higgs p_{T} distribution in the HTL agrees [43] with the non-resummed part of the program `HqT` [342, 343, 346].
- We found agreement at the sub-percent level for the NNLO HTL jet-vetoed cross section by comparing with the program `HNNLO` [116, 197, 408].
- We verified the independence of our cross sections on the α-parameter [409, 410], which restricts the phase space of the Catani-Seymour dipoles.

4

RESULTS AND DISCUSSION

4.1 INPUT PARAMETERS AND NOTATION

We study finite top-mass effects on Higgs+jet and jet-vetoed cross sections in gluon fusion at the LHC with a center of mass energy of 13 TeV. The renormalization scale μ_R and factorization scale μ_F are set to $m_H = 125.6\,\text{GeV}$, unless indicated otherwise. The convolution of the partonic parts with PDFs is performed with the set MSTW2008 68%CL at required orders [411]. It implies values for the strong coupling of $\alpha_s(m_Z) = 0.139$ at LO, $\alpha_s(m_Z) = 0.120$ at NLO and $\alpha_s(m_Z) = 0.117$ at NNLO. The top-quark mass is set to its on-shell value of 173.5 GeV [130].

Jets are defined using the anti-k_T algorithm [403] with jet radius $R = 0.5$. Our default choice of the minimum jet transverse momentum $p_{T,\text{min}}^{\text{jet}}$ is 30 GeV, unless stated otherwise. We checked that with these choices our results generalize to experimentally applied jet definitions, which usually imply $p_{T,\text{min}}^{\text{jet}} \gtrsim 25$–$30$ GeV and a rapidity cut [233, 412].

NOTATION The cross sections at $\{\text{LO,NLO,NNLO}\} \ni X$ perturbative accuracy in the asymptotic expansion, truncated at $1/m_t^k$, are denoted as

$$\left[\sigma^X\right]_{1/m_t^k}, \quad k \in \{0,2,4,\ldots\},$$

where $k = 0$ equals the HTL. If the square brackets are absent, the cross section is not truncated in the $1/m_t^2$-expansion, but is exact in the top-mass dependence.

All our results are reweighted by the exact top-mass dependence at LO, unless stated otherwise:

$$\left[\sigma^X\right]_{1/m_t^k} \equiv \left[\tilde{\sigma}^X\right]_{1/m_t^k} \cdot \frac{\sigma^{\text{LO}}}{\left[\tilde{\sigma}^{\text{LO}}\right]_{1/m_t^k}}, \tag{4.1}$$

where $\bar{\sigma}$ refers to the unweighted cross section.

The K-factor is defined by

$$K_k^X(b) = \frac{[\sigma^X(b)]_{1/m_t^k}}{[\sigma^{\mathrm{LO}}(b)]_{1/m_t^k}}, \tag{4.2}$$

where the argument b is introduced to denote the kinematic variable over which no integration is performed in distributions. We consider $b = p_{\mathrm{T},1}^{\mathrm{jet}}$ for the hardest jet transverse momentum, and $b = y_1^{\mathrm{jet}}$ for the hardest jet rapidity here. For example, $K_0^{\mathrm{NLO}}(p_{\mathrm{T},1}^{\mathrm{jet}})$ is the NLO K-factor in the HTL of the transverse momentum distribution of the hardest jet.

4.2 JET-VETO AT NNLO

We first consider the NLO jet-veto, where the exact top-mass dependence is available and can be compared to the asymptotic expansion. Despite having found the Higgs boson with a mass of $\simeq 125\,\mathrm{GeV}$, it can be instructive to look at the veto in dependence of the Higgs mass: Firstly, it introduces another scale that can be large with respect to the top-mass. Thus, we can see if and in how far this degrades the asymptotic expansion. Secondly, BSM theories usually require additional heavier Higgs particles, extending our results to heavy BSM Higgs-like scalars.

A main goal of our study for the different jet quantities is to justify the use of the HTL in calculations of similar or higher order, and give reliable error estimates of the mass effects in the HTL. The normalization of results to the HTL then allows us to perform these estimations if the asymptotic expansion behaves convergently and does not deviate much from the HTL result. The HTL error can then be estimated, by looking at the spread between the curves of the expansion, or predicted for a well-convergent series.

Since we do not expect the asymptotic expansion to converge beyond scales $\gg m_t$, we can, indeed, usually only assess validity of the HTL for the low and intermediate range of scales, comparable in size to m_t.

In fig. 4.1 we show the NLO jet-veto in dependence of the Higgs mass without normalization (fig. 4.1a) and with normalization to the HTL (fig. 4.1b). For small

values of m_H, the mass effects are at the percent level. While the $1/m_t^2$ curve remains close to the full result over the whole mass range, the $1/m_t^4$ corrections reduce the cross section significantly toward larger m_H. Assuming that the full result was unknown, as in the forthcoming NNLO results, we could give a reasonable estimate of mass effects at most up to $m_H \simeq 200\,\text{GeV}$, where the expansion clearly starts to diverge. The mass effects would then be conservatively estimated by the spread between the curves to $\simeq 5\%$. Fortunately, all orders of the $1/m_t$ expansion agree very well at $m_H \simeq 125\,\text{GeV}$.

We now have a closer look at the jet-veto for a Higgs boson mass of $m_H = 125.6\,\text{GeV}$ in fig. 4.2, in dependence of the jet-veto cut $p_{\text{T,veto}}^{\text{jet}}$. Again the absolute results, see fig. 4.2a, and the normalization to the HTL, see fig. 4.2b, are shown. The horizontal lines denote the total cross sections in the asymptotic expansion, corresponding to $p_{\text{T,veto}}^{\text{jet}} \to \infty$. For cuts of order 30 GeV we would estimate mass effects to at most half a percent. For large cuts of up to 600 GeV, the worst case estimate of top-mass effects from the asymptotic expansion is still just $\simeq 2.5\%$.

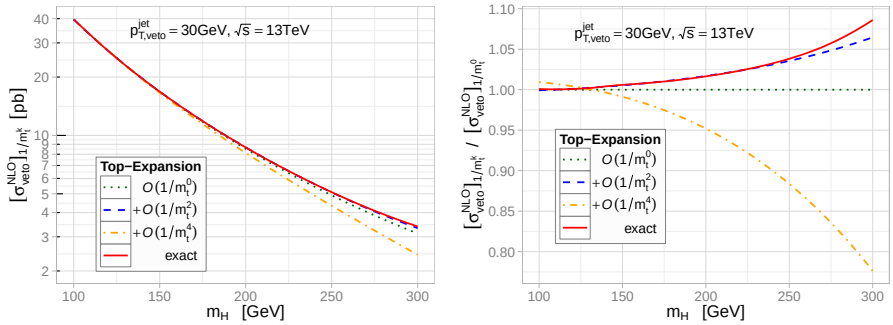

(a) No normalization **(b)** Normalized to $k = 0$

Figure 4.1: Higgs+0-jet cross section at NLO including terms up to $1/m_t^4$ as a function of m_H for $p_{\text{T,veto}}^{\text{jet}} = 30\,\text{GeV}$. As in ref. [115, fig. 4].

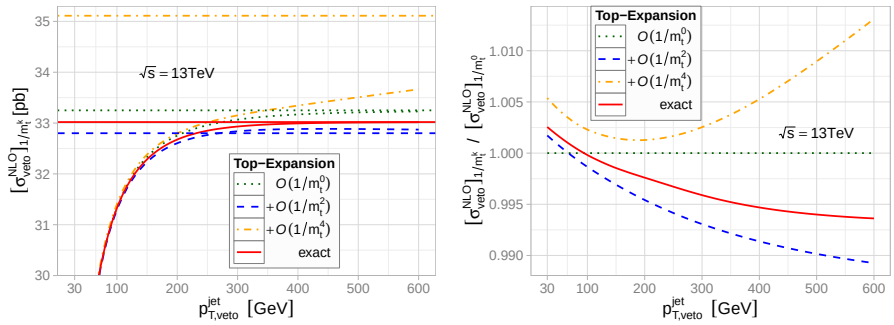

(a) No normalization. **(b)** Normalized to $k = 0$.

Figure 4.2: Higgs+0-jet cross section at NLO including terms up to $1/m_t^4$ as a function of $p_{\mathrm{T,veto}}^{\mathrm{jet}}$. As in ref. [115, fig. 5].

The success of the HTL for the jet-vetoed cross section is, firstly, set by the fact that only low energy contributions remain, analogously as for the NNLO case in eq. (3.1):

$$\sigma_{\mathrm{veto}}^{\mathrm{NLO}} \equiv \sigma_{\text{0-jet}}^{\mathrm{NLO}} = \sigma_{\mathrm{tot}}^{\mathrm{NLO}} - \sigma_{\geq 1\,\mathrm{jet}}^{\mathrm{LO'}} ,$$

where LO' denotes the convolution with NLO PDFs. The high p_{T}/energy tail included in the total inclusive cross section is subtracted accurately. Secondly, for larger veto scales, the high p_{T} jets are suppressed by the PDFs. However, the latter PDF suppression cannot fix the breakdown of the asymptotic expansion for higher orders and large scales: the expansion up to $1/m_t^4$ is not a good description of the full result at large $p_{\mathrm{T,veto}}^{\mathrm{jet}}$. Note that the total inclusive cross section in the expansion up to $1/m_t^4$ also differs a lot from the lower order terms (horizontal lines in fig. 4.2a) due to just this breakdown.

For the NNLO jet-vetoed cross section we can apply the same reasoning to estimate mass effects. Consider fig. 4.3, where the vetoed cross section is displayed in dependence of $p_{\mathrm{T,veto}}^{\mathrm{jet}}$, absolutely (fig. 4.3a) and normalized to the HTL (fig. 4.3b). At first sight, these plot looks remarkably similar to the NLO ones in fig. 4.2, just without the full result curve. One could be tempted to draw the red full result line similarly in this plot. For small values of $p_{\mathrm{T,veto}}^{\mathrm{jet}} \lesssim 200\,\mathrm{GeV}$ the spread between the curves is at most 0.5%. For $p_{\mathrm{T,veto}}^{\mathrm{jet}} \lesssim 600\,\mathrm{GeV}$ the deviation between the curves stays below 2%.

The mass dependence for the jet-vetoed cross section at NNLO is displayed in fig. 4.4. The asymptotic expansion shows nearly identical behavior as at NLO,

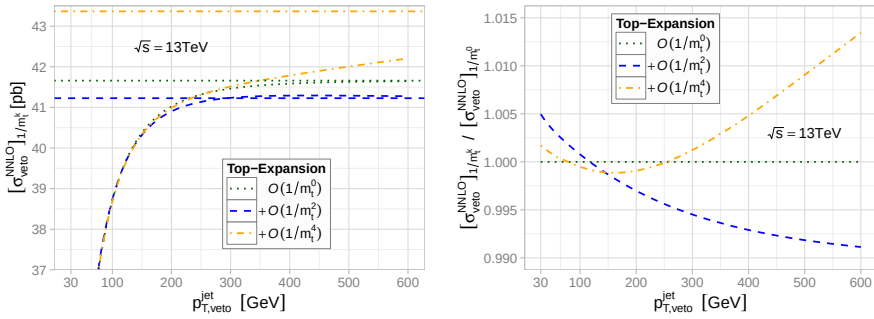

(a) No normalization. **(b)** Normalized to $k = 0$.

Figure 4.3: Higgs+0-jet cross section at NNLO including terms up to $1/m_t^4$ as a function of $p_{\mathrm{T,veto}}^{\mathrm{jet}}$. For reference, the horizontal lines indisplay the corresponding total cross sections in the asymptotic expansion. As in ref. [115, fig. 8].

and one could be tempted to claim that the $1/m_t^2$ result matches the full result up to $m_H \simeq 250\,\mathrm{GeV}$, see fig. 4.1b. Overcoming this temptation, we can only give conservative estimates of $\simeq 6$–$20\,\%$ top-mass effects for $m_H = 200$–$300\,\mathrm{GeV}$.

In summary, for the SM Higgs boson with a mass of $\simeq 125\,\mathrm{GeV}$, it is fully justified to trust the effective field theory approach to determine radiative corrections to the jet-vetoed cross section at NNLO. Remember that in all cases our cross sections were obtained by reweighting with the full LO result. Higher order perturbative corrections to the full LO result are taken into account as a K-factor,

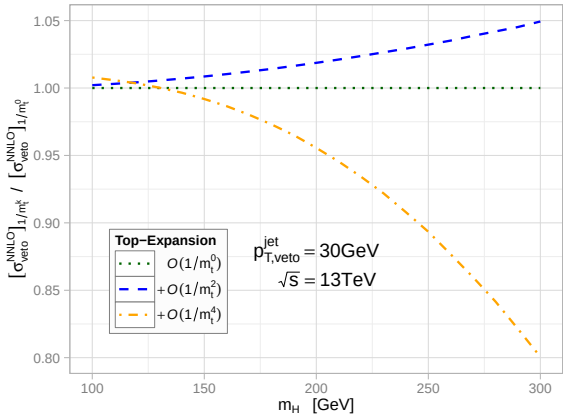

Figure 4.4: Higgs+0-jet cross section at NNLO including terms up to $1/m_t^4$ as a function of m_H normalized to heavy-top limit ($k = 0$) for $p_{\mathrm{T,veto}}^{\mathrm{jet}} = 30\,\mathrm{GeV}$. As in ref. [115, fig. 9].

which is either determined in the HTL or in higher orders of the asymptotic expansion, see eq. (4.1).

We expect our results to directly generalize to resummed jet-vetoed cross sections evaluated in the HTL, since the resummation of logarithms from soft-gluon emission is predominantly described by process independent QCD effects.[1]

4.2.1 *Other approximations*

Reweighting the results obtained in the asymptotic expansion by the full LO one, as in eq. (4.1), is not a unique approximation of the full result at NLO or NNLO. Since we know the full top-mass dependence even at NLO, we can, for example, reweight by using the full NLO result.[2]

For this, we consider the following approximations of the jet-vetoed cross section at NNLO:

$$\sigma^{\text{NNLO}}_{\text{veto},k}(\kappa_i) \equiv \sigma^{\text{NLO'}}_{\text{veto}} + \kappa_i \left(\left[\sigma^{\text{NNLO}}_{\text{veto},k}\right]_{1/m_t^k} - \left[\sigma^{\text{NLO'}}_{\text{veto}}\right]_{1/m_t^k} \right) , \tag{4.3}$$

where

$$\kappa_0 = 1\,, \quad \kappa_1 = \sigma^{\text{LO}}_{\text{veto}} / \left[\sigma^{\text{LO}}_{\text{veto}}\right]_{1/m_t^k} = \sigma^{\text{LO}} / \left[\sigma^{\text{LO}}\right]_{1/m_t^k}\,,$$
$$\kappa_2 = \sigma^{\text{NLO'}}_{\text{veto}} / \left[\sigma^{\text{NLO}'}_{\text{veto}}\right]_{1/m_t^k}\,,$$

and the primed quantities are calculated with NNLO PDFs. With this scheme we always take into account the full NLO result and add the NNLO perturbative corrections from the asymptotic expansion, reweighted by κ_0,κ_1 or κ_2. Using κ_2 corresponds to calculating the K-factor from NLO to NNLO in the asymptotic expansion and multiplying it with the NLO cross section in the full theory.

In fig. 4.5 we use these approximations to study the mass effects on the jet-vetoed cross section. For each approximation we normalize to the respective HTL result $k = 0$. Compare this to fig. 4.3b, where the result was obtained by reweighting the full LO result. For the approximations κ_1 and κ_2 the mass effects are even smaller, at a few per mill level for the whole range up to cuts of 600 GeV. This,

1 See chapter 2 for references to such resummation studies, for example ref. [350].
2 We thank the referee of ref. [115] for this suggestion.

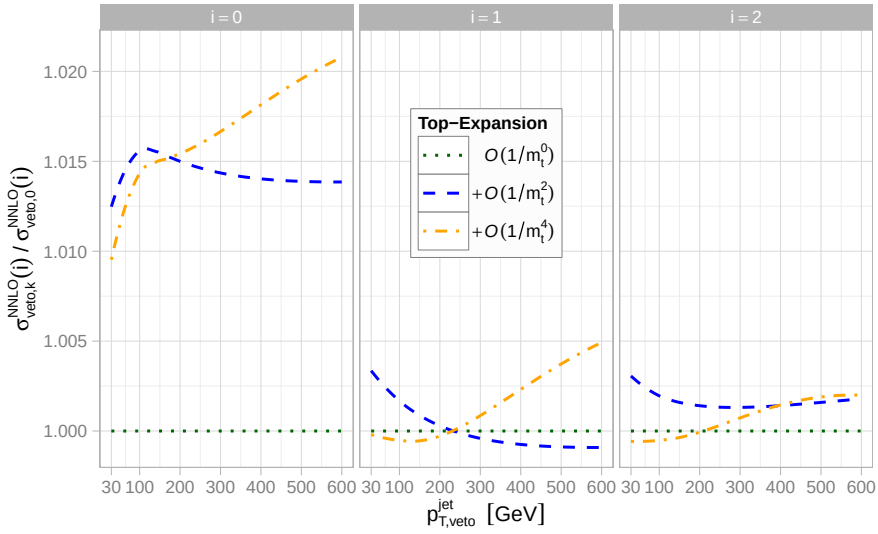

Figure 4.5: Same as fig. 4.3b, but for the approximations defined in eq. (4.3). Left/center/right plot show the approximations for κ_0,κ_1,κ_2, defined in eq. (4.3). As in ref. [115, fig. 14].

and the observation that the mass effects for $\kappa_0 = 1$ are larger, about 1.5–2 %, confirm that the HTL works well to describe perturbative *corrections* as in a K-factor, and not absolute cross sections.

4.3 INCLUSIVE HIGGS+JET AT NLO

The semi-inclusive Higgs+jet cross section is defined by the integral of $\mathrm{d}\sigma/\mathrm{d}p_{\mathrm{T}}^{\mathrm{jet}}$, where the integration is performed from a lower limit of $p_{\mathrm{T,min}}^{\mathrm{jet}}$ to the maximum kinematically possible value. Since in this case, compared to the jet-vetoed cross section, the full high p_{T} jet tail is explicitly included, we cannot expect the asymptotic expansion to reliably estimate mass effects beyond some $p_{\mathrm{T,min}}^{\mathrm{jet}}$ or for higher orders in the asymptotic expansion.

Figure 4.6a compares the $1/m_t^2$-expansion for the H+jet rate at LO to the exact result. If we were to estimate the mass effects by looking at the spread between the curves, including $1/m_t^4$, we would already be forced to give an upper limit on the mass effects of $\simeq 27\%$ for $p_{\mathrm{T,min}}^{\mathrm{jet}} = 30\,\mathrm{GeV}$.

The same problem of the quickly diverging asymptotic expansion exists for the total inclusive cross section (see horizontal lines in fig. 4.3a). In that case, a matching to the high energy limit of the full theory was performed to control the region $\sqrt{\hat{s}} \gtrsim 2m_t$ [357, 363–365]. This matching was performed by the construction of interpolation functions[1] between the full result in the high energy limit and the low energy result. The latter is given in the $1/m_t^2$-expansion and simultaneously in a soft expansion in $(1-x)$ to a high order, where $x = m_H^2/\hat{s}$. The interpolation functions are constructed to smoothly and correctly interpolate between the limits $x \to 0$ and $x \to 1$. Additionally, the expressions of the high energy limit work as a higher order term in the soft expansion. It has been shown that the error induced by the soft expansion and the interpolation procedure are small. Similarly, a matching to the high p_T limit would temper the power effects of $(p_\mathrm{T}^2/m_t^2)^k$, $k \in 0,2,4$ contributions that are not damped sufficiently by PDF suppression.

We will assume that the contribution of large $\hat{s}$ to the cross section corresponds also to large jet p_T. Then, a construction of a matched H+jet cross section is possible by subtracting the difference between the unmatched and the matched total inclusive cross section. More precisely, we remove the difference between the asymptotic expansion in each order and the matching to the full high energy limit beyond large $\sqrt{\hat{s}} \gtrsim 2m_t$.

As long as $p_{\mathrm{T,min}}^{\mathrm{jet}}$, the minimum jet transverse momentum, stays sufficiently below the region where the interpolated result begins to deviate from the non interpolated result in the asymptotic expansion, we expect that our procedure works. The high energy region gets 'fixed' as for the total inclusive cross section, and the result is largely independent of the interpolation specifics due to PDF suppression.

As a formula, this procedure is described at LO by

$$\begin{aligned}\left[\sigma^{\mathrm{LO}}_{\geq 1\text{-jet, matched}}\right]_{1/m_t^k} \equiv \left[\sigma^{\mathrm{LO}}_{\geq 1\text{-jet, unmatched}}\right]_{1/m_t^k} \\ - \left(\left[\sigma^{\mathrm{NLO}^*}_{\mathrm{tot, unmatched}}\right]_{1/m_t^k} - \left[\sigma^{\mathrm{NLO}^*}_{\mathrm{tot, matched}}\right]_{1/m_t^k}\right), \quad (4.4)\end{aligned}$$

where the starred cross sections are calculated with LO PDFs. The result is shown in fig. 4.6b. Up to $p_{\mathrm{T,min}}^{\mathrm{jet}} \simeq 150\,\mathrm{GeV}$ the asymptotic expansion is hardly

1 The NLO and NNLO coefficients in the perturbative expansion in α_s are each interpolated by a different function due to the different form of the high energy limits.

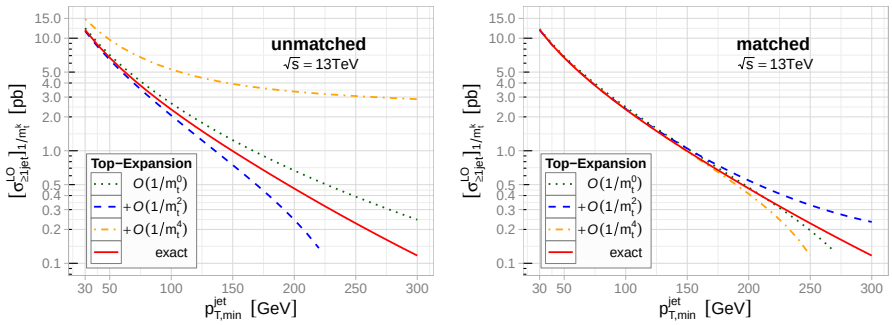

(a) unmatched **(b)** matched according to eq. (4.4)

Figure 4.6: Inclusive Higgs+jet cross section at LO including terms up to $1/m_t^k$ as a function of $p_{\mathrm{T,min}}^{\mathrm{jet}}$. As in ref. [115, fig. 6].

distinguishable from the full theory result. Beyond that, our assumptions seem to become invalid, and the expansion diverges. For a closer look, we modified fig. 4.6b by normalizing all curves to the HTL of the *unmatched* result. This is shown in fig. 4.7.

The overall agreement of the exact result with increasingly higher orders of the $1/m_t^2$-expansion is remarkable. For $p_{\mathrm{T,min}}^{\mathrm{jet}} \lesssim 150\,\mathrm{GeV}$ the spread between the matched curves is less than 5 %. An important observation has to be made with respect to the unmatched HTL result: The difference to the exact result varies between 3–10 % for $p_{\mathrm{T,veto}}^{\mathrm{jet}}$ between 30–100 GeV and can be read off as the exact

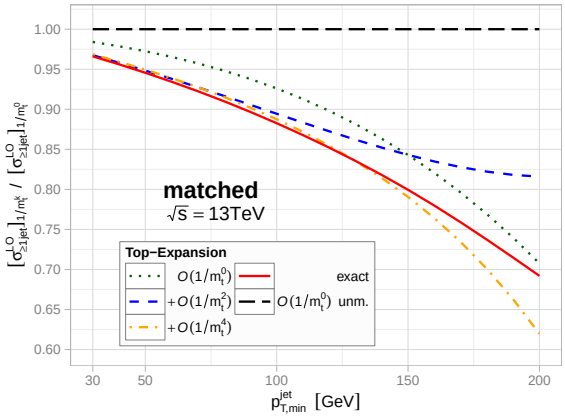

Figure 4.7: Same as fig. 4.6b, but normalized to the unmatched $1/m_t^0$ cross section (dotted curve of fig. 4.6a). As in ref. [115, fig. 7].

error that will be made by using the HTL. Using the matched HTL result, already improves the error to 2–3 % in that range. But, since the asymptotic expansion converges so well in that region, we can use the $1/m_t^2$ or $1/m_t^4$ matched result to predict the exact result with negligible uncertainty.

If the asymptotic expansion shows the same convergence behavior at NLO, the same reasoning can be applied. For values of $p_{\mathrm{T,min}}^{\mathrm{jet}} \simeq 30\,\mathrm{GeV}$, as used in analyses, one can then avoid the error due to an infinite top-mass by using this matching procedure and taking into account the subleading $1/m_t^2$ and $1/m_t^4$ terms.

At NLO the matching is described as

$$\left[\sigma^{\mathrm{NLO}}_{\geq 1\text{-jet, matched}}\right]_{1/m_t^k} \equiv \left[\sigma^{\mathrm{NLO}}_{\geq 1\text{-jet, unmatched}}\right]_{1/m_t^k} - \left(\left[\sigma^{\mathrm{NNLO}^*}_{\mathrm{tot, unmatched}}\right]_{1/m_t^k} - \left[\sigma^{\mathrm{NNLO}^*}_{\mathrm{tot, matched}}\right]_{1/m_t^k}\right), \quad (4.5)$$

where the starred cross sections are calculated with NLO PDFs. The result is displayed in fig. 4.8a. For comparison, the unmatched result is shown in fig. 4.8b. The matching allows us, again, to make quantitative estimates, and not just give qualitative upper limits from the spread of the quickly diverging asymptotic expansion. Normalization of the matched result to the unmatched HTL results are shown in fig. 4.9. Since the asymptotic expansion works so well for jets with $p_{\mathrm{T,min}}^{\mathrm{jet}} \lesssim 100\,\mathrm{GeV}$, we predict the exact result to be the $1/m_t^2$ or $1/m_t^4$ result with negligible error. It is interesting to note that the unmatched HTL is closer to our predicted exact result than to the matched HTL.

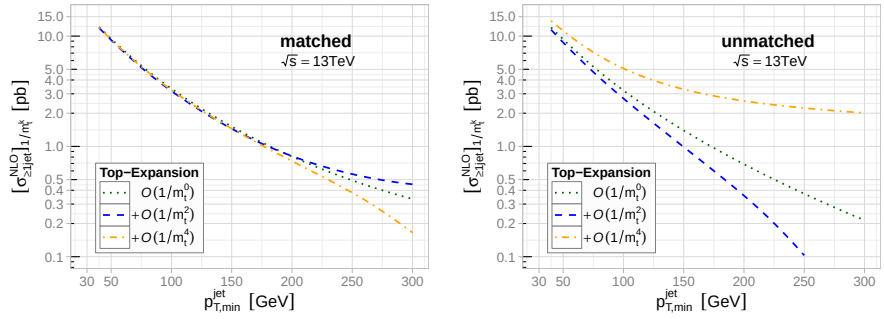

(a) matched according to eq. (4.5) **(b)** unmatched

Figure 4.8: Inclusive Higgs+jet cross section at NLO including terms up to $1/m_t^k$ as a function of $p_{\mathrm{T,min}}^{\mathrm{jet}}$. As in ref. [115, fig. 10].

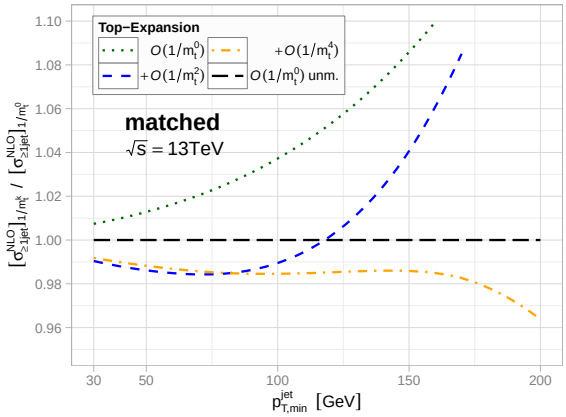

Figure 4.9: Same as fig. 4.8a, but normalized to the unmatched $1/m_t^0$ cross section (dotted curve of fig. 4.8b). As in ref. [115, fig. 11].

Conclusively, we can justify the commonly used unmatched NLO HTL H+jet cross sections at the level of 1–2 % for $p_{\mathrm{T,min}}^{\mathrm{jet}} \lesssim 100\,\mathrm{GeV}$.

4.4 Distributions of the hardest jet at NLO

Lastly, we consider kinematical distributions of the hardest jet, namely the transverse momentum and the rapidity spectra.[1]

Figure 4.10 shows the p_{T}-dependent K-factors $K_k^{\mathrm{NLO}}(p_{\mathrm{T,1}}^{\mathrm{jet}})$ of the cross sections up to $1/m_t^{k=4}$, as defined in eq. (4.2), with variable scales

$$\mu_R = \mu_F = \sqrt{m_H^2 + (p_{\mathrm{T,1}}^{\mathrm{jet}})^2}\,.$$

In the gg-channel, the K-factors differ little in the asymptotic expansion. Thus, the QCD corrections are well described by the HTL. This is different for the quark-gluon channel: The QCD corrections are sensitive to the resolved Higgs-gluon coupling once $p_{\mathrm{T,1}}^{\mathrm{jet}} \gtrsim 100\,\mathrm{GeV}$. The expansion for this channel begins to diverge at $p_{\mathrm{T,1}}^{\mathrm{jet}} \simeq 225\,\mathrm{GeV}$. Since the qg channel is only subleading with respect to gg, we can estimate the mass effects to remain below 1.5 % for $p_{\mathrm{T,1}}^{\mathrm{jet}} \lesssim 150\,\mathrm{GeV}$. They

1 Distributions of the Higgs were considered in ref. [43].

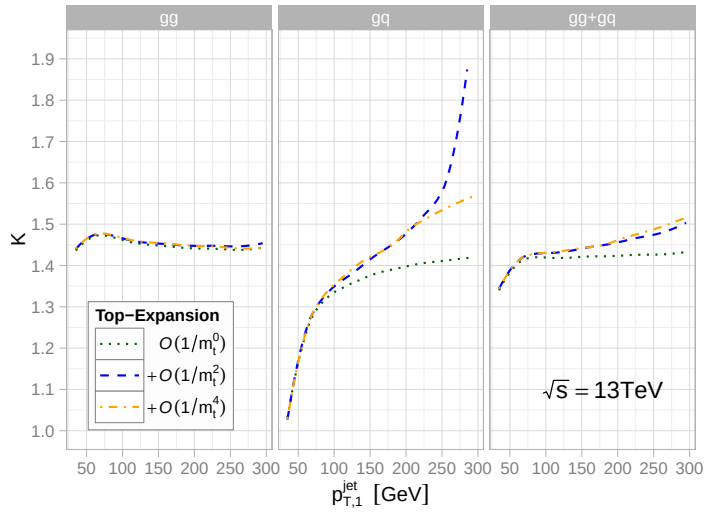

Figure 4.10: K-factors as defined in eq. (4.2), for the transverse momentum distribution of the hardest jet, i. e. $K_k^{\mathrm{NLO}}(p_{\mathrm{T},1}^{\mathrm{jet}})$. As in ref. [115, fig. 12].

reach 6 % at $p_{\mathrm{T},1}^{\mathrm{jet}} = 300\,\mathrm{GeV}$.

Comparing this result to the Higgs p_{T} distribution in fig. 2.4, we notice that the effects are of similar size, yet the asymptotic expansion works much better here. It allows us to predict the mass effects, as shown in fig. 4.10, with sub-percent error for $p_{\mathrm{T},1}^{\mathrm{jet}}$ by using the higher order $1/m_t$ terms.

For the K-factor $K_k^{\mathrm{NLO}}(y_1^{\mathrm{jet}})$ of the rapidity distribution of the hardest jet, consider fig. 4.11. The bottom right plot shows how the asymptotic expansion evolves when no further cuts, except for the jet algorithm itself, are used. In the central region, the contributions of high energy jets spoil the convergence. Unfortunately, it is not possible to determine a matched cross section by means of a subtraction, similar as for the inclusive H+jet cross section in the previous section 4.3. Instead, we introduce a cut $p_{\mathrm{T}}^{\mathrm{jet}} < p_{\mathrm{T,max}}^{\mathrm{jet}}$ which removes the problematic high-p_{T} jets. This cut is arbitrary, but, of course, modifies the distribution. When this cut is large enough, it should not affect the result noticeably, because due to PDF/phase-space suppression, the main contribution comes from low p_{T} jets. Our reasoning is as follows: Since we know that the HTL is insensitive toward power terms $\sim (\hat{s}/m_t^2)^{k=0}$ that can spoil the asymptotic expansion ($k > 0$) at higher energies, we increase the $p_{\mathrm{T,max}}^{\mathrm{jet}}$ cut until the HTL result no longer changes visibly. Then we can estimate the finite top-mass effects by looking at the higher

order asymptotic expansion terms. For this purpose we choose three different values of $p_{\mathrm{T,max}}^{\mathrm{jet}}$: 200 GeV, 400 GeV and 600 GeV, as in the top-left, top-right and bottom-left plots in fig. 4.11. For $p_{\mathrm{T,max}}^{\mathrm{jet}} = 600\,\mathrm{GeV}$ we consider the cut large enough to be, firstly, representative for the uncut result, and, secondly, to give a reasonable estimate of top-mass effects. In the central region ($y_1^{\mathrm{jet}} < 2.5$) the effect is less than two percent, while in the forward region the effects are below one percent.

In conclusion, the behavior of K-factors of the hardest jet distributions suggest that QCD corrections can safely be calculated in the HTL. Finite top-mass effects stay below 1.5 % (6 %) for $p_{\mathrm{T,1}}^{\mathrm{jet}} \leq 150\,\mathrm{GeV}$ ($p_{\mathrm{T,1}}^{\mathrm{jet}} \leq 300\,\mathrm{GeV}$), and for the rapidity, as a representative p_{T} integrated quantity, at the percent level.

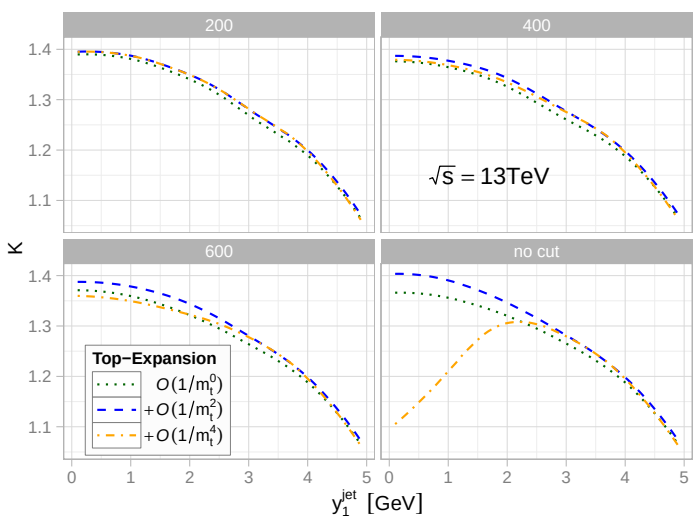

Figure 4.11: K-factors as defined in eq. (4.2), for the rapidity distribution of the hardest jet, i. e. $K_k^{\mathrm{NLO}} \equiv K_k^{\mathrm{NLO}}(y_1^{\mathrm{jet}})$. Left-top/right-top/left-bottom/right-bottom plot: $p_{\mathrm{T,max}}^{\mathrm{jet}} = 200\,\mathrm{GeV}$, 400 GeV and 600 GeV, and no cut. As in ref. [115, fig. 13].

5

SUMMARY

We extended our previous study of top-mass effects in differential Higgs production through gluon fusion [43, 185, 186] to the jet-vetoed cross section at NNLO, to inclusive jet production, and to kinematical distributions of the hardest jet. To determine these mass effects, we used the NLO H+jet matrix elements in a $1/m_t^2$ asymptotic expansion, and implemented them up to $1/m_t^4$ in a program, allowing the calculation of fully differential cross sections. By combination with the NNLO total inclusive cross section, also given in the $1/m_t^2$-expansion, the jet-vetoed rate was constructed. Our method to estimate mass effects was then to look how well the expansion converges, and examine the spread between different orders:

- For the NNLO jet-vetoed rate we found mass effects to be negligible. Even at large values of the jet-veto cut, the use of the HTL is fully justified.

- In case of the inclusive H+jet cross section, the high p_T region is pronounced, and the asymptotic expansion diverges quickly for higher orders. We introduced a matching procedure, utilizing the finite top-quark mass high energy limit of the total cross section, that allowed us to estimate and predict mass effects at the 1–2 % level for $p_{T,\text{min}}^{\text{jet}} < 100\,\text{GeV}$, relative to the unmatched HTL. Beyond 100 GeV, the $1/m_t^2$-expansion runs out of control and does not allow for a useful estimation.

- The p_T distribution of the hardest jet shows mass effects less than 1.5 % for $p_{T,1}^{\text{jet}} \lesssim 150\,\text{GeV}$ and less than 6 % for $p_{T,1}^{\text{jet}} \lesssim 600\,\text{GeV}$. The $1/m_t^2$-expansion converges well, such that mass effects are predicted with less than one percent error. For the rapidity distribution, effects of one to two percent are estimated.

We have checked that our results also hold for different center of mass energies at the LHC. By choosing a center of mass energy of 13 TeV, we considered what could be called the worst case. For smaller energies the HTL always works better, since, on the one hand, finite mass corrections to the HTL become only

significant at energies comparable to the top-quark mass, and, on the other hand, for the dominating gg channel, the bulk contribution comes from PDF enhanced low energies[1]. Still today, the accuracy of the HTL approach is better than the uncertainty on the cross section induced by PDFs. Just recently it became closer to missing higher order QCD corrections, due to the completion of the N^3LO Higgs inclusive and NNLO H+jet cross section calculations.

1 For a plot of partonic contributions to the total cross section, differentiated between gg, qg and $q\bar{q}$ channels, below and above the top-quark threshold $\sqrt{\hat{s}} = 2m_t$, see ref. [365, fig. 2].

Part III

PROBING THE HIGGS-GLUON COUPLING

This part is based on our publication 'Probing the nature of the Higgs-gluon coupling' [413]. We study one- and two-jet observables of dimension-7 Higgs-gluon coupling operators as a probe of possible deviations from the top-loop induced gluon-Higgs coupling. We focus on shape deviations in the Higgs p_T distribution, and show that some operators provide a much harder p_T spectrum than in the SM. This allows one to constrain corresponding Wilson coefficients, or give upper limits on the scale of new physics.

6

INTRODUCTION TO THE HIGGS-GLUON COUPLING

We started the last part with the observation that currently there is no reason, motivated by raw experimental results, to believe that the found Higgs-like particle is not the SM Higgs boson. Signal significances match the predicted SM values [59–62], even measured kinematical distributions match increasingly more the SM predictions [58].

Is it still possible that EWSB is not realized in the minimal form as in the SM? EWSB in the SM has the problem of naturalness. Only additional symmetries from extended models can, more or less elegantly, solve this problem. Simultaneously, these models often solve a number of other questions in particle physics, such as dark matter, gauge coupling unification, missing CP violation or cosmic inflation. Whatever the specific model is, it must have an effective description in terms of the SM fields, since we observe a SM-like Higgs boson.

For example, only with data from LHC Run II will we be able to begin the determination of the direct top-Yukawa coupling in $t\bar{t}$ associated H production [414–417]. Up to now, only indirect measurements (through gluon fusion) were done. Possibly, we fell for a SM Higgs imposter, so far? Is gluon fusion, constituting the largest H production cross section in the SM at the LHC, and mediated through a top-quark loop, possibly not at all induced by a top-quark loop? After all, the Higgs boson could have a reduced – or even vanishing – top-quark Yukawa coupling. Then, since current signals are already found to be SM-like, this would mean that BSM contributions must mimic the SM top-Yukawa coupling for the correct total gluon fusion cross section. It is, after the Higgs discovery, now one of the prior goals to determine the precise nature of the Higgs-gluon coupling.

In this work we consider an effective field theory consisting of Higgs-gluon coupling operators of dimension-5 and -7, and calculate kinematical distributions of Higgs+n-jet production, where n = 1,2. This allows us to quantify deviations from the SM Higgs-gluon coupling model-independently. Additionally, it allows constraining specific models and the mass scale of new physics.

To leading order, the effective field theory description of the Higgs-gluon coupling is given by the dimension 5 operator $HF^a_{\mu\nu}F^{\mu\nu,a}$. Put next to the SM, it is suppressed by a scale of new physics Λ. In general, operators of arbitrarily high dimension contribute, but they are increasingly more suppressed by Λ (see also section 1.2).

The operators of dimension-7 are suppressed by Λ^3, so in principle not relevant for the near future. Nevertheless, as mentioned, an 'imposter' Higgs could have a reduced top-quark Yukawa coupling, forcing these contributions to become relevant. Note that for the SM, when integrating out the top-quark, the Wilson coefficients are itself proportional to $\Lambda = m_t$ due to the top-Yukawa coupling. This leads to a reduced suppression, where, indeed, the operator of dimension 5 is not suppressed at all. Such a mechanism could make dimension 7 operators relevant for BSM physics.

In any case, we will show that the operators of dimension-7 lead to kinematical distributions with shapes well distinguished from the SM, allowing constraints on new physics. We consider the Higgs p_{T} distribution in one-jet production and $\Delta\Phi_{jj}$ and $\Delta\eta_{jj}$[1] jet distributions in two-jet production, all in LO QCD. Our analysis covers both scalar and pseudo-scalar Higgs bosons separately. Both will be denoted as H in what follows.

Since we assume that gluon fusion is the dominant Higgs production mechanism at the LHC, we do not need to take into account the full set of SM-EFT operators [83–85]. These other operators, constructed from electroweak fields, typically affect the branching ratios of the Higgs boson. A comprehensive list of references for studies in this direction can be found in refs. [81, 238].

In the following chapter we introduce the SM-EFT basis of dimension-5 and -7 operators to couple either a scalar or a pseudo-scalar particle to gluons. We describe the implementation of these operators for obtaining kinematical distributions in Higgs+n-jet production, where n = 1,2. In chapter 8 we present these distributions, normalized to compare their shapes, and discuss them. Additionally, we show distributions with SM top-quark induced Wilson coefficients. Finally, in chapter 9 we conclude.

1 $\Delta\Phi_{jj}$ is the modulus of the azimuthal angle difference between the two jets, and $\Delta\eta_{jj}$ the modulus of the rapidity difference between the two jets.

7

BASIS OF DIMENSION-7 OPERATORS AND THEIR IMPLEMENTATION

In this chapter we describe the operator basis used in our study, and its implementation for kinematical distributions in Higgs production with one and two jets.

The effective Lagrangian involving operators through mass dimension-7 that couple a scalar Higgs boson H to gluons can be written as [418, 419] (see also ref. [420])

$$\mathcal{L} = \frac{C_1}{\Lambda}\mathcal{O}_1 + \sum_{n=2}^{5}\frac{C_n}{\Lambda^3}\mathcal{O}_n\,, \tag{7.1}$$

$$\begin{aligned}\mathcal{O}_1 &= HF^a_{\mu\nu}F^{a\,\mu\nu}\,, \quad \mathcal{O}_2 = HD_\alpha F^a_{\mu\nu}D^\alpha F^{a\,\mu\nu}\,, \quad \mathcal{O}_3 = HF^{a\,\mu}_{\nu}F^{b\,\nu}_{\sigma}F^{c\,\sigma}_{\mu}f^{abc}\,,\\ \mathcal{O}_4 &= HD^\alpha F^a_{\alpha\nu}D_\beta F^{a\,\beta\nu}\,, \quad \mathcal{O}_5 = HF^a_{\alpha\nu}D^\nu D^\beta F^{a\,\alpha}_{\beta}\,,\end{aligned} \tag{7.2}$$

where

$$\begin{aligned}F^a_{\mu\nu} &= \partial_\mu A^a_\nu - \partial_\nu A^a_\mu - g f^{abc}A^b_\mu A^c_\nu\,,\\ D_\mu A^a_\nu &= \partial_\mu A^a_\nu - g f^{abc}A^b_\mu A^c_\nu\,,\end{aligned} \tag{7.3}$$

and A^a_μ is the gluon field. The strong coupling is denoted by g, and f^{abc} are the $\mathrm{SU}(3)$ structure constants. We remark that, for an on-shell Higgs boson, the operators in eq. (7.2) are not linearly independent. Instead, one finds $m_H^2\mathcal{O}_1 = 4\mathcal{O}_5 - 2\mathcal{O}_2 + 4g\mathcal{O}_3$. Thus, one of the operators $\mathcal{O}_1$,$\mathcal{O}_2$,$\mathcal{O}_3$ or $\mathcal{O}_5$ could be eliminated from our analysis. Nevertheless, we find the generating set in eq. (7.2) convenient and stick to this redundancy.

Nominally, contributions of $\mathcal{O}_1$ are suppressed by $1/\Lambda^2$ in physical quantities, and mixed terms of $\mathcal{O}_1$ with $\mathcal{O}_2$ to $\mathcal{O}_5$ are suppressed by $1/\Lambda^4$. As discussed in the introductory chapter 6, the suppression could be lifted when $C_i \propto \Lambda$, as in the SM (see following eq. (7.5)). Since we want to keep the discussion as general

as possible, we will mostly ignore the suppression of the higher dimensional operators by normalizing all distributions to their integrated total cross section. Only the shapes of the distributions, generated from the individual operators, are relevant for us.

Note that the operators $\mathcal{O}_4$ and $\mathcal{O}_5$ can be rewritten as operators containing two and one quark bilinears, respectively, through the QCD equations of motion [421–423]:

$$D^\mu F^a_{\mu\nu}(x) = g\bar{\Psi}(x)\gamma_\nu t^a \Psi(x)\,, \tag{7.4}$$

where $\Psi(x)$ are quark fields with the sum over all flavors implied, and t^a are $\mathrm{SU}(3)$ color matrices in the fundamental representation. They only contribute when their corresponding quark representation can occur in the Feynman diagrams for considered processes. In the case of gluodynamics these two operators then, of course, vanish [418].

STANDARD MODEL MATCHING. For the SM, when the top-quark is integrated out and a matching to the set of operators in eq. (7.2) is performed, the mass parameter Λ equals the top-quark mass m_t. Taking the operator $\mathcal{O}_1$ with Wilson coefficient C_1 corresponds to using the HTL, thus is well known in higher order perturbative Higgs calculations. C_1 has been obtained through $\mathcal{O}(\alpha_s^4)$ [253, 254]. The other Wilson coefficients of dimension-7 are known through $\mathcal{O}(\alpha_s^2)$ [419]. We will give the LO expressions, for an illustration of their size, as follows:

$$\begin{aligned}
C_1^{\mathrm{SM}} &= \frac{g^2\lambda_t}{48\pi^2} + \mathcal{O}(g^4) \simeq 2.2\cdot 10^{-3}\,,\\
C_2^{\mathrm{SM}} &= \frac{-7g^2\lambda_t}{2880\pi^2} + \mathcal{O}(g^4) \simeq -2.6\cdot 10^{-4}\,,\\
C_3^{\mathrm{SM}} &= -\frac{g^3\lambda_t}{240\pi^2} + \mathcal{O}(g^5) \simeq -5.3\cdot 10^{-4}\,,\\
C_4^{\mathrm{SM}} &= \frac{g^2\lambda_t}{1440\pi^2} + \mathcal{O}(g^4) \simeq 7.3\cdot 10^{-5}\,,\\
C_5^{\mathrm{SM}} &= \frac{g^2\lambda_t}{80\pi^2} + \mathcal{O}(g^4) \simeq 1.3\cdot 10^{-3}\,,
\end{aligned} \tag{7.5}$$

where $\lambda_t = m_t/v$ is the top-quark Yukawa coupling, and the values $m_t = 172\,\mathrm{GeV}$, $v = 246\,\mathrm{GeV}$ and $g^2 = 4\pi\alpha_s$ with $\alpha_s = 0.118$ have been inserted to obtain the numerical values.

PSEUDOSCALAR OPERATORS. We also consider the pseudoscalar analogue, where the operators are obtained from the previous scalar case by replacing one of the field strength tensors by its dual $\tilde{F}^a_{\mu\nu} = \frac{1}{2}\varepsilon_{\mu\nu\rho\sigma}F^{a,\rho\sigma}$, where $\varepsilon_{\mu\nu\rho\sigma}$ is the Levi-Civita symbol. Our generating system for dimension-5 and dimension-7 pseudoscalar Higgs-gluon coupling operators is then given by

$$\mathcal{L} = \frac{\tilde{C}_1}{\Lambda}\tilde{\mathcal{O}}_1 + \sum_{n=2}^{5}\frac{\tilde{C}_n}{\Lambda^3}\tilde{\mathcal{O}}_n\,, \tag{7.6}$$

where

$$\begin{aligned}&\tilde{\mathcal{O}}_1 = H\tilde{F}^a_{\mu\nu}F^{a\,\mu\nu}\,, \quad \tilde{\mathcal{O}}_2 = HD_\alpha\tilde{F}^a_{\mu\nu}D^\alpha F^{a\,\mu\nu}\,, \quad \tilde{\mathcal{O}}_3 = H\tilde{F}^{a\,\mu}_{\nu}F^{b\,\nu}_{\sigma}F^{c\,\sigma}_{\mu}f^{abc}\,,\\ &\tilde{\mathcal{O}}_4 = HD^\alpha\tilde{F}^a_{\alpha\nu}D_\beta F^{a\,\beta\nu}\,, \quad \tilde{\mathcal{O}}_5 = H\tilde{F}^a_{\alpha\nu}D^\nu D^\beta F^{a\,\alpha}_{\beta}\,.\end{aligned} \tag{7.7}$$

IMPLEMENTATION. We generated the Feynman rules for the operators $\mathcal{O}_n$ and $\tilde{\mathcal{O}}_n$, $n = 1,\ldots,5$, using `LanHEP` [424] and confirmed their validity with `FeynRules` [425]. A nonzero contribution of the operator $\tilde{\mathcal{O}}_4$ involves at least six gluons; therefore, it does not appear in our numerical analysis below. Similarly to the scalar case, the remaining operators are not linearly independent for an on-shell Higgs boson, but for convenience we will include all of them.

Using the obtained vertices, we generated the LO Feynman graphs for H + 1-jet and H + 2-jet amplitudes with `Diana` [426] and `qgraf` [427] as `FORM` [428] code. The matrix elements were calculated in Feynman gauge with Faddeev-Popov ghosts and in an axial gauge for cross-checking. Integration was performed with a standard VEGAS integrator [429–431].

8

KINEMATICAL DISTRIBUTIONS

We consider kinematical distributions for the Higgs transverse momentum p_{T} in Higgs+jet production, and two-jet distributions in their azimuthal angle difference $\Delta\Phi_{jj}$ and their rapidity difference $\Delta\eta_{jj}$. Latter observables are motivated by studies in gluon fusion and weak boson fusion with two jets [263, 264, 366], for example to examine the charge parity (CP) nature of the Higgs-gluon coupling [432–439]. The observables can also be used to distinguish between gluon fusion and weak boson fusion in H + 2-jet production [264]. By considering the higher dimensional operators, we see how their kinematics may affect the conclusions drawn from previous studies.

In the following sections 8.1 and 8.2, the leading and subleading terms in $1/\Lambda$ for the scalar operators in eq. (7.2) and pseudo-scalar operators in eq. (7.7) are taken into account. This means that cross sections will receive contributions with Wilson coefficients proportional to C_1^2, C_1C_2, . . ., up to C_1C_5. Thus, they are truncated at $1/\Lambda^4$. In the later section 8.3 we also consider terms suppressed by $1/\Lambda^6$ with Wilson coefficients C_jC_k, $j,k \in \{2,\ldots,5\}$. They are only relevant if the Higgs-gluon coupling is predominantly mediated by one of the dimension-7 operators, and we can then, additionally, neglect interference terms of $\mathcal{O}_1$ and dimension-9 operators.

We write the differential cross sections based on the Lagrangian of eq. (7.1) (eq. (7.6)) as

$$\mathrm{d}\sigma = \sum_{i,j=1}^{5} \mathrm{d}\sigma_{ij} \,, \tag{8.1}$$

where $\mathrm{d}\sigma_{ij}$ is due to terms of the form $\mathcal{O}_i\mathcal{O}_j^\dagger$ ($\tilde{\mathcal{O}}_i\tilde{\mathcal{O}}_j^\dagger$). As mentioned, to be independent of the actual size of the Wilson coefficients, we normalize the kinematical distributions to their respective contribution to the inclusive cross section σ_{ij}, i.e., we display $\mathrm{d}\sigma_{ij}/\sigma_{ij}$. Absolute effects on the distribution within a given model, that is for concrete values of the Wilson coefficients C_i and the mass scale Λ, can be derived by combining these normalized distributions with

their numerical values for the total cross sections σ_{ij} provided in appendix C.

The shown distributions are calculated for LHC proton-proton collisions, split into the partonic gluon-gluon (gg), gluon-quark (gq) and quark-quark (qq) initial states, where qq includes quark-antiquark as well as different-flavor initial states. Furthermore, we chose a Higgs mass of $m_H = 125\,\text{GeV}$ and a center of mass energy of $\sqrt{s} = 13\,\text{TeV}$. The renormalization and factorization scales are set to the common value of $\mu = \sqrt{m_H^2 + p_\text{T}^2}$, and in the case of the H + 2-jet cross sections to the jet-p_T geometric mean $\mu = \sqrt{p_{\text{T,j1}} p_{\text{T,j2}}}$. Because of our normalization, the results are largely independent by variations of m_H and $\sqrt{s}$.

Let us remark that for the H + 1-jet cross sections the operator $\mathcal{O}_4$ does not contribute, because it can be rewritten in terms of two quark bilinears according to the equation of motion in eq. (7.4). The operator $\mathcal{O}_5$ only contributes to the gq and qq channels, having a representation with one quark bilinear. Operator $\mathcal{O}_3$ only contributes to the gg channel, as it involves at least three gluons. For the H + 2-jet cross sections $\mathcal{O}_3$ does, for the same reason, not contribute in the qq channel and $\mathcal{O}_4$ contributes only in the qq channel. Similar observations hold for the distributions in the pseudoscalar case.

8.1 HIGGS+1-JET CROSS SECTIONS

We consider the normalized Higgs transverse momentum distributions in H + 1-jet production for scalar and pseudoscalar Higgs bosons in figs. 8.1 and 8.2, respectively. The panel named 'sum' shows the sum over the partonic channels for fixed i, j. In both cases, scalar and pseudoscalar, one observes large differences in the distribution shapes of the individual terms, pronounced toward higher p_T. The operator $\mathcal{O}_5$, which contributes at LO only in the gq and qq channels, also leads to a visible deviation at small transverse momenta.

For comparison, we show the result that corresponds to SM Higgs production through a top-loop, obtained from the program `SusHi` [404]. It is denoted as 'SM' for the scalar and 'top-loop' for the pseudoscalar case. Note that these distributions would receive an additional p_T dependence through its proportionality to $\alpha_s^2(\mu)$, with $\mu = \sqrt{m_H^2 + p_\text{T}^2}$; to properly compare them to the predictions from our effective theory, we have divided the SM and top-loop distributions by this factor.

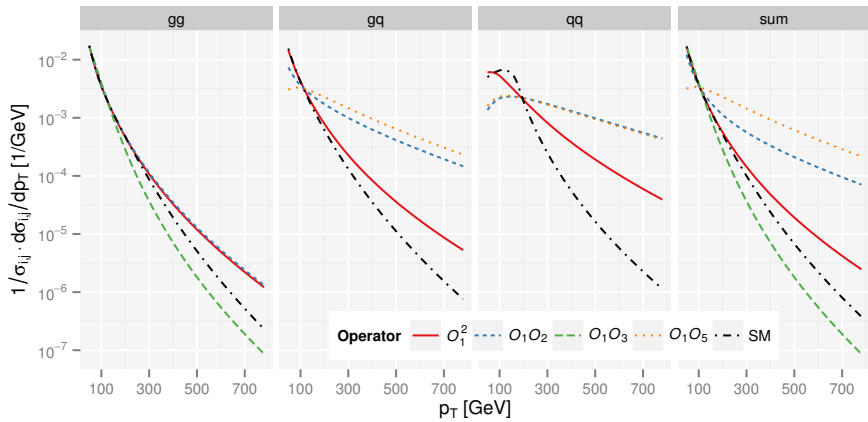

Figure 8.1: Normalized Higgs transverse momentum distribution for scalar coupling operators. The normalization factors σ_{ij} are given in table C.1.

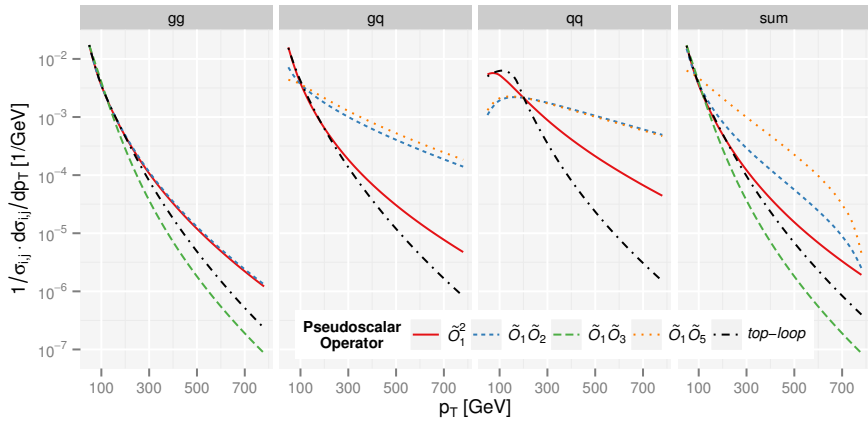

Figure 8.2: Normalized Higgs transverse momentum distributions for pseudoscalar coupling operators. Note that the gg channel is identical to the scalar case. σ_{ij} are given in table C.2.

For fig. 8.3 we performed the calculation of the distributions in fig. 8.1 with SM Wilson coefficients, given in eq. (7.5), where the top-quark has been integrated out. The expansion scale Λ is set to the top-quark mass m_t in this case. This reproduces the first two non-vanishing terms, that is, terms up to $1/m_t^2$, in the asymptotic $1/m_t^2$-expansion for the Higgs p_T distribution[1], and serves as an additional check.

Having the asymptotic expansion partitioned through the distinct operator contributions, we gain some deeper insight into the observations made earlier in part II and refs. [43, 115]: In case of the gg channel, which is the predominating and well-converging partonic channel in the asymptotic expansion, the interference terms of $\mathcal{O}_1$ with the higher order operators have a very similar shape as the leading $\mathcal{O}_1\mathcal{O}_1^\dagger$ contribution, which itself is much like the full SM shape. For the partonic subleading gq and qq channels the various contributions differ rather strongly among each other. The contribution $\mathcal{O}_1\mathcal{O}_5^\dagger$ in the gq channel is even negative, and, since its magnitude hardly decreases toward larger p_T, it drives this channel to negative values.

Higgs rapidity distributions do not show significant differences between the different operator contributions. We thus do not display them here.

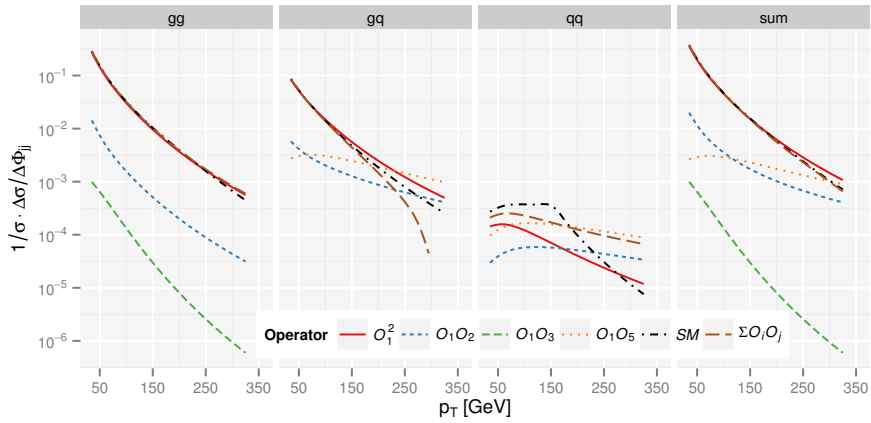

Figure 8.3: Higgs transverse momentum distributions with SM matching coefficients resulting in a total $1/m_t^2$ suppression with respect to C_1^2. Note that in the case of the gq and summed channel the cross term $\mathcal{O}_1\mathcal{O}_5$ has been multiplied with -1. For the qq channel the cross term $\mathcal{O}_1\mathcal{O}_2$ has been multiplied with -1.

1 See fig. 2.3 for the asymptotic expansion up to $1/m_t^6$.

8.2 HIGGS+2-JET CROSS SECTIONS

Rapidity separation $\Delta\eta_{jj}$ and azimuthal angle difference $\Delta\Phi_{jj}$ between two jets are well known observables in H + 2-jet production through gluon fusion and weak boson fusion. They can be used to distinguish these two production channels and peruse the Higgs CP nature; see the beginning of chapter 8.

In the following we will use 'inclusive' cuts for the $\Delta\eta_{jj}$ distribution:

$$p_{\mathrm{T,j}} > 20\,\mathrm{GeV}\,, \quad |\eta_j| < 5\,, \quad R_{jj} > 0.6\,, \tag{8.2}$$

where $R_{jj} = \sqrt{(\Delta\eta_{jj})^2 + (\Delta\Phi_{jj})^2}$, and additional 'WBF cuts'

$$\Delta\eta_{jj} = |\eta_{j1} - \eta_{j2}| > 4.2\,, \quad \eta_{j1}\cdot\eta_{j2} < 0\,, \quad m_{jj} > 600\,\mathrm{GeV} \tag{8.3}$$

for the $\Delta\Phi_{jj}$ distribution, where m_{jj} is the invariant mass of the two jets.

The $\Delta\Phi_{jj}$ distributions for scalar and pseudoscalar Higgs are shown in fig. 8.4 and fig. 8.5, respectively. The red curves, corresponding to the contributions from $\mathcal{O}_1\mathcal{O}_1^\dagger$ and $\tilde{\mathcal{O}}_1\tilde{\mathcal{O}}_1^\dagger$, respectively, reproduce the results of ref. [433], where the CP nature of the Higgs boson is studied in $\Delta\Phi_{jj}$ distributions. We calculated the distributions for a top-loop with VBFNLO [440–442] and found that they hardly differ from the results of $\mathcal{O}_1\mathcal{O}_1^\dagger$ and $\tilde{\mathcal{O}}_1\tilde{\mathcal{O}}_1^\dagger$, respectively. Therefore, we skip their inclusion in our figures.

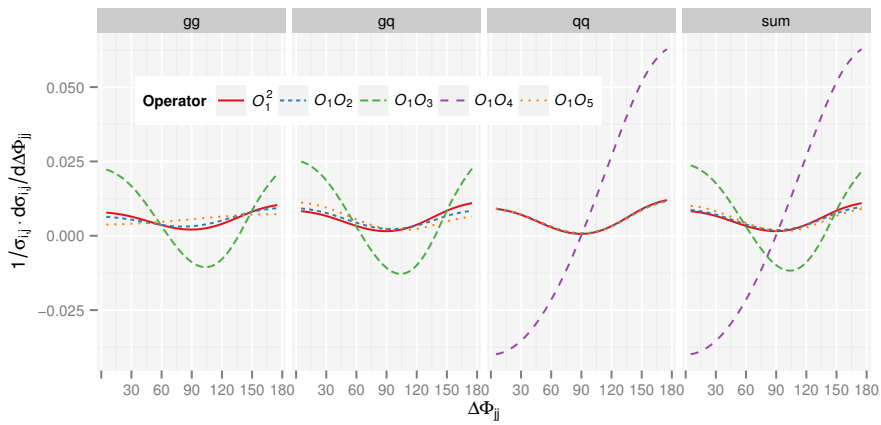

Figure 8.4: Normalized distributions for azimuthal angle difference of the two final state jets for scalar operators. σ_{ij} are given in table C.3.

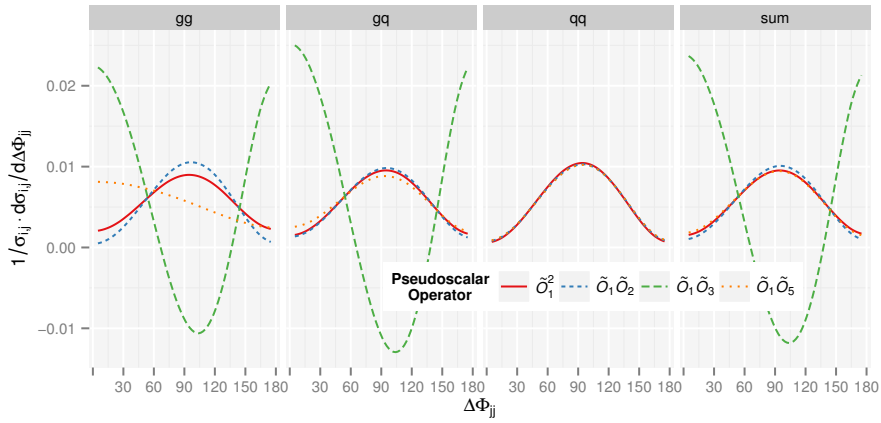

Figure 8.5: Normalized distributions for azimuthal angle difference of the two final state jets for pseudoscalar operators. σ_{ij} are given in table C.4.

The CP property of the Higgs boson can be distinguished by its $\Delta\Phi_{jj}$ distribution curvature, being either positive or negative. The distribution for the scalar Higgs exhibits a negative curvature, with maximums for planar events ($\Delta\Phi_{jj} \simeq 0°$ or $\Delta\Phi_{jj} \simeq 180°$). For the CP-odd coupling, planar events are suppressed, because, in that case, the occurring epsilon-tensor is contracted with (four) linearly dependent momentum vectors of the incoming and outgoing partons [433].

Only few operators differ from the leading (top-loop-like induced) behavior: The term generated by the operator $\mathcal{O}_3$ ($\tilde{\mathcal{O}}_3$) has a much stronger curvature than the other terms. In the scalar case the '4-quark-operator' $\mathcal{O}_4$ leads to a remarkable deviation from the other terms.

In figs. 8.6 and 8.7 we show the jet rapidity separation distributions for scalar and pseudoscalar operators, respectively. One can compare these with the SM case [264, fig. 8], in which $\Delta\eta_{jj}$ is used to distinguish H + 2-jet gluon fusion and weak boson fusion production modes. While gluon fusion exhibits a peak at small $\Delta\eta_{jj}$ due to the jet radius constraint $R_{jj} > 0.6$, for weak boson fusion the peak is at a rapidity separation $\Delta\eta_{jj} \simeq 5$ and considerably smaller. Again, we compared our results to the top-loop induced case with VBFNLO, and found that they are almost identical to the curves for $\mathcal{O}_1\mathcal{O}_1^\dagger$ and $\tilde{\mathcal{O}}_1\tilde{\mathcal{O}}_1^\dagger$, respectively. We thus refrain from including them in our plots.

While there are quantitative differences among the various contributions for

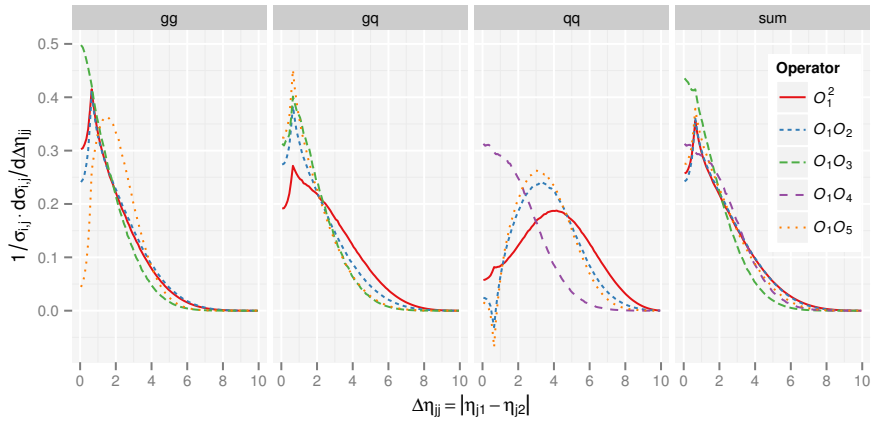

Figure 8.6: Normalized distributions for rapidity separation of the two final state jets for scalar operators. σ_{ij} are given in table C.5.

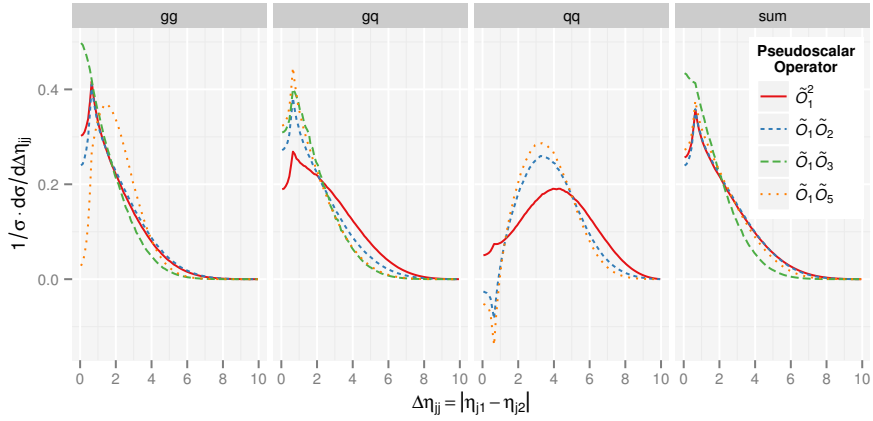

Figure 8.7: Normalized distributions for rapidity separation of the two final state jets for pseudoscalar operators. σ_{ij} are given in table C.6.

the scalar and pseudoscalar operators considered here, we conclude that the qualitative differences are probably too small to be used in an experimental analysis in order to classify the Higgs-gluon coupling. Then, since we observed in figs. 8.1 and 8.2 that differences between the individual operators increase with the Higgs' transverse momentum, it is suggestive to consider the $\Delta\Phi_{jj}$ and $\Delta\eta_{jj}$ distributions for these high-p_T events only. Figures 8.8 and 8.9 show these distributions in the scalar case, when the Higgs' transverse momentum is restricted to $p_T > 200\,\text{GeV}$. Compared to figs. 8.4 and 8.6, some features are enhanced, but, since such a cut will significantly decrease the data sample, it

remains to be seen whether it would lead to an improvement of an experimental analysis.

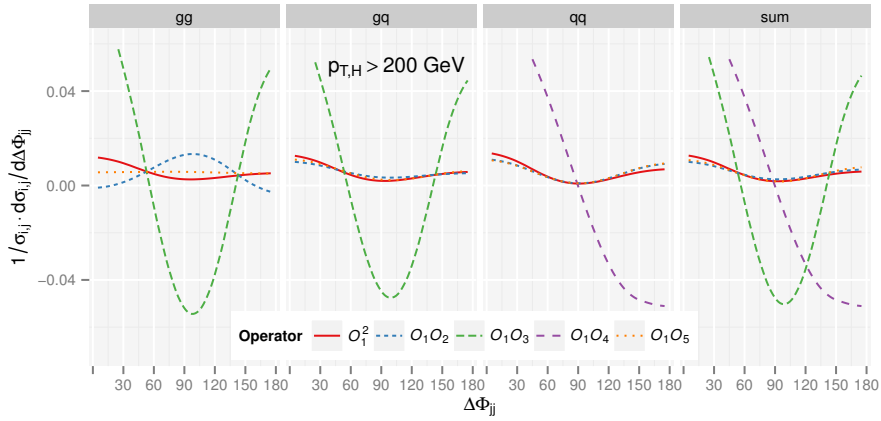

Figure 8.8: Normalized azimuthal angle difference distributions for scalar operators as in fig. 8.4, but restricted to events with $p_{T,H} > 200\,\text{GeV}$, where $p_{T,H}$ is the transverse momentum of the Higgs boson. σ_{ij} are given in table C.7.

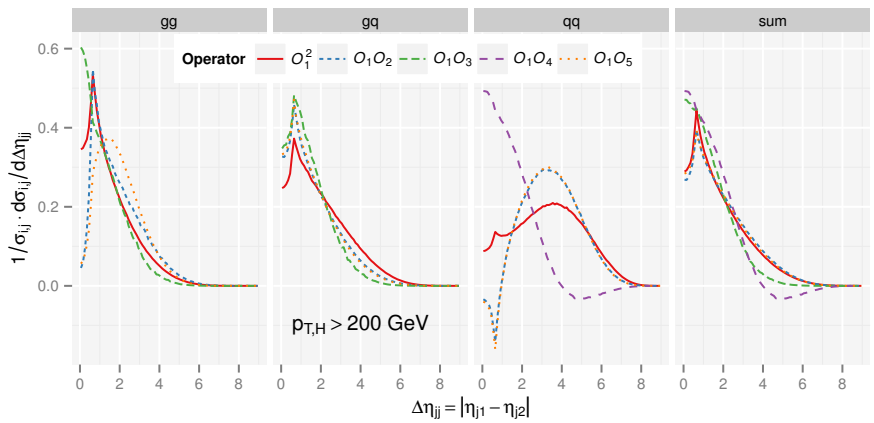

.

Figure 8.9: Normalized rapidity separation distributions for scalar operators as in fig. 8.6, but restricted to events with $p_{T,H} > 200\,\text{GeV}$, where $p_{T,H}$ is the transverse momentum of the Higgs boson. σ_{ij} are given in table C.8.

8.3 HIGHER ORDER SUPPRESSED TERMS

Up to this point, we only considered contributions due to the effective theory Lagrangian in eqs. (7.1) and (7.6) up to order $1/\Lambda^4$, originating from squares of $\mathcal{O}_1$ and interferences of $\mathcal{O}_1$ with $\mathcal{O}_2$ to $\mathcal{O}_5$, and equivalents for pseudoscalar operators. Terms arising from squares of $\mathcal{O}_2$ ($\tilde{\mathcal{O}}_2$) to $\mathcal{O}_5$ ($\tilde{\mathcal{O}}_5$) and their interferences are suppressed by $1/\Lambda^6$ and in principle negligible. Only can they become important when the Higgs-gluon coupling is predominantly mediated by dimension-7 operators, meaning that $C_1 \lll 1$. Then we can neglect interferences of $\mathcal{O}_1$ with dimension-9 operators, which are also of order $1/\Lambda^6$.

We begin, as before, with the Higgs p_T distributions in association with one jet, displayed in figs. 8.10 and 8.11. For comparison, the leading contributions due to $\mathcal{O}_1\mathcal{O}_1^\dagger$ and $\tilde{\mathcal{O}}_1\tilde{\mathcal{O}}_1^\dagger$, respectively, are also included. It is remarkable that, on the one hand, the spectrum is drastically different from the leading term; it shows a maximum at high p_T and falls off only very slowly. On the other hand, the higher order terms themselves are all very close to each other. The scalar and pseudoscalar cases are virtually indistinguishable.

The H + 2-jet distributions with respect to $\Delta\Phi jj$ are shown in figs. 8.12 and 8.13, and for $\Delta\eta_{jj}$ in figs. 8.14 and 8.15, where again the leading contributions $\mathcal{O}_1\mathcal{O}_1^\dagger$ and $\tilde{\mathcal{O}}_1\tilde{\mathcal{O}}_1^\dagger$, resp., are included. Quite large qualitative differences are visible in the $\Delta\Phi_{jj}$ distributions, while they are far less prominent in the $\Delta\eta_{jj}$ shapes.

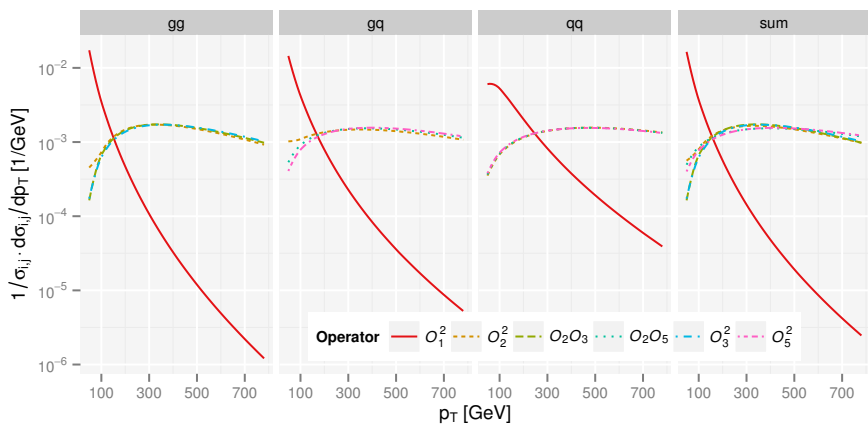

Figure 8.10: Normalized Higgs transverse momentum distributions, suppressed by $1/\Lambda^6$, for scalar coupling operators. σ_{ij} are given in table C.9.

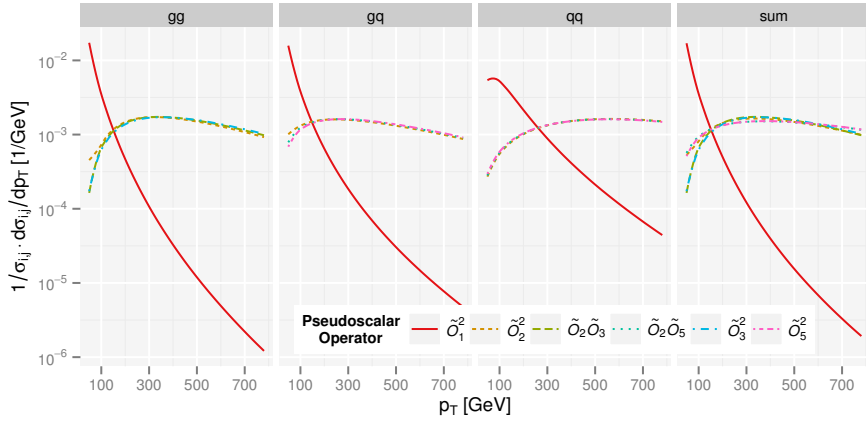

Figure 8.11: Normalized Higgs transverse momentum distributions suppressed by $1/\Lambda^6$ for pseudoscalar coupling operators. σ_{ij} are given in table C.10.

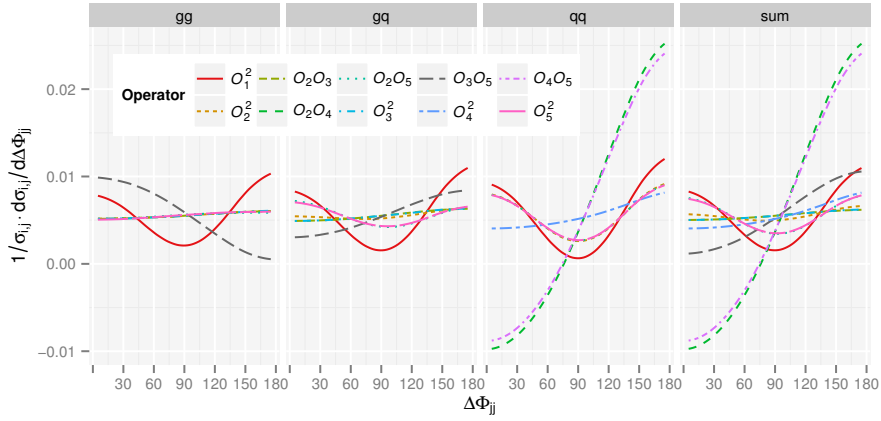

Figure 8.12: Normalized azimuthal angle difference distributions suppressed by $1/\Lambda^6$ for scalar coupling operators. σ_{ij} are given in table C.11.

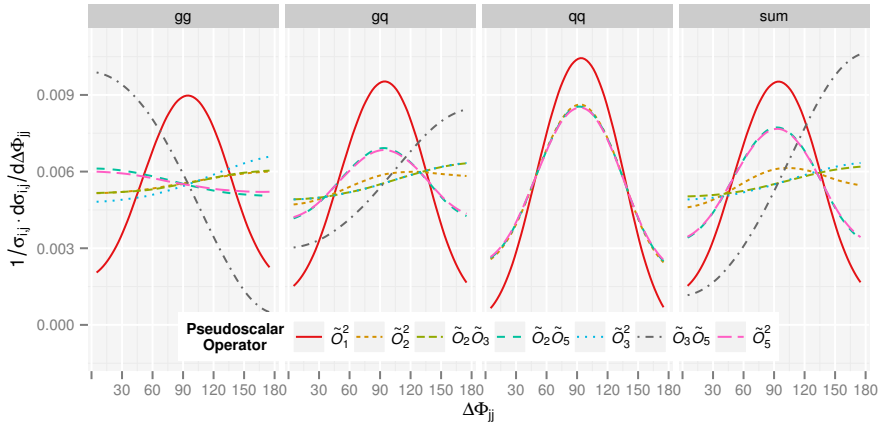

Figure 8.13: Normalized azimuthal angle difference distributions suppressed by $1/\Lambda^6$ for pseudoscalar coupling operators. σ_{ij} are given in table C.12.

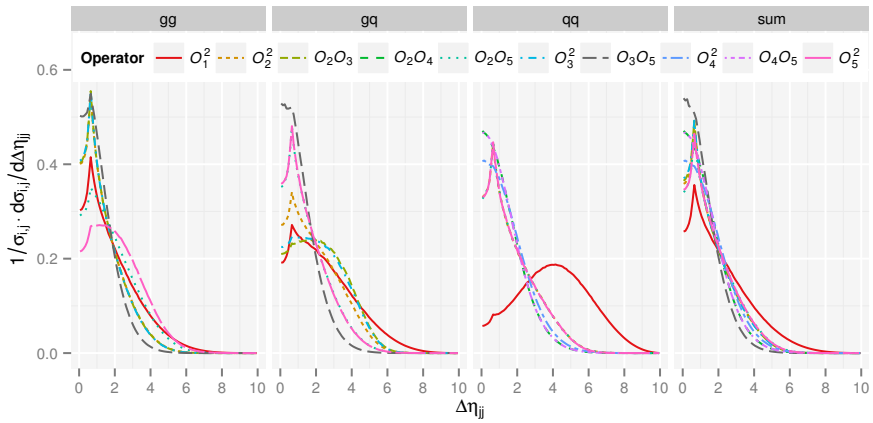

Figure 8.14: Normalized rapidity separation distributions suppressed by $1/\Lambda^6$ for scalar coupling operators. σ_{ij} are given in table C.13.

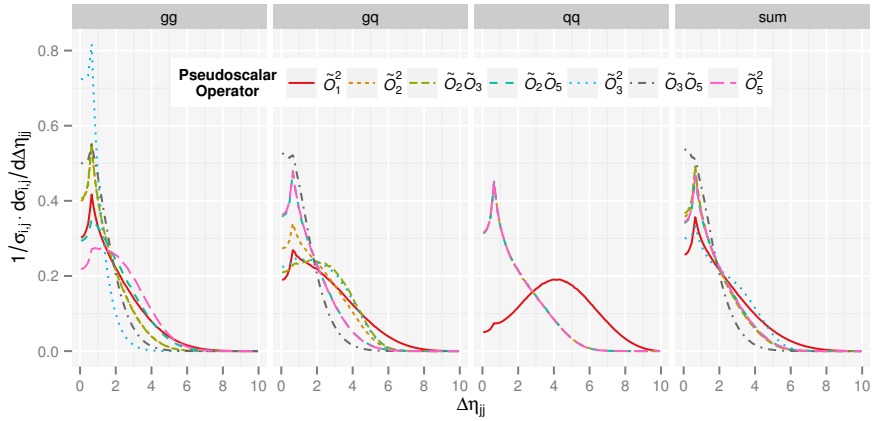

Figure 8.15: Normalized rapidity separation distributions suppressed by $1/\Lambda^6$ for scalar coupling operators. σ_{ij} are given in table C.14.

9

CONCLUSIONS

We have studied the effects of dimension-5 and -7 Higgs-gluon coupling SM-EFT operators on kinematical distributions in H + 1-jet and H + 2-jet production. While in the SM the Higgs-gluon coupling is predominantly mediated by a top-quark loop, new physics could augment or even replace this coupling. Our analysis allows searching for, constraining and quantifying such coupling modifications. We found that dimension-7 operators can significantly deform the Higgs p_{T} distribution toward a harder spectrum than in the SM. Additionally, we have shown that for two-jet observables certain operators can be sensitive to effects of new physics.

CLOSING REMARKS. Meanwhile, two years have passed since this study has been published, and several studies based on it and extending it have been done. For an overview of such studies see section 1.2 in part I. For example ref. [114] covers the matching to two generic models with heavy colored scalars and heavy top partners, and concludes that dimension-7 operators are unlikely to produce relevant information about UV physics, at LHC energies, beyond the leading dimension-5 operator.

A specific analysis of the Higgs-gluon coupling in the $H \to \gamma\gamma$ channel with the ATLAS experiment was performed using the Higgs transverse momentum as discriminating variable [443]. Instead of considering the kinematical distributions shown in this work, interference terms between the Standard Model and $\mathcal{O}_1, \ldots, \mathcal{O}_5$ were considered. These terms were provided by us in a collaboration and show a less emphasized behavior of the $\mathcal{O}_1\mathcal{O}_i$, $i = 2 \ldots 5$ interference contributions as considered above. They rather have more SM-like shapes. Furthermore, the operators are considered one by one in addition to the SM and not altogether in a combined analysis with the SM.

From this ATLAS analysis no limit on C_1 could be derived, since the p_{T} spectrum using $\mathcal{O}_1$ is too similar to the SM shape at low p_{T}. Here, once again, we point out the importance of top-mass effects, which distinguish $\mathcal{O}_1$ from the SM top-loop

induced coupling. It will be very important to calculate the Higgs p_{T} distribution at higher perturbative orders with an exact quark-loop induced Higgs-gluon coupling. Only through such a calculation the exact SM shape can be predicted at high p_{T}. For the Wilson coefficients C_2,C_3 and C_5, divided by Λ^3, limits of $\mathcal{O}(10^{-11}\mathrm{GeV}^{-3})$ were derived [443]. For example, new physics from $\mathcal{O}_2$ in addition to the SM, and assuming $C_2 = 1$, are limited to $\Lambda \gtrsim 7$–8 TeV. $\mathcal{O}_3$ and $\mathcal{O}_5$ are even stronger constrained.

Part IV

THE PERTURBATIVE QCD GRADIENT FLOW TO THREE LOOPS

This part is based on our upcoming publication 'The perturbative QCD gradient flow to three loops' [444]. The gradient flow encodes physical properties of QCD through a diffusion equation of the gauge fields. Different scales can be probed, determined by the flowtime t. Through its smoothing properties, gradient flow correlation functions are calculable in lattice QCD to high precisions. A perturbative expansion is possible and allows connecting QCD in the perturbative and non-perturbative regimes. In particular, an extraction of the strong coupling constant α_s is possible.

10

INTRODUCTION TO PERTURBATIVE GRADIENT FLOW

A huge amount of work is put into the development of algorithms to extract non-perturbative properties of QCD from calculations on a finite space time lattice. At first sight, it is straightforward to perform the continuum and infinite volume limits, necessary to compare results with experiments. When working in detail on such calculations, many problems connected to multiple scales and for example fermions turn up. Generally, the lattice size must be large compared to the hadron size $\simeq {\Lambda_{\mathrm{QCD}}}^{-1}$; but the spacing a must also be sufficiently small to make contact with the perturbative regime: $1/a \gg \mu_R$.

Lüscher firstly introduced the Yang-Mills gradient flow[1] in the context of improving the efficiency of lattice QCD calculations [445, 446]. The gradient flow evolves the gauge fields as a function of the so called flow time t, which allows for an interpretation as a smearing range, and sets a physical scale for observables within this framework. Later, Lüscher and Weisz showed that correlation functions of the flowtime dependent fields can be expanded in perturbation theory and that the obtained Feynman rules correspond to those of a renormalizable field theory on $\mathbb{R}^4 \times [0,\infty]$ [154, 155]. The extra dimension corresponds to the introduced flowtime. Moreover, due to the smoothing property of the gradient flow, correlation functions do not require additional renormalization, once the underlying theory (QCD) is renormalized as usual. The gauge fields evaluated at flowtime t probe the theory at length scales of the order $\sqrt{t}$.

The gradient flow can be calculated to a very high precision on the lattice, and, from a pure lattice point of view, can serve to define a high precision scale setting reference variable [154, 157]. It can be extended into a regime of t that is also perturbatively accessible. This opens a new way to connect the non-perturbative part of QCD with the perturbative part. One specific observable, the action density $\langle E \rangle$ (to be introduced below), is especially useful here. It allows an easy definition of a running coupling on the lattice at a scale given by t [159, 162, 447],

1 In lattice gauge theory, the gradient flow is commonly referred to as the Wilson flow. We will usually stick to gradient flow as in the mathematical literature.

and can be compared to the perturbative expansion at the renormalization scale $\mu = 1/\sqrt{8t}$. Thus, this gives us a way to extract the perturbative QCD running coupling $\alpha_s(\mu)$ from hadronic observables. This will be elaborated in the final chapter of this part.

In the following section we will recapitulate the general gradient flow formalism and the perturbative calculation of correlation functions of flowfields, based on refs. [154, 155].

The action density $\langle E \rangle$ has been obtained to NLO analytically [154].[1] For calculations beyond NLO, we will argue that an analytical integration of the occurring integrals is not feasible with current methods. This, and our approach to calculate $\langle E \rangle$ numerically to NNLO by sector decomposition [210] will be shown in chapter 11. We present checks that serve to validate our calculation.

The whole setup for the perturbative expansion of the observable and generation of the integrals is done in `Mathematica`. The numerical integration itself is done in C++ with gluing code in Haskell. A description of the setup with implementation details is given in appendix A.

In the final chapter of this part, chapter 12, we estimate the uncertainty, introduced by the finite perturbative expansion, through a variation of the renormalization scale. Further error sources are also discussed. The most interesting application of our result might indeed be an extraction of the strong coupling $\alpha_s^{(5)}(m_Z)$ in the $\overline{\text{MS}}$-scheme through a combination with lattice QCD results. Such high precision lattice data is not accessible to us at the time of writing. Nevertheless, we can use our perturbative result to check what precision in the extraction of α_s can be achieved at NNLO.

1 Except for the NLO calculation of $\langle E \rangle$, up to now, no other perturbative gradient flow calculations in the continuum have been performed.

10.1 FORMALISM

This section largely recapitulates the introductory parts of refs. [154, 155]. The flow $B_\mu(t,x)$ of Euclidean SU(N) gauge fields is defined by the equations

$$\begin{aligned} &\dot{B}_\mu = D_\nu G_{\nu\mu}, \quad B_\mu\,|_{t=0} = g_0 A_\mu\,, \\ &G_{\mu\nu} = \partial_\mu B_\nu - \partial_\nu B_\mu + [B_\mu, B_\nu], \quad D_\mu = \partial_\mu + [B_\mu, \cdot]\,, \end{aligned} \tag{10.1}$$

where A_μ is the fundamental SU(N) gauge field and g_0 is the bare gauge coupling. The dot denotes differentiation with respect to the flowtime t. Since the flow equation 10.1 is invariant under gauge transformations [154], it allows the introduction of a gauge parameter α_0:

$$\dot{B}_\mu = D_\nu G_{\nu\mu} + \alpha_0 D_\mu \partial_\nu B_\nu\,. \tag{10.2}$$

Taking gauge invariant observables then allows us to choose $\alpha_0 = 1$, which makes the resulting expressions simpler. Additionally, by checking independence of α_0, this gives us another possibility to check the correctness of the calculation.

Gradient flow is formulated for general SU(N) gauge theory. In the following we will restrict our presentations to SU(3) gauge theory, and also take into account N_f massless fermions in the fundamental representation; that is, we use massless N_f-flavor QCD as the underlying theory. We will thus refer to the fundamental gauge field also as gluon field. The fermions (quarks) are taken into account in the perturbative expansion of correlation functions of fundamental gauge fields, as elaborated later. An extension where the fermions itself are taken into account in the flow equations has been developed in ref. [156], but will not be considered here.

Let us remark that the flow eq. (10.2) has the form of a diffusion equation

$$\frac{\partial \Phi(\boldsymbol{x},t)}{\partial t} = \nabla\left(\mathcal{D}(\Phi,\boldsymbol{x}) \cdot \nabla \Phi(\boldsymbol{x},t)\right)\,,$$

where $\Phi(\boldsymbol{x},t)$ is the density of the diffusing material and $\mathcal{D}(\Phi,\boldsymbol{x})$ is a diffusion coefficient. If $\mathcal{D}$ is independent of Φ, the equation is linear and reduces to the heat equation. Similar to the smoothing effect of the diffusion equation on a density field, the gradient flow smooths the gauge field over a range determined by the flowtime t. The linear part of the flow eq. (10.2), which equals

$$\dot{B}_\mu = \partial_\nu \partial_\nu B_\mu + (\alpha_0 - 1)\partial_\mu \partial_\nu B_\nu\,,$$

can be solved by a Fourier transformation. With the heat kernel

$$K_t(x)_{\mu\nu} = \int\limits_p \frac{e^{ipx}}{p^2} \left\{ (\delta_{\mu\nu} p^2 - p_\mu p_\nu)\, \mathrm{e}^{-tp^2} + p_\mu p_\nu\, \mathrm{e}^{-\alpha_0 t p^2} \right\},$$

$$\text{where} \quad \int\limits_p = \int \frac{\mathrm{d}^D p}{(2\pi)^D},$$

and D is the space-time dimension in dimensional regularization, the solution to the linearized equation is then

$$B_{\mu,1}(t,x) = \int \mathrm{d}^D y\, K_t(x-y) A_\mu(y). \tag{10.3}$$

This is also perturbatively the lowest order approximation in the series

$$B_\mu = \sum_{k=1}^{\infty} g_0^k B_{\mu,k} \tag{10.4}$$

for the full non-linearized solution.

For $\alpha_0 = 1$ the heat kernel $K_t(x)_{\mu\nu}$ reduces to the simple form

$$K_t(x)_{\mu\nu} = \delta_{\mu\nu} \int\limits_p \mathrm{e}^{ipx}\, \mathrm{e}^{-tp^2} = \delta_{\mu\nu} \frac{\mathrm{e}^{-x^2/(4t)}}{(4\pi t)^{(D/2)}},$$

and thus shows (see eq. (10.3)) that the flow equation Gauss smooths the gauge potential over a spherical range with mean-square radius $\sqrt{2t \cdot D}$, that is, in $D = 4$ dimensions over $\sqrt{8t}$. This is therefore the scale of the involved physics and sets a natural choice of the renormalization scale in dimensional regularization to $\mu = 1/\sqrt{8t}$.

The solution to the complete flow equation can be written down in momentum space in terms of an integral equation as follows [154, 155]:

$$\begin{aligned}
\tilde{B}_\mu(t,p) &= g_0 \tilde{K}_t(p)_{\mu\nu} \tilde{A}_\nu(p) + \int\limits_0^t \mathrm{d}s\, \tilde{K}_{t-s}(p)_{\mu\nu} \tilde{R}_\nu(s,p), \\
\tilde{R}^a_\mu(t,p) &= \sum_{n=2}^{3} \frac{1}{n!} \int\limits_{q_1} \cdots \int\limits_{q_n} (2\pi)^D \delta(p + q_1 + \cdots + q_n) \\
&\qquad \times X^{(n,0)}(p, q_1, \ldots, q_n)^{a b_1 \ldots b_n}_{\mu \nu_1 \ldots \nu_n}\, \tilde{B}^{b_1}_{\nu_1}(t, -q_1) \cdots \tilde{B}^{b_n}_{\nu_n}(t, -q_n),
\end{aligned} \tag{10.5}$$

where the flowtime vertices $X^{(2,0)}$ and $X^{(3,0)}$ read

$$X^{(2,0)}(p,q,r)^{abc}_{\mu\nu\rho} = if^{abc}\Big\{(r-q)_\mu\delta_{\nu\rho} + 2q_\rho\delta_{\mu\nu} - 2r_\nu\delta_{\mu\rho} + (\alpha_0-1)(q_\nu\delta_{\mu\rho} - r_\rho\delta_{\mu\nu})\Big\}, \tag{10.6}$$

$$\begin{aligned} X^{(3,0)}(p,q,r,s)^{abcd}_{\mu\nu\rho\sigma} = {} & f^{abe}f^{cde}(\delta_{\mu\sigma}\delta_{\nu\rho} - \delta_{\mu\rho}\delta_{\sigma\nu}) \\ & + f^{ade}f^{bce}(\delta_{\mu\rho}\delta_{\nu\sigma} - \delta_{\mu\nu}\delta_{\rho\sigma}) \\ & + f^{ace}f^{dbe}(\delta_{\mu\nu}\delta_{\rho\sigma} - \delta_{\mu\sigma}\delta_{\nu\rho}), \end{aligned} \tag{10.7}$$

and the heat kernel $\tilde{K}_t(p)$ in momentum space is

$$\tilde{K}_t(p)_{\mu\nu} = \frac{1}{p^2}\left\{(\delta_{\mu\nu}p^2 - p_\mu p_\nu)\,\mathrm{e}^{-tp^2} + p_\mu p_\nu\,\mathrm{e}^{-\alpha_0 tp^2}\right\}. \tag{10.8}$$

Note that when we set the gauge parameter α_0 to one, a minimal number of terms is obtained.

The solution in terms of the fundamental gauge field A is thus obtained iteratively through eq. (10.5), leading to the solution series (10.4).

To illustrate the form of the solution series, we print the first two terms for $\alpha_0 = 1$:

$$B^a_{\mu,1}(t,x) = \int_p \mathrm{e}^{ipx}\,\mathrm{e}^{-tp^2}\,\tilde{A}^a_\mu(p),$$

$$\begin{aligned} B^a_{\mu,2}(t,x) = {} & if^{abc}\int_0^t \mathrm{d}s \int_{q,r} \mathrm{e}^{i(q+r)x}\,\mathrm{e}^{-s(q^2+r^2)-(t-s)(q+r)^2} \\ & \times\left\{\delta_{\mu\lambda}r_\sigma - \delta_{\mu\sigma}q_\lambda + \frac{1}{2}\delta_{\sigma\lambda}(q-r)_\mu\right\}\tilde{A}^b_\sigma(q)\tilde{A}^c_\lambda(r). \end{aligned}$$

Correlation functions in the flowfields B can then be calculated perturbatively in g_0, by firstly expanding B_μ as above, and secondly expanding the correlators in A as usual. More details for this step are given later.

For a diagrammatic approach [155], the Feynman rules can be derived from a field theory in $D+1$ dimensions, where the additional dimension in the half-space $[0,\infty]$ is the flowtime. One has to introduce an auxiliary Lagrange-

multiplier field L to describe the propagation of flowtime. In the end, one obtains, additionally to the gauge field (A) propagators and B field propagators, mixed propagators between A and B, and B and L. The auxiliary field only propagates through its mixing with other fields. The two earlier introduced vertices $X^{(2,0)}$ and $X^{(3,0)}$ correspond to vertices with interactions LB^2 and LB^3. Other vertices of SU(N) gauge theory are unmodified.

If one wants to calculate a correlation function (including vacuum expectation values) in perturbation theory, one can generate all possible contributing Feynman diagrams and insert the Feynman rules. With regard to our specific observable $\langle E \rangle$, which is a vacuum expectation value, we are not aware of any publicly available program that supports the generation of vacuum diagrams with mixed propagators, thus, it would have to be written from scratch. Alternatively, we can perform Wick contractions of the fundamental gauge fields in the perturbatively expanded correlation functions. This approach does not require a Feynman diagram generator but creates a huge amount of duplicate and equivalent expressions, and also includes vacuum bubbles and scaleless integrals that vanish in dimensional regularization. Care has to be taken for these instead. In this work, we took the Wick-contraction approach.

In the next chapter our specific observable $\langle E \rangle$ is introduced, as well as the setup to perform its calculation to NNLO. Finally, in chapter 12 the result with an application to extract $\alpha_s(m_Z)$ is discussed.

11

CALCULATION OF THE ACTION DENSITY

In this thesis we will compute the vacuum expectation value of the observable

$$\mathcal{O} := E(t,x) = \frac{1}{4} G^a_{\mu\nu} G^a_{\mu\nu}$$

to NNLO perturbative accuracy, corresponding to a three-loop calculation. The calculation is done in Euclidean space-time and dimensional regularization with $\overline{\text{MS}}$ renormalization. The result at NLO accuracy is known analytically.[1] [154]

To perform the calculation of $\langle E \rangle$, one firstly inserts the solution series for $B_\mu(t,x)$ (eq. (10.4)) into

$$\langle E \rangle = \frac{1}{2} \langle \partial_\mu B^a_\nu \partial_\mu B^a_\nu - \partial_\mu B^a_\nu \partial_\nu B^a_\mu \rangle + f^{abc} \langle \partial_\mu B^a_\nu B^b_\mu B^c_\nu \rangle + \frac{1}{4} f^{abe} f^{cde} \langle B^a_\mu B^b_\nu B^c_\mu B^d_\nu \rangle \,. \tag{11.1}$$

Secondly, higher orders of the fundamental perturbative (QCD) vacuum are taken into account as follows:

$$\langle \mathcal{O} \rangle = \frac{\langle 0 | \mathcal{O} \exp(-S_{\text{QCD}}(g_0)) | 0 \rangle}{\langle 0 | \exp(-S_{\text{QCD}}(g_0)) | 0 \rangle} \,, \tag{11.2}$$

where S_{QCD} is the interaction part of the fundamental QCD action, which depends on the fundamental gauge fields A^a_μ and quark fields.

Since $\langle E \rangle$ includes at least two B fields, it follows from the expansion of B_μ in eq. (10.4) that to leading order $\langle E \rangle$ is proportional to g_0^2. The next non-vanishing term in the perturbative series is of order g_0^4, since odd powers in g_0 vanish due to an odd number of fields in the matrix elements. At order g_0^4 now also the other terms in eq. (11.1) contribute.

1 We wish to thank Martin Lüscher for providing us his personal notes on the complete NLO calculation, which helped us to lift a misunderstanding in the calculation of vacuum expectation values.

Generally, higher orders in the flowfield expansion (eq. (10.4)), lead to a larger number of flowtime integrations, while the perturbative expansion (eq. (11.2)) leads to the well known corrections due to fundamental QCD. To be precise, the B field, perturbatively expanded to order g_0^n, $B_{\mu,n}$, contains terms with n fundamental gauge fields and terms with a number of flowtime integrations between $\lceil n/2 \rceil$ and $n-1$.

We symbolize the general form of a matrix element to be evaluated at order g_0^n by

$$M_n(k,m) := \langle 0 | (B_{m_1} \cdots B_{m_k}) \times (S_{\mathrm{QCD}})^{n-m} | 0 \rangle \,, \quad m = \sum_{i=1}^{k} m_i \,, \tag{11.3}$$

where B_{m_i} is the m_i^{th} coefficient of the asymptotic series in eq. (10.4). We choose this classification because our subsequent simplifications are applied for each class of integrals $M_n(k,m)$ separately. This is advisable from a computational point of view, since there is no overlap of equivalent integrals among those classes, saving time for algorithms that do not scale linearly with the number of integrals.

To get a feeling for these classes, let us recap: For our observable $\langle E(t,x) \rangle$, $k \in \{2,3,4\}$ thus denotes the second, third and fourth term in eq. (11.1). The number m tells us how many flowtime integrations will be involved, while n denotes an expansion order in fundamental QCD.[1]

At LO, $M_2(2,2)$ is the only class that contributes, corresponding to just the first term in eq. (11.1), with flowfields B expanded to the lowest order (being proportional to A), and no additional QCD corrections. At NLO, there are six classes with at most two flowtime integrations, and at NNLO twelve classes with at most four flowtime integrations.

This classification in $M_n(k,m)$ also allows us to highlight $M_n(2,2)$, which is fully and analytically determined by the expression for the $(n-2)$-loop self-energy of the fundamental gauge field. Since the gluon self-energy has been computed before analytically, we can compare it to the result of our setup as a check of correctness.

1 The maximum number of flowtime integrations for integrals in $M_n(k,m)$ is $m-k$, and since $m \leq n$, the maximum number of flowtime integrations at order g_0^n is $n-2$. For a k-point function, the maximum number of flowtime integrations is $n-k$.

11.1 ANALYTICAL CALCULATION OF FLOWTIME INTEGRALS

In the end, the complete calculation has been performed numerically through sector decomposition. Before coming to that, we would like to emphasize that we have studied the feasibility of an analytical integration. Some reasons why an analytical integration is not feasible with currently available methods for usual Feynman integrals are given in this section. We will use dimensional regularization with space-time dimension $D = 4 - 2\varepsilon$.

Stepping ahead a bit of the next section, where our setup for the perturbative expansion is described, one finally ends up with integrals of the following form at order g_0^6:

$$I(t,\boldsymbol{\nu},\boldsymbol{a},D) = \left(\prod_{f=0}^{N}\int_0^{t_f^{\mathrm{up}}} \mathrm{d}t_f\right)\int_{p_1,p_2,p_3} \frac{\exp\left(\sum_{k,i,j} a_{kij} t_k p_i p_j\right)}{p_1^{2\nu_1} p_2^{2\nu_2} p_3^{2\nu_3} p_4^{2\nu_4} p_5^{2\nu_5} p_6^{2\nu_6}} \tag{11.4}$$

where

$$\begin{aligned}
&\boldsymbol{\nu} = \{\nu_1,\nu_2,\nu_3,\nu_4,\nu_5,\nu_6\}\,, \quad \nu_i \leq 3\,,\\
&\boldsymbol{a} = \{a_{kij} : k = 1,\ldots,N\,,\, i = 1,2,3\,,\, j = 1,2,3\}\,,
\end{aligned}$$

are sets of integers, $N \leq 4, t_0 \equiv t$, and the upper limits for the flowtime integrations are linear combinations of the other flowtime observables, $t_f^{\mathrm{up}} = t_f^{\mathrm{up}}(t_0,\ldots,t_{f-1})$. The momenta p_4,p_5,p_6 are linear combinations of the integration momenta p_1,p_2,p_3.

The only mass scale in the problem (quark masses are neglected) is the flow time t, such that this scale completely factorizes as

$$I(t,\boldsymbol{\nu},\boldsymbol{a},D) = t^d\, c(\boldsymbol{\nu},\boldsymbol{a},D)\,, \quad d = 3D - 2N - 2\sum_{i=1}^{6}\nu_i\,, \tag{11.5}$$

where $c(\boldsymbol{\nu},\boldsymbol{a},D)$ is dimensionless.

At this point it already becomes clear that direct Feynman parametrization of the propagators through a formula like

$$\frac{1}{A_1^{\alpha_1}\cdots A_n^{\alpha_n}} = \frac{\Gamma(\alpha_1+\ldots+\alpha_n)}{\Gamma(\alpha_1)\cdots\Gamma(\alpha_n)}\int_0^1 du_1\cdots\int_0^1 du_n \frac{\delta\left(\sum_{k=1}^n u_k - 1\right) u_1^{\alpha_1-1}\cdots u_n^{\alpha_n-1}}{\left[u_1A_1+\cdots+u_nA_n\right]^{\sum_{k=1}^n \alpha_k}}$$

is not possible due to the additional exponential factor with momenta. The latter exponential factor prevents the subsequent integration over the momenta. Instead, we have to use the Schwinger parametrization

$$\frac{1}{A^n} = \frac{1}{\Gamma(n)} \int_0^\infty \mathrm{d}\alpha\, \alpha^{n-1}\, \mathrm{e}^{-\alpha A} .$$

Applying it to each propagator, and handling numerator factors as in

$$\frac{1}{p^{2n}} = \frac{1}{\Gamma(n)} \int_0^\infty \mathrm{d}\alpha\, \alpha^{n-1}\, \mathrm{e}^{-\alpha p^2} , \quad p^{2n} = \frac{\mathrm{d}^n}{\mathrm{d}s^n}\, \mathrm{e}^{s p^2} \bigg|_{s=1} ,$$

where $n \in \mathbb{N}$, the momentum integration reduces to a Gaussian integral:

$$\int_{p_1,p_2,p_3} \exp[-\mathbf{p}^T A(\boldsymbol{\alpha},\mathbf{t})\mathbf{p}] = \left(\det A(\alpha,\mathbf{t})\right)^{-D/2} (4\pi)^{-3D/2} ,$$

where $\mathbf{p} = (p_1,p_2,p_3)$, and $A(\alpha,\mathbf{t})$ is a coefficient matrix which is linear in the Schwinger parameters $\boldsymbol{\alpha} = \{\alpha_1,\ldots,\alpha_6\}$ and the flowtime variables $\mathbf{t} = \{t_0,\ldots,t_N\}$.

Through a simple rescaling of the flowtime variables and the Schwinger parameters to the unit interval,

$$t_n \to \frac{t_n}{t_n^{\mathrm{up}}} , \qquad \alpha_n \to \frac{\alpha_n}{\alpha_n - 1} ,$$

making them also dimensionless, one ends up with integrals of the form

$$J(t,D) = \int_0^1 \mathrm{d}x_1 \cdots \int_0^1 \mathrm{d}x_M \prod_i P_i^{a_i}(t,x_1,\ldots,x_M) , \tag{11.6}$$

where $M > 0$, the P_i are polynomials in $x_1,\ldots,x_M$, and the exponents a_i can be D-dependent. In the limit $4 - D = 2\varepsilon \to 0$, the integrals develop divergences.

It is important to remark that divergences are not just introduced through the integrals over Schwinger parameters, but also through the flowtime integrations.

If one then performs all the simplification steps, and steps to eliminate equivalent integrals as described in the next section, the number of integrals involving f flowtime integrals at NLO (NNLO) are given in table 11.2 (table 11.1). For now let

us summarize that over 80% of the total number of integrals have three or four flowtime integrations. Half of the total number have four.

What does that mean for our goal to calculate $\langle E \rangle$ analytically at three-loop precision? We should at least be able to compute 'most' (also corresponding to the most difficult) integrals analytically. If only some small amount of simpler integrals can be solved analytically, we could just solve all of them numerically. Under this premise, we will have a look at various techniques, present them for the two-loop case and discuss the feasibility for three loops. If one technique does not apply to the integrals with three or four flowtime integrations, but is barely applicable to one or two flowtime integrations, we do not consider it further.

Let us first observe how two-loop integrals, where at most two flowtime integrations occur, can be solved analytically: just in the most simple way, by performing Schwinger parametrization and subsequently doing the integration in D dimensions in terms of hypergeometric functions. All integrals can then be written down analytically in a $1/\varepsilon$ expansion. The result is a sum of rational numbers and logarithms of 2 and 3 for the finite parts.

We can simplify the computation in few cases further by replacing numerator momentum factors with a derivative with respect to a flowtime integration variable:

$$\int_0^t \mathrm{d}s\; \mathrm{e}^{sX} X = \int_0^t \mathrm{d}s\; \frac{\mathrm{d}}{\mathrm{d}s}\, \mathrm{e}^{sX} = \mathrm{e}^{sX}\Big|_0^t , \tag{11.7}$$

where X contains momenta and possibly other flowtime integration variables; the momentum integrations are not important for this example.

Let us define 'nested' flowtime integrations for the following discussion: Higher order expansions of the flowfield B are constructed iteratively from lower order B fields, such that the flowtime integration structure to a contribution to a fourth order expansion B_4 looks like

$$\begin{aligned}
&\int_0^t \mathrm{d}s_1 \int_0^{s_1} \mathrm{d}s_2 \int_0^{s_2} \mathrm{d}s_3 \int_0^{s_3} \mathrm{d}s_4\, f(s_1,s_2,s_3,s_4) \\
&\qquad = t^4 \int_0^1 \!\!\iiiint \mathrm{d}s_1\, \mathrm{d}s_2\, \mathrm{d}s_3\, \mathrm{d}s_4\, s_1^3 s_2^2 s_3 f(s_1 t, s_1 s_2 t, s_1 s_2 s_3 t, s_1 s_2 s_3 s_4 t)\,,
\end{aligned}$$

when scaled to unit intervals. The integration intervals are interlinked by the other integration variables, such that we call this a nested integration.

With more flowtime integrations, the exponential factor is considerably more complicated in addition to the numerator flowtime factors for nested integrals. In general, trying to use the trick in eq. (11.7) for one or even multiple derivatives is not possible anymore for the three-loop integrals.

DIRECT INTEGRATION OVER FLOWTIMES. What comes to our mind next is a direct integration over flowtimes:

$$\int_0^t \mathrm{d}s\; \mathrm{e}^{sX} = \frac{1}{X}\,\mathrm{e}^{sX}\Big|_0^t = \frac{\mathrm{e}^{tX}-1}{X}\,.$$

By doing this, we introduce new denominators[1], thus providing no net benefit in the number of resulting parametric integrals after Schwinger parametrization. In case of nested flowtime integrations, even higher propagator powers are introduced in addition to a large increase of numerator terms.

TWO-LOOP EXAMPLE. For completeness, let us look at a two-loop example. For the following example we perform the direct integration of the flowtime, resulting in two terms:

$$\begin{aligned}\int_0^t \mathrm{d}s \int_{p,q} \frac{e^{-s(p^2+q^2)-(2t-s)(p+q)^2}}{p^2} \\ = \int_{p,q} \frac{e^{-2t(p+q)^2}}{p^2(p^2+q^2-(p+q)^2)} - \int_{p,q} \frac{e^{-t(p^2+q^2+(p+q)^2)}}{p^2(p^2+q^2-(p+q)^2)}\,.\end{aligned}$$

1 The denominators, interpreted as propagators, correspond to linear propagators, like those appearing in asymptotic expansions by regions

After Schwinger parametrization, this equation has the form

$$\int_0^t \mathrm{d}s \int_0^\infty \mathrm{d}\alpha \left(4\,ts - s^2 + 2\,t\alpha\right)^{-D/2} = \int_0^\infty \mathrm{d}\alpha \int_0^\infty \mathrm{d}\beta \left(4\,t\beta - \beta^2 + 2\,t\alpha\right)^{-D/2} - \int_0^\infty \mathrm{d}\alpha \int_0^\infty \mathrm{d}\beta \left(3\,t^2 + 2\,t\beta - \beta^2 + 2\,t\alpha\right)^{-D/2} .$$

Doing the substitution $\beta = s - t$ on the rightmost integral, we see that the original integral has been restored:

$$\int_0^t \mathrm{d}s \int_0^\infty \mathrm{d}\alpha \left(4\,ts - s^2 + 2\,t\alpha\right)^{-D/2} = \left(\int_0^\infty \mathrm{d}s - \int_t^\infty \mathrm{d}s\right) \int_0^\infty \mathrm{d}\alpha \left(4\,ts - s^2 + 2\,t\alpha\right)^{-D/2} .$$

Our procedure of integration over the flowtime corresponds to extending the flowtime integration interval up to infinity, and subtracting the just added interval again in terms of a new integral. It should be clear that in general we have introduced new divergences that must cancel between both integrals.

Indeed, now trying to perform the integration for both parts shows divergences that require additional regularization for a direct integration. Other integration techniques introduce imaginary parts that cancel between both parts.

In fact, this is the general behavior when one integrates over the flowtime first: The momenta in the exponential function, prefixed with flowtime integration variable s, get pushed into the denominator as a new propagator by integration over s. These momenta are then pushed back into the exponential function by Schwinger-parametrization, this time integrated from 0 to ∞.

INTEGRATION BY PARTS. One important technique, and essential requirement for approaches like dimensional recurrence relations or differential equations, but useful by itself, is integration by parts [217].

Clearly, integration by parts reduction can only be applied with respect to the momentum integrations and not to the flowtime integrations. The flowtime integration variables have to be treated as external scales for the IBP reduction.

What does this mean? Including t itself, the IBP reduction will at most include five scales for three-loop integrals. The sizes of the reduced expressions are just too huge to be of any use. The coefficients, as rational functions of the five scales, still have to be integrated over. Remembering that the flowtime integrations themselves can lead to $1/\varepsilon$ poles, this makes it completely infeasible for an analytical treatment.

Another caveat is that, even in the simplest cases with just one flowtime integration

$$\int_0^t \mathrm{d}s\, f(t,s)\,,$$

where $f(t,s)$ refers to the remaining (momentum) integrations, after an IBP reduction of $f(t,s)$, new unregularized poles in the flowtime integration are introduced as in

$$\int_0^t \mathrm{d}s\, \frac{\tilde{f}_1(t,s)}{t-s} + \cdots .$$

These new poles only cancel in the sum of all contributing reduced integrals $\tilde{f}_i$ with complicated coefficient functions in s. This could be somewhat manageable, but not for many (> 1) flowtime integrations, where even more complicated pole structures are introduced. The construction of a basis $\tilde{f}_i$ with finite coefficients for $D \to 4$ (like in ref. [448]) and no singularities introduced through the flowtime integrations could be possible. But this does not help further the problem of huge five scale coefficients.

In principle one could try to do the integration over flowtimes, and do a subsequent IBP reduction of the integrals with high propagator and numerator powers. This reduction would have to be done for a very large number of integrals, namely for each integral with different flowtime integrations and different exponential factors, leading to different new linear propagators, for which the reduction has to be performed. We did not follow this approach.

All techniques so far are with more or less effort feasible to solve the two-loop case with at most two flowtime integrations. These two-loop integrals are not even a problem by direct integration of flowtime and Schwinger parameters. Going to higher orders, the increased number of flowtime integrations makes them unusable. Particularly, methods that *rely* on an IBP reduction are invalidated.

MELLIN-BARNES INTEGRATION. By using the Mellin-Barnes representation of a propagator as in

$$\frac{1}{(m^2-k^2)^\lambda} = \frac{1}{\Gamma(\lambda)}\frac{1}{2\pi i}\int\limits_{-i\infty}^{+i\infty} \mathrm{d}z\,\Gamma(\lambda+z)\Gamma(-z)\frac{(m^2)^z}{(-k^2)^{\lambda+z}}\,,$$

where the contour of integration is chosen such that the poles with a $\Gamma(\ldots+z)$ dependence are separated from those with a $\Gamma(\ldots-z)$ dependence [216], we can factorize a massive propagator in exchange for a general propagator power $\lambda+z$.

Given our integral structure, we can only make use of the Mellin-Barnes representation after Schwinger parametrization to transform a sum of integration variables in the denominator into a product:

$$\begin{aligned}\frac{1}{(x_1+\ldots+x_n)^\lambda} = \frac{1}{\Gamma(\lambda)}\frac{1}{(2\pi i)^{n-1}}\int\limits_{-i\infty}^{+i\infty} \mathrm{d}z_2\ldots\mathrm{d}z_n\,\Gamma(\lambda+z_2+\ldots+z_n)\\ \times\Gamma(-z_2)\ldots\Gamma(-z_n)x_2^{z_2}\ldots x_n^{z_n}x_1^{-\lambda-z_2-\cdots-z_n}\,,\end{aligned}\quad (11.8)$$

where x_i can be Schwinger or flowtime integration parameters. After Schwinger and flowtime integrations, all parameters $2\varepsilon = 4-D$, etc. are chosen in such a way that for straight integration contours of the MB variables z_i the arguments of all gamma functions in the numerator are positive when crossing the real axis.[1] One then tends $\varepsilon\to 0$ and picks up crossed poles with their residues.

But first, the MB parametrization leads us to integrals of the form

$$\int \mathrm{d}z \int\limits_0^\infty \mathrm{d}\alpha\,\alpha^{z+\cdots}\ldots\,,$$

where the Schwinger parameter integration over α must be performed. Obviously the integral is divergent. We are required to introduce an artificial regularization. This can be a cutoff Λ for the α integration that is sent to ∞ in the end. It seems to work, as was checked for simple cases, but is not very elegant and leads to more complicated series of residues for the MB integrals.

1 This simple strategy of choosing the integration contour for the resolution of poles in ε is known as 'Strategy B' [216]. See also ref. [216] for other strategies and detailed examples.

Another idea is to regularize these integrals in the following way:

$$\int_0^\infty \mathrm{d}x\, x^a = \int_0^\infty \mathrm{d}x \lim_{\delta\to 0} x^{a+\delta}(1+x)^\delta$$
$$\to \lim_{\delta\to 0} \int_0^\infty \mathrm{d}x\, x^{a+\delta}(1+x)^\delta = \lim_{\delta\to 0} \frac{\Gamma(-2\delta-1-a)\Gamma(1+a+\delta)}{\Gamma(-\delta)} \tag{11.9}$$

The step '→' is, of course, not allowed in general, but should be acceptable in our case, as we know that the composite overall result is finite / analytical in the δ parameter. We can then use this regularization to integrate over the Schwinger parameters and perform the MB pole resolution: the limits $\delta \to 0$ and $\varepsilon \to 0$ are taken, and all residues that are crossed are taken into account. In the results, δ can be set to zero and we can expand in ε.

This way of regularization was tested in simple two-loop cases with the help of `MB.m` [449] and `MBresolve.m` [450]. We give one example as follows. Starting with the Schwinger parametrized integral

$$F := \int_0^t \mathrm{d}s \int_{p,q} \frac{e^{-s(p^2+q^2)-(2t-s)(p+q)^2}}{(p+q)^2} = \int_0^t \mathrm{d}s \int_0^\infty \mathrm{d}\alpha\, (2t\alpha - 4ts - s^2)^{-D/2},$$

we use eq. (11.8) to derive

$$F = \frac{1}{\Gamma(D/2)} \frac{1}{(2\pi i)^2} \int_0^t \mathrm{d}s \int_0^\infty \mathrm{d}\alpha \int_{-i\infty}^{i\infty} \mathrm{d}z_2 \int_{-i\infty}^{i\infty} \mathrm{d}z_3 \frac{(4ts)^{z_2}(-s^2)^{z_3}}{(2t\alpha)^{D/2+z_2+z_3}}$$
$$\times \Gamma(D/2+z_2+z_3)\Gamma(-z_2)\Gamma(-z_3).$$

Performing the integration over flowtime and Schwinger parameters, while using the regularization in eq. (11.9), we obtain

$$F \stackrel{\to}{=} \lim_{\delta\to 0} \frac{1}{\Gamma(D/2)} \frac{1}{(2\pi i)^2} \int_{-i\infty}^{i\infty} \mathrm{d}z_2 \int_{-i\infty}^{i\infty} \mathrm{d}z_3 \frac{(4t)^{z_2}(-1)^{z_3}(2t)^{-D/2-z_2-z_3}}{z_2+2z_3+1}$$
$$\times \Gamma(D/2+z_2+z_3)\Gamma(-z2)\Gamma(-z_3)$$
$$\times \frac{\Gamma(D/2+z_2+z_3-1-2\delta)\Gamma(-D/2-z_2-z_3+1+\delta)}{\Gamma(-\delta)}.$$

Using `MB.m` we found the following choices for straight contour lines: $\varepsilon = 7/8$, $\delta = -3/8$, $\mathfrak{Re}(z_2) = -1/2$, $\mathfrak{Re}(z_3) = -1/8$. Performing the continuations to zero by taking crossed residues into account, taking the limit $\delta \to 0$, expanding in ε, and subsequently performing the MB integrals by summing up residues, we obtain the correct result:

$$F = \frac{1}{8}\frac{1}{t^2\varepsilon} - \frac{1}{8}\frac{-2\log(t) - 1 + \log(3) - 4\log(2)}{t^2}.$$

More complicated cases require the evaluation of many-fold nested sums. A numerical evaluation of the MB integrals is also possible. What prevents the adaption to three-loop integrals is the number of terms $x_1, \ldots, x_n$ in eq. (11.8). They can easily grow beyond $n = 20$ for many propagators and flowtimes, thus leading to $\sim 20+$ fold Mellin-Barnes integrals. Even the construction of contours for this amount of integrations and the introduction of regularizations for the Schwinger integrations are not practical anymore.

11.2 Numerical evaluation of the perturbative series

What will be sketched in this section, is our setup to perturbatively calculate the observable $\langle E \rangle$ in eq. (11.1) to three-loop order (NNLO). The perturbative order is just one parameter of the setup, such that, in principle, even higher orders could be calculated. Due to the already large number of difficult integrals at NNLO, to be evaluated numerically to a high precision, this would require a significant increase in computing resources.[1] Also, the specific observable $\langle E \rangle$ is a simple 'parameter' which could be replaced by other vacuum expectation values. For implementation details we refer to appendix A.

Except for the final numerical integration, all stages of the calculation are implemented as a `Mathematica` [451] code. As already mentioned, we did not follow a diagrammatic approach but directly implemented the Wick contractions of gauge and quark fields. This step is performed after the iterative expansion of the flowfields (eqs. (10.4) and (10.5)), the perturbative expansion of $\exp(-S_{\mathrm{QCD}})$ (eq. (11.2)), and the insertion of QCD Feynman rules. The Dirac algebra is performed with the package `FeynCalc` [452]. Color factors are calculated using

1 The real limitation in the current implementation are the Wick contractions though, which scale factorially with the number of involved fields.

`ColorMath` [453]. Vacuum bubble contributions are discarded as required by the normalization factor in eq. (11.2).

After these algebraic and symbolic manipulations, we obtain the momentum space integrals in the form of eq. (11.4). Since we did Wick contractions, we now have many integrals that are equivalent under either renaming and/or permutation of integration variable names, or linear transformations of the loop momenta. We account for these possibilities using the Schwinger parametrized form (eq. (11.6)), which is invariant under shifts of loop momenta, and comparing term by term all permutations of integration variable names. Additionally, we cancel numerator factors with denominators (propagators) as far as possible and discard scaleless integrals, which vanish in dimensional regularization, using the technique in ref. [454].

These simplifications (reductions) lead to a certain number of integrals, which are given in table 11.2 for the NLO case and in table 11.1 for the NNLO case. They are split according to the classification defined in eq. (11.3) and according to the number of flowtime integrations. Due to our exhaustive reduction steps, a diagrammatic approach would lead to a similar amount of integrals.

To extract the terms that become singular for $\varepsilon \to 0$, we use the sector decomposition [210] implementation in the `Mathematica` package `FIESTA` [220]. It provides us with the result in the form

$$J(t,D) = \frac{1}{\varepsilon^2} J_2 + \frac{1}{\varepsilon} J_1 + J_0 + \dots ,$$

Table 11.1: Number of integrals at NNLO (a) in class $M_6(k,m)$, and (b) involving f flowtime integrations. The numbers may not strictly be minimal; they are to be understood as a reference, in particular in comparison to the NLO numbers given in table 11.2.

k	2					3				4			Σ
m	2	3	4	5	6	3	4	5	6	4	5	6	
#	24	45	219	683	2244	13	43	110	244	5	7	14	3651

(a)

f	0	1	2	3	4	Σ
#	42	117	412	1229	1851	3651

(b)

Table 11.2: Number of integrals at NLO (a) in class $M_4(k,m)$, and (b) involving f flowtime integrations. The numbers may not strictly be minimal; they are to be understood as a reference, in particular in comparison to the NNLO numbers given in table 11.1.

k	2			3		4	Σ
m	2	3	4	3	4	4	
#	1	4	11	1	2	1	20

(a)

f	0	1	2	Σ
#	3	7	10	20

(b)

where the ellipsis denotes higher order terms in ε. $J_i(t)$ are convergent integrals over rational functions times logarithms of the integration parameters $x_1, \ldots, x_M$, as in eq. (11.6). We prevented `FIESTA` from performing this integration, and rather used our own implementation of the fully symmetric Genz-Malik rule of order 13 [455] in a global adaptive bi-sectioning [456]. The implementation uses high precision arithmetics using the C++ `MPFR` wrapper `MPFR C++` [457, 458].

NON-LINEAR TRANSFORMATIONS. An attractive alternative or complementary approach to sector decomposition for the subtraction of singularities are non-linear transformations [221]. These have, in principle, the advantage that no iterative decomposition into more and more sub sectors is necessary to get a form of the integrands suitable for a subtraction.

One problem with these transformations is that an algorithmic automatization has not been achieved yet. We could only handle a subset of integrals with this approach in an automatized way. It also turned out that for our integrals the numerical integration did not improve significantly over plain sector decomposition. We thus abandoned this idea and completely switched to sector decomposition.

REMARKS ON NUMERICAL INTEGRATION. The sector decomposition implementation `FIESTA` with option `SeperateTerms=False` will return one integrand expression for each obtained sector by default. One can then integrate these integrands and compare the integration result and error with the case of split up integrands, where the splitting is such that terms with different denominator pole structures and different logarithmic numerator structures are separated.

It turned out that a splitting is not ultimately necessary to get a high precision result, but the estimate for the numerical integration error can be severely overestimated in the case of combined terms. The errors for the split terms, as used for our final result, are usually overestimated by a factor of one to ten. They can drift to an underestimation for single cases if the integration runs for too long. Then, the global adaptive bi-sectioning algorithm reaches too far into the singular (but integrable) border regions. It is clear that at some point an integration based on polynomial interpolation is inefficient in these regions. Ways to lift this singular behavior like Iri-Moriguti-Takasawa (IMT) transformations [459, 460] did not show improvements.

For our final result of $\langle E(t)\rangle$, a huge number of integrals has been evaluated, some for which the error is underestimated, and many for which the error is overestimated. We checked that our error estimation is conservative, as elaborated in the next section, where we give validating checks of our setup and result.

Let us give the explicit result for one particular non-trivial momentum integral of the type in eq. (11.4) which occurs in the calculation of $\langle E\rangle$. It has four flowtime integrations and thus belongs to the class $M_6(2,6)$. Furthermore, from the flowtime integration limits, we see that it originates from the iterated insertion of four three-point flowtime vertices $X^{(2,0)}$:

$$\begin{aligned}
&\int_{k,q,r} \int_0^t \mathrm{d}s_0 \int_0^{s_0} \mathrm{d}s_1 \int_0^{s_1} \mathrm{d}s_2 \int_0^{s_2} \mathrm{d}s_3 \, \frac{(k+q)^2(k+r)^2}{(k-q)^2(q-r)^2} \times \\
&\exp\left[2r(r-q)(s_0+s_3)+2kr(s_0-s_1)+2kq(s_1-s_2-2t)+2k^2t+2q^2(s_2+t)\right] \\
&\quad = \frac{t^{-2+3\varepsilon}}{(4\pi)^{3D/2}} \left(-0.858906438(2) + \frac{0.0078125}{\varepsilon^2} - \frac{0.0037791975(3)}{\varepsilon} \right) .
\end{aligned} \tag{11.10}$$

The numerical result in the last line is obtained by following the evaluation procedure described above. The numbers in brackets indicate the integration error; for the $1/\varepsilon^2$ terms we were able to perform the integrals analytically, for which we simply quote the first few digits of its numerical value. The precision of order 10^{-9} as quoted in eq. (11.10) for the $1/\varepsilon^0$-term corresponds to about 250 CPU minutes on an 3 GHz AMD A8 processor; a precision of $10^{-6}(10^{-4})$ could be achieved within about ten (two) minutes. The CPU time for the $1/\varepsilon$ term is typically several orders of magnitude smaller.

11.3 VALIDATION OF THE CALCULATION

We successfully completed the following checks for the validity of our calculation. They also provide proof that our numerical integration error estimation is conservative.

LOWER ORDER RESULTS. It is important to note that our calculation does not rely on any of the results of refs. [154, 155]. The fact that we reproduced the NLO results evaluated in these papers is therefore an important check of the setup in general. Since the NLO result is known analytically, we can use it also to cross check the numerical accuracy claimed by our integration routine. We find rather conservative estimates, and our numerical result agrees with the analytical expression through 10^{-15}.

RENORMALIZATION: SUBTRACTION OF UV-POLES. The terms of order $1/\varepsilon^2$ and $1/\varepsilon$ obtained in our three-loop calculation need to be canceled by the corresponding terms due to the renormalization of the strong coupling at lower orders. We verify this cancellation by analytical integration for the $1/\varepsilon^2$ terms, and numerically through one part in 10^{10} for the $1/\varepsilon$ terms.

The cancellation of poles is equivalent to the renormalization group (RG) invariance of the final result:

$$\mu^2 \frac{\mathrm{d}}{\mathrm{d}\mu^2} \langle E(t) \rangle = 0 \,,$$

where μ is the renormalization scale. $\langle E(t) \rangle$ depends on μ implicitly through $\alpha_s(\mu)$, and explicitly through terms of the form $\log(\mu^2 t)$, since t is the only physical scale for our quantity. Knowing the logarithmic dependence in μ is then equivalent to knowing the one in t. The latter is directly obtained from expanding eq. (11.5) for $\varepsilon \to 0$, while the former follows from RG-invariance and can be derived from lower order terms through the perturbative solution of the QCD renormalization group equation:

$$\mu^2 \frac{\mathrm{d}}{\mathrm{d}\mu^2} \alpha_s(\mu) = \alpha_s(\mu) \beta(\alpha_s) \,, \quad \beta(\alpha_s) = -\sum_{n \geq 0} \beta_n \left(\frac{\alpha_s}{\pi} \right)^{n+1} \,,$$

leading to

$$\alpha_s(q) = \alpha_s(\mu)\left[1 + \frac{\alpha_s(\mu)}{\pi}\beta_0 \ln\frac{\mu^2}{q^2} + \left(\frac{\alpha_s(\mu)}{\pi}\right)^2\left[\beta_1 \ln\frac{\mu^2}{q^2} + \beta_0^2 \ln^2\frac{\mu^2}{q^2}\right] + \ldots\right],$$

with the first two coefficients of the β function given by

$$\beta_0 = \frac{11}{4} - \frac{1}{6}N_f\,, \qquad \beta_1 = \frac{51}{8} - \frac{19}{24}N_f\,,$$

where N_f is the number of active quark flavors. If we then quote our result for the physical choice $\mu = 1/\sqrt{8t}$, the full dependence on μ and t can be easily reconstructed.

TWO-LOOP GLUON PROPAGATOR. As already pointed out above (see the discussion after eq. (11.3)), one class of integrals, namely $M_n(2,2)$, stemming from the first two terms in eq. (11.1), with flowfields of the lowest order $B^a_{\mu,1}$ inserted, is fully determined by the fundamental gluon self energy $D(p)_{\mu\nu}$. Adopting the notation of ref. [154], we may write for SU(N)

$$\begin{aligned}\mathcal{E}_0 &\equiv \frac{g_0^2}{2}\langle \partial_\mu B^a_{1,\nu}\partial_\mu B^a_{1,\nu} - \partial_\nu B^a_{1,\mu}\partial_\nu B^a_{1,\mu}\rangle \\ &= \frac{1}{2}g_0^2(N^2-1)\int_p \mathrm{e}^{-2tp^2}(p^2\delta_{\mu\nu} - p_\mu p_\nu)D(p)_{\mu\nu}\,, \quad (11.11)\end{aligned}$$

where $D(p)_{\mu\nu}$ denotes the unrenormalized full gluon propagator and reads

$$\begin{aligned}D(p)_{\mu\nu} &= \frac{1}{(p^2)^2}\left\{\frac{p^2\delta_{\mu\nu} - p_\mu p_\nu}{1-\omega(p)} + p_\mu p_\nu\right\}, \\ \omega(p) &= \sum_{k=1}^{\infty} g_0^{2k}(p^2)^{-k\varepsilon}\frac{\tilde{\omega}_k\,\mathrm{e}^{-k\varepsilon\gamma_E}}{(4\pi)^{kD/2}}\,.\end{aligned}$$

The perturbative expansion of eq. (11.11) can be calculated analytically. The

coefficients $\tilde{\omega}_i$ can be taken from literature.[1] In Feynman gauge, they read

$$\begin{aligned}
\tilde{\omega}_1 &= C_A\left(\frac{5}{3\varepsilon}+\frac{31}{9}\right) - N_f T_R\left(\frac{4}{3\varepsilon}+\frac{20}{9}\right) + \mathcal{O}(\varepsilon)\,,\\
\tilde{\omega}_2 &= -C_A^2\left(\frac{25}{12\varepsilon^2}+\frac{583}{72\varepsilon}+\frac{14311}{432}-\zeta(3)-\frac{25}{12}\zeta(2)\right)\\
&\quad + 2N_f C_F T_R\left(\frac{1}{\varepsilon}+\frac{55}{6}-8\zeta(3)\right)\\
&\quad + 2N_f C_A T_R\left(\frac{5}{6\varepsilon^2}+\frac{101}{36\varepsilon}+\frac{1961}{216}+4\zeta(3)-\frac{5}{6}\zeta(2)\right)+\mathcal{O}(\varepsilon)\,,
\end{aligned}$$

where C_A and C_F are the $\mathrm{SU}(N)$ Casimir operators, T_R is the trace normalization (in QCD $C_A = 3$, $C_F = 4/3$, and $T_R = 1/2$ as commonly used). $\zeta(z)$ is Riemann's zeta function.

Comparing the result $\mathcal{E}_0$ obtained analytically in this way with our numerical result, we find agreement at the level of one part in 10^8, and observe that the error for the finite part is overestimated by a factor of five.

DERIVATIVES IN THE FLOWTIME. For an integral of the form $I(t,\boldsymbol{a},\boldsymbol{\nu},D)$, as in eq. (11.4), we can compute the derivative with respect to t in two ways: either by applying it to the integrand on the l.h.s. of eq. (11.4) and then calculating the resulting integrals with our setup, or by using eq. (11.5), which implies

$$t\frac{\mathrm{d}}{\mathrm{d}t}I(t,\boldsymbol{a},\boldsymbol{\nu},D) = d\cdot I(t,\boldsymbol{a},\boldsymbol{\nu},D)\,,$$

with d given in eq. (11.5). We have confirmed the equivalence of both approaches in our setup for some of the most complicated integrals at the level of one part in 10^{10}.

GAUGE PARAMETER INDEPENDENCE. Our setup allows us in principle to perform the calculation for arbitrary gauge parameter $\alpha_0 \neq 1$ (see eq. (10.2)). We have confirmed general α_0-independence at NLO, where the number of terms to be evaluated increases by about a factor of ten compared to the case $\alpha_0 = 1$. At NNLO, however, with a choice of $\alpha_0 \neq 1$ the number of terms makes it impractical to efficiently generate, reduce and integrate the resulting integrals

1 Two-loop calculations of the gluon propagator were first reported in [461–464]; we use the result quoted in [465] here.

with meaningful precision in reasonable time. A much more practical way, though still powerful, is to perform an expansion around $\alpha_0 = 1$ and consider only the term of first order $c_1 \delta\alpha_0$ as in:

$$\langle E \rangle = \langle E \rangle \,|_{\alpha_0=1} + c_1 \delta\alpha_0 + \ldots + c_n (\delta\alpha_0)^n \,, \quad \delta\alpha_0 = (\alpha_0 - 1).$$

Since α_0 appears in a non-polynomial way in eq. (10.8), infinitely many terms contribute.

In this way, the number of integrals contributing to c_1 increases again only by a factor of ~ 10 with respect to $\langle E \rangle \,|_{\alpha_0=1}$. We find gauge parameter independence of the NNLO result for $\langle E \rangle$ at $\mathcal{O}(\delta\alpha_0)$ through 10^{-3} for the finite term and 10^{-10} for the $1/\varepsilon$ pole terms. The reported integration error for the finite terms is two times larger than the result. Assuming that gauge invariance indeed holds we can conclude for a conservative error estimate by this fact.

12

RESULTS AND DISCUSSION

Having calculated the integrals at order $1/\varepsilon^2$, $1/\varepsilon$ and $1/\varepsilon^0$ we renormalize the bare coupling g_0 in the $\overline{\text{MS}}$ scheme with an associated renormalization scale μ according to [397, 466]

$$g_0^2 = g^2 \mu^{2\varepsilon} \left(4\pi\, \mathrm{e}^{-\gamma_E}\right)^{-\varepsilon} \left\{1 + b_0 \frac{g^2}{(4\pi)^2} + b_1 \frac{g^4}{(4\pi)^4} + \mathcal{O}(g^6)\right\}, \tag{12.1}$$

$$b_0 = \frac{-11}{3} + \frac{2}{3}\frac{N_f}{\varepsilon}, \quad b_1 = \frac{121}{\varepsilon^2} - \frac{51}{\varepsilon} - \frac{44}{3}\frac{N_f}{\varepsilon^2} + \frac{19}{3}\frac{N_f}{\varepsilon} + \frac{4}{9}\frac{N_f^2}{\varepsilon^2}. \tag{12.2}$$

We write our result for the vacuum expectation value of the action density as

$$\mathcal{E} := t^2 \langle E(t) \rangle = \frac{3\alpha_s}{4\pi} \left(1 + \alpha_s k_1 + \alpha_s^2 k_2\right), \tag{12.3}$$

where $\alpha_s \equiv \alpha_s^{(N_f)}(\mu)$ is the strong coupling renormalized at the scale μ with N_f active quark flavors, which are assumed massless. We also set $\mu = 1/\sqrt{8t}$ to obtain the perturbative coefficients k_1 and k_2 as in eq. (12.4). With respect to the interpretation of $\sqrt{8t}$ as the gauge field smoothing range, $q_8 \equiv 1/\sqrt{8t}$ is a natural choice for the central value of μ. We find

$$\begin{aligned} k_1 &= 1.097787 + 0.0075552 N_f\,, \\ k_2 &= -0.98224(5) - 0.069913(2) N_f + 0.00187223 N_f^2\,. \end{aligned} \tag{12.4}$$

The NLO coefficient k_1 has been obtained analytically in ref. [154], the NNLO coefficient k_2 is our main result here. The numbers in brackets denote the numerical uncertainty. For the N_f^2-term in k_2 the analytical result is known through the NNLO gluon propagator. Thus, for k_1 and the k_2 N_f^2-term we simply quote the first few digits of their numerical values.

The result for a general simple Lie-algebra reads

$$
\begin{aligned}
t^2 \langle E(t) \rangle &= \frac{3\alpha_s}{4\pi} \frac{N_A}{8} \left(1 + \alpha_s k_1 + \alpha_s^2 k_2\right) , \\
k_1 &= 8 \cdot \left(0.045741114\, C_A + 0.001888798\, T_R N_f\right) , \\
k_2 &= 8 \cdot \Big(- 0.0136423(7)\, C_A^2 \\
&\quad + T_R N_f \, \left(0.006440134(5)\, C_F - 0.0086884(2)\, C_A\right) \\
&\quad + T_R^2 N_f^2\, 0.000936117\Big) ,
\end{aligned}
$$

where, as aforementioned, C_A and C_F are the Casimir operators of the adjoint and fundemental representations, respectively, T_R is the trace normalization, and N_A is the dimension of the adjoint representation. For $\mathrm{SU}(N)$ the identities $C_A = 2\, T_R N$, $C_F = T_R(N^2 - 1)/N$ and $N_A = N^2 - 1$ hold.

Since this is a one-scale problem, one can reconstruct the full logarithmic dependence of μ and t through the QCD renormalization group equation (see paragraph about renormalization in section 11.3).

12.1 PERTURBATIVE UNCERTAINTY OF $t^2 \langle E(t) \rangle$

In fig. 12.1 we show the effect of a μ variation for different values of the flowtime t. Since t has the unit of inverse energy squared ($1/\mathrm{GeV}^2$), we rather use $q_8 = 1/\sqrt{8t}$ as a representative for t, which has the unit GeV. The value of $\alpha_s^{(N_f)}(\mu)$ is derived from the reference input value $\alpha_s^{(5)}(m_Z) = 0.118$ [130] as follows. We perform a four-loop running [396, 397] down to $\alpha_s^{(3)}(\mu_c)$, where $\mu_c = 2m_c = 2 \times 1.67\,\mathrm{GeV}$, while the bottom and charm quark thresholds $\mu_b = 4.78\,\mathrm{GeV}$ and μ_c, respectively, are crossed with three-loop on-shell decouplings[1, 2] [250]. Additionally, we evolve to $\mu = q_8$ with four loops. This value is our input starting value for α_s at the physical scale q_8 for the observable. For the variation of μ around q_8, we run up and down with (one, two and three) loops for the (LO, NLO and NNLO) perturbative expansions of $t^2 \langle E(t) \rangle$ to obtain the curves. This procedure is also depicted in fig. 12.2.

1 Public codes for running and decoupling are available through refs. [467, 468], for example.

2 Consistency for n loop running only requires $n - 1$ loop decoupling relations. Four-loop decoupling relations are available in refs. [253, 254].

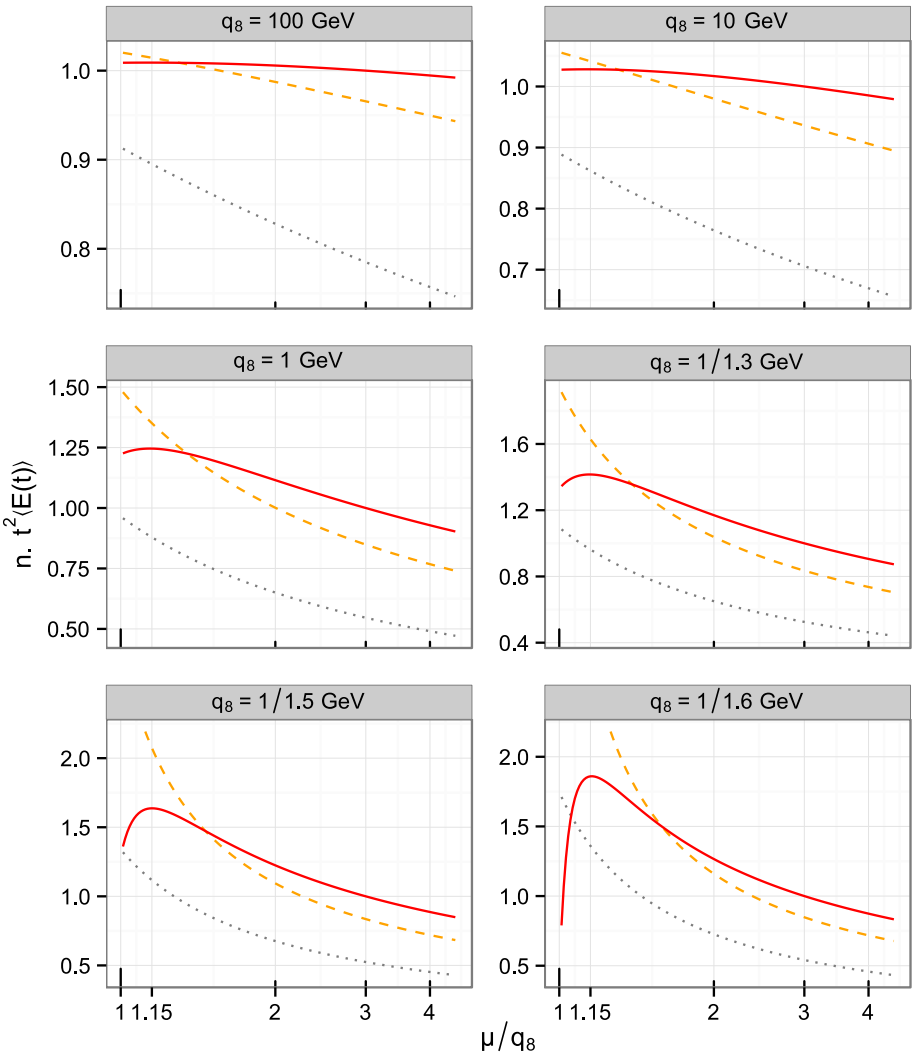

Figure 12.1: $t^2 \langle E(t) \rangle$ for $N_f = 3$ as a function of μ/q_8 for various values of q_8 at LO (black dotted), NLO (orange dashes), NNLO (red solid). All curves are normalized to the NNLO result at $\mu = 3q_8$. Note the different scales for each plot.

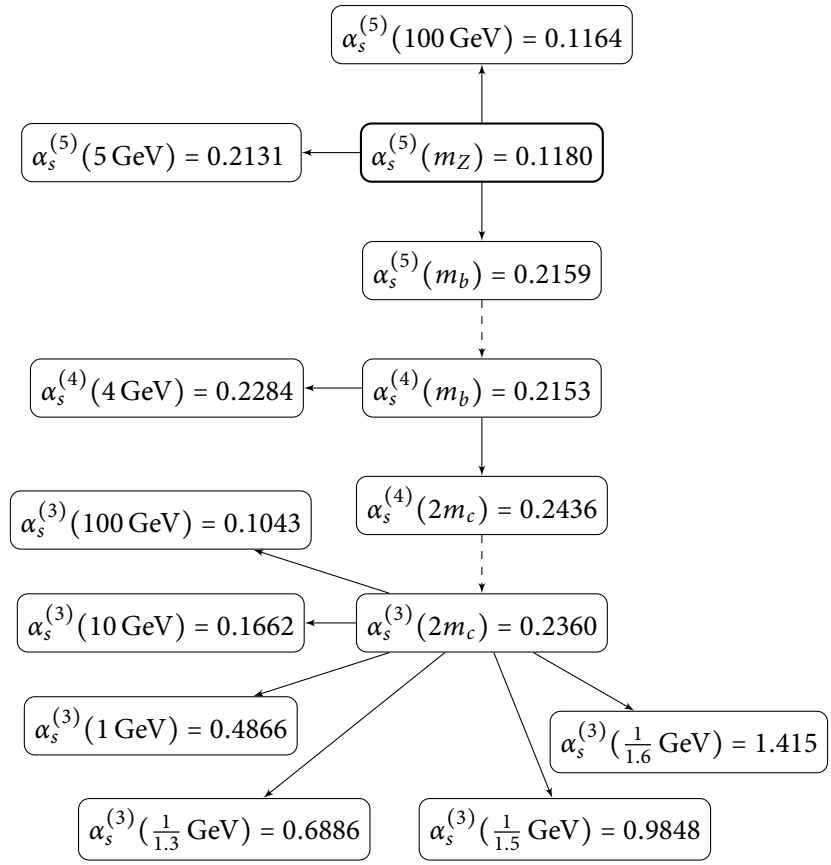

Figure 12.2: Evolution of α_s from the input value $\alpha_s^{(5)}(m_Z)$ as in ref. [444]. Solid arrows denote four-loop RG evolution, dashed arrows three-loop decoupling of heavy quarks.

As expected, as long as the energy scale q_8 is not too small, the dependence on μ decreases significantly with increasing loop order. Going toward values below $q_8 = 1\,\text{GeV}$, we see the breakdown of the perturbative expansion, where α_s approaches a numerical value of one. The minimum energy allowing still a quantitative prediction is around $q_8 \sim 0.7\,\text{GeV}$, corresponding to a distance of about 0.3 fm. For lower energies the uncertainty at NNLO becomes of the order of 100%.

Let us remark that in any case the NNLO result exhibits a maximum for about $\mu = 1.15 q_8$, which is especially pronounced at small energies. Because of this and the fact that varying μ below q_8 for small q_8 will reach into the non-perturbative regime, we estimate the perturbative uncertainty through μ variation between

$1.15q_8$ and $3q_8$. We define the relative uncertainty of $\mathcal{E} = t^2 \langle E(t) \rangle$ as

$$\frac{\Delta\mathcal{E}}{\mathcal{E}} = \frac{\mathcal{E}(\mu = 1.15q_8) - \mathcal{E}(\mu = 3q_8)}{\mathcal{E}(\mu = 1.15q_8) + \mathcal{E}(\mu = 3q_8)} \,. \tag{12.5}$$

With this definition we get uncertainties for $q_8 = 1\,\text{GeV}$, 3 GeV and 100 GeV as written in table 12.1. Clearly there is a large improvement going from LO to NLO and then to NNLO, allowing for quantitative predictions even at lower energies.

Plotting $t^2 \langle E(t) \rangle$ as a function of $1/q_8 = \sqrt{8t}$ at LO, NLO and NNLO with bands displaying the variation of μ between $1.15q_8$ and $3q_8$, we obtain fig. 12.3. The input value is derived as above, that is, we start with $\alpha_s^{(5)}(m_Z) = 0.118$ from which we derive $\alpha_s^{(3)}(q_8)$ by four-loop running and three-loop matching (see fig. 12.2). One observes that the NLO and NNLO bands nicely overlap, which gives confidence in using these bands to measure the theoretical uncertainty. At LO though there is hardly any overlap with the other bands. At $q_8 = 1/1.7\,\text{GeV}$ the four-loop evolution of α_s from m_Z to q_8 breaks down.

Table 12.1: Uncertainties for $t^2 \langle E(t) \rangle$ obtained by a μ variation between $1.15q_8$ and $3q_8$ following eq. (12.5) for different values of $q_8 = 1/\sqrt{8t}$.

loops	$q_8 = 1\,\text{GeV}$	$q_8 = 4\,\text{GeV}$	$q_8 = 100\,\text{GeV}$
one	23.3	12.7	6.6
two	22.8	8.2	2.5
three	10.9	2.6	0.4

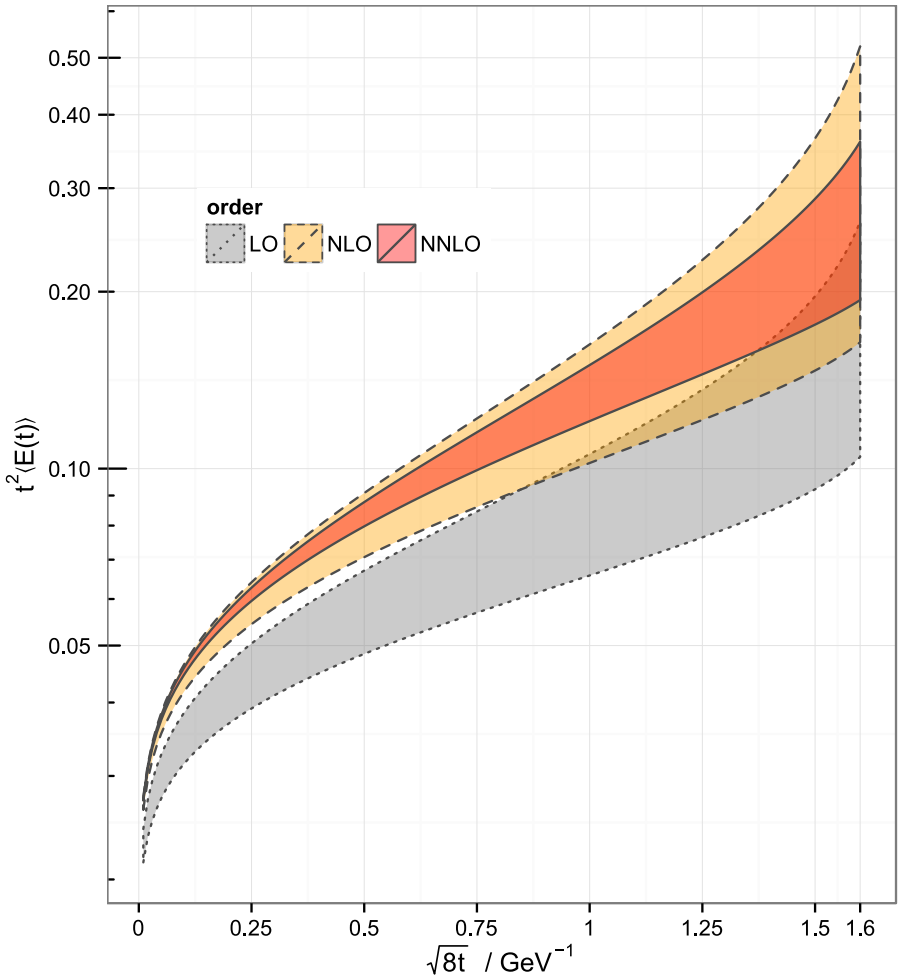

Figure 12.3: $t^2 \langle E(t) \rangle$ for $N_f = 3$ as a function of $\sqrt{8t}$ (in GeV^{-1}) for $\mu = 3q_8$ (lower) and $\mu = 1.15q_8$ (upper) at LO (gray), NLO (orange), and NNLO (red).

12.2 EXTRACTION OF α_s

To our knowledge, one of the most interesting applications of our result could be the determination of $\alpha_s(m_Z)$ using lattice data as input. $t^2 \langle E(t) \rangle$ can be computed in lattice QCD relatively easily to a high precision and can also be used for a running coupling definition. By means of a technique called step scaling [151] it can even be calculated in principle to high energies, reaching into the perturbative regime accessible from our result [159, 162, 447].

The idea is to solve the following equation for $\alpha_s(\mu)$:

$$e(t) \stackrel{!}{=} t^2 \langle E(t) \rangle = \frac{3\alpha_s}{4\pi} \left(1 + \alpha_s k_1 + \alpha_s^2 k_2\right) , \tag{12.6}$$

where $e(t)$ is assumed to be $t^2 \langle E(t) \rangle$ obtained non-perturbatively (lattice QCD) with a high precision, while the right hand side is our perturbative NNLO result. By solving this equation for $\alpha_s^{(N_f)}(\mu)$, we can extract α_s at the renormalization scale μ in the N_f-flavor scheme. Evolving it perturbatively up to m_Z, we extract the reference value $\alpha_s^{(5)}(m_Z)$. For our NNLO result and $N_f = 3$, the evolution is performed with three-loops, and matching is performed at the charm and bottom thresholds, specified as above, with two-loops. For lower order results of $t^2 \langle E(t) \rangle$ the running and matching is performed with correspondingly fewer loops. The uncertainty can be estimated by varying the extraction scale. That means that we first solve the equation for our central value of $\mu = q_8$ and evolve $\alpha_s^{(3)}(\mu = q_8)$ to $\mu = m_Z$. Then, for the error estimation we additionally solve it for values of $1.15 q_8$ and $3 q_8$ and again evolve the coupling to $\mu = m_Z$. In each case we take into account the matching at the charm and bottom thresholds, of course.

Since we do not have a lattice QCD result at hand, we assume a value for $e(t)$. We choose it to be our perturbative NNLO expression for $t^2 \langle E(t) \rangle$ at $\mu = q_8$ and $N_f = 3$, where the numerical value for $\alpha_s^{(3)}(q_8)$ is derived by three-loop running and two-loop matching ($\mu_b = m_b$, $\mu_c = 2m_c$) from the input value $\alpha_s^{(5)}(m_Z) = 0.118$.

The result of this procedure is shown in fig. 12.4. By construction, the red NNLO band always includes the value 0.118. The uncertainty value is calculated by taking the relative width of the bands of the plot:

$$\frac{\Delta\alpha_s}{\alpha_s} = \frac{\alpha_s^{\max}(m_Z) - \alpha_s^{\min}(m_Z)}{\alpha_s^{\max}(m_Z) + \alpha_s^{\min}(m_Z)} . \tag{12.7}$$

Similarly to $t^2 \langle E(t) \rangle$ in fig. 12.3, the width of the bands decreases remarkably toward higher orders of perturbation theory, and the NNLO band lies completely within the NLO band, while LO has no overlap with NLO. If $e(t)$ was given at $q_8 = 10\,\text{GeV}$, the NNLO uncertainty on $\alpha_s(m_Z)$ would be about one percent. Trying to reach world average accuracy of 0.5% on $\alpha_s(m_Z)$ requires an extraction at about $q_8 = m_Z$.

Once one reaches sub percent accuracy of this leading uncertainty source, that

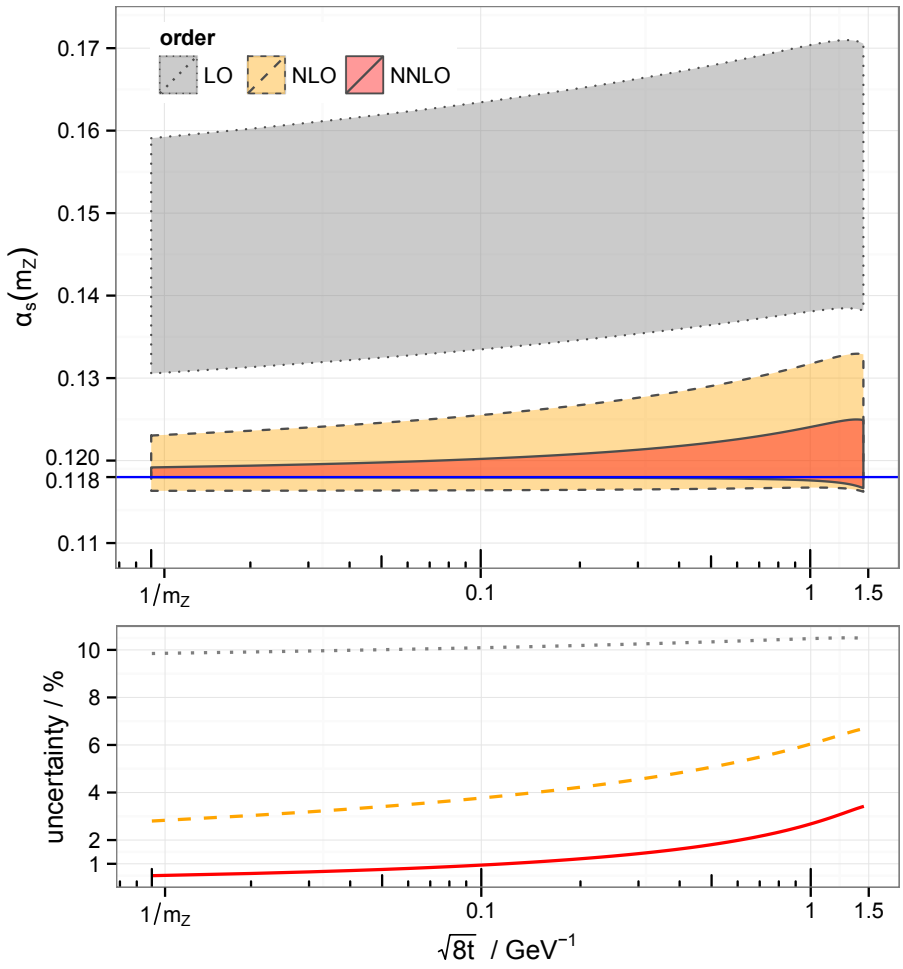

Figure 12.4: Upper plot: numerical value for $\alpha_s^{(5)}(m_Z)$ derived at LO (gray), NLO (orange), and NNLO (red) from a hypothetical exact value of $t^2 \langle E(t) \rangle$. Lower plot: corresponding theoretical uncertainty (see eq. (12.7)).

is the perturbative truncation of $t^2 \langle E(t) \rangle$, one also has to consider sub-leading uncertainties like the decoupling scheme dependence. While we decoupled and coupled the heavy quarks with on-shell masses in the on-shell scheme, we checked that changing the scheme to $\overline{\text{MS}}$ with $\overline{\text{MS}}$ masses has an impact of only a few per mill. This only becomes relevant if the extraction takes place at values $q_8 \sim m_Z$. Also the variation of the charm and bottom decoupling scales has to be accounted for then. Lastly, non-perturbative effects for $\alpha_s \simeq 1$ could become important for energies reaching as low as the charm quark mass.

The uncertainty for $e(t)$ obtained from lattice QCD is expected to be small, but will also have to be considered.

12.3 SUMMARY AND OUTLOOK

We calculated the action density $\langle E \rangle$ for the QCD gradient flow at three-loop (NNLO) level. We used Wick contractions to derive the integrals in the perturbative expansion. The integrals were regularized in dimensional regularization, and pole terms for $D \to 4$ were separated by sector decomposition. Afterwards, the resulting finite integrals were evaluated with a high precision integration routine. A validation of the result through a number of strong checks has been performed.

The expansion of $\langle E \rangle$ up to NNLO shows a well converging perturbative series down to scales of about $q_8 \sim 0.7\,\text{GeV}$. We showed that an extraction of α_s is possible at percent or sub-percent accuracy when lattice QCD results for a comparison reach energy scales q_8 of a few GeV. This seems well within reach of current means.

Inclusion of quark mass effects, induced by quark loops from fundamental QCD, could become important for smaller energies q_8 or in the vicinity of quark thresholds. This could become one of the next tasks. The application of the flow equation to quark fields [156] itself might also be interesting to consider perturbatively.

Though *in principle* our setup has no limitation to three loops, for a higher number of loops, firstly, the Wick contraction approach becomes impractical, which could be overcome by a diagrammatic generation of integrals. Secondly, the number of integrals increases considerably, and a reduction to a small number

of master integrals does not seem feasible. With a diagrammatic approach the N^3LO calculation via sector decomposition is not out of reach though.

A

DOCUMENTATION OF THE GRADIENT FLOW SETUP

This appendix serves as a documentation of the perturbative gradient flow setup, developed for the calculation of $t^2 \langle E(t) \rangle$ at NNLO using Wick contractions and sector decomposition. The aim is, firstly, to give an overview of the setup to someone who would want to use it to reproduce the results and, secondly, to give a general impression of methodologies and implementation details.

The first part of the setup, the generation of the momentum integral expressions, up to obtaining the sector decomposed parameter integrals, is implemented in `Mathematica 7` [451]. The second part, consisting of the numerical integration of such obtained integrals, is performed by a C++ integration routine and a light wrapper, written in Haskell, to manage the huge amount of integrals and files. Since each integrand is compiled as a simple function in a library, the wrapper allows for choosing different integration routines and precision goals.

A.1 GENERATION OF MOMENTUM INTEGRALS

The code for the perturbative expansion step is completely contained in the files `FlowfieldExpansion.m`, `FlowUtilities.m`, `Reduction.m` and `FIntegrate.m`. Usually all files should be included in a notebook to work with the setup. A global variable `$FlowBaseDir` specifies the output directory for intermediate and result files.

We have discussed in section 11.1 that IBP reduction does not help in the gradient flow calculation since integral coefficients develop new unregularized singularities in the flowtime integrations. Nevertheless, with the help of `FIRE4` and functions in `IBP.m`, an IBP reduction can be performed.

A.1.1 *Expansion in fundamental gauge fields*

In the first step, the perturbative expansion of $\langle E \rangle$ in terms of vertex functions and fundamental fields is performed in the function

```
IntegralsA[numA_,order:6,numB_:{2,3,4}],
```

where `numB` is a set of different k in the categorization $M_n(k,m)$ in eq. (11.3), `order` denotes the expansion order n in the gauge coupling g_0^n, and `numA` corresponds to m – it specifies how many fundamental gauge fields A, obtained from the expansion of the flowfields B in terms of A's, should be kept.

The observable $\langle E(t) \rangle$ in `IntegralsA` is expressed as

```
  1/2*Diff[Bn[nu, a, p], mu] * Diff[Bn[nu, a, q], mu] * MomInt[p, q]
- 1/2*Diff[Bn[nu, a, p], mu] * Diff[Bn[mu, a, q], nu] * MomInt[p, q]
+ ColorMath`f[a, b, c] * Diff[Bn[nu, a, p], mu] * Bn[mu, b, q] *
      Bn[nu, c, r] * MomInt[p, q, r]
+ 1/4*ColorMath`f[a, b, e]*ColorMath`f[c, d, e] *
     Bn[mu, a, p] * Bn[nu, b, q] * Bn[mu, c, l] * Bn[nu, d, m]*
      MomInt[p, q, l, m],
```

where the meaning of the individual expressions should be clear from the general context. If `numB` contains only 2, then only the first two terms with two `Bn` field expressions are taken, otherwise if numB contains 3 (4), also the third (fourth) terms are taken. In principle any other observable can be implemented here.

The flowfields `Bn[mu,a,p]` are replaced by a sum `g0^i Bexp[i,mu,a,p]` for $i = 1,\ldots,$`order` $- 1$ as the first terms in the recursive B-field expansion. The derivatives are taken into account as in

```
Diff[Bexp[n_,mu_,a_,p_],nu_] -> I*FVD[p,nu]*Bexp[n,mu,a,p],
```

where `FVD[p,nu]` specifies the four-vector p_ν. Subsequently, the perturbative expansion in the fundamental QCD vacuum is performed by multiplying with

```
Exp[g0*3GluonVertex + g0*QuarkGluonVertex +
                g0*GhostGluonVertex + g0^2*Gluon4Vertex],
```

and expanding the whole expression up to the order specified as argument to `IntegralsA`. The vertex factors are expressed in terms of the fundamental fields,

Dirac delta functions, metric tensors (MTD) and color factors as follows:

```
Gluon4Vertex := -1/4*
        Module[{mu, mup, nu, nup, a, ap, b, bp, c, cp, p1, p2, p3, p4},
                DiracDelta[p1 + p2 + p3 + p4]*MTD[mu, mup]*MTD[nu, nup]*
                ColorMath`\[Delta\][a,ap] * MomInt[p1, p2, p3, p4] *
                ColorMath`f[a,b,c] * ColorMath`f[ap,bp,cp]*
                A[mu, b, p1] * A[nu, c, p2] *
                        A[mup, bp, p3] * A[nup, cp, p4]];

Gluon3Vertex := -I*
        Module[{p1, p2, p3, a1, a2, a3, mu1, mu2, mu3},
                MomInt[p1, p2, p3]*DiracDelta[p1 + p2 + p3]*
                ColorMath`f[a1, a2, a3]*
                FVD[p1, mu2]*MTD[mu1, mu3]*
                A[mu1, a1, p1] * A[mu2, a2, p2] * A[mu3, a3, p3]];

GhostGluonVertex := -I*
        Module[{p1,p2,p3, a,b,c, mu3},
                MomInt[p1,p2,p3]*DiracDelta[p1+p2+p3]*
                ColorMath`f[a,b,c]*(FVD[p2,mu3]+FVD[p3,mu3])*
                A[mu3, b, p3] * NC[AntiGhost[a,p1], Ghost[c,p2]]];

QuarkGluonVertex :=
        Module[{p,a,mu, ci,cj, i,j, q,r},
                A[mu,a,p]*NC[AntiQuark[i,ci,q],Quark[j,cj,r]]*
                DiracGammaC[mu,i,j]*ColorMath`t[{a},ci,cj]*
                MomInt[p,q,r]*DiracDelta[p+q+r]];
```

In the end of the function, only terms that contain numA fundamental gauge fields from the B-expansion are returned by counting the n's from the multiple Bexp[n,mu,a,p] expressions for all terms. The placeholder B-field expressions Bexp[n,mu,a,p], to be evaluated up to order n, are then replaced by B[n,mu,a,t,p]. The latter are implemented as the recursive expansion of the flowfield up to order n in terms of expressions like MomInt[p,q,..], representing momentum integrations, Dirac delta functions DiracDelta[p+q,...], flowfield vertices X20[p,q,r,a,b,c,mu,nu,rho] and X30[...] (eq. (10.6)), K[mu,nu,t,p] (eq. (10.8)), gauge fields A[nu,a,p], as well as factors representing flowtime integrations FInt[s,0,t].

Remark: The uniqueness of integration variables and indices is ensured by using initially module scoped variables in the returned expressions, as in the definition of the vertices above, for example.

A.1.2 *Simplifications and reductions*

The next steps are performed in `ProcessInts[expr_, file_,loops_:3]`, where `expr` denotes the expressions obtained from `IntegralsA`, `file` is an output filename to which the final results will be written with the `Mathematica` function `Export`, and `loops` is the number of loops, a parameter which helps to eliminate vacuum bubble terms after evaluation of the delta functions.

`ProcessInts` calls step by step `NewFullExpand`, `LightCanonicalizeTerms`, `CancelPropagators`, `CanonicalizeTerms`, then `ZeroScalelessIntegral`, and finally `PermutationDuplicates` on the sum of integrals. In the following subsections these functions are explained.

Wick and other contractions

The function `NewFullExpand[expr_,loops_:3]` applies the following actions on the integrals:

- Perform Wick contractions of gauge and fermionic fields (quarks, ghosts) with the functions `MultiWick` and `FermiWick` (implemented for any number of fields, giving $(2n-1)!!$ terms for n involved fields). For example, gauge field Wick contractions lead to expressions of the form `MTD[mu,nu]*DiracDelta[p+q]*Prop[p]` times a color factor, where `MTD[mu,nu]` corresponds to the metric tensor $g_{\mu\nu} \equiv \delta_{\mu\nu}$ and `Prop[p]` to a propagator term $1/p^2$.

- Combine multiple `MomInt`, `Prop`, `DiracDelta` factors in each summand with `ContractLabels` to sequence arguments, for example as in `Prop[a_]*Prop[b_] -> Prop[a,b]`.

- Evaluate expressions like `DiracDelta[k1,..,kn] * MomInt[p,q,..]` with the function `EnforceDelta` by trying to solve the system $\{k_1 = 0, \ldots, k_n = 0\}$ for all appearing momentum variables in `MomInt`. Subsequently, the momentum replacements are done in the integral expression.

- Filter trivial vacuum bubbles by removing remaining terms with the wrong number ($\neq$ `loops`) of momentum integrations.

- Calculate gamma matrix traces (with `FeynCalc` [452]) and insert factors of N_f for each trace.

- Insert the vertex expressions for `K`, `X20`, `X30` in terms of metric tensors `MTD[mu,nu]`, four vectors `FVD[p,rho]`, color factors and exponential factors `Exp[-t*p^2]`.

  Remark: If we want to calculate the first term in the expansion of the gauge parameter α_0 around 1, we insert additional factors for `K` and `X20` here.

- Calculate color factors in `OnlyColorSimplify` with `ColorMath` [453] wrapped in a memoization function that stores previously computed color factors.

- Contract metric tensors and four vector expressions. Scalar products $p \cdot q$ are represented as `Pair[Momentum[p,D],Momentum[q,D]]` to match `FeynCalc` syntax, although the contractions are performed independently for performance reasons.

At this point the momentum integral expressions are in a syntactic form that can be directly used to generate the Schwinger parameter representation. But before we do this, we apply a series of further reductions that will completely eliminate duplicate integrals which are equivalent under renaming of dummy names and under linear shifts in momenta. Furthermore, we will remove scaleless integrals.

Cancellation of numerators with propagators

The first large step in the simplifications is to cancel numerator terms with propagators. Before that, we apply a 'light' reduction of integrals as follows.

Firstly, `LightCanonicalizeTerms`, called with the integrals as argument, renames all dummy names (like p$4320, a$921, etc. from module scope) with the functions `SimplifyNames` and `SimplifyMomNames` to well defined sets: all flow-time integration variables are taken from the set $\{s,u,s2,s3\}$, Schwinger parameters (to be introduced later) from $\{\alpha,\beta,\gamma,\delta,\varepsilon,\ldots\}$, and momentum names from k,q,r. Secondly, it factors expressions like `Exp[..]`, `FInt[..]`, `Prop[..]` into an argument of a new function `Integral[Exp[..] FInt[..] Prop[..] ..]`,

such that only prefactors independent of the integration remain outside. Through the function `ReduceCanonical`, integrals are reduced as in the replacement

```
a_*Integral[x_] + b_*Integral[x_] :> Simplify[a+b]*Integral[x],
```

but considerably faster.

Finally, `CancelPropagators` is used to cancel numerator factors with propagators. It relies on a few auxiliary functions, explained in what follows. First off, `CancelPropagators` acts as expected: it takes a momentum integral and cancels all numerator scalar products against a constructed propagator basis as far as possible. It uses the function `ToPropagatorBasis[lmom,lprop]`, where `lmom` is a list of integration momenta and `lprop` is a list of propagators in the same form as in the `Prop[p,q,p+q,..]` expressions. We will call this form of denoting propagators 'linear', and 'squared' when they are squared, i.e. $(p+q)^2 = p^2 + 2pq + q^2$. `ToPropagatorBasis` returns a tuple (list) of:

1. the replacement rules necessary to replace all numerator scalar products to `PropIncr[i]` and `PropDecr[j]` expressions, denoting operators to increase or decrease a specific propagator power of the propagator basis.

2. the complete basis (a possible extension of the list of given propagators), which `i` and `j` refer to. The basis is given in 'linear' form.

`ToPropagatorBasis` itself uses `CompletePropBasis[lmom,lprop]`, which returns a triple (list) of:

1. a basis transformation matrix from propagator to trivial basis.

2. the propagator basis (extended from given list `lprop`) in linear form.

3. the trivial basis in squared form.

By trivial basis we mean the set of all scalar products between the integration momenta, including themselves. For example in case of momenta p,q the trivial basis is the set $\{p^2,q^2,r^2,pq,pr,qr\}$. The propagator basis denotes the elements in `lprop` extended by additional elements of the trivial basis.

The provided list of propagators must not contain any duplicates, except for those that can be removed by `DeleteDuplicates`. Also, linearly dependent

propagators will pose a problem. That is, if enough elements in `lprop` are provided, which do not form a basis, just these will be returned.

The propagator elements are augmented to a basis by additional elements from the trivial basis as follows. We know that a basis must have $n+\binom{n}{2}$ elements, where n is the number of integration momenta. Assuming that propagators in `lprop` are linearly independent, we thus know how many propagators x are missing for a basis. We take x-subsets of the trivial basis and check if the combined basis of `lprop` and the x-subset provides a transformation from the trivial basis to the newly constructed set. The transformation from the propagator basis to the trivial basis is trivially obtained by just expanding all scalar products. We can just construct this transformation matrix and check if the inverse exists. If this is the case, we will keep the new set as the propagator basis in a slightly modified way: Instead of using scalar products $p \cdot q$, we will use in these cases $(p+q)^2$. For new elements of the simple form k^2 we just keep them.

Canonicalization and scaleless integrals

The next step in `ProcessInts`, after the cancellation of numerator factors with propagators, is to feed the integrals to `CanonicalizeTerms`. It is a heavier version of the previously introduced `LightCanonicalizeTerms`, and again factors off prefactors by putting all ingredients which are relevant for the integration in a `Integral[..]` expression and combines identical integrals with different prefactors. Additionally, it then derives the Schwinger parametrization (with `PrepareShift` as elaborated in appendix A.2 on page 125) for all integrals and compares these naively, that is, permutations of variable names are not taken into account.

`ProcessInts` then calls `ZeroScalelessIntegral` for all remaining integrals. Again through the Schwinger parametrization, with `PrepareShift`, and a procedure described in ref. [454, see eq. (16)], we nullify scaleless integrals. The idea is to check, algebraically, if a subset of Schwinger parameters exists, that, when scaled by a parameter, can be completely factorized off as a single factor in the integrand; that is, to check if the integrand is homogeneous with respect to such a subset [216, ch. 9.4].

Checking variable name permutations

The last step in `ProcessInts` is the final elimination of equivalent integrals by checking all integration variable name permutations: `PermutationDuplicates` checks in the Schwinger parameter representation of all integrals, which only contain the integrations over Schwinger and flowtime parameters, all permutations of said parameters and compare them with all other integrals one by one. It is clear that integrals with different numbers of flowtime and Schwinger parameter integrations need no comparison. The cases of different number of integrations are all treated separately. It is a very hard task to check the equivalence of two symbolic expressions efficiently, such that we use a numerical solution here.

This is done in the function `IntegralHash`. Firstly, for a given list of (random) numbers we set the flowtime and Schwinger parameters one by one to the values in the list and also take a value for the space-time dimension. Then we take all other permutations of parameters and also set them to the values in the list. This results in a list with numbers, where each number stems from a different permutation. We sort and apply a mathematical hash function, resulting in a final 'integral hash', representing the integral irrespective of integration variable name permutations.

If the integral hashes of two integrals do not match, nothing specific happens. If they match, we make sure they match analytically to a high confidence level by comparing the hashes with 10 other sets of numbers.

After this step we can be certain to have a nearly minimal set[1] of integrals after the inflation by performing Wick contractions.

A.1.3 *Integration by parts*

During the development of the setup the following functions were created to help performing an IBP reduction, though at some point it became clear that IBP reduction is not viable:

1 In principle there are some ambiguities. For example, a different way to extend the propagators to a basis could lead to a different number of integrals.

`CreateIBP` takes an integral in momentum representation and returns a list of IBP equations with symbols `Nu[j]`, corresponding to propagator powers ν_j, and `PropIncr[i]`, `PropDecr[k]` functions, representing increase and decrease operators for propagator powers. Additionally, the propagator basis itself is printed.

With `FIREForm` the list of IBP equations returned by `CreateIBP` is brought into a form that can be directly read by `FIRE4` as the 'startinglist', essentially replacing `Nu[i_]->a[i]`, `PropIncr[j_]->Y[j]`, `PropDecr[k_]->Ym[k]`.

`PropToIBpForm` is an auxiliary function that takes a momentum integral, augmented by an expression `PropBasis[p,q,..]`, representing the propagator basis (which can be added by `AppendPropBasis`), and extends it by a topology identifier `Topology[nu1,..]`.

A.2 Schwinger parameter representation and sector decomposition

The file written by `ProcessInts` after all steps, contains the sum of all integrals. One example term is given as follows:

```
((-30 + 11*D)*Nc^2*(-1 + Nc^2)*TR^2)/8 *
        Integral[ (FInt[s, 0, t]*FInt[s2, 0, u]*
                  FInt[s3, 0, s2]*FInt[u, 0, s]*IntMom[k, q, r]*
                Pair[Momentum[k + q, D], Momentum[k + q, D]]*
                Pair[Momentum[k + r, D], Momentum[k + r, D]]*
                Prop[k - q, q - r]) /
                E^(2*(-(q*r*(s + s3)) + r^2*(s + s3)
                                + k^2*t + q^2*(s2 + t) +
                                  k*(r*(s - u) + q*(-s2 - 2*t + u))))
                ]
```

The next step is to derive the Schwinger representation and feed the resulting expression to the sector decomposition code `FIESTA`.

The Schwinger parametrization of an integral written in momentum representation is obtained by calling `PrepareShift`. It performs the following steps on the integral with small auxiliary functions:

1. Write scalar products $p \cdot q$ as `Diff[xi]*Exp[xi*p*q]`, as a representation

for the identity

$$pq = \frac{\mathrm{d}}{\mathrm{d}\xi} \exp(\xi \cdot pq)\Big|_{\xi=0} .$$

2. Propagators in `Prop[p1,p2,...]` are Schwinger parametrized like `SInt[a]*Exp[-a*p1^2]`. Higher propagator powers are accounted for with `1/Factorial[N-1]*a^(N-1)*Exp[-a*p^2]`, where `N` denotes how often `p` appears in `Prop[...]`.

3. Having all momentum dependence in the form $\exp(-\boldsymbol{p}^T A \boldsymbol{p})$, the integration is performed by taking the determinant of A:

$$\int \mathrm{d}^D \boldsymbol{p_1} \cdots \mathrm{d}^D \boldsymbol{p_n} \exp(-\boldsymbol{p}^T A \boldsymbol{p}) = (4\pi)^{-nD/2} (\det A)^{-D/2} .$$

4. Derivatives with respect to `xi` in `Diff[xi]` factors are evaluated, and `xi` is set to zero afterwards.

5. All flowtime integrations `FInt[si,0,sj]` are scaled to unit intervals. All Schwinger parameter integrations `SInt[a]` are scaled by the flowtime t to make them dimensionless. In principle we know the one scale t dependence beforehand, but such a scaling allows us to factorize t as an additional consistency check:

6. All t dependence is factored out to a global prefactor.

Having obtained the Schwinger representation, we are ready to perform the sector decomposition. The function `WriteIntegralSD` takes an integral and transforms it into a suitable way for the `FIESTA` [220] function `SDEvaluateDirect`, which does the decomposition. Different parameters, specifying if `FIESTA` should combine expressions from different sectors, etc., can be set. For our integrals the best numerical integration results are obtained by not combining any expressions.

Subsequently, `WriteIntegralSD` writes C, C++ and `Mathematica` files of the sector decomposed integrals to `$FlowBaseDir<>"/src/"`. By applying a hash-function to the integral expressions, unique filenames are obtained, which are then returned by `WriteIntegralSD` and must be saved with a reference to the originating momentum integral. The generated C file contains the following

functions, where `f` specifies the integrand:

```
int f (unsigned dim, const double *xx, void *params,
                        unsigned fdim, double *retval);
int f_dim();
char* f_prefac();
int f_pole_order();
double f_scale();
```

The C++ file uses an MPFR [457, 458] based high-precision arithmetics integrand `mpreal f (unsigned dim, std::vector<mpreal> xx)` instead.

`f_dim` returns the integrand dimensionality, `f_prefac` a string of an additional integral prefactor, `f_pole_order` the power of ε for the integral, and `f_scale` a scale factor that should be accounted for with a given integration precision goal. For example, a large color factor of the integral could make it important relative to other integrals. When altogether for the sum of all integrals a fixed absolute precision is demanded, each integral's absolute precision goal is multiplied by `f_scale`.

Finally, the C and C++ files can be compiled into dynamically linked libraries. Then, the wrapper program `calcHashgroup` loads a specified library with an integrand and calls an integration routine for it. The result is saved to the directory `$FlowBaseDir<>"/out/"`. A small `Mathematica` script (`collect.m`) can be used to go through all momentum integrals and load the integration results of the associated sector decomposed expressions. The integrals, which can reach dimensions up to seven for our three-loop calculation, require evaluations with absolute and relative precisions up to 10^{-10} due to, firstly, the large amount of integrals, and, secondly, integrals with large color/dimension prefactors. This precision cannot be reached with Monte-Carlo integrations, and, due to the high required precision, plain `double` integration will lead to problems in singular regions. For these reasons we have implemented our own cubature routine with high-precision arithmetics and based on a high order rule. This is elaborated in appendix B.

A.3 Global structure of the setup

This final section serves as an *explicit* guide to reproduce the results for an arbitrary integral class. To be definite, we work out the steps for the class $M_6(2,2)$,

denoted as 'B2A2' in what follows. In fig. A.1 the steps are visualized in a flow-diagram.

1. Set `$FlowBaseDir` and generate its subdirectories `in`, `out`, `src` and `tmp` (with `mkDir.hs`).

   `/in/` will contain one file for each momentum integral. It will also hold files referring to the sector decomposed representation.

   `/out/` is where the result files and possible error files from the numerical integration will reside.

   `/src/` will contain the C, C++, `Mathematica` integral source files.

   `/tmp/` is the directory for the compiled source files. Progress dumps of the numerical integration, allowing a resumption of an aborted integration, will also be saved here.

2. Use `ints=IntegralsA[2,6,{2}]` to generate raw expression from the B-field and QCD vacuum expansion in terms of the fundamental gauge fields. Of course, integrals from other classes could be added to `ints` here.

3. Perform simplifications with `ProcessInts[ints,"B2A2_3loop.m",3]`. This saves the integrals to `$FlowBaseDir<>"/B2A2_3loop.m"`.

4. Write each integral from `B2A2_3loop.m` with `WriteIn` to a distinct file `B2A2_3loop_i.m` in `$FlowBaseDir<>"/in/"`, where `i` is a counter. This is done in the script `generate.m`.

5. Use `generateSingle.hs` to perform the following steps: Schwinger parametrize each integral in `/in/` with `PrepareShift`, then perform the sector decomposition with `WriteIntegralSD`, which writes the resulting integrals to `/src/`:

   Note that each momentum integral can result in multiple Schwinger parametrized integrals due to the numerator structures. And each Schwinger parametrized integral results in multiple integrals from sector decomposition. Additionally, bubble type integrals with higher propagator powers require a splitting of the Schwinger integration intervals to be convergent after sector decomposition: $(0,\infty)$ is split into $(0,1)$ + $(1,\infty)$ with subsequent scaling to the unit interval. This is handled in `generateSingle.hs`

by using the function `ExpandAllSInts` in `FIntegrate.m`.

`WriteIntegralSD` returns a list of group hashes that each refer to a Schwinger parametrized source integral. The group hashes are written to `in/B2A2_3loop_i.m.hashes`, with the counter `i` running as above over all momentum space integrals. The group hashes refer to the file `/src/<gp>/group_<gh>.m`, where `<gp>` are the first three characters of the group hash `<gh>`. These files contain the hashes for the distinct sector decomposed integrals, each saved in `/src/<prefix>/<hash>.{m,c,c++}`, where `<prefix>` specifies the first three characters of the integral hash `<hash>`.

6. Run `calcHashgroup`, specifying the precision goal and one integral hash. Do this for all integrals generated. Temporary files, like the compiled integrand functions and dumps of the integration progress are saved in `/tmp/<prefix>/<hash>.{so,heap}`. The results are written to the files `/out/<prefix>/<hash>.m`.

7. Go through all hash groups stored in the files `/in/*.hashes`. Lookup all integral hashes in the `group_<gh>.m` files, where `<gh>` denotes the group hash. Subsequently, add all results for these referenced integrals with the prefactors in the `/in/*.m` files. This is done in the `collect.m` script.

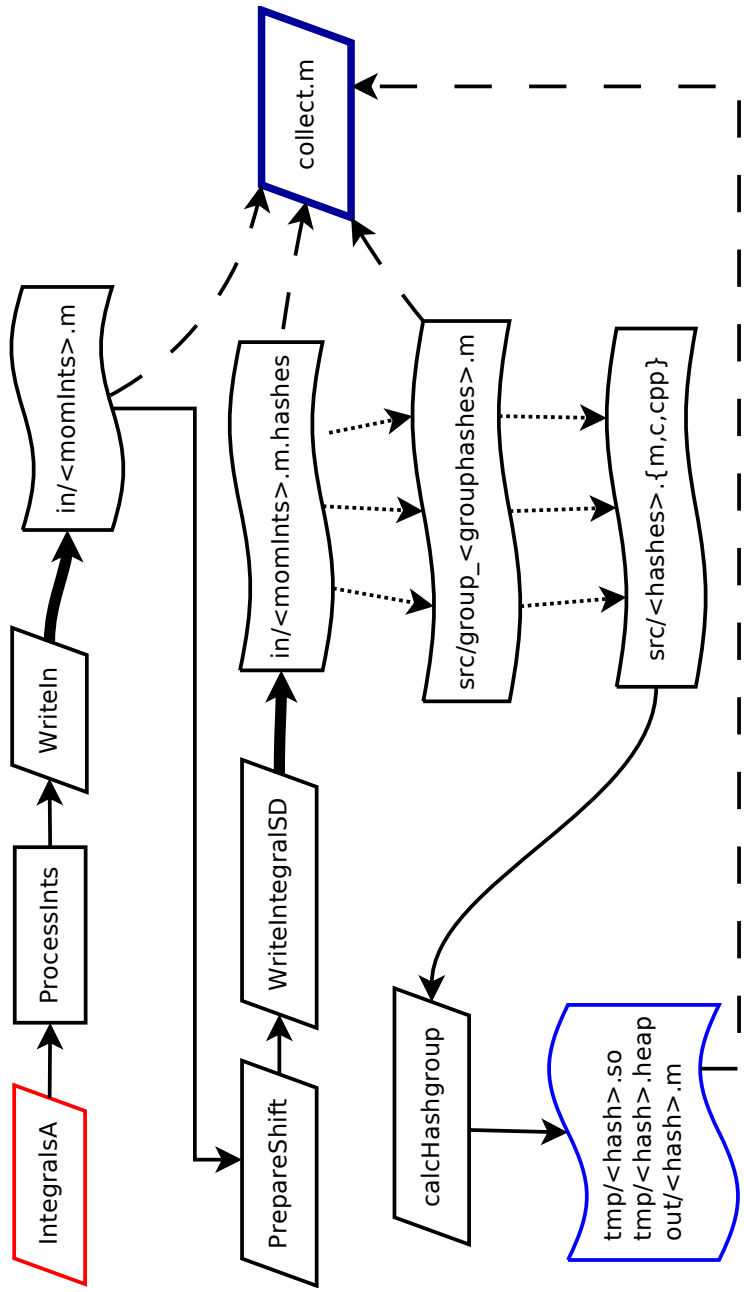

Figure A.1: Schematic overview of the perturbative gradient flow setup. The prefix subdirectories are not shown.

B

NUMERICAL INTEGRATION

The integrals obtained by sector decomposition for our three-loop perturbative gradient flow setup require high absolute and relative numerical precisions. This is, firstly, due to the high number of $\mathcal{O}(10^6)$ integrals, and, secondly, because of single integrals with large prefactors that require a comparatively higher precision. The dimension of the integrals is large, namely seven, but not intractable by non-probabilistic methods [469]. Monte-Carlo approaches, even with importance sampling and subdivision techniques, are not suitable for such high-precision needs.

For moderate precision goals we have had good experience with the double-precision h-adaptive[1] cubature integration in ref. [470]. For our high precision goals of $\sim 10^{-10}$, the error can either become severely mis-estimated, or the integration breaks down in a singular region. In many cases the precision simply cannot be reached. The h-adaptive integration is based on the integration rules of order 5/7 by Genz and Malik [456], and, since it works quite well, we use the same integration rule, but of higher order.

Our multivariate integration routine is based on the embedded family of fully symmetric [471] integration rules in ref. [455] of order 11/13. This means that all multivariate polynomials up to order 11/13, are integrated exactly. The rule of order 13 is used to estimate the error by subtraction from the embedded rule of order 11. Even though the error is estimated for the order 11 rule, we keep the order 13 approximation as the final result, thus, in principle overestimating the error. The error is reduced, up to a certain specified precision goal, by recursively subdividing the region with the largest estimated error. The region is bisected along the coordinate axis where the integrand has the largest local absolute fourth difference [456].

All weights and evaluation points are pre-generated with 300 decimal digits

1 Recursively partitioning the integration domain into smaller subdomains, applying the same integration rule to each, until convergence is achieved.

precision via `Mathematica`. Our routine uses the library `MPFR C++` [457, 458] to perform all parts of the integration with a default precision of 256 bits, corresponding to ~ 77 decimal digits. The precision can be adjusted by setting a variable.

We also implemented the IMT-transformation [460], which can be used to regularize endpoint singularities. The transformation can be activated by specifying the minimum number of bisections from which on the transformation is applied to the subdivisioned interval. Subsequently, the IMT-transformed interval will be adaptively subdivided, and the rules of order 11/13 are applied. For our integrals this lead to no noticeable improvements.

The routine is able to save and load snapshots of the integration progress to a file. The snapshot includes the total integral estimate and error, as well as all subdivisions with their estimates and errors. To limit the number of saved subdivisions, one can specify an error cutoff, below which regions with a smaller error are no longer subdivided nor saved, and just accounted for in the total value and error.

To test the integration, we checked that it successfully integrates multivariate polynomials of seven and more variables and total order 13 to the full 300 decimal digits precision. Additionally, we reproduced the two-loop result of $t^2 \langle E(t) \rangle$ in chapter 10 to a high precision and checked that the results for single integrals are compatible with the result of the h-adaptive cubature routine.

Finally, we note that the integration is largely independent from the rest of the perturbative gradient flow setup, and we plan to release the integration routine for general use in precision critical applications.

C

NORMALIZATION FACTORS FOR KINEMATICAL DISTRIBUTIONS IN CHAPTER 8

This appendix contains all normalization factors σ_{ij} used in the kinematical distributions in chapter 8. They are obtained by integrating corresponding distributions over the whole kinematical range considered, and allow the reconstruction of the distributions absolute values for Wilson coefficients C_i set to one and scales Λ to 1 GeV.

Specifically, the absolute cross sections $\mathrm{d}\sigma_{ij}$ in picobarns are obtained by multiplying the numbers for $\mathrm{d}\sigma_{ij}/\sigma_{ij}$, read off from the figures, by the normalization factors σ_{ij}, given below, times $\mathfrak{Re}(C_i^\dagger C_j)/(\Lambda/\mathrm{GeV})^{n_i+n_j}$, where $n_1 = 1$ and $n_k = 3$ for $k \neq 1$. This factor is not required for the cross sections labeled "SM" or "top-loop", of course.

Table C.1: Normalization factors for p_T distributions in H+1-jet production for a scalar Higgs. They are obtained by integrating the distributions of fig. 8.1 over the complete p_T interval of 30–800 GeV.

σ_{ij}/pb for H+1-jet (scalar)			
ij	gg	gq	qq
SM/α_s^2	$4.79 \cdot 10^2$	$1.78 \cdot 10^2$	3.13
11	$3.88 \cdot 10^{10}$	$1.59 \cdot 10^{10}$	$1.03 \cdot 10^8$
12	$-5.55 \cdot 10^{14}$	$-6.59 \cdot 10^{14}$	$3.05 \cdot 10^{13}$
13	$-2.00 \cdot 10^{13}$	–	–
15	–	$-2.05 \cdot 10^{14}$	$1.60 \cdot 10^{13}$

Table C.2: Same as table C.1, but for a pseudo-scalar Higgs (see fig. 8.2).

σ_{ij}/pb for H+1-jet (pseudo-scalar)			
ij	gg	gq	qq
top-loop/α_s^2	$1.11 \cdot 10^3$	$4.16 \cdot 10^2$	6.67
11	$3.88 \cdot 10^{10}$	$5.06 \cdot 10^9$	$3.13 \cdot 10^8$
12	$-5.56 \cdot 10^{14}$	$-3.22 \cdot 10^{14}$	$8.87 \cdot 10^{13}$
13	$-2.00 \cdot 10^{13}$	–	–
15	–	$-1.21 \cdot 10^{14}$	$4.68 \cdot 10^{13}$

Table C.3: Normalization factors for $\Delta\Phi_{jj}$ distributions in H+2-jets production for a scalar Higgs. They are obtained by integrating the distributions of fig. 8.4 over the interval $\Delta\Phi_{jj} \in [0,\pi]$, with the cuts described in eq. (8.2) and (eq. (8.3)).

σ_{ij}/pb for H+2-jet (scalar), WBF cuts			
ij	gg	gq	qq
11	$1.43 \cdot 10^9$	$2.27 \cdot 10^9$	$8.42 \cdot 10^8$
12	$-2.14 \cdot 10^{13}$	$-6.54 \cdot 10^{13}$	$-4.47 \cdot 10^{13}$
13	$-7.13 \cdot 10^{11}$	$-7.59 \cdot 10^{11}$	–
14	–	–	$-1.19 \cdot 10^{12}$
15	$-4.65 \cdot 10^{11}$	$-1.60 \cdot 10^{13}$	$-1.58 \cdot 10^{13}$

Table C.4: Same as table C.3, but for a pseudo-scalar Higgs (see fig. 8.5).

σ_{ij}/pb for H+2-jet (pseudo-scalar), WBF cuts			
ij	gg	gq	qq
11	$1.42 \cdot 10^9$	$2.24 \cdot 10^9$	$8.29 \cdot 10^8$
12	$-2.11 \cdot 10^{13}$	$-6.66 \cdot 10^{13}$	$-4.41 \cdot 10^{13}$
13	$-7.12 \cdot 10^{11}$	$-7.57 \cdot 10^{11}$	–
14	–	–	–
15	$-4.43 \cdot 10^{11}$	$-1.68 \cdot 10^{13}$	$-1.55 \cdot 10^{13}$

Table C.5: Normalization factors for $\Delta\eta_{jj}$ distributions in H+2-jets production for a scalar Higgs. They are obtained by integrating the distributions of fig. 8.6 over the interval $\Delta\eta_{jj} \in [0,10]$, with the cuts described in eq. (8.2).

σ_{ij}/pb for H+2-jet (scalar), incl. cuts			
ij	gg	gq	qq
11	$5.00 \cdot 10^{10}$	$2.67 \cdot 10^{10}$	$2.50 \cdot 10^9$
12	$-6.41 \cdot 10^{14}$	$-1.05 \cdot 10^{15}$	$-1.48 \cdot 10^{14}$
13	$-6.11 \cdot 10^{13}$	$-3.11 \cdot 10^{13}$	–
14	–	–	$-1.71 \cdot 10^{13}$
15	$-1.42 \cdot 10^{13}$	$-3.59 \cdot 10^{14}$	$-5.51 \cdot 10^{13}$

Table C.6: Same as table C.5, but for a pseudo-scalar Higgs (see fig. 8.7).

σ_{ij}/pb for H+2-jet (pseudo-scalar), incl. cuts			
ij	gg	gq	qq
11	$4.94 \cdot 10^{10}$	$2.62 \cdot 10^{10}$	$2.39 \cdot 10^{9}$
12	$-6.32 \cdot 10^{14}$	$-1.07 \cdot 10^{15}$	$-1.31 \cdot 10^{14}$
13	$-6.11 \cdot 10^{13}$	$-3.11 \cdot 10^{13}$	–
14	–	–	–
15	$-1.36 \cdot 10^{13}$	$-3.70 \cdot 10^{14}$	$-4.74 \cdot 10^{13}$

Table C.7: Normalization factors for $\Delta\Phi_{jj}$ distributions in H+2-jets production for a scalar Higgs with $p_{\mathrm{T,H}} > 200\,\mathrm{GeV}$. They are obtained by integrating the distributions of fig. 8.8 over the interval $\Delta\Phi_{jj} \in [0,\pi]$, with the cuts described in eq. (8.2) and eq. (8.3).

σ_{ij}/pb for H+2-jet (scalar), WBF cuts $p_{\mathrm{T,H}} > 200\,\mathrm{GeV}$			
ij	gg	gq	qq
11	$1.14 \cdot 10^{8}$	$2.36 \cdot 10^{8}$	$1.23 \cdot 10^{8}$
12	$-1.91 \cdot 10^{12}$	$-2.32 \cdot 10^{13}$	$-2.25 \cdot 10^{13}$
13	$-1.28 \cdot 10^{11}$	$-1.93 \cdot 10^{11}$	–
14	–	–	$3.82 \cdot 10^{11}$
15	$-2.34 \cdot 10^{11}$	$-1.00 \cdot 10^{13}$	$-1.03 \cdot 10^{13}$

Table C.8: Normalization factors for $\Delta\eta_{jj}$ distributions in H+2-jets production for a scalar Higgs with $p_{\mathrm{T,H}} > 200\,\mathrm{GeV}$. They are obtained by integrating the distributions of fig. 8.9 over the interval $\Delta\eta_{jj} \in [0,10]$, with the cuts described in eq. (8.2).

σ_{ij}/pb for H+2-jet (scalar), incl. cuts $p_{\mathrm{T,H}} > 200\,\mathrm{GeV}$			
ij	gg	gq	qq
11	$3.58 \cdot 10^{9}$	$2.95 \cdot 10^{9}$	$3.84 \cdot 10^{8}$
12	$-3.83 \cdot 10^{13}$	$-5.05 \cdot 10^{14}$	$-7.00 \cdot 10^{13}$
13	$-1.21 \cdot 10^{13}$	$-1.30 \cdot 10^{13}$	–
14	–	–	$-6.14 \cdot 10^{12}$
15	$-6.57 \cdot 10^{12}$	$-2.46 \cdot 10^{14}$	$-3.23 \cdot 10^{13}$

Table C.9: Normalization factors for p_T distributions suppressed by $1/\Lambda^6$ in H+1-jet production for a scalar Higgs. They are obtained by integrating the distributions of fig. 8.10 over the complete p_T interval of 30–800 GeV.

σ_{ij}/pb for H+1-jet (scalar)			
ij	gg	gq	qq
22	$1.35 \cdot 10^{20}$	$3.60 \cdot 10^{19}$	$1.00 \cdot 10^{19}$
23	$-1.12 \cdot 10^{20}$	–	–
25	–	$3.35 \cdot 10^{19}$	$1.01 \cdot 10^{19}$
33	$2.38 \cdot 10^{19}$	–	–
55	–	$7.97 \cdot 10^{18}$	$2.57 \cdot 10^{18}$

Table C.10: Same as table C.9, but for a pseudoscalar Higgs (see fig. 8.11).

σ_{ij}/pb for H+1-jet (pseudo-scalar)			
ij	gg	gq	qq
22	$1.35 \cdot 10^{20}$	$3.61 \cdot 10^{19}$	$2.67 \cdot 10^{19}$
23	$-1.12 \cdot 10^{20}$	–	–
25	–	$3.48 \cdot 10^{19}$	$2.71 \cdot 10^{19}$
33	$2.38 \cdot 10^{19}$	–	–
55	–	$8.47 \cdot 10^{18}$	$6.87 \cdot 10^{18}$

Table C.11: Normalization factors for $\Delta\Phi_{jj}$ distributions suppressed by $1/\Lambda^6$ in H+2-jets production for a scalar Higgs. They are obtained by integrating the distributions of fig. 8.12 over the interval $\Delta\Phi_{jj} \in [0,\pi]$, with the cuts described in eq. (8.2) and eq. (8.3).

σ_{ij}/pb for H+2-jet (scalar), WBF cuts			
ij	gg	gq	qq
22	$1.40 \cdot 10^{19}$	$2.01 \cdot 10^{19}$	$5.14 \cdot 10^{18}$
23	$-1.07 \cdot 10^{19}$	$-1.24 \cdot 10^{19}$	–
24	–	–	$3.09 \cdot 10^{17}$
25	$2.28 \cdot 10^{17}$	$4.17 \cdot 10^{18}$	$4.96 \cdot 10^{18}$
33	$2.08 \cdot 10^{18}$	$2.45 \cdot 10^{18}$	–
34	–	–	–
35	$-2.06 \cdot 10^{15}$	$9.60 \cdot 10^{15}$	–
44	–	–	$1.20 \cdot 10^{17}$
45	–	–	$1.49 \cdot 10^{17}$
55	$5.48 \cdot 10^{16}$	$1.02 \cdot 10^{18}$	$1.21 \cdot 10^{18}$

Table C.12: Same as table C.11, but for a pseudoscalar Higgs (see fig. 8.13).

σ_{ij}/pb for H+2-jet (pseudo-scalar), WBF cuts			
ij	gg	gq	qq
22	$1.40 \cdot 10^{19}$	$2.01 \cdot 10^{19}$	$4.88 \cdot 10^{18}$
23	$-1.07 \cdot 10^{19}$	$-1.24 \cdot 10^{19}$	–
24	–	–	–
25	$2.28 \cdot 10^{17}$	$4.12 \cdot 10^{18}$	$4.71 \cdot 10^{18}$
33	$2.26 \cdot 10^{15}$	$2.45 \cdot 10^{18}$	–
34	–	–	–
35	$-2.06 \cdot 10^{15}$	$9.62 \cdot 10^{15}$	–
44	–	–	–
45	–	–	–
55	$5.49 \cdot 10^{16}$	$1.01 \cdot 10^{18}$	$1.15 \cdot 10^{18}$

Table C.13: Normalization factors for $\Delta\eta_{jj}$ distributions suppressed by $1/\Lambda^6$ in H+2-jets production for a scalar Higgs. They are obtained by integrating the distributions of fig. 8.14 over the interval $\Delta\eta_{jj} \in [0,10]$, with the cuts described in eq. (8.2).

σ_{ij}/pb for H+2-jet (scalar), incl. cuts			
ij	gg	gq	qq
22	$7.10 \cdot 10^{20}$	$3.10 \cdot 10^{20}$	$9.56 \cdot 10^{19}$
23	$-5.62 \cdot 10^{20}$	$-1.36 \cdot 10^{20}$	–
24	–	–	$1.69 \cdot 10^{19}$
25	$4.21 \cdot 10^{18}$	$1.38 \cdot 10^{20}$	$9.38 \cdot 10^{19}$
33	$1.12 \cdot 10^{20}$	$2.86 \cdot 10^{19}$	–
34	–	–	–
35	$-4.94 \cdot 10^{17}$	$1.65 \cdot 10^{18}$	–
44	–	–	$4.26 \cdot 10^{18}$
45	–	–	$8.37 \cdot 10^{18}$
55	$7.18 \cdot 10^{17}$	$3.49 \cdot 10^{19}$	$2.32 \cdot 10^{19}$

Table C.14: Same as table C.13, but for a pseudo-scalar Higgs (see fig. 8.15).

σ_{ij}/pb for H+2-jet (pseudo-scalar), incl. cuts			
ij	gg	gq	qq
22	$7.11 \cdot 10^{20}$	$3.10 \cdot 10^{20}$	$8.33 \cdot 10^{19}$
23	$-5.62 \cdot 10^{20}$	$-1.37 \cdot 10^{20}$	–
24	–	–	–
25	$4.19 \cdot 10^{18}$	$1.39 \cdot 10^{20}$	$8.15 \cdot 10^{19}$
33	$5.12 \cdot 10^{18}$	$2.86 \cdot 10^{19}$	–
34	–	–	–
35	$-4.94 \cdot 10^{17}$	$1.65 \cdot 10^{18}$	–
44	–	–	–
45	–	–	–
55	$7.15 \cdot 10^{17}$	$3.50 \cdot 10^{19}$	$2.01 \cdot 10^{19}$

PUBLICATIONS

1. Harlander, R. V., **T. Neumann**, K. J. Ozeren, and M. Wiesemann: 'Top-mass effects in differential Higgs production through gluon fusion at order α_s^4'. *JHEP* (2012) 1208: p. 139. doi: 10.1007/JHEP08(2012)139. arXiv: 1206.0157 [hep-ph].
2. Harlander, R. V. and **T. Neumann**: 'Probing the nature of the Higgs-gluon coupling'. *Phys. Rev.* (2013) D88: p. 074015. doi: 10.1103/PhysRevD.88.074015. arXiv: 1308.2225 [hep-ph].
3. **Neumann, T.** and M. Wiesemann: 'Finite top-mass effects in gluon-induced Higgs production with a jet-veto at NNLO'. *JHEP* (2014) 1411: p. 150. doi: 10.1007/JHEP11(2014)150. arXiv: 1408.6836 [hep-ph].
4. Harlander, R. V. and **T. Neumann**: 'The perturbative QCD gradient flow to three loops'. 2015.

BIBLIOGRAPHY

REFERENCES FOR PART I

1. Glashow, S. L.: 'Partial-symmetries of weak interactions'. *Nucl. Phys.* (1961) 22: pp. 579–588. DOI: 10.1016/0029-5582(61)90469-2 (cit. on p. 3).
2. Weinberg, S.: 'A Model of Leptons'. *Phys. Rev. Lett.* (1967) 19: pp. 1264–1266. DOI: 10.1103/PhysRevLett.19.1264 (cit. on p. 3).
3. Salam, A.: 'Weak and Electromagnetic Interactions'. *Conf. Proc.* (1968) C680519: pp. 367–377 (cit. on p. 3).
4. 't Hooft, G.: 'Renormalization of massless Yang-Mills fields'. *Nucl. Phys.* (1971) B33: pp. 173–199. DOI: 10.1016/0550-3213(71)90395-6 (cit. on p. 3).
5. 't Hooft, G.: 'Renormalizable Lagrangians for massive Yang-Mills fields'. *Nucl. Phys.* (1971) B35: pp. 167–188. DOI: 10.1016/0550-3213(71)90139-8 (cit. on p. 3).
6. Politzer, H. D.: 'Reliable Perturbative Results for Strong Interactions?' *Phys. Rev. Lett.* (1973) 30: pp. 1346–1349. DOI: 10.1103/PhysRevLett.30.1346 (cit. on p. 3).
7. Gross, D. J. and F. Wilczek: 'Asymptotically Free Gauge Theories. 1.' *Phys. Rev.* (1973) D8: pp. 3633–3652. DOI: 10.1103/PhysRevD.8.3633 (cit. on p. 3).
8. Gross, D. J. and F. Wilczek: 'Ultraviolet Behavior of Nonabelian Gauge Theories'. *Phys. Rev. Lett.* (1973) 30: pp. 1343–1346. DOI: 10.1103/PhysRevLett.30.1343 (cit. on p. 3).
9. Gross, D. J. and F. Wilczek: 'Asymptotically Free Gauge Theories. 2.' *Phys. Rev.* (1974) D9: pp. 980–993. DOI: 10.1103/PhysRevD.9.980 (cit. on p. 3).
10. Fritzsch, H., M. Gell-Mann, and H. Leutwyler: 'Advantages of the Color Octet Gluon Picture'. *Phys. Lett.* (1973) B47: pp. 365–368. DOI: 10.1016/0370-2693(73)90625-4 (cit. on p. 3).

11. Politzer, H. D.: 'Asymptotic Freedom: An Approach to Strong Interactions'. *Phys. Rept.* (1974) 14: pp. 129–180. doi: 10.1016/0370-1573(74)90014-3 (cit. on p. 3).
12. Wilczek, F.: 'Quantum Chromodynamics (QCD): The Modern Theory of the Strong Interaction'. *Ann. Rev. Nucl. Part. Sci.* (1982) 32: pp. 177–209. doi: 10.1146/annurev.ns.32.120182.001141 (cit. on p. 3).
13. Ellis, J.: 'The discovery of the gluon'. *Int. J. Mod. Phys.* (2014) A29.31: p. 1430072. doi: 10.1142/S0217751X14300725. arXiv: 1409.4232 [hep-ph] (cit. on p. 3).
14. Brambilla, N., S. Eidelman, P. Foka, S. Gardner, A. S. Kronfeld, et al.: 'QCD and Strongly Coupled Gauge Theories: Challenges and Perspectives'. *Eur. Phys. J.* (2014) C74.10: p. 2981. doi: 10.1140/epjc/s10052-014-2981-5. arXiv: 1404.3723 [hep-ph] (cit. on pp. 3, 15, 16).
15. Hewett, J. L.: 'The Standard model and why we believe it'. (1997): pp. 3–83. arXiv: hep-ph/9810316 [hep-ph] (cit. on pp. 3, 4).
16. Nakamura, K. et al. (The Particle Data Group collaboration): 'Review of particle physics'. *J. Phys.* (2010) G37: p. 075021. doi: 10.1088/0954-3899/37/7A/075021 (cit. on p. 3).
17. Aad, G. et al. (The ATLAS collaboration): 'Observation of a new particle in the search for the Standard Model Higgs boson with the ATLAS detector at the LHC'. *Phys. Lett.* (2012) B716: pp. 1–29. doi: 10.1016/j.physletb.2012.08.020. arXiv: 1207.7214 [hep-ex] (cit. on pp. 3, 8, 25).
18. Chatrchyan, S. et al. (The CMS collaboration): 'Observation of a new boson at a mass of 125 GeV with the CMS experiment at the LHC'. *Phys. Lett.* (2012) B716: pp. 30–61. doi: 10.1016/j.physletb.2012.08.021. arXiv: 1207.7235 [hep-ex] (cit. on pp. 3, 8, 25).
19. Ellis, J.: 'Outstanding questions: Physics beyond the Standard Model'. *Phil. Trans. Roy. Soc. Lond.* (2012) A370: pp. 818–830. doi: 10.1098/rsta.2011.0452 (cit. on p. 4).
20. 't Hooft, G.: 'Naturalness, chiral symmetry, and spontaneous chiral symmetry breaking'. *NATO Adv. Sci. Inst. Ser. B Phys.* (1980) 59: p. 135 (cit. on p. 4).
21. Friederich, S., R. V. Harlander, and K. Karaca: 'Philosophical perspectives on ad hoc-hypotheses and the Higgs mechanism'. (2013). arXiv: 1305.5110 [physics.hist-ph] (cit. on p. 4).

22. Weinberg, S.: 'Implications of Dynamical Symmetry Breaking'. *Phys. Rev.* (1976) D13: pp. 974–996. doi: 10.1103/PhysRevD.13.974 (cit. on p. 4).

23. Gildener, E.: 'Gauge Symmetry Hierarchies'. *Phys. Rev.* (1976) D14: p. 1667. doi: 10.1103/PhysRevD.14.1667 (cit. on p. 4).

24. Susskind, L.: 'Dynamics of Spontaneous Symmetry Breaking in the Weinberg-Salam Theory'. *Phys. Rev.* (1979) D20: pp. 2619–2625. doi: 10.1103/PhysRevD.20.2619 (cit. on p. 4).

25. Weinberg, S.: 'Implications of Dynamical Symmetry Breaking: An Addendum'. *Phys. Rev.* (1979) D19: pp. 1277–1280. doi: 10.1103/PhysRevD.19.1277 (cit. on p. 4).

26. Peskin, M. E.: 'On the Trail of the Higgs Boson'. (2015). arXiv: 1506.08185 [hep-ph] (cit. on p. 4).

27. Fayet, P. and S. Ferrara: 'Supersymmetry'. *Phys. Rept.* (1977) 32: pp. 249–334. doi: 10.1016/0370-1573(77)90066-7 (cit. on p. 5).

28. Martin, S. P.: 'A Supersymmetry primer'. *Adv. Ser. Direct. High Energy Phys.* (2010) 21: pp. 1–153. doi: 10.1142/9789814307505_0001. arXiv: hep-ph/9709356 [hep-ph] (cit. on p. 5).

29. Arkani-Hamed, N., S. Dimopoulos, and G. Dvali: 'The Hierarchy problem and new dimensions at a millimeter'. *Phys. Lett.* (1998) B429: pp. 263–272. doi: 10.1016/S0370-2693(98)00466-3. arXiv: hep-ph/9803315 [hep-ph] (cit. on p. 5).

30. Arkani-Hamed, N., S. Dimopoulos, and G. Dvali: 'Phenomenology, astrophysics and cosmology of theories with submillimeter dimensions and TeV scale quantum gravity'. *Phys. Rev.* (1999) D59: p. 086004. doi: 10.1103/PhysRevD.59.086004. arXiv: hep-ph/9807344 [hep-ph] (cit. on p. 5).

31. Randall, L. and R. Sundrum: 'A Large mass hierarchy from a small extra dimension'. *Phys. Rev. Lett.* (1999) 83: pp. 3370–3373. doi: 10.1103/PhysRevLett.83.3370. arXiv: hep-ph/9905221 [hep-ph] (cit. on p. 5).

32. Schmaltz, M.: 'Physics beyond the standard model (theory): Introducing the little Higgs'. *Nucl. Phys. Proc. Suppl.* (2003) 117: pp. 40–49. doi: 10.1016/S0920-5632(03)01409-9. arXiv: hep-ph/0210415 [hep-ph] (cit. on p. 5).

33. Schmaltz, M. and D. Tucker-Smith: 'Little Higgs review'. *Ann. Rev. Nucl. Part. Sci.* (2005) 55: pp. 229–270. doi: 10.1146/annurev.nucl.55.090704.151502. arXiv: hep-ph/0502182 [hep-ph] (cit. on p. 5).

34. Marques Tavares, G., M. Schmaltz, and W. Skiba: 'Higgs mass naturalness and scale invariance in the UV'. *Phys. Rev.* (2014) D89.1: p. 015009. doi: 10.1103/PhysRevD.89.015009. arXiv: 1308.0025 [hep-ph] (cit. on p. 5).

35. Hill, C. T. and E. H. Simmons: 'Strong dynamics and electroweak symmetry breaking'. *Phys. Rept.* (2003) 381: pp. 235–402. doi: 10.1016/S0370-1573(03)00140-6. arXiv: hep-ph/0203079 [hep-ph] (cit. on p. 5).

36. Giudice, G. F., C. Grojean, A. Pomarol, and R. Rattazzi: 'The Strongly-Interacting Light Higgs'. *JHEP* (2007) 0706: p. 045. doi: 10.1088/1126-6708/2007/06/045. arXiv: hep-ph/0703164 [hep-ph] (cit. on p. 5).

37. Bellazzini, B., C. Csáki, and J. Serra: 'Composite Higgses'. *Eur. Phys. J.* (2014) C74.5: p. 2766. doi: 10.1140/epjc/s10052-014-2766-x. arXiv: 1401.2457 [hep-ph] (cit. on p. 5).

38. Panico, G. and A. Wulzer: 'The Composite Nambu-Goldstone Higgs'. (2015). arXiv: 1506.01961 [hep-ph] (cit. on p. 5).

39. Graham, P. W., D. E. Kaplan, and S. Rajendran: 'Cosmological Relaxation of the Electroweak Scale'. (2015). arXiv: 1504.07551 [hep-ph] (cit. on p. 5).

40. Espinosa, J. R., C. Grojean, G. Panico, A. Pomarol, O. Pujolàs, and G. Servant: 'Cosmological Higgs-Axion Interplay for a Naturally Small Electroweak Scale'. (2015). arXiv: 1506.09217 [hep-ph] (cit. on p. 5).

41. Ellis, G. and J. Silk: 'Scientific method: Defend the integrity of physics'. *Nature* (2014) 516: pp. 321–323. doi: 10.1038/516321a (cit. on p. 5).

42. Ellis, G.: 'Does the Multiverse Really Exist?' *Sci. Amer.* (2011) 305: pp. 38–43. doi: 10.1038/scientificamerican0811-38 (cit. on p. 5).

43. Harlander, R. V., T. Neumann, K. J. Ozeren, and M. Wiesemann: 'Top-mass effects in differential Higgs production through gluon fusion at order α_s^4'. *JHEP* (2012) 1208: p. 139. doi: 10.1007/JHEP08(2012)139. arXiv: 1206.0157 [hep-ph] (cit. on pp. 6, 14, 19, 23, 26, 31, 32, 34–37, 39, 40, 42, 53, 57, 70).

44. Arnison, G. et al. (The UA1 collaboration): 'Experimental Observation of Isolated Large Transverse Energy Electrons with Associated Missing Energy at $\sqrt{s} = 540\,\text{GeV}$'. *Phys. Lett.* (1983) B122: pp. 103–116. doi: 10.1016/0370-2693(83)91177-2 (cit. on p. 8).

45. Banner, M. et al. (The UA2 collaboration): 'Observation of Single Isolated Electrons of High Transverse Momentum in Events with Missing Transverse Energy at the CERN anti-p p Collider'. *Phys. Lett.* (1983) B122: pp. 476–485. doi: 10.1016/0370-2693(83)91605-2 (cit. on p. 8).

46. Arnison, G. et al. (The UA1 collaboration): 'Experimental Observation of Lepton Pairs of Invariant Mass Around 95 GeV/c^2 at the CERN SPS Collider'. *Phys. Lett.* (1983) B126: pp. 398–410. DOI: 10.1016/0370-2693(83)90188-0 (cit. on p. 8).

47. Arnison, G. et al. (The UA1 collaboration): 'Observation of Muonic Z^0 Decay at the $\bar{p}p$ Collider'. *Phys. Lett.* (1984) B147: p. 241. DOI: 10.1016/0370-2693(84)90628-2 (cit. on p. 8).

48. Bagnaia, P. et al. (The UA2 collaboration): 'Evidence for $Z^0 \to e^+e^-$ at the CERN $\bar{p}p$ Collider'. *Phys. Lett.* (1983) B129: pp. 130–140. DOI: 10.1016/0370-2693(83)90744-X (cit. on p. 8).

49. Denegri, D.: 'The discovery of the *W* and *Z*'. *Phys. Rept.* (2004) 403-404: pp. 107–145. DOI: 10.1016/j.physrep.2004.09.006 (cit. on p. 8).

50. Barate, R. et al. (The LEP Working Group for Higgs boson searches, ALEPH, DELPHI, L3, and OPAL collaborations): 'Search for the standard model Higgs boson at LEP'. *Phys. Lett.* (2003) B565: pp. 61–75. DOI: 10.1016/S0370-2693(03)00614-2. arXiv: hep-ex/0306033 [hep-ex] (cit. on p. 8).

51. Lafaye, R., T. Plehn, M. Rauch, D. Zerwas, and M. Dührssen: 'Measuring the Higgs Sector'. *JHEP* (2009) 0908: p. 009. DOI: 10.1088/1126-6708/2009/08/009. arXiv: 0904.3866 [hep-ph] (cit. on p. 8).

52. Plehn, T. and M. Rauch: 'Higgs Couplings after the Discovery'. *Europhys. Lett.* (2012) 100: p. 11002. DOI: 10.1209/0295-5075/100/11002. arXiv: 1207.6108 [hep-ph] (cit. on p. 8).

53. Klute, M., R. Lafaye, T. Plehn, M. Rauch, and D. Zerwas: 'Measuring Higgs Couplings from LHC Data'. *Phys. Rev. Lett.* (2012) 109: p. 101801. DOI: 10.1103/PhysRevLett.109.101801. arXiv: 1205.2699 [hep-ph] (cit. on p. 8).

54. Ellis, J. and T. You: 'Updated Global Analysis of Higgs Couplings'. *JHEP* (2013) 1306: p. 103. DOI: 10.1007/JHEP06(2013)103. arXiv: 1303.3879 [hep-ph] (cit. on pp. 8, 11).

55. Englert, C., A. Freitas, M. M. Mühlleitner, T. Plehn, M. Rauch, et al.: 'Precision Measurements of Higgs Couplings: Implications for New Physics Scales'. *J. Phys.* (2014) G41: p. 113001. DOI: 10.1088/0954-3899/41/11/113001. arXiv: 1403.7191 [hep-ph] (cit. on pp. 8, 13).

56. Peskin, M. E.: 'Comparison of LHC and ILC Capabilities for Higgs Boson Coupling Measurements'. (2012). arXiv: 1207.2516 [hep-ph] (cit. on p. 8).

57. Bechtle, P., S. Heinemeyer, O. Stål, T. Stefaniak, and G. Weiglein: 'Probing the Standard Model with Higgs signal rates from the Tevatron, the LHC and a future ILC'. *JHEP* (2014) 1411: p. 039. doi: 10.1007/JHEP11(2014)039. arXiv: 1403.1582 [hep-ph] (cit. on pp. 8, 9).

58. Aad, G. et al. (The ATLAS collaboration): 'Measurements of the Total and Differential Higgs Boson Production Cross Sections Combining the $H \to \gamma\gamma$ and $H \to ZZ^* \to 4\ell$ Decay Channels at $\sqrt{s} = 8$ TeV with the ATLAS Detector'. (2015). arXiv: 1504.05833 [hep-ex] (cit. on pp. 8, 25, 61).

59. *Measurements of the Higgs boson production and decay rates and coupling strengths using pp collision data at $\sqrt{s} = 7$ and 8 TeV in the ATLAS experiment*. Tech. rep. ATLAS-CONF-2015-007. Geneva: CERN, Mar. 2015 (cit. on pp. 8, 25, 61).

60. Aad, G. et al. (The ATLAS collaboration): 'Study of the spin and parity of the Higgs boson in diboson decays with the ATLAS detector'. (2015). arXiv: 1506.05669 [hep-ex] (cit. on pp. 8, 25, 61).

61. Khachatryan, V. et al. (The CMS collaboration): 'Precise determination of the mass of the Higgs boson and tests of compatibility of its couplings with the standard model predictions using proton collisions at 7 and 8 TeV'. (2014). arXiv: 1412.8662 [hep-ex] (cit. on pp. 8, 25, 61).

62. Giardino, P. P., K. Kannike, I. Masina, M. Raidal, and A. Strumia: 'The universal Higgs fit'. *JHEP* (2014) 1405: p. 046. doi: 10.1007/JHEP05(2014)046. arXiv: 1303.3570 [hep-ph] (cit. on pp. 8, 25, 61).

63. *Cross Sections Figures*. Feb. 4, 2015. LHC Higgs Cross Section Working Group. https://twiki.cern.ch/twiki/bin/view/LHCPhysics/LHCHXSWGCrossSectionsFigures, revision r40 (cit. on pp. 9, 10).

64. Ellis, J. and T. You: 'Global Analysis of the Higgs Candidate with Mass 125 GeV'. *JHEP* (2012) 1209: p. 123. doi: 10.1007/JHEP09(2012)123. arXiv: 1207.1693 [hep-ph] (cit. on p. 9).

65. Dicus, D. A. and S. S. D. Willenbrock: 'Photon Pair Production and the Intermediate Mass Higgs Boson'. *Phys. Rev.* (1988) D37: p. 1801. doi: 10.1103/PhysRevD.37.1801 (cit. on p. 10).

66. Dixon, L. J. and M. S. Siu: 'Resonance continuum interference in the diphoton Higgs signal at the LHC'. *Phys. Rev. Lett.* (2003) 90: p. 252001. doi: 10.1103/PhysRevLett.90.252001. arXiv: hep-ph/0302233 [hep-ph] (cit. on p. 10).

67. Campbell, J. M., R. K. Ellis, and C. Williams: 'Gluon-gluon contributions to W^+W^- production and Higgs interference effects'. *JHEP* (2011) 1110: p. 005. DOI: 10.1007/JHEP10(2011)005. arXiv: 1107.5569 [hep-ph] (cit. on p. 10).

68. Kauer, N. and G. Passarino: 'Inadequacy of zero-width approximation for a light Higgs boson signal'. *JHEP* (2012) 1208: p. 116. DOI: 10.1007/JHEP08(2012)116. arXiv: 1206.4803 [hep-ph] (cit. on p. 10).

69. Kauer, N.: 'Inadequacy of zero-width approximation for a light Higgs boson signal'. *Mod. Phys. Lett.* (2013) A28: p. 1330015. DOI: 10.1142/S0217732313300152. arXiv: 1305.2092 [hep-ph] (cit. on p. 10).

70. Caola, F. and K. Melnikov: 'Constraining the Higgs boson width with ZZ production at the LHC'. *Phys. Rev.* (2013) D88: p. 054024. DOI: 10.1103/PhysRevD.88.054024. arXiv: 1307.4935 [hep-ph] (cit. on p. 10).

71. Campbell, J. M., R. K. Ellis, and C. Williams: 'Bounding the Higgs width at the LHC using full analytic results for $gg- > e^-e^+\mu^-\mu^+$'. *JHEP* (2014) 1404: p. 060. DOI: 10.1007/JHEP04(2014)060. arXiv: 1311.3589 [hep-ph] (cit. on p. 10).

72. Campbell, J. M., R. K. Ellis, and C. Williams: 'Bounding the Higgs width at the LHC: Complementary results from $H \to WW$'. *Phys. Rev.* (2014) D89.5: p. 053011. DOI: 10.1103/PhysRevD.89.053011. arXiv: 1312.1628 [hep-ph] (cit. on p. 10).

73. Gainer, J. S., J. Lykken, K. T. Matchev, S. Mrenna, and M. Park: 'Beyond Geolocating: Constraining Higher Dimensional Operators in $H \to 4\ell$ with Off-Shell Production and More'. *Phys. Rev.* (2015) D91.3: p. 035011. DOI: 10.1103/PhysRevD.91.035011. arXiv: 1403.4951 [hep-ph] (cit. on p. 10).

74. Cacciapaglia, G., A. Deandrea, G. Drieu La Rochelle, and J.-B. Flament: 'Higgs couplings: disentangling New Physics with off-shell measurements'. *Phys. Rev. Lett.* (2014) 113.20: p. 201802. DOI: 10.1103/PhysRevLett.113.201802. arXiv: 1406.1757 [hep-ph] (cit. on p. 10).

75. Englert, C., Y. Soreq, and M. Spannowsky: 'Off-Shell Higgs Coupling Measurements in BSM scenarios'. *JHEP* (2015) 1505: p. 145. DOI: 10.1007/JHEP05(2015)145. arXiv: 1410.5440 [hep-ph] (cit. on p. 10).

76. Azatov, A., C. Grojean, A. Paul, and E. Salvioni: 'Taming the off-shell Higgs boson'. *J. Exp. Theor. Phys.* (2015) 120: pp. 354–368. DOI: 10.1134/S1063776115030140. arXiv: 1406.6338 [hep-ph] (cit. on p. 10).

77. Liebler, S., G. Moortgat-Pick, and G. Weiglein: 'Off-shell effects in Higgs processes at a linear collider and implications for the LHC'. (2015). arXiv: 1502.07970 [hep-ph] (cit. on p. 10).

78. Degrassi, G., S. Di Vita, J. Elias-Miro, J. R. Espinosa, G. F. Giudice, G. Isidori, and A. Strumia: 'Higgs mass and vacuum stability in the Standard Model at NNLO'. *JHEP* (2012) 1208: p. 098. doi: 10.1007/JHEP08(2012)098. arXiv: 1205.6497 [hep-ph] (cit. on p. 11).

79. Bezrukov, F., M. Y. Kalmykov, B. A. Kniehl, and M. Shaposhnikov: 'Higgs Boson Mass and New Physics'. *JHEP* (2012) 1210: p. 140. doi: 10.1007/JHEP10(2012)140. arXiv: 1205.2893 [hep-ph] (cit. on p. 11).

80. Buttazzo, D., G. Degrassi, P. P. Giardino, G. F. Giudice, F. Sala, et al.: 'Investigating the near-criticality of the Higgs boson'. *JHEP* (2013) 1312: p. 089. doi: 10.1007/JHEP12(2013)089. arXiv: 1307.3536 [hep-ph] (cit. on pp. 11, 12).

81. David, A. et al. (The LHC Higgs Cross Section Working Group collaboration): 'LHC HXSWG interim recommendations to explore the coupling structure of a Higgs-like particle'. (2012). arXiv: 1209.0040 [hep-ph] (cit. on pp. 12, 62).

82. Skiba, W.: 'TASI Lectures on Effective Field Theory and Precision Electroweak Measurements'. (2010). arXiv: 1006.2142 [hep-ph] (cit. on p. 12).

83. Grzadkowski, B., M. Iskrzynski, M. Misiak, and J. Rosiek: 'Dimension-Six Terms in the Standard Model Lagrangian'. *JHEP* (2010) 1010: p. 085. doi: 10.1007/JHEP10(2010)085. arXiv: 1008.4884 [hep-ph] (cit. on pp. 13, 62).

84. Buchmüller, W. and D. Wyler: 'Effective Lagrangian Analysis of New Interactions and Flavor Conservation'. *Nucl. Phys.* (1986) B268: pp. 621–653. doi: 10.1016/0550-3213(86)90262-2 (cit. on pp. 13, 62).

85. Lehman, L.: 'Extending the Standard Model Effective Field Theory with the Complete Set of Dimension-7 Operators'. *Phys. Rev.* (2014) D90.12: p. 125023. doi: 10.1103/PhysRevD.90.125023. arXiv: 1410.4193 [hep-ph] (cit. on pp. 13, 62).

86. Jenkins, E. E., A. V. Manohar, and M. Trott: 'Renormalization group evolution of the Standard Model dimension six operators I: formalism and λ dependence'. *JHEP* (2013) 1310: p. 087. doi: 10.1007/JHEP10(2013)087. arXiv: 1308.2627 [hep-ph] (cit. on p. 13).

87. Jenkins, E. E., A. V. Manohar, and M. Trott: 'Renormalization group evolution of the Standard Model dimension six operators II: Yukawa dependence'. *JHEP* (2014) 1401: p. 035. doi: 10.1007/JHEP01(2014)035. arXiv: 1310.4838 [hep-ph] (cit. on p. 13).

88. Alonso, R., E. E. Jenkins, A. V. Manohar, and M. Trott: 'Renormalization group evolution of the Standard Model dimension six operators III: gauge coupling dependence and phenomenology'. *JHEP* (2014) 1404: p. 159. doi: 10.1007/JHEP04(2014)159. arXiv: 1312.2014 [hep-ph] (cit. on p. 13).

89. Elias-Miró, J., J. R. Espinosa, E. Masso, and A. Pomarol: 'Higgs windows to new physics through d=6 operators: constraints and one-loop anomalous dimensions'. *JHEP* (2013) 1311: p. 066. doi: 10.1007/JHEP11(2013)066. arXiv: 1308.1879 [hep-ph] (cit. on p. 13).

90. Elias-Miró, J., C. Grojean, R. S. Gupta, and D. Marzocca: 'Scaling and tuning of EW and Higgs observables'. *JHEP* (2014) 1405: p. 019. doi: 10.1007/JHEP05(2014)019. arXiv: 1312.2928 [hep-ph] (cit. on p. 13).

91. Grojean, C., E. E. Jenkins, A. V. Manohar, and M. Trott: 'Renormalization group scaling of Higgs operators and $h \to \gamma\gamma$ decay'. *JHEP* (2013) 1304: p. 016. doi: 10.1007/JHEP04(2013)016. arXiv: 1301.2588 [hep-ph] (cit. on p. 13).

92. Elias-Miró, J., J. R. Espinosa, E. Masso, and A. Pomarol: 'Renormalization of dimension-six operators relevant for the Higgs decays $h \to \gamma\gamma, \gamma Z$'. *JHEP* (2013) 1308: p. 033. doi: 10.1007/JHEP08(2013)033. arXiv: 1302.5661 [hep-ph] (cit. on p. 13).

93. Bonnet, F., M. B. Gavela, T. Ota, and W. Winter: 'Anomalous Higgs couplings at the LHC, and their theoretical interpretation'. *Phys. Rev.* (2012) D85: p. 035016. doi: 10.1103/PhysRevD.85.035016. arXiv: 1105.5140 [hep-ph] (cit. on p. 13).

94. Bonnet, F., T. Ota, M. Rauch, and W. Winter: 'Interpretation of precision tests in the Higgs sector in terms of physics beyond the Standard Model'. *Phys. Rev.* (2012) D86: p. 093014. doi: 10.1103/PhysRevD.86.093014. arXiv: 1207.4599 [hep-ph] (cit. on p. 13).

95. Contino, R., M. Ghezzi, C. Grojean, M. Mühlleitner, and M. Spira: 'Effective Lagrangian for a light Higgs-like scalar'. *JHEP* (2013) 1307: p. 035. doi: 10.1007/JHEP07(2013)035. arXiv: 1303.3876 [hep-ph] (cit. on p. 13).

96. Dumont, B., S. Fichet, and G. von Gersdorff: 'A Bayesian view of the Higgs sector with higher dimensional operators'. *JHEP* (2013) 1307: p. 065. doi: 10.1007/JHEP07(2013)065. arXiv: 1304.3369 [hep-ph] (cit. on p. 13).

97. Boos, E., V. Bunichev, M. Dubinin, and Y. Kurihara: 'Higgs boson signal at complete tree level in the SM extension by dimension-six operators'. *Phys. Rev.* (2014) D89: p. 035001. doi: 10.1103/PhysRevD.89.035001. arXiv: 1309.5410 [hep-ph] (cit. on p. 13).

98. Degrande, C.: 'A basis of dimension-eight operators for anomalous neutral triple gauge boson interactions'. *JHEP* (2014) 1402: p. 101. doi: 10.1007/JHEP02(2014)101. arXiv: 1308.6323 [hep-ph] (cit. on p. 13).

99. Brivio, I., T. Corbett, O. J. P. Éboli, M. B. Gavela, J. Gonzalez-Fraile, et al.: 'Disentangling a dynamical Higgs'. *JHEP* (2014) 1403: p. 024. doi: 10.1007/JHEP03(2014)024. arXiv: 1311.1823 [hep-ph] (cit. on p. 13).

100. Einhorn, M. B. and J. Wudka: 'Higgs-Boson Couplings Beyond the Standard Model'. *Nucl. Phys.* (2013) B877: pp. 792–806. doi: 10.1016/j.nuclphysb.2013.11.004. arXiv: 1308.2255 [hep-ph] (cit. on p. 13).

101. Banerjee, S., S. Mukhopadhyay, and B. Mukhopadhyaya: 'Higher dimensional operators and the LHC Higgs data: The role of modified kinematics'. *Phys. Rev.* (2014) D89.5: p. 053010. doi: 10.1103/PhysRevD.89.053010. arXiv: 1308.4860 [hep-ph] (cit. on p. 13).

102. Gavela, M. B., J. Gonzalez-Fraile, M. C. Gonzalez-Garcia, L. Merlo, S. Rigolin, et al.: 'CP violation with a dynamical Higgs'. *JHEP* (2014) 1410: p. 44. doi: 10.1007/JHEP10(2014)044. arXiv: 1406.6367 [hep-ph] (cit. on p. 13).

103. Alloul, A., B. Fuks, and V. Sanz: 'Phenomenology of the Higgs Effective Lagrangian via FEYNRULES'. *JHEP* (2014) 1404: p. 110. doi: 10.1007/JHEP04(2014)110. arXiv: 1310.5150 [hep-ph] (cit. on p. 13).

104. Appelquist, T. and J. Carazzone: 'Infrared Singularities and Massive Fields'. *Phys. Rev.* (1975) D11: p. 2856. doi: 10.1103/PhysRevD.11.2856 (cit. on p. 13).

105. Banfi, A., A. Martin, and V. Sanz: 'Probing top-partners in Higgs+jets'. *JHEP* (2014) 1408: p. 053. doi: 10.1007/JHEP08(2014)053. arXiv: 1308.4771 [hep-ph] (cit. on p. 14).

106. Azatov, A. and A. Paul: 'Probing Higgs couplings with high p_T Higgs production'. *JHEP* (2014) 1401: p. 014. doi: 10.1007/JHEP01(2014)014. arXiv: 1309.5273 [hep-ph] (cit. on p. 14).

107. Grojean, C., E. Salvioni, M. Schlaffer, and A. Weiler: 'Very boosted Higgs in gluon fusion'. *JHEP* (2014) 1405: p. 022. doi: 10.1007/JHEP05(2014)022. arXiv: 1312.3317 [hep-ph] (cit. on p. 14).

108. Schlaffer, M., M. Spannowsky, M. Takeuchi, A. Weiler, and C. Wymant: 'Boosted Higgs Shapes'. *Eur. Phys. J.* (2014) C74.10: p. 3120. doi: 10.1140/epjc/s10052-014-3120-z. arXiv: 1405.4295 [hep-ph] (cit. on p. 14).

109. Langenegger, U., M. Spira, and I. Strebel: 'Testing the Higgs Boson Coupling to Gluons'. (2015). arXiv: 1507.01373 [hep-ph] (cit. on p. 14).

110. Englert, C. and M. Spannowsky: 'Effective Theories and Measurements at Colliders'. *Phys. Lett.* (2015) B740: pp. 8–15. doi: 10.1016/j.physletb.2014.11.035. arXiv: 1408.5147 [hep-ph] (cit. on p. 14).

111. Buschmann, M., C. Englert, D. Goncalves, T. Plehn, and M. Spannowsky: 'Resolving the Higgs-Gluon Coupling with Jets'. *Phys. Rev.* (2014) D90.1: p. 013010. doi: 10.1103/PhysRevD.90.013010. arXiv: 1405.7651 [hep-ph] (cit. on p. 14).

112. Ghosh, D. and M. Wiebusch: 'Dimension-six triple gluon operator in Higgs+jet observables'. *Phys. Rev.* (2015) D91.3: p. 031701. doi: 10.1103/PhysRevD.91.031701. arXiv: 1411.2029 [hep-ph] (cit. on p. 14).

113. Dawson, S., I. M. Lewis, and M. Zeng: 'Effective field theory for Higgs boson plus jet production'. *Phys. Rev.* (2014) D90.9: p. 093007. doi: 10.1103/PhysRevD.90.093007. arXiv: 1409.6299 [hep-ph] (cit. on p. 14).

114. Dawson, S., I. M. Lewis, and M. Zeng: 'Usefulness of effective field theory for boosted Higgs production'. *Phys. Rev.* (2015) D91: p. 074012. doi: 10.1103/PhysRevD.91.074012. arXiv: 1501.04103 [hep-ph] (cit. on pp. 14, 79).

115. Neumann, T. and M. Wiesemann: 'Finite top-mass effects in gluon-induced Higgs production with a jet-veto at NNLO'. *JHEP* (2014) 1411: p. 150. doi: 10.1007/JHEP11(2014)150. arXiv: 1408.6836 [hep-ph] (cit. on pp. 14, 19, 23, 26, 32, 37, 45–49, 51–55, 70).

116. Grazzini, M. and H. Sargsyan: 'Heavy-quark mass effects in Higgs boson production at the LHC'. *JHEP* (2013) 1309: p. 129. doi: 10.1007/JHEP09(2013)129. arXiv: 1306.4581 [hep-ph] (cit. on pp. 14, 31, 42).

117. Buschmann, M., D. Goncalves, S. Kuttimalai, M. Schönherr, F. Krauss, et al.: 'Mass Effects in the Higgs-Gluon Coupling: Boosted vs Off-Shell Production'. *JHEP* (2015) 1502: p. 038. doi: 10.1007/JHEP02(2015)038. arXiv: 1410.5806 [hep-ph] (cit. on p. 14).

118. Hamilton, K., P. Nason, and G. Zanderighi: 'Finite quark-mass effects in the NNLOPS POWHEG+MiNLO Higgs generator'. *JHEP* (2015) 1505: p. 140. doi: 10.1007/JHEP05(2015)140. arXiv: 1501.04637 [hep-ph] (cit. on p. 14).

119. Hands, S.: 'The Phase diagram of QCD'. *Contemp. Phys.* (2001) 42: pp. 209–225. doi: 10.1080/00107510110063843. arXiv: physics/0105022 [physics.ed-ph] (cit. on p. 15).

120. Collins, J. C., D. E. Soper, and G. F. Sterman: 'Factorization of Hard Processes in QCD'. *Adv. Ser. Direct. High Energy Phys.* (1988) 5: pp. 1–91. arXiv: hep-ph/0409313 [hep-ph] (cit. on pp. 15, 19).

121. Soper, D. E.: 'Basics of QCD perturbation theory'. (1996). arXiv: hep-ph/9702203 [hep-ph] (cit. on pp. 15, 19).

122. Kronfeld, A. S.: 'Twenty-first Century Lattice Gauge Theory: Results from the QCD Lagrangian'. *Ann. Rev. Nucl. Part. Sci.* (2012) 62: pp. 265–284. doi: 10.1146/annurev-nucl-102711-094942. arXiv: 1203.1204 [hep-lat] (cit. on pp. 15, 16).

123. Borsányi, S., S. Dürr, Z. Fodor, C. Hölbling, S. D. Katz, et al.: 'Ab initio calculation of the neutron-proton mass difference'. *Science* (2015) 347: pp. 1452–1455. doi: 10.1126/science.1257050. arXiv: 1406.4088 [hep-lat] (cit. on p. 15).

124. Aoki, S., Y. Aoki, C. Bernard, T. Blum, G. Colangelo, et al.: 'Review of lattice results concerning low-energy particle physics'. *Eur. Phys. J.* (2014) C74: p. 2890. doi: 10.1140/epjc/s10052-014-2890-7. arXiv: 1310.8555 [hep-lat] (cit. on pp. 15, 16).

125. Goldstone, J.: 'Field Theories with Superconductor Solutions'. *Nuovo Cim.* (1961) 19: pp. 154–164. doi: 10.1007/BF02812722 (cit. on p. 16).

126. Goldstone, J., A. Salam, and S. Weinberg: 'Broken Symmetries'. *Phys. Rev.* (1962) 127: pp. 965–970. doi: 10.1103/PhysRev.127.965 (cit. on p. 16).

127. DeGrand, T., Z. Liu, and S. Schaefer: 'Quark condensate in two-flavor QCD'. *Phys. Rev.* (2006) D74: p. 094504. doi: 10.1103/PhysRevD.74.094504,10.1103/PhysRevD.74.099904. arXiv: hep-lat/0608019 [hep-lat] (cit. on p. 16).

128. Fukaya, H. et al. (The JLQCD collaboration): 'Determination of the chiral condensate from 2+1-flavor lattice QCD'. *Phys. Rev. Lett.* (2010) 104: p. 122002. doi: 10.1103/PhysRevLett.104.122002,10.1103/PhysRevLett.105.159901. arXiv: 0911.5555 [hep-lat] (cit. on p. 16).

129. Fukaya, H. et al. (The JLQCD and TWQCD collaborations): 'Determination of the chiral condensate from QCD Dirac spectrum on the lattice'. *Phys. Rev.* (2011) D83: p. 074501. doi: 10.1103/PhysRevD.83.074501. arXiv: 1012.4052 [hep-lat] (cit. on p. 16).

130. Olive, K. A. et al. (The Particle Data Group collaboration): 'Review of Particle Physics'. *Chin. Phys* (2014) C38: p. 090001. doi: 10.1088/1674-1137/38/9/090001 (cit. on pp. 16, 43, 108).

131. Demartin, F., S. Forte, E. Mariani, J. Rojo, and A. Vicini: 'Impact of parton distribution function and α_s uncertainties on Higgs boson production in gluon fusion at hadron colliders'. *Phys. Rev.* (2010) D82: p. 014002. doi: 10.1103/PhysRevD.82.014002. arXiv: 1004.0962 [hep-ph] (cit. on pp. 16, 30).

132. Baglio, J. and A. Djouadi: 'Predictions for Higgs production at the Tevatron and the associated uncertainties'. *JHEP* (2010) 1010: p. 064. doi: 10.1007/JHEP10(2010)064. arXiv: 1003.4266 [hep-ph] (cit. on pp. 16, 30).

133. Martin, A. D., W. J. Stirling, R. S. Thorne, and G. Watt: 'Uncertainties on α_S in global PDF analyses and implications for predicted hadronic cross sections'. *Eur. Phys. J.* (2009) C64: pp. 653–680. doi: 10.1140/epjc/s10052-009-1164-2. arXiv: 0905.3531 [hep-ph] (cit. on p. 16).

134. Dissertori, G.: 'The Determination of the Strong Coupling Constant'. (2015). arXiv: 1506.05407 [hep-ex] (cit. on p. 16).

135. Bethke, S.: 'Determination of the QCD coupling α_s'. *J. Phys.* (2000) G26: R27. doi: 10.1088/0954-3899/26/7/201. arXiv: hep-ex/0004021 [hep-ex] (cit. on p. 16).

136. Chatrchyan, S. et al. (The CMS collaboration): 'Determination of the top-quark pole mass and strong coupling constant from the t t-bar production cross section in pp collisions at $\sqrt{s} = 7$ TeV'. *Phys. Lett.* (2014) B728: pp. 496–517. doi: 10.1016/j.physletb.2014.08.040,10.1016/j.physletb.2013.12.009. arXiv: 1307.1907 [hep-ex] (cit. on p. 16).

137. Czakon, M., M. L. Mangano, A. Mitov, and J. Rojo: 'Constraints on the gluon PDF from top quark pair production at hadron colliders'. *JHEP* (2013) 1307: p. 167. DOI: 10.1007/JHEP07(2013)167. arXiv: 1303.7215 [hep-ph] (cit. on p. 16).

138. McNeile, C., C. T. H. Davies, E. Follana, K. Hornbostel, and G. P. Lepage: 'High-Precision c and b Masses, and QCD Coupling from Current-Current Correlators in Lattice and Continuum QCD'. *Phys. Rev.* (2010) D82: p. 034512. DOI: 10.1103/PhysRevD.82.034512. arXiv: 1004.4285 [hep-lat] (cit. on p. 16).

139. Shintani, E., S. Aoki, H. Fukaya, S. Hashimoto, T. Kaneko, et al.: 'Strong coupling constant from vacuum polarization functions in three-flavor lattice QCD with dynamical overlap fermions'. *Phys. Rev.* (2010) D82.7: p. 074505. DOI: 10.1103/PhysRevD.82.074505, 10.1103/PhysRevD.89.099903. arXiv: 1002.0371 [hep-lat] (cit. on p. 16).

140. Aoki, S. et al. (The PACS-CS collaboration): 'Precise determination of the strong coupling constant in N(f) = 2+1 lattice QCD with the Schrodinger functional scheme'. *JHEP* (2009) 0910: p. 053. DOI: 10.1088/1126-6708/2009/10/053. arXiv: 0906.3906 [hep-lat] (cit. on p. 16).

141. Blossier, B., P. Boucaud, M. Brinet, F. De Soto, X. Du, et al.: 'The Strong running coupling at τ and Z_0 mass scales from lattice QCD'. *Phys. Rev. Lett.* (2012) 108: p. 262002. DOI: 10.1103/PhysRevLett.108.262002. arXiv: 1201.5770 [hep-ph] (cit. on p. 16).

142. Lepage, G. P. and P. B. Mackenzie: 'On the viability of lattice perturbation theory'. *Phys. Rev.* (1993) D48: pp. 2250–2264. DOI: 10.1103/PhysRevD.48.2250. arXiv: hep-lat/9209022 [hep-lat] (cit. on p. 17).

143. Lepage, G. P.: 'Redesigning lattice QCD'. *Lect. Notes Phys.* (1997) 479: pp. 1–48. DOI: 10.1007/BFb0104288. arXiv: hep-lat/9607076 [hep-lat] (cit. on p. 17).

144. Capitani, S.: 'Lattice perturbation theory'. *Phys. Rept.* (2003) 382: pp. 113–302. DOI: 10.1016/S0370-1573(03)00211-4. arXiv: hep-lat/0211036 [hep-lat] (cit. on p. 17).

145. Mason, Q. et al. (The HPQCD and UKQCD collaborations): 'Accurate determinations of α_s from realistic lattice QCD'. *Phys. Rev. Lett.* (2005) 95: p. 052002. DOI: 10.1103/PhysRevLett.95.052002. arXiv: hep-lat/0503005 [hep-lat] (cit. on p. 17).

146. Lüscher, M., R. Narayanan, P. Weisz, and U. Wolff: 'The Schrodinger functional: A renormalizable probe for non-abelian gauge theories'. *Nucl. Phys.* (1992) B384: pp. 168–228. doi: 10.1016/0550-3213(92)90466-0. arXiv: hep-lat/9207009 [hep-lat] (cit. on p. 17).

147. Lüscher, M.: 'Schrödinger Representation In Quantum Field Theory'. *Nucl. Phys.* (1985) B254: pp. 52–57. doi: 10.1016/0550-3213(85)90210-X (cit. on p. 17).

148. Lüscher, M. and P. Weisz: 'Two loop relation between the bare lattice coupling and the MS coupling in pure SU(N) gauge theories'. *Phys. Lett.* (1995) B349: pp. 165–169. doi: 10.1016/0370-2693(95)00250-0. arXiv: hep-lat/9502001 [hep-lat] (cit. on p. 17).

149. Lüscher, M. and P. Weisz: 'Computation of the relation between the bare lattice coupling and the MS coupling in SU(N) gauge theories to two loops'. *Nucl. Phys.* (1995) B452: pp. 234–260. doi: 10.1016/0550-3213(95)00338-S. arXiv: hep-lat/9505011 [hep-lat] (cit. on p. 17).

150. Narayanan, R. and U. Wolff: 'Two loop computation of a running coupling lattice Yang-Mills theory'. *Nucl. Phys.* (1995) B444: pp. 425–446. doi: 10.1016/0550-3213(95)00170-W. arXiv: hep-lat/9502021 [hep-lat] (cit. on p. 17).

151. Lüscher, M., P. Weisz, and U. Wolff: 'A Numerical method to compute the running coupling in asymptotically free theories'. *Nucl. Phys.* (1991) B359: pp. 221–243. doi: 10.1016/0550-3213(91)90298-C (cit. on pp. 17, 112).

152. Lüscher, M., R. Sommer, U. Wolff, and P. Weisz: 'Computation of the running coupling in the SU(2) Yang-Mills theory'. *Nucl. Phys.* (1993) B389: pp. 247–264. doi: 10.1016/0550-3213(93)90292-W. arXiv: hep-lat/9207010 [hep-lat] (cit. on p. 17).

153. Lüscher, M., R. Sommer, P. Weisz, and U. Wolff: 'A Precise determination of the running coupling in the SU(3) Yang-Mills theory'. *Nucl. Phys.* (1994) B413: pp. 481–502. doi: 10.1016/0550-3213(94)90629-7. arXiv: hep-lat/9309005 [hep-lat] (cit. on p. 17).

154. Lüscher, M.: 'Properties and uses of the Wilson flow in lattice QCD'. *JHEP* (2010) 1008: p. 071. doi: 10.1007/JHEP08(2010)071,10.1007/JHEP03(2014)092. arXiv: 1006.4518 [hep-lat] (cit. on pp. 17, 83–86, 89, 103, 104, 107).

155. Lüscher, M. and P. Weisz: 'Perturbative analysis of the gradient flow in non-abelian gauge theories'. *JHEP* (2011) 1102: p. 051. DOI: 10.1007/JHEP02(2011)051. arXiv: 1101.0963 [hep-th] (cit. on pp. 17, 83–87, 103).

156. Lüscher, M.: 'Chiral symmetry and the Yang–Mills gradient flow'. *JHEP* (2013) 1304: p. 123. DOI: 10.1007/JHEP04(2013)123. arXiv: 1302.5246 [hep-lat] (cit. on pp. 17, 85, 115).

157. Borsányi, S., S. Dürr, Z. Fodor, C. Hölbling, S. D. Katz, et al.: 'High-precision scale setting in lattice QCD'. *JHEP* (2012) 1209: p. 010. DOI: 10.1007/JHEP09(2012)010. arXiv: 1203.4469 [hep-lat] (cit. on pp. 17, 83).

158. Sommer, R.: 'Scale setting in lattice QCD'. *PoS* (2014) LATTICE2013: p. 015. arXiv: 1401.3270 [hep-lat] (cit. on p. 17).

159. Fodor, Z., K. Holland, J. Kuti, D. Nogradi, and C. H. Wong: 'The Yang-Mills gradient flow in finite volume'. *JHEP* (2012) 1211: p. 007. DOI: 10.1007/JHEP11(2012)007. arXiv: 1208.1051 [hep-lat] (cit. on pp. 17, 83, 112).

160. Fritzsch, P. and A. Ramos: 'The gradient flow coupling in the Schrödinger Functional'. *JHEP* (2013) 1310: p. 008. DOI: 10.1007/JHEP10(2013)008. arXiv: 1301.4388 [hep-lat] (cit. on p. 17).

161. Ramos, A.: 'The gradient flow running coupling with twisted boundary conditions'. *JHEP* (2014) 1411: p. 101. DOI: 10.1007/JHEP11(2014)101. arXiv: 1409.1445 [hep-lat] (cit. on p. 17).

162. Lüscher, M.: 'Step scaling and the Yang-Mills gradient flow'. *JHEP* (2014) 1406: p. 105. DOI: 10.1007/JHEP06(2014)105. arXiv: 1404.5930 [hep-lat] (cit. on pp. 17, 83, 112).

163. Lüscher, M.: 'Future applications of the Yang-Mills gradient flow in lattice QCD'. *PoS* (2014) LATTICE2013: p. 016. arXiv: 1308.5598 [hep-lat] (cit. on p. 17).

164. Ramos, A.: 'The Yang-Mills gradient flow and renormalization'. (2015). arXiv: 1506.00118 [hep-lat] (cit. on p. 17).

165. Suzuki, H.: 'Energy–momentum tensor from the Yang–Mills gradient flow'. *Prog. Theor. Exp. Phys.* (2013) 2013.8. DOI: 10.1093/ptep/ptt059. arXiv: 1304.0533 [hep-lat] (cit. on p. 17).

166. Del Debbio, L., A. Patella, and A. Rago: 'Space-time symmetries and the Yang-Mills gradient flow'. *JHEP* (2013) 1311: p. 212. DOI: 10.1007/JHEP11(2013)212. arXiv: 1306.1173 [hep-th] (cit. on p. 17).

167. Makino, H. and H. Suzuki: 'Lattice energy–momentum tensor from the Yang–Mills gradient flow—inclusion of fermion fields'. *Prog. Theor. Exp. Phys.* (2014) 2014.6. doi: 10.1093/ptep/ptu070. arXiv: 1403.4772 [hep-lat] (cit. on p. 17).

168. Asakawa, M., T. Hatsuda, E. Itou, M. Kitazawa, and H. Suzuki (The FlowQCD collaboration): 'Thermodynamics of SU(3) gauge theory from gradient flow on the lattice'. *Phys. Rev.* (2014) D90.1: p. 011501. doi: 10.1103/PhysRevD.90.011501. arXiv: 1312.7492 [hep-lat] (cit. on p. 17).

169. Kitazawa, M., M. Asakawa, T. Hatsuda, T. Iritani, E. Itou, et al.: 'Measurement of thermodynamics using gradient flow'. *PoS* (2014) LATTICE2014: p. 022. arXiv: 1412.4508 [hep-lat] (cit. on p. 17).

170. Bollini, C. G. and J. J. Giambiagi: 'Dimensional Renormalization: The Number of Dimensions as a Regularizing Parameter'. *Nuovo Cim.* (1972) B12: pp. 20–26. doi: 10.1007/BF02895558 (cit. on p. 18).

171. 't Hooft, G. and M. J. G. Veltman: 'Regularization and Renormalization of Gauge Fields'. *Nucl. Phys.* (1972) B44: pp. 189–213. doi: 10.1016/0550-3213(72)90279-9 (cit. on p. 18).

172. Bardeen, W. A., A. J. Buras, D. W. Duke, and T. Muta: 'Deep-inelastic scattering beyond the leading order in asymptotically free gauge theories'. *Phys. Rev.* (1978) D18: p. 3998. doi: 10.1103/PhysRevD.18.3998 (cit. on p. 18).

173. Pittau, R.: 'A four-dimensional approach to quantum field theories'. *JHEP* (2012) 1211: p. 151. doi: 10.1007/JHEP11(2012)151. arXiv: 1208.5457 [hep-ph] (cit. on p. 18).

174. Hernandez-Pinto, R. J., G. F. R. Sborlini, and G. Rodrigo: 'Gauge theories in four dimensions'. (2015). arXiv: 1506.04617 [hep-ph] (cit. on p. 18).

175. Bloch, F. and A. Nordsieck: 'Note on the Radiation Field of the electron'. *Phys. Rev.* (1937) 52: pp. 54–59. doi: 10.1103/PhysRev.52.54 (cit. on p. 18).

176. Kinoshita, T.: 'Mass singularities of Feynman amplitudes'. *J. Math. Phys.* (1962) 3: pp. 650–677. doi: 10.1063/1.1724268 (cit. on p. 18).

177. Lee, T. D. and M. Nauenberg: 'Degenerate Systems and Mass Singularities'. *Phys. Rev.* (1964) B133: pp. 1549–1562. doi: 10.1103/PhysRev.133.B1549 (cit. on p. 18).

178. Lavelle, M. and D. McMullan: 'Collinearity, convergence and cancelling infrared divergences'. *JHEP* (2006) 0603: p. 026. doi: 10.1088/1126-6708/2006/03/026. arXiv: hep-ph/0511314 [hep-ph] (cit. on p. 18).

179. Chetyrkin, K. G. and V. A. Smirnov: 'Dimensional Regularization And Infrared Divergences'. *Theor. Math. Phys.* (1984) 56: pp. 770–776 (cit. on p. 18).

180. Catani, S. and M. H. Seymour: 'A General algorithm for calculating jet cross-sections in NLO QCD'. *Nucl. Phys.* (1997) B485: pp. 291–419. doi: 10.1016/S0550-3213(96)00589-5. arXiv: hep-ph/9605323 [hep-ph]. Erratum ibid. *Nucl. Phys.* (1998) B510.1–2 (cit. on pp. 19, 33, 42).

181. Catani, S., S. Dittmaier, M. H. Seymour, and Z. Trocsanyi: 'The Dipole formalism for next-to-leading order QCD calculations with massive partons'. *Nucl. Phys.* (2002) B627: pp. 189–265. doi: 10.1016/S0550-3213(02)00098-6. arXiv: hep-ph/0201036 [hep-ph] (cit. on p. 19).

182. Fabricius, K., I. Schmitt, G. Schierholz, and G. Kramer: 'Order α_s^2 Correction to Jet Cross-Sections in $e^+ e^-$ Annihilation'. *Phys. Lett.* (1980) B97: p. 431. doi: 10.1016/0370-2693(80)90635-8 (cit. on pp. 19, 33).

183. Fabricius, K., I. Schmitt, G. Kramer, and G. Schierholz: 'Higher Order Perturbative QCD Calculation of Jet Cross-Sections in e+ e- Annihilation'. *Z. Phys.* (1981) C11: p. 315. doi: 10.1007/BF01578281 (cit. on pp. 19, 33).

184. Gutbrod, F., G. Kramer, and G. Schierholz: 'Higher Order QCD Corrections to the Three Jet Cross-Sections: Bare Versus Dressed Jets'. *Z. Phys.* (1984) C21: p. 235. doi: 10.1007/BF01577037 (cit. on pp. 19, 33).

185. Neumann, T.: 'Topmassen-Effekte in der differentiellen Higgsproduktion an Hadronenbeschleunigern'. Universität Wuppertal, 2011 (cit. on pp. 19, 32, 57).

186. Wiesemann, M.: 'Kinematische Verteilungen bei der Higgsproduktion im Standardmodell und seiner supersymmetrischen Erweiterung'. PhD thesis. Universität Wuppertal, 2013 (cit. on pp. 19, 32, 57).

187. Ellis, R. K., D. A. Ross, and A. E. Terrano: 'The Perturbative Calculation of Jet Structure in e+ e- Annihilation'. *Nucl. Phys.* (1981) B178: p. 421. doi: 10.1016/0550-3213(81)90165-6 (cit. on pp. 19, 33).

188. Giele, W. T. and E. W. N. Glover: 'Higher order corrections to jet cross-sections in e+ e- annihilation'. *Phys. Rev.* (1992) D46: pp. 1980–2010. doi: 10.1103/PhysRevD.46.1980 (cit. on pp. 19, 33).

189. Giele, W. T., E. W. N. Glover, and D. A. Kosower: 'Higher order corrections to jet cross-sections in hadron colliders'. *Nucl. Phys.* (1993) B403: pp. 633–670. doi: 10.1016/0550-3213(93)90365-V. arXiv: hep-ph/9302225 [hep-ph] (cit. on p. 19).

190. Harris, B. W. and J. F. Owens: 'The Two cutoff phase space slicing method'. *Phys. Rev.* (2002) D65: p. 094032. doi: 10.1103/PhysRevD.65.094032. arXiv: hep-ph/0102128 [hep-ph] (cit. on p. 19).

191. Frixione, S., Z. Kunszt, and A. Signer: 'Three jet cross-sections to next-to-leading order'. *Nucl. Phys.* (1996) B467: pp. 399–442. doi: 10.1016/0550-3213(96)00110-1. arXiv: hep-ph/9512328 [hep-ph] (cit. on p. 19).

192. Frixione, S.: 'A General approach to jet cross-sections in QCD'. *Nucl. Phys.* (1997) B507: pp. 295–314. doi: 10.1016/S0550-3213(97)00574-9. arXiv: hep-ph/9706545 [hep-ph] (cit. on p. 19).

193. Anastasiou, C., K. Melnikov, and F. Petriello: 'A new method for real radiation at NNLO'. *Phys. Rev.* (2004) D69: p. 076010. doi: 10.1103/PhysRevD.69.076010. arXiv: hep-ph/0311311 [hep-ph] (cit. on pp. 19, 33).

194. Anastasiou, C., K. Melnikov, and F. Petriello: 'Fully differential Higgs boson production and the di-photon signal through next-to-next-to-leading order'. *Nucl. Phys.* (2005) B724: pp. 197–246. doi: 10.1016/j.nuclphysb.2005.06.036. arXiv: hep-ph/0501130 [hep-ph] (cit. on pp. 19, 32).

195. Binoth, T. and G. Heinrich: 'Numerical evaluation of phase space integrals by sector decomposition'. *Nucl. Phys.* (2004) B693: pp. 134–148. doi: 10.1016/j.nuclphysb.2004.06.005. arXiv: hep-ph/0402265 [hep-ph] (cit. on pp. 19, 33).

196. Gehrmann-De Ridder, A., T. Gehrmann, and E. W. N. Glover: 'Antenna subtraction at NNLO'. *JHEP* (2005) 0509: p. 056. doi: 10.1088/1126-6708/2005/09/056. arXiv: hep-ph/0505111 [hep-ph] (cit. on pp. 19, 33).

197. Catani, S. and M. Grazzini: 'An NNLO subtraction formalism in hadron collisions and its application to Higgs boson production at the LHC'. *Phys. Rev. Lett.* (2007) 98: p. 222002. doi: 10.1103/PhysRevLett.98.222002. arXiv: hep-ph/0703012 [hep-ph] (cit. on pp. 19, 32, 33, 42).

198. Czakon, M.: 'A novel subtraction scheme for double-real radiation at NNLO'. *Phys. Lett.* (2010) B693: pp. 259–268. doi: 10.1016/j.physletb.2010.08.036. arXiv: 1005.0274 [hep-ph] (cit. on pp. 19, 33).

199. Gaunt, J., M. Stahlhofen, F. J. Tackmann, and J. R. Walsh: 'N-jettiness Subtractions for NNLO QCD Calculations'. (2015). arXiv: 1505.04794 [hep-ph] (cit. on pp. 19, 33).

200. Weinzierl, S.: 'Subtraction terms at NNLO'. *JHEP* (2003) 0303: p. 062. doi: 10.1088/1126-6708/2003/03/062. arXiv: hep-ph/0302180 [hep-ph] (cit. on p. 19).

201. Weinzierl, S.: 'Subtraction terms for one loop amplitudes with one unresolved parton'. *JHEP* (2003) 0307: p. 052. doi: 10.1088/1126-6708/2003/07/052. arXiv: hep-ph/0306248 [hep-ph] (cit. on p. 19).

202. Gehrmann-De Ridder, A., T. Gehrmann, and G. Heinrich: 'Four particle phase space integrals in massless QCD'. *Nucl. Phys.* (2004) B682: pp. 265–288. doi: 10.1016/j.nuclphysb.2004.01.023. arXiv: hep-ph/0311276 [hep-ph] (cit. on p. 19).

203. Gehrmann-De Ridder, A., T. Gehrmann, and E. W. N. Glover: 'Infrared structure of e+ e- —> 2 jets at NNLO'. *Nucl. Phys.* (2004) B691: pp. 195–222. doi: 10.1016/j.nuclphysb.2004.05.017. arXiv: hep-ph/0403057 [hep-ph] (cit. on p. 19).

204. Gehrmann-De Ridder, A., T. Gehrmann, and E. W. N. Glover: 'Infrared structure of $e^+e^- \to 3$ jets at NNLO - the C_F^2 contribution'. *Nucl. Phys. Proc. Suppl.* (2004) 135: pp. 97–101. doi: 10.1016/j.nuclphysbps.2004.09.042. arXiv: hep-ph/0407023 [hep-ph] (cit. on p. 19).

205. Kilgore, W. B.: 'Subtraction terms for hadronic production processes at next-to-next-to-leading order'. *Phys. Rev.* (2004) D70: p. 031501. doi: 10.1103/PhysRevD.70.031501. arXiv: hep-ph/0403128 [hep-ph] (cit. on p. 19).

206. Frixione, S. and M. Grazzini: 'Subtraction at NNLO'. *JHEP* (2005) 0506: p. 010. doi: 10.1088/1126-6708/2005/06/010. arXiv: hep-ph/0411399 [hep-ph] (cit. on p. 19).

207. Kosower, D. A.: 'Multiple singular emission in gauge theories'. *Phys. Rev.* (2003) D67: p. 116003. doi: 10.1103/PhysRevD.67.116003. arXiv: hep-ph/0212097 [hep-ph] (cit. on p. 19).

208. Kosower, D. A.: 'All orders singular emission in gauge theories'. *Phys. Rev. Lett.* (2003) 91: p. 061602. doi: 10.1103/PhysRevLett.91.061602. arXiv: hep-ph/0301069 [hep-ph] (cit. on p. 19).

209. Binoth, T. and G. Heinrich: 'An automatized algorithm to compute infrared divergent multiloop integrals'. *Nucl. Phys.* (2000) B585: pp. 741–759. doi: 10.1016/S0550-3213(00)00429-6. arXiv: hep-ph/0004013 [hep-ph] (cit. on pp. 19, 20, 30).

210. Binoth, T. and G. Heinrich: 'Numerical evaluation of multiloop integrals by sector decomposition'. *Nucl. Phys.* (2004) B680: pp. 375–388. doi: 10.1016/j.nuclphysb.2003.12.023. arXiv: hep-ph/0305234 [hep-ph] (cit. on pp. 19, 20, 30, 84, 100).

211. Collins, J.: 'Parton distribution functions (definition)'. *Scholarpedia* (2012) 7.7. revision #128140: p. 10851 (cit. on p. 19).

212. Dokshitzer, Y. L.: 'Calculation of the Structure Functions for Deep Inelastic Scattering and e+ e- Annihilation by Perturbation Theory in Quantum Chromodynamics.' *Sov. Phys. JETP* (1977) 46: pp. 641–653 (cit. on p. 19).

213. Gribov, V. N. and L. N. Lipatov: 'Deep inelastic e p scattering in perturbation theory'. *Sov. J. Nucl. Phys.* (1972) 15: pp. 438–450 (cit. on p. 19).

214. Gribov, V. N. and L. N. Lipatov: 'e+ e- pair annihilation and deep inelastic e p scattering in perturbation theory'. *Sov. J. Nucl. Phys.* (1972) 15: pp. 675–684 (cit. on p. 19).

215. Altarelli, G. and G. Parisi: 'Asymptotic Freedom in Parton Language'. *Nucl. Phys.* (1977) B126: p. 298. doi: 10.1016/0550-3213(77)90384-4 (cit. on p. 19).

216. Smirnov, V. A.: *Analytic tools for Feynman integrals*. Vol. 250. 2012: pp. 1–296. doi: 10.1007/978-3-642-34886-0 (cit. on pp. 20, 21, 30, 97, 123).

217. Chetyrkin, K. G. and F. V. Tkachov: 'Integration by parts: The algorithm to calculate β-functions in 4 loops'. *Nucl. Phys.* (1981) B192: pp. 159–204. doi: 10.1016/0550-3213(81)90199-1 (cit. on pp. 20, 30, 95).

218. Laporta, S.: 'High precision calculation of multiloop Feynman integrals by difference equations'. *Int. J. Mod. Phys.* (2000) A15: pp. 5087–5159. doi: 10.1016/S0217-751X(00)00215-7. arXiv: hep-ph/0102033 [hep-ph] (cit. on pp. 20, 30).

219. Gehrmann, T. and E. Remiddi: 'Differential equations for two loop four point functions'. *Nucl. Phys.* (2000) B580: pp. 485–518. doi: 10.1016/S0550-3213(00)00223-6. arXiv: hep-ph/9912329 [hep-ph] (cit. on pp. 20, 30).

220. Smirnov, A. V.: 'FIESTA 3: cluster-parallelizable multiloop numerical calculations in physical regions'. *Comput. Phys. Commun.* (2014) 185: pp. 2090–2100. doi: 10.1016/j.cpc.2014.03.015. arXiv: 1312.3186 [hep-ph] (cit. on pp. 20, 100, 126).

221. Anastasiou, C., F. Herzog, and A. Lazopoulos: 'On the factorization of overlapping singularities at NNLO'. *JHEP* (2011) 1103: p. 038. doi: 10.1007/JHEP03(2011)038. arXiv: 1011.4867 [hep-ph] (cit. on pp. 22, 101).

references for part II

17. Aad, G. et al. (The ATLAS collaboration): 'Observation of a new particle in the search for the Standard Model Higgs boson with the ATLAS detector at the LHC'. *Phys. Lett.* (2012) B716: pp. 1–29. doi: 10.1016/j.physletb.2012.08.020. arXiv: 1207.7214 [hep-ex] (cit. on pp. 3, 8, 25).

18. Chatrchyan, S. et al. (The CMS collaboration): 'Observation of a new boson at a mass of 125 GeV with the CMS experiment at the LHC'. *Phys. Lett.* (2012) B716: pp. 30–61. doi: 10.1016/j.physletb.2012.08.021. arXiv: 1207.7235 [hep-ex] (cit. on pp. 3, 8, 25).

43. Harlander, R. V., T. Neumann, K. J. Ozeren, and M. Wiesemann: 'Top-mass effects in differential Higgs production through gluon fusion at order α_s^4'. *JHEP* (2012) 1208: p. 139. doi: 10.1007/JHEP08(2012)139. arXiv: 1206.0157 [hep-ph] (cit. on pp. 6, 14, 19, 23, 26, 31, 32, 34–37, 39, 40, 42, 53, 57, 70).

58. Aad, G. et al. (The ATLAS collaboration): 'Measurements of the Total and Differential Higgs Boson Production Cross Sections Combining the $H \to \gamma\gamma$ and $H \to ZZ^* \to 4\ell$ Decay Channels at $\sqrt{s} = 8$ TeV with the ATLAS Detector'. (2015). arXiv: 1504.05833 [hep-ex] (cit. on pp. 8, 25, 61).

59. *Measurements of the Higgs boson production and decay rates and coupling strengths using pp collision data at $\sqrt{s} = 7$ and 8 TeV in the ATLAS experiment*. Tech. rep. ATLAS-CONF-2015-007. Geneva: CERN, Mar. 2015 (cit. on pp. 8, 25, 61).

60. Aad, G. et al. (The ATLAS collaboration): 'Study of the spin and parity of the Higgs boson in diboson decays with the ATLAS detector'. (2015). arXiv: 1506.05669 [hep-ex] (cit. on pp. 8, 25, 61).

61. Khachatryan, V. et al. (The CMS collaboration): 'Precise determination of the mass of the Higgs boson and tests of compatibility of its couplings with the standard model predictions using proton collisions at 7 and 8 TeV'. (2014). arXiv: 1412.8662 [hep-ex] (cit. on pp. 8, 25, 61).

62. Giardino, P. P., K. Kannike, I. Masina, M. Raidal, and A. Strumia: 'The universal Higgs fit'. *JHEP* (2014) 1405: p. 046. doi: 10.1007/JHEP05(2014)046. arXiv: 1303.3570 [hep-ph] (cit. on pp. 8, 25, 61).

115. Neumann, T. and M. Wiesemann: 'Finite top-mass effects in gluon-induced Higgs production with a jet-veto at NNLO'. *JHEP* (2014) 1411: p. 150. doi: 10.1007/JHEP11(2014)150. arXiv: 1408.6836 [hep-ph] (cit. on pp. 14, 19, 23, 26, 32, 37, 45–49, 51–55, 70).

116. Grazzini, M. and H. Sargsyan: 'Heavy-quark mass effects in Higgs boson production at the LHC'. *JHEP* (2013) 1309: p. 129. doi: 10.1007/JHEP09(2013)129. arXiv: 1306.4581 [hep-ph] (cit. on pp. 14, 31, 42).

130. Olive, K. A. et al. (The Particle Data Group collaboration): 'Review of Particle Physics'. *Chin. Phys* (2014) C38: p. 090001. doi: 10.1088/1674-1137/38/9/090001 (cit. on pp. 16, 43, 108).

131. Demartin, F., S. Forte, E. Mariani, J. Rojo, and A. Vicini: 'Impact of parton distribution function and α_s uncertainties on Higgs boson production in gluon fusion at hadron colliders'. *Phys. Rev.* (2010) D82: p. 014002. doi: 10.1103/PhysRevD.82.014002. arXiv: 1004.0962 [hep-ph] (cit. on pp. 16, 30).

132. Baglio, J. and A. Djouadi: 'Predictions for Higgs production at the Tevatron and the associated uncertainties'. *JHEP* (2010) 1010: p. 064. doi: 10.1007/JHEP10(2010)064. arXiv: 1003.4266 [hep-ph] (cit. on pp. 16, 30).

180. Catani, S. and M. H. Seymour: 'A General algorithm for calculating jet cross-sections in NLO QCD'. *Nucl. Phys.* (1997) B485: pp. 291–419. doi: 10.1016/S0550-3213(96)00589-5. arXiv: hep-ph/9605323 [hep-ph]. Erratum ibid. *Nucl. Phys.* (1998) B510.1–2 (cit. on pp. 19, 33, 42).

182. Fabricius, K., I. Schmitt, G. Schierholz, and G. Kramer: 'Order α_s^2 Correction to Jet Cross-Sections in $e^+ e^-$ Annihilation'. *Phys. Lett.* (1980) B97: p. 431. doi: 10.1016/0370-2693(80)90635-8 (cit. on pp. 19, 33).

183. Fabricius, K., I. Schmitt, G. Kramer, and G. Schierholz: 'Higher Order Perturbative QCD Calculation of Jet Cross-Sections in e+ e- Annihilation'. *Z. Phys.* (1981) C11: p. 315. doi: 10.1007/BF01578281 (cit. on pp. 19, 33).

184. Gutbrod, F., G. Kramer, and G. Schierholz: 'Higher Order QCD Corrections to the Three Jet Cross-Sections: Bare Versus Dressed Jets'. *Z. Phys.* (1984) C21: p. 235. doi: 10.1007/BF01577037 (cit. on pp. 19, 33).

185. Neumann, T.: 'Topmassen-Effekte in der differentiellen Higgsproduktion an Hadronenbeschleunigern'. Universität Wuppertal, 2011 (cit. on pp. 19, 32, 57).

186. Wiesemann, M.: 'Kinematische Verteilungen bei der Higgsproduktion im Standardmodell und seiner supersymmetrischen Erweiterung'. PhD thesis. Universität Wuppertal, 2013 (cit. on pp. 19, 32, 57).

187. Ellis, R. K., D. A. Ross, and A. E. Terrano: 'The Perturbative Calculation of Jet Structure in e+ e- Annihilation'. *Nucl. Phys.* (1981) B178: p. 421. doi: 10.1016/0550-3213(81)90165-6 (cit. on pp. 19, 33).

188. Giele, W. T. and E. W. N. Glover: 'Higher order corrections to jet cross-sections in e+ e- annihilation'. *Phys. Rev.* (1992) D46: pp. 1980–2010. doi: 10.1103/PhysRevD.46.1980 (cit. on pp. 19, 33).

193. Anastasiou, C., K. Melnikov, and F. Petriello: 'A new method for real radiation at NNLO'. *Phys. Rev.* (2004) D69: p. 076010. doi: 10.1103/PhysRevD.69.076010. arXiv: hep-ph/0311311 [hep-ph] (cit. on pp. 19, 33).

194. Anastasiou, C., K. Melnikov, and F. Petriello: 'Fully differential Higgs boson production and the di-photon signal through next-to-next-to-leading order'. *Nucl. Phys.* (2005) B724: pp. 197–246. doi: 10.1016/j.nuclphysb.2005.06.036. arXiv: hep-ph/0501130 [hep-ph] (cit. on pp. 19, 32).

195. Binoth, T. and G. Heinrich: 'Numerical evaluation of phase space integrals by sector decomposition'. *Nucl. Phys.* (2004) B693: pp. 134–148. doi: 10.1016/j.nuclphysb.2004.06.005. arXiv: hep-ph/0402265 [hep-ph] (cit. on pp. 19, 33).

196. Gehrmann-De Ridder, A., T. Gehrmann, and E. W. N. Glover: 'Antenna subtraction at NNLO'. *JHEP* (2005) 0509: p. 056. doi: 10.1088/1126-6708/2005/09/056. arXiv: hep-ph/0505111 [hep-ph] (cit. on pp. 19, 33).

197. Catani, S. and M. Grazzini: 'An NNLO subtraction formalism in hadron collisions and its application to Higgs boson production at the LHC'. *Phys. Rev. Lett.* (2007) 98: p. 222002. doi: 10.1103/PhysRevLett.98.222002. arXiv: hep-ph/0703012 [hep-ph] (cit. on pp. 19, 32, 33, 42).

198. Czakon, M.: 'A novel subtraction scheme for double-real radiation at NNLO'. *Phys. Lett.* (2010) B693: pp. 259–268. doi: 10.1016/j.physletb.2010.08.036. arXiv: 1005.0274 [hep-ph] (cit. on pp. 19, 33).

199. Gaunt, J., M. Stahlhofen, F. J. Tackmann, and J. R. Walsh: 'N-jettiness Subtractions for NNLO QCD Calculations'. (2015). arXiv: 1505.04794 [hep-ph] (cit. on pp. 19, 33).

209. Binoth, T. and G. Heinrich: 'An automatized algorithm to compute infrared divergent multiloop integrals'. *Nucl. Phys.* (2000) B585: pp. 741–759. doi: 10.1016/S0550-3213(00)00429-6. arXiv: hep-ph/0004013 [hep-ph] (cit. on pp. 19, 20, 30).

210. Binoth, T. and G. Heinrich: 'Numerical evaluation of multiloop integrals by sector decomposition'. *Nucl. Phys.* (2004) B680: pp. 375–388. doi: 10.1016/j.nuclphysb.2003.12.023. arXiv: hep-ph/0305234 [hep-ph] (cit. on pp. 19, 20, 30, 84, 100).

216. Smirnov, V. A.: *Analytic tools for Feynman integrals*. Vol. 250. 2012: pp. 1–296. doi: 10.1007/978-3-642-34886-0 (cit. on pp. 20, 21, 30, 97, 123).

217. Chetyrkin, K. G. and F. V. Tkachov: 'Integration by parts: The algorithm to calculate β-functions in 4 loops'. *Nucl. Phys.* (1981) B192: pp. 159–204. doi: 10.1016/0550-3213(81)90199-1 (cit. on pp. 20, 30, 95).

218. Laporta, S.: 'High precision calculation of multiloop Feynman integrals by difference equations'. *Int. J. Mod. Phys.* (2000) A15: pp. 5087–5159. doi: 10.1016/S0217-751X(00)00215-7. arXiv: hep-ph/0102033 [hep-ph] (cit. on pp. 20, 30).

219. Gehrmann, T. and E. Remiddi: 'Differential equations for two loop four point functions'. *Nucl. Phys.* (2000) B580: pp. 485–518. doi: 10.1016/S0550-3213(00)00223-6. arXiv: hep-ph/9912329 [hep-ph] (cit. on pp. 20, 30).

222. Englert, F. and R. Brout: 'Broken Symmetry and the Mass of Gauge Vector Mesons'. *Phys. Rev. Lett.* (1964) 13: pp. 321–323. doi: 10.1103/PhysRevLett.13.321 (cit. on p. 25).

223. Higgs, P. W.: 'Broken symmetries, massless particles and gauge fields'. *Phys. Lett.* (1964) 12: pp. 132–133. doi: 10.1016/0031-9163(64)91136-9 (cit. on p. 25).

224. Higgs, P. W.: 'Broken Symmetries and the Masses of Gauge Bosons'. *Phys. Rev. Lett.* (1964) 13: pp. 508–509. doi: 10.1103/PhysRevLett.13.508 (cit. on p. 25).

225. Guralnik, G. S., C. R. Hagen, and T. W. B. Kibble: 'Global Conservation Laws and Massless Particles'. *Phys. Rev. Lett.* (1964) 13: pp. 585–587. doi: 10.1103/PhysRevLett.13.585 (cit. on p. 25).

226. Anderson, P. W.: 'Plasmons, Gauge Invariance, and Mass'. *Phys. Rev.* (1963) 130: pp. 439–442. doi: 10.1103/PhysRev.130.439 (cit. on p. 25).

227. Nambu, Y.: 'Quasiparticles and Gauge Invariance in the Theory of Superconductivity'. *Phys. Rev.* (1960) 117: pp. 648–663. doi: 10.1103/PhysRev.117.648 (cit. on p. 25).

228. Aad, G. et al. (The ATLAS and CMS collaborations): 'Combined Measurement of the Higgs Boson Mass in pp Collisions at $\sqrt{s} = 7$ and 8 TeV with the ATLAS and CMS Experiments'. (2015). arXiv: 1503.07589 [hep-ex] (cit. on p. 25).

229. Aad, G. et al. (The ATLAS collaboration): 'Measurements of Higgs boson production and couplings in diboson final states with the ATLAS detector at the LHC'. *Phys. Lett.* (2013) B726: pp. 88–119. doi: 10.1016/j.physletb.2014.05.011,10.1016/j.physletb.2013.08.010. arXiv: 1307.1427 [hep-ex] (cit. on p. 26).

230. Khachatryan, V. et al. (The CMS collaboration): 'Observation of the diphoton decay of the Higgs boson and measurement of its properties'. *Eur. Phys. J.* (2014) C74.10: p. 3076. doi: 10.1140/epjc/s10052-014-3076-z. arXiv: 1407.0558 [hep-ex] (cit. on p. 26).

231. Chatrchyan, S. et al. (The CMS collaboration): 'Measurement of the properties of a Higgs boson in the four-lepton final state'. *Phys. Rev.* (2014) D89.9: p. 092007. doi: 10.1103/PhysRevD.89.092007. arXiv: 1312.5353 [hep-ex] (cit. on p. 26).

232. Aad, G. et al. (The ATLAS collaboration): 'Observation and measurement of Higgs boson decays to WW^* with the ATLAS detector'. (2014). arXiv: 1412.2641 [hep-ex] (cit. on p. 26).

233. Chatrchyan, S. et al. (The CMS collaboration): 'Measurement of Higgs boson production and properties in the WW decay channel with leptonic final states'. *JHEP* (2014) 1401: p. 096. doi: 10.1007/JHEP01(2014)096. arXiv: 1312.1129 [hep-ex] (cit. on pp. 26, 43).

234. Dittmar, M. and H. K. Dreiner: 'How to find a Higgs boson with a mass between 155-GeV - 180-GeV at the LHC'. *Phys. Rev.* (1997) D55: pp. 167–172. doi: 10.1103/PhysRevD.55.167. arXiv: hep-ph/9608317 [hep-ph] (cit. on p. 26).

235. Anastasiou, C., G. Dissertori, F. Stockli, and B. R. Webber: 'QCD radiation effects on the $H \to WW \to l\nu l\nu$ signal at the LHC'. *JHEP* (2008) 0803: p. 017. doi: 10.1088/1126-6708/2008/03/017. arXiv: 0801.2682 [hep-ph] (cit. on p. 26).

236. Dittmaier, S. et al. (The LHC Higgs Cross Section Working Group collaboration): 'Handbook of LHC Higgs Cross Sections: 1. Inclusive Observables'. (2011). DOI: 10.5170/CERN-2011-002. arXiv: 1101.0593 [hep-ph] (cit. on p. 26).

237. Dittmaier, S. et al. (The LHC Higgs Cross Section Working Group collaboration): 'Handbook of LHC Higgs Cross Sections: 2. Differential Distributions'. (2012). DOI: 10.5170/CERN-2012-002. arXiv: 1201.3084 [hep-ph] (cit. on p. 26).

238. Heinemeyer, S. et al. (The LHC Higgs Cross Section Working Group collaboration): 'Handbook of LHC Higgs Cross Sections: 3. Higgs Properties'. (2013). Ed. by Heinemeyer, S. DOI: 10.5170/CERN-2013-004. arXiv: 1307.1347 [hep-ph] (cit. on pp. 26, 62).

239. Georgi, H. M., S. L. Glashow, M. E. Machacek, and D. V. Nanopoulos: 'Higgs Bosons from Two Gluon Annihilation in Proton Proton Collisions'. *Phys. Rev. Lett.* (1978) 40: p. 692. DOI: 10.1103/PhysRevLett.40.692 (cit. on p. 27).

240. Wilczek, F.: 'Decays of Heavy Vector Mesons Into Higgs Particles'. *Phys. Rev. Lett.* (1977) 39: p. 1304. DOI: 10.1103/PhysRevLett.39.1304 (cit. on p. 27).

241. Ellis, J. R., M. K. Gaillard, D. V. Nanopoulos, and C. T. Sachrajda: 'Is the Mass of the Higgs Boson About 10-GeV?' *Phys. Lett.* (1979) B83: p. 339. DOI: 10.1016/0370-2693(79)91122-5 (cit. on p. 27).

242. Rizzo, T. G.: 'Gluon Final States in Higgs Boson Decay'. *Phys. Rev.* (1980) D22: p. 178. DOI: 10.1103/PhysRevD.22.178 (cit. on p. 27).

243. Baur, U. and E. W. N. Glover: 'Higgs Boson Production at Large Transverse Momentum in Hadronic Collisions'. *Nucl. Phys.* (1990) B339: pp. 38–66. DOI: 10.1016/0550-3213(90)90532-I (cit. on pp. 27, 28, 31).

244. Ellis, R. K., I. Hinchliffe, M. Soldate, and J. J. van der Bij: 'Higgs Decay to tau+ tau-: A Possible Signature of Intermediate Mass Higgs Bosons at the SSC'. *Nucl. Phys.* (1988) B297: p. 221. DOI: 10.1016/0550-3213(88)90019-3 (cit. on pp. 27, 31).

245. Dawson, S.: 'Radiative corrections to Higgs boson production'. *Nucl. Phys.* (1991) B359: pp. 283–300. DOI: 10.1016/0550-3213(91)90061-2 (cit. on p. 27).

246. Djouadi, A., M. Spira, and P. M. Zerwas: 'Production of Higgs bosons in proton colliders: QCD corrections'. *Phys. Lett.* (1991) B264: pp. 440–446. DOI: 10.1016/0370-2693(91)90375-Z (cit. on p. 27).

247. Shifman, M. A., A. I. Vainshtein, M. B. Voloshin, and V. I. Zakharov: 'Low-Energy Theorems for Higgs Boson Couplings to Photons'. *Sov. J. Nucl. Phys.* (1979) 30: pp. 711–716 (cit. on p. 27).

248. Vainshtein, A. I., V. I. Zakharov, and M. A. Shifman: 'Higgs Particles'. *Sov. Phys. Usp.* (1980) 23: pp. 429–449. DOI: 10.1070/PU1980v023n08ABEH005019 (cit. on p. 27).

249. Voloshin, M. B.: 'Once Again About the Role of Gluonic Mechanism in Interaction of Light Higgs Boson with Hadrons'. *Sov. J. Nucl. Phys.* (1986) 44: p. 478 (cit. on p. 27).

250. Chetyrkin, K. G., B. A. Kniehl, and M. Steinhauser: 'Decoupling relations to $\mathcal{O}(\alpha_s^3)$ and their connection to low-energy theorems'. *Nucl. Phys.* (1998) B510: pp. 61–87. DOI: 10.1016/S0550-3213(97)00649-4. arXiv: hep-ph/9708255 [hep-ph] (cit. on pp. 27, 108).

251. Krämer, M., E. Laenen, and M. Spira: 'Soft gluon radiation in Higgs boson production at the LHC'. *Nucl. Phys.* (1998) B511: pp. 523–549. DOI: 10.1016/S0550-3213(97)00679-2. arXiv: hep-ph/9611272 [hep-ph] (cit. on pp. 27, 30).

252. Chetyrkin, K. G., B. A. Kniehl, and M. Steinhauser: 'Hadronic Higgs decay to order α_s^4'. *Phys. Rev. Lett.* (1997) 79: pp. 353–356. DOI: 10.1103/PhysRevLett.79.353. arXiv: hep-ph/9705240 [hep-ph] (cit. on p. 27).

253. Schröder, Y. and M. Steinhauser: 'Four-loop decoupling relations for the strong coupling'. *JHEP* (2006) 0601: p. 051. DOI: 10.1088/1126-6708/2006/01/051. arXiv: hep-ph/0512058 [hep-ph] (cit. on pp. 27, 64, 108).

254. Chetyrkin, K. G., J. H. Kühn, and C. Sturm: 'QCD decoupling at four loops'. *Nucl. Phys.* (2006) B744: pp. 121–135. DOI: 10.1016/j.nuclphysb.2006.03.020. arXiv: hep-ph/0512060 [hep-ph] (cit. on pp. 27, 64, 108).

255. Graudenz, D., M. Spira, and P. M. Zerwas: 'QCD corrections to Higgs boson production at proton proton colliders'. *Phys. Rev. Lett.* (1993) 70: pp. 1372–1375. DOI: 10.1103/PhysRevLett.70.1372 (cit. on p. 28).

256. Spira, M., A. Djouadi, D. Graudenz, and P. M. Zerwas: 'SUSY Higgs production at proton colliders'. *Phys. Lett.* (1993) B318: pp. 347–353. DOI: 10.1016/0370-2693(93)90138-8 (cit. on p. 28).

257. Spira, M., A. Djouadi, D. Graudenz, and P. M. Zerwas: 'Higgs boson production at the LHC'. *Nucl. Phys.* (1995) B453: pp. 17–82. doi: 10.1016/0550-3213(95)00379-7. arXiv: hep-ph/9504378 [hep-ph] (cit. on pp. 28, 31).

258. Dawson, S. and R. Kauffman: 'QCD corrections to Higgs boson production: nonleading terms in the heavy quark limit'. *Phys. Rev.* (1994) D49: pp. 2298–2309. doi: 10.1103/PhysRevD.49.2298. arXiv: hep-ph/9310281 [hep-ph] (cit. on p. 28).

259. Harlander, R. and P. Kant: 'Higgs production and decay: Analytic results at next-to-leading order QCD'. *JHEP* (2005) 0512: p. 015. doi: 10.1088/1126-6708/2005/12/015. arXiv: hep-ph/0509189 [hep-ph] (cit. on p. 28).

260. Anastasiou, C., S. Beerli, S. Bucherer, A. Daleo, and Z. Kunszt: 'Two-loop amplitudes and master integrals for the production of a Higgs boson via a massive quark and a scalar-quark loop'. *JHEP* (2007) 0701: p. 082. doi: 10.1088/1126-6708/2007/01/082. arXiv: hep-ph/0611236 [hep-ph] (cit. on p. 28).

261. Dawson, S. and R. P. Kauffman: 'Higgs boson plus multi - jet rates at the SSC'. *Phys. Rev. Lett.* (1992) 68: pp. 2273–2276. doi: 10.1103/PhysRevLett.68.2273 (cit. on pp. 28, 30).

262. Kauffman, R. P., S. V. Desai, and D. Risal: 'Production of a Higgs boson plus two jets in hadronic collisions'. *Phys. Rev.* (7 Apr. 1997) D55: pp. 4005–4015. doi: 10.1103/PhysRevD.55.4005. arXiv: hep-ph/9610541 [hep-ph]. Erratum ibid. *Phys. Rev.* (11 Oct. 1998) D58 (cit. on p. 28).

263. Del Duca, V., W. Kilgore, C. Oleari, C. Schmidt, and D. Zeppenfeld: 'Higgs + 2 jets via gluon fusion'. *Phys. Rev. Lett.* (2001) 87: p. 122001. doi: 10.1103/PhysRevLett.87.122001. arXiv: hep-ph/0105129 [hep-ph] (cit. on pp. 28, 31, 67).

264. Del Duca, V., W. Kilgore, C. Oleari, C. Schmidt, and D. Zeppenfeld: 'Gluon fusion contributions to H + 2 jet production'. *Nucl. Phys.* (2001) B616: pp. 367–399. doi: 10.1016/S0550-3213(01)00446-1. arXiv: hep-ph/0108030 [hep-ph] (cit. on pp. 28, 31, 67, 72).

265. Kauffman, R. P.: 'Higgs boson p_T in gluon fusion'. *Phys. Rev.* (1991) D44: pp. 1415–1425. doi: 10.1103/PhysRevD.44.1415 (cit. on pp. 29, 30).

266. Sjöstrand, T.: 'A Model for Initial State Parton Showers'. *Phys. Lett.* (1985) B157: p. 321. doi: 10.1016/0370-2693(85)90674-4 (cit. on p. 29).

267. Balazs, C., J. Huston, and I. Puljak: 'Higgs production: A Comparison of parton showers and resummation'. *Phys. Rev.* (2001) D63: p. 014021. doi: 10.1103/PhysRevD.63.014021. arXiv: hep-ph/0002032 [hep-ph] (cit. on p. 29).

268. Collins, J. C. and D. E. Soper: 'Back-to-back Jets in QCD: Comparison With Experiment'. *Phys. Rev. Lett.* (1982) 48: p. 655. doi: 10.1103/PhysRevLett.48.655 (cit. on p. 29).

269. Collins, J. C. and D. E. Soper: 'Back-To-Back Jets in QCD'. *Nucl. Phys.* (1981) B193: p. 381. doi: 10.1016/0550-3213(81)90339-4 (cit. on p. 29).

270. Collins, J. C. and D. E. Soper: 'Back-To-Back Jets: Fourier Transform from B to K-Transverse'. *Nucl. Phys.* (1982) B197: p. 446. doi: 10.1016/0550-3213(82)90453-9 (cit. on p. 29).

271. Collins, J. C., D. E. Soper, and G. F. Sterman: 'Transverse Momentum Distribution in Drell-Yan Pair and W and Z Boson Production'. *Nucl. Phys.* (1985) B250: p. 199. doi: 10.1016/0550-3213(85)90479-1 (cit. on p. 29).

272. Ellis, R. K., D. A. Ross, and S. Veseli: 'Vector boson production in hadronic collisions'. *Nucl. Phys.* (1997) B503: pp. 309–338. doi: 10.1016/S0550-3213(97)00403-3. arXiv: hep-ph/9704239 [hep-ph] (cit. on p. 29).

273. Ellis, R. K. and S. Veseli: 'W and Z transverse momentum distributions: Resummation in q_T space'. *Nucl. Phys.* (1998) B511: pp. 649–669. doi: 10.1016/S0550-3213(97)00655-X. arXiv: hep-ph/9706526 [hep-ph] (cit. on p. 29).

274. Bauer, C. W., S. Fleming, D. Pirjol, and I. W. Stewart: 'An Effective field theory for collinear and soft gluons: Heavy to light decays'. *Phys. Rev.* (2001) D63: p. 114020. doi: 10.1103/PhysRevD.63.114020. arXiv: hep-ph/0011336 [hep-ph] (cit. on p. 29).

275. Bauer, C. W., D. Pirjol, and I. W. Stewart: 'Soft collinear factorization in effective field theory'. *Phys. Rev.* (2002) D65: p. 054022. doi: 10.1103/PhysRevD.65.054022. arXiv: hep-ph/0109045 [hep-ph] (cit. on p. 29).

276. Bauer, C. W., S. Fleming, D. Pirjol, I. Z. Rothstein, and I. W. Stewart: 'Hard scattering factorization from effective field theory'. *Phys. Rev.* (2002) D66: p. 014017. doi: 10.1103/PhysRevD.66.014017. arXiv: hep-ph/0202088 [hep-ph] (cit. on p. 29).

277. Luisoni, G. and S. Marzani: 'Resummation in QCD'. (2015). arXiv: 1505.04084 [hep-ph] (cit. on p. 29).

278. Becher, T., A. Broggio, and A. Ferroglia: 'Introduction to Soft-Collinear Effective Theory'. (2014). arXiv: 1410.1892 [hep-ph] (cit. on p. 29).

279. Gao, Y., C. S. Li, and J. J. Liu: 'Transverse momentum resummation for Higgs production in soft-collinear effective theory'. *Phys. Rev.* (2005) D72: p. 114020. doi: 10.1103/PhysRevD.72.114020. arXiv: hep-ph/0501229 [hep-ph] (cit. on pp. 29, 31).

280. Idilbi, A., X.-d. Ji, and F. Yuan: 'Transverse momentum distribution through soft-gluon resummation in effective field theory'. *Phys. Lett.* (2005) B625: pp. 253–263. doi: 10.1016/j.physletb.2005.08.038. arXiv: hep-ph/0507196 [hep-ph] (cit. on pp. 29, 31).

281. Mantry, S. and F. Petriello: 'Factorization and Resummation of Higgs Boson Differential Distributions in Soft-Collinear Effective Theory'. *Phys. Rev.* (2010) D81: p. 093007. doi: 10.1103/PhysRevD.81.093007. arXiv: 0911.4135 [hep-ph] (cit. on pp. 29, 31).

282. Mantry, S. and F. Petriello: 'Transverse Momentum Distributions from Effective Field Theory with Numerical Results'. *Phys. Rev.* (2011) D83: p. 053007. doi: 10.1103/PhysRevD.83.053007. arXiv: 1007.3773 [hep-ph] (cit. on pp. 29, 31).

283. Becher, T., M. Neubert, and D. Wilhelm: 'Higgs-Boson Production at Small Transverse Momentum'. *JHEP* (2013) 1305: p. 110. doi: 10.1007/JHEP05(2013)110. arXiv: 1212.2621 [hep-ph] (cit. on pp. 29, 31).

284. Huang, F. P., C. S. Li, H. T. Li, and J. Wang: 'Renormalization-group improved predictions for Higgs boson production at large p_T'. *Phys. Rev.* (2014) D90.9: p. 094024. doi: 10.1103/PhysRevD.90.094024. arXiv: 1406.2591 [hep-ph] (cit. on pp. 29, 30).

285. Neill, D., I. Z. Rothstein, and V. Vaidya: 'The Higgs Transverse Momentum Distribution at NNLL and its Theoretical Errors'. (2015). arXiv: 1503.00005 [hep-ph] (cit. on pp. 29, 31).

286. Hinchliffe, I. and S. F. Novaes: 'Transverse-momentum distribution of Higgs bosons at the Superconducting Super Collider'. *Phys. Rev.* (1988) D38: pp. 3475–3480. doi: 10.1103/PhysRevD.38.3475 (cit. on p. 29).

287. Catani, S., E. D'Emilio, and L. Trentadue: 'The Gluon Form-factor to Higher Orders: Gluon Gluon Annihilation at Small Q^-transverse'. *Phys. Lett.* (1988) B211: pp. 335–342. doi: 10.1016/0370-2693(88)90912-4 (cit. on p. 29).

288. Yuan, C. P.: 'Kinematics of the Higgs boson at hadron colliders: NLO QCD gluon resummation'. *Phys. Lett.* (1992) B283: pp. 395–402. doi: 10.1016/0370-2693(92)90038-6 (cit. on p. 29).

289. Sterman, G. F.: 'Summation of Large Corrections to Short Distance Hadronic Cross-Sections'. *Nucl. Phys.* (1987) B281: p. 310. doi: 10.1016/0550-3213(87)90258-6 (cit. on p. 30).

290. Catani, S. and L. Trentadue: 'Resummation of the QCD Perturbative Series for Hard Processes'. *Nucl. Phys.* (1989) B327: p. 323. doi: 10.1016/0550-3213(89)90273-3 (cit. on p. 30).

291. Kauffman, R. P.: 'Higher order corrections to Higgs boson p_T'. *Phys. Rev.* (1992) D45: pp. 1512–1517. doi: 10.1103/PhysRevD.45.1512 (cit. on p. 30).

292. Florian, D. de and M. Grazzini: 'Next-to-next-to-leading logarithmic corrections at small transverse momentum in hadronic collisions'. *Phys. Rev. Lett.* (2000) 85: pp. 4678–4681. doi: 10.1103/PhysRevLett.85.4678. arXiv: hep-ph/0008152 [hep-ph] (cit. on p. 30).

293. Qiu, J. and X. Zhang: 'QCD prediction for heavy boson transverse momentum distributions'. *Phys. Rev. Lett.* (2001) 86: pp. 2724–2727. doi: 10.1103/PhysRevLett.86.2724. arXiv: hep-ph/0012058 [hep-ph] (cit. on p. 30).

294. Balazs, C. and C. P. Yuan: 'Higgs boson production at the LHC with soft gluon effects'. *Phys. Lett.* (2000) B478: pp. 192–198. doi: 10.1016/S0370-2693(00)00270-7. arXiv: hep-ph/0001103 [hep-ph] (cit. on p. 30).

295. Vogt, A.: 'Next-to-next-to-leading logarithmic threshold resummation for deep inelastic scattering and the Drell-Yan process'. *Phys. Lett.* (2001) B497: pp. 228–234. doi: 10.1016/S0370-2693(00)01344-7. arXiv: hep-ph/0010146 [hep-ph] (cit. on p. 30).

296. Florian, D. de and M. Grazzini: 'The Structure of large logarithmic corrections at small transverse momentum in hadronic collisions'. *Nucl. Phys.* (2001) B616: pp. 247–285. doi: 10.1016/S0550-3213(01)00460-6. arXiv: hep-ph/0108273 [hep-ph] (cit. on p. 30).

297. Berger, E. L. and J. Qiu: 'Differential cross-section for Higgs boson production including all orders soft gluon resummation'. *Phys. Rev.* (2003) D67: p. 034026. doi: 10.1103/PhysRevD.67.034026. arXiv: hep-ph/0210135 [hep-ph] (cit. on p. 30).

298. Catani, S., D. de Florian, M. Grazzini, and P. Nason: 'Soft gluon resummation for Higgs boson production at hadron colliders'. *JHEP* (2003) 0307: p. 028. doi: 10.1088/1126-6708/2003/07/028. arXiv: hep-ph/0306211 [hep-ph] (cit. on p. 30).

299. Schmidt, C. R.: 'H —> g g g (g q anti-q) at two loops in the large M(t) limit'. *Phys. Lett.* (1997) B413: pp. 391–395. doi: 10.1016/S0370-2693(97)01102-7. arXiv: hep-ph/9707448 [hep-ph] (cit. on p. 30).

300. Harlander, R. V.: 'Virtual corrections to g g —> H to two loops in the heavy top limit'. *Phys. Lett.* (2000) B492: pp. 74–80. doi: 10.1016/S0370-2693(00)01042-X. arXiv: hep-ph/0007289 [hep-ph] (cit. on p. 30).

301. Catani, S., D. de Florian, and M. Grazzini: 'Higgs production in hadron collisions: Soft and virtual QCD corrections at NNLO'. *JHEP* (2001) 0105: p. 025. doi: 10.1088/1126-6708/2001/05/025. arXiv: hep-ph/0102227 [hep-ph] (cit. on p. 30).

302. Harlander, R. V. and W. B. Kilgore: 'Soft and virtual corrections to proton proton → H + x at NNLO'. *Phys. Rev.* (2001) D64: p. 013015. doi: 10.1103/PhysRevD.64.013015. arXiv: hep-ph/0102241 [hep-ph] (cit. on p. 30).

303. Harlander, R. V. and W. B. Kilgore: 'Next-to-next-to-leading order Higgs production at hadron colliders'. *Phys. Rev. Lett.* (2002) 88: p. 201801. doi: 10.1103/PhysRevLett.88.201801. arXiv: hep-ph/0201206 [hep-ph] (cit. on pp. 30, 39).

304. Anastasiou, C. and K. Melnikov: 'Higgs boson production at hadron colliders in NNLO QCD'. *Nucl. Phys.* (2002) B646: pp. 220–256. doi: 10.1016/S0550-3213(02)00837-4. arXiv: hep-ph/0207004 [hep-ph] (cit. on p. 30).

305. Ravindran, V., J. Smith, and W. L. van Neerven: 'NNLO corrections to the total cross-section for Higgs boson production in hadron hadron collisions'. *Nucl. Phys.* (2003) B665: pp. 325–366. doi: 10.1016/S0550-3213(03)00457-7. arXiv: hep-ph/0302135 [hep-ph] (cit. on p. 30).

306. Ahrens, V., T. Becher, M. Neubert, and L. L. Yang: 'Origin of the Large Perturbative Corrections to Higgs Production at Hadron Colliders'. *Phys. Rev.* (2009) D79: p. 033013. doi: 10.1103/PhysRevD.79.033013. arXiv: 0808.3008 [hep-ph] (cit. on p. 30).

307. Ahrens, V., T. Becher, M. Neubert, and L. L. Yang: 'Renormalization-Group Improved Prediction for Higgs Production at Hadron Colliders'. *Eur. Phys. J.* (2009) C62: pp. 333–353. doi: 10.1140/epjc/s10052-009-1030-2. arXiv: 0809.4283 [hep-ph] (cit. on p. 30).

308. Florian, D. de, M. Grazzini, and Z. Kunszt: 'Higgs production with large transverse momentum in hadronic collisions at next-to-leading order'. *Phys. Rev. Lett.* (1999) 82: pp. 5209–5212. doi: 10.1103/PhysRevLett.82.5209. arXiv: hep-ph/9902483 [hep-ph] (cit. on p. 30).

309. Ravindran, V., J. Smith, and W. L. Van Neerven: 'Next-to-leading order QCD corrections to differential distributions of Higgs boson production in hadron hadron collisions'. *Nucl. Phys.* (2002) B634: pp. 247–290. doi: 10.1016/S0550-3213(02)00333-4. arXiv: hep-ph/0201114 [hep-ph] (cit. on p. 30).

310. Anastasiou, C., L. J. Dixon, and K. Melnikov: 'NLO Higgs boson rapidity distributions at hadron colliders'. *Nucl. Phys. Proc. Suppl.* (2003) 116: pp. 193–197. doi: 10.1016/S0920-5632(03)80168-8. arXiv: hep-ph/0211141 [hep-ph] (cit. on p. 30).

311. Smith, J. and W. L. van Neerven: 'An Approximation for NLO single Higgs boson inclusive transverse momentum distributions in hadron-hadron collisions'. *Nucl. Phys.* (2005) B720: pp. 182–202. doi: 10.1016/j.nuclphysb.2005.05.008. arXiv: hep-ph/0501098 [hep-ph] (cit. on p. 30).

312. Glosser, C. J. and C. R. Schmidt: 'Next-to-leading corrections to the Higgs boson transverse momentum spectrum in gluon fusion'. *JHEP* (2002) 0212: p. 016. doi: 10.1088/1126-6708/2002/12/016. arXiv: hep-ph/0209248 [hep-ph] (cit. on p. 30).

313. Florian, D. de, A. Kulesza, and W. Vogelsang: 'Threshold resummation for high-transverse-momentum Higgs production at the LHC'. *JHEP* (2006) 0602: p. 047. doi: 10.1088/1126-6708/2006/02/047. arXiv: hep-ph/0511205 [hep-ph] (cit. on p. 30).

314. Becher, T., G. Bell, C. Lorentzen, and S. Marti: 'The transverse-momentum spectrum of Higgs bosons near threshold at NNLO'. *JHEP* (2014) 1411: p. 026. doi: 10.1007/JHEP11(2014)026. arXiv: 1407.4111 [hep-ph] (cit. on pp. 30, 33).

315. Campbell, J. M., R. K. Ellis, and G. Zanderighi: 'Next-to-Leading order Higgs + 2 jet production via gluon fusion'. *JHEP* (2006) 0610: p. 028. doi: 10.1088/1126-6708/2006/10/028. arXiv: hep-ph/0608194 [hep-ph] (cit. on p. 30).

316. Campbell, J. M., R. K. Ellis, and C. Williams: 'Hadronic production of a Higgs boson and two jets at next-to-leading order'. *Phys. Rev.* (2010) D81: p. 074023. doi: 10.1103/PhysRevD.81.074023. arXiv: 1001.4495 [hep-ph] (cit. on p. 30).

317. Smirnov, V. A.: 'Analytical result for dimensionally regularized massless on shell double box'. *Phys. Lett.* (1999) B460: pp. 397–404. doi: 10.1016/S0370-2693(99)00777-7. arXiv: hep-ph/9905323 [hep-ph] (cit. on p. 30).

318. Smirnov, V. A. and O. L. Veretin: 'Analytical results for dimensionally regularized massless on-shell double boxes with arbitrary indices and numerators'. *Nucl. Phys.* (2000) B566: pp. 469–485. doi: 10.1016/S0550-3213(99)00686-0. arXiv: hep-ph/9907385 [hep-ph] (cit. on p. 30).

319. Tausk, J. B.: 'Nonplanar massless two loop Feynman diagrams with four on-shell legs'. *Phys. Lett.* (1999) B469: pp. 225–234. doi: 10.1016/S0370-2693(99)01277-0. arXiv: hep-ph/9909506 [hep-ph] (cit. on p. 30).

320. Kotikov, A. V.: 'Differential equations method: New technique for massive Feynman diagrams calculation'. *Phys. Lett.* (1991) B254: pp. 158–164. doi: 10.1016/0370-2693(91)90413-K (cit. on p. 30).

321. Remiddi, E.: 'Differential equations for Feynman graph amplitudes'. *Nuovo Cim.* (1997) A110: pp. 1435–1452. arXiv: hep-th/9711188 [hep-th] (cit. on p. 30).

322. Djouadi, A. and P. Gambino: 'Leading electroweak correction to Higgs boson production at proton colliders'. *Phys. Rev. Lett.* (1994) 73: pp. 2528–2531. doi: 10.1103/PhysRevLett.73.2528. arXiv: hep-ph/9406432 [hep-ph] (cit. on p. 31).

323. Aglietti, U., R. Bonciani, G. Degrassi, and A. Vicini: 'Two loop light fermion contribution to Higgs production and decays'. *Phys. Lett.* (2004) B595: pp. 432–441. doi: 10.1016/j.physletb.2004.06.063. arXiv: hep-ph/0404071 [hep-ph] (cit. on p. 31).

324. Degrassi, G. and F. Maltoni: 'Two-loop electroweak corrections to Higgs production at hadron colliders'. *Phys. Lett.* (2004) B600: pp. 255–260. doi: 10.1016/j.physletb.2004.09.008. arXiv: hep-ph/0407249 [hep-ph] (cit. on p. 31).

325. Aglietti, U., R. Bonciani, G. Degrassi, and A. Vicini: 'Two-loop electroweak corrections to Higgs production in proton-proton collisions'. (2006). arXiv: hep-ph/0610033 [hep-ph] (cit. on p. 31).

326. Actis, S., G. Passarino, C. Sturm, and S. Uccirati: 'NNLO Computational Techniques: The Cases $H \to \gamma\gamma$ and $H \to gg$'. *Nucl. Phys.* (2009) B811: pp. 182–273. doi: 10.1016/j.nuclphysb.2008.11.024. arXiv: 0809.3667 [hep-ph]; Actis, S., G. Passarino, C. Sturm, and S. Uccirati: 'NLO Electroweak Corrections to Higgs Boson Production at

Hadron Colliders'. *Phys. Lett.* (2008) B670: pp. 12–17. DOI: 10.1016/j.physletb.2008.10.018. arXiv: 0809.1301 [hep-ph]. Cit. on p. 31.

327. Anastasiou, C., R. Boughezal, and F. Petriello: 'Mixed QCD-electroweak corrections to Higgs boson production in gluon fusion'. *JHEP* (2009) 0904: p. 003. DOI: 10.1088/1126-6708/2009/04/003. arXiv: 0811.3458 [hep-ph] (cit. on p. 31).

328. Keung, W.-Y. and F. J. Petriello: 'Electroweak and finite quark-mass effects on the Higgs boson transverse momentum distribution'. *Phys. Rev.* (2009) D80: p. 013007. DOI: 10.1103/PhysRevD.80.013007. arXiv: 0905.2775 [hep-ph] (cit. on p. 31).

329. Brein, O.: 'Electroweak and Bottom Quark Contributions to Higgs Boson plus Jet Production'. *Phys. Rev.* (2010) D81: p. 093006. DOI: 10.1103/PhysRevD.81.093006. arXiv: 1003.4438 [hep-ph] (cit. on p. 31).

330. Alwall, J., Q. Li, and F. Maltoni: 'Matched predictions for Higgs production via heavy-quark loops in the SM and beyond'. *Phys. Rev.* (2012) D85: p. 014031. DOI: 10.1103/PhysRevD.85.014031. arXiv: 1110.1728 [hep-ph] (cit. on p. 31).

331. Bagnaschi, E., G. Degrassi, P. Slavich, and A. Vicini: 'Higgs production via gluon fusion in the POWHEG approach in the SM and in the MSSM'. *JHEP* (2012) 1202: p. 088. DOI: 10.1007/JHEP02(2012)088. arXiv: 1111.2854 [hep-ph] (cit. on p. 31).

332. Mantler, H. and M. Wiesemann: 'Top- and bottom-mass effects in hadronic Higgs production at small transverse momenta through LO+NLL'. *Eur. Phys. J.* (2013) C73.6: p. 2467. DOI: 10.1140/epjc/s10052-013-2467-x. arXiv: 1210.8263 [hep-ph] (cit. on p. 31).

333. Banfi, A., P. F. Monni, and G. Zanderighi: 'Quark masses in Higgs production with a jet veto'. *JHEP* (2014) 1401: p. 097. DOI: 10.1007/JHEP01(2014)097. arXiv: 1308.4634 [hep-ph] (cit. on p. 31).

334. Moch, S. and A. Vogt: 'Higher-order soft corrections to lepton pair and Higgs boson production'. *Phys. Lett.* (2005) B631: pp. 48–57. DOI: 10.1016/j.physletb.2005.09.061. arXiv: hep-ph/0508265 [hep-ph] (cit. on pp. 31, 33).

335. Laenen, E. and L. Magnea: 'Threshold resummation for electroweak annihilation from DIS data'. *Phys. Lett.* (2006) B632: pp. 270–276. DOI: 10.1016/j.physletb.2005.10.038. arXiv: hep-ph/0508284 [hep-ph] (cit. on pp. 31, 33).

336. Idilbi, A., X.-d. Ji, J.-P. Ma, and F. Yuan: 'Threshold resummation for Higgs production in effective field theory'. *Phys. Rev.* (2006) D73: p. 077501. doi: 10.1103/PhysRevD.73.077501. arXiv: hep-ph/0509294 [hep-ph] (cit. on p. 31).

337. Ravindran, V.: 'On Sudakov and soft resummations in QCD'. *Nucl. Phys.* (2006) B746: pp. 58–76. doi: 10.1016/j.nuclphysb.2006.04.008. arXiv: hep-ph/0512249 [hep-ph] (cit. on p. 31).

338. Ravindran, V.: 'Higher-order threshold effects to inclusive processes in QCD'. *Nucl. Phys.* (2006) B752: pp. 173–196. doi: 10.1016/j.nuclphysb.2006.06.025. arXiv: hep-ph/0603041 [hep-ph] (cit. on p. 31).

339. Catani, S., L. Cieri, D. de Florian, G. Ferrera, and M. Grazzini: 'Threshold resummation at N^{3}LL accuracy and soft-virtual cross sections at N^{3}LO'. *Nucl. Phys.* (2014) B888: pp. 75–91. doi: 10.1016/j.nuclphysb.2014.09.012. arXiv: 1405.4827 [hep-ph] (cit. on p. 31).

340. Bonvini, M. and S. Marzani: 'Resummed Higgs cross section at N^{3}LL'. *JHEP* (2014) 1409: p. 007. doi: 10.1007/JHEP09(2014)007. arXiv: 1405.3654 [hep-ph] (cit. on p. 31).

341. Kulesza, A. and W. J. Stirling: 'Nonperturbative effects and the resummed Higgs transverse momentum distribution at the LHC'. *JHEP* (2003) 0312: p. 056. doi: 10.1088/1126-6708/2003/12/056. arXiv: hep-ph/0307208 [hep-ph] (cit. on p. 31).

342. Bozzi, G., S. Catani, D. de Florian, and M. Grazzini: 'The q_T spectrum of the Higgs boson at the LHC in QCD perturbation theory'. *Phys. Lett.* (2003) B564: pp. 65–72. doi: 10.1016/S0370-2693(03)00656-7. arXiv: hep-ph/0302104 [hep-ph] (cit. on pp. 31, 42).

343. Bozzi, G., S. Catani, D. de Florian, and M. Grazzini: 'Transverse-momentum resummation and the spectrum of the Higgs boson at the LHC'. *Nucl. Phys.* (2006) B737: pp. 73–120. doi: 10.1016/j.nuclphysb.2005.12.022. arXiv: hep-ph/0508068 [hep-ph] (cit. on pp. 31, 42).

344. Bozzi, G., S. Catani, D. de Florian, and M. Grazzini: 'Higgs boson production at the LHC: Transverse-momentum resummation and rapidity dependence'. *Nucl. Phys.* (2008) B791: pp. 1–19. doi: 10.1016/j.nuclphysb.2007.09.034. arXiv: 0705.3887 [hep-ph] (cit. on p. 31).

345. Catani, S. and M. Grazzini: 'QCD transverse-momentum resummation in gluon fusion processes'. *Nucl. Phys.* (2011) B845: pp. 297–323. doi: 10.1016/j.nuclphysb.2010.12.007. arXiv: 1011.3918 [hep-ph] (cit. on p. 31).

346. Florian, D. de, G. Ferrera, M. Grazzini, and D. Tommasini: 'Transverse-momentum resummation: Higgs boson production at the Tevatron and the LHC'. *JHEP* (2011) 1111: p. 064. doi: 10.1007/JHEP11(2011)064. arXiv: 1109.2109 [hep-ph] (cit. on pp. 31, 42).

347. Berger, C. F., C. Marcantonini, I. W. Stewart, F. J. Tackmann, and W. J. Waalewijn: 'Higgs Production with a Central Jet Veto at NNLL+NNLO'. *JHEP* (2011) 1104: p. 092. doi: 10.1007/JHEP04(2011)092. arXiv: 1012.4480 [hep-ph] (cit. on p. 31).

348. Banfi, A., G. P. Salam, and G. Zanderighi: 'NLL+NNLO predictions for jet-veto efficiencies in Higgs-boson and Drell-Yan production'. *JHEP* (2012) 1206: p. 159. doi: 10.1007/JHEP06(2012)159. arXiv: 1203.5773 [hep-ph] (cit. on p. 31).

349. Tackmann, F. J., J. R. Walsh, and S. Zuberi: 'Resummation Properties of Jet Vetoes at the LHC'. *Phys. Rev.* (2012) D86: p. 053011. doi: 10.1103/PhysRevD.86.053011. arXiv: 1206.4312 [hep-ph] (cit. on p. 31).

350. Banfi, A., P. F. Monni, G. P. Salam, and G. Zanderighi: 'Higgs and Z-boson production with a jet veto'. *Phys. Rev. Lett.* (2012) 109: p. 202001. doi: 10.1103/PhysRevLett.109.202001. arXiv: 1206.4998 [hep-ph] (cit. on pp. 31, 48).

351. Becher, T. and M. Neubert: 'Factorization and NNLL Resummation for Higgs Production with a Jet Veto'. *JHEP* (2012) 1207: p. 108. doi: 10.1007/JHEP07(2012)108. arXiv: 1205.3806 [hep-ph] (cit. on p. 31).

352. Liu, X. and F. Petriello: 'Resummation of jet-veto logarithms in hadronic processes containing jets'. *Phys. Rev.* (2013) D87.1: p. 014018. doi: 10.1103/PhysRevD.87.014018. arXiv: 1210.1906 [hep-ph] (cit. on p. 31).

353. Becher, T., M. Neubert, and L. Rothen: 'Factorization and N^3LL_p + NNLO predictions for the Higgs cross section with a jet veto'. *JHEP* (2013) 1310: p. 125. doi: 10.1007/JHEP10(2013)125. arXiv: 1307.0025 [hep-ph] (cit. on p. 31).

354. Stewart, I. W., F. J. Tackmann, J. R. Walsh, and S. Zuberi: 'Jet p_T resummation in Higgs production at $NNLL' + NNLO$'. *Phys. Rev.* (2014) D89.5: p. 054001. doi: 10.1103/PhysRevD.89.054001. arXiv: 1307.1808 (cit. on p. 31).

355. Catani, S., D. de Florian, and M. Grazzini: 'Direct Higgs production and jet veto at the Tevatron and the LHC in NNLO QCD'. *JHEP* (2002) 0201: p. 015. doi: 10.1088/1126-6708/2002/01/015. arXiv: hep-ph/0111164 [hep-ph] (cit. on p. 31).

356. Hautmann, F.: 'Heavy top limit and double-logarithmic contributions to Higgs production at $m_H^2/s \ll 1$'. *Phys. Lett.* (2002) B535: pp. 159–162. doi: 10.1016/S0370-2693(02)01761-6. arXiv: hep-ph/0203140 [hep-ph] (cit. on p. 31).

357. Harlander, R. V. and K. J. Ozeren: 'Finite top mass effects for hadronic Higgs production at next-to-next-to-leading order'. *JHEP* (2009) 0911: p. 088. doi: 10.1088/1126-6708/2009/11/088. arXiv: 0909.3420 [hep-ph] (cit. on pp. 31, 33, 39, 40, 42, 50).

358. Pak, A., M. Rogal, and M. Steinhauser: 'Finite top quark mass effects in NNLO Higgs boson production at LHC'. *JHEP* (2010) 1002: p. 025. doi: 10.1007/JHEP02(2010)025. arXiv: 0911.4662 [hep-ph] (cit. on pp. 31, 42).

359. Harlander, R. V. and K. J. Ozeren: 'Top mass effects in Higgs production at next-to-next-to-leading order QCD: Virtual corrections'. *Phys. Lett.* (2009) B679: pp. 467–472. doi: 10.1016/j.physletb.2009.08.012. arXiv: 0907.2997 [hep-ph] (cit. on p. 31).

360. Pak, A., M. Rogal, and M. Steinhauser: 'Virtual three-loop corrections to Higgs boson production in gluon fusion for finite top quark mass'. *Phys. Lett.* (2009) B679: pp. 473–477. doi: 10.1016/j.physletb.2009.08.016. arXiv: 0907.2998 [hep-ph] (cit. on p. 31).

361. Smirnov, V. A.: 'Applied asymptotic expansions in momenta and masses'. *Springer Tracts Mod. Phys.* (2002) 177: pp. 1–262 (cit. on pp. 31, 40).

362. Harlander, R.: 'Asymptotic expansions: Methods and applications'. *Acta Phys. Polon.* (1999) B30: pp. 3443–3462. arXiv: hep-ph/9910496 [hep-ph] (cit. on pp. 31, 40).

363. Marzani, S., R. D. Ball, V. Del Duca, S. Forte, and A. Vicini: 'Finite-top-mass effects in NNLO Higgs production'. *Nucl. Phys. Proc. Suppl.* (2009) 186: pp. 98–101. doi: 10.1016/j.nuclphysbps.2008.12.019. arXiv: 0809.4934 [hep-ph] (cit. on pp. 31, 50).

364. Marzani, S., R. D. Ball, V. Del Duca, S. Forte, and A. Vicini: 'Higgs production via gluon-gluon fusion with finite top mass beyond next-to-leading order'. *Nucl. Phys.* (2008) B800: pp. 127–145. doi: 10.1016/j.nuclphysb.2008.03.016. arXiv: 0801.2544 [hep-ph] (cit. on pp. 31, 50).

365. Harlander, R. V., H. Mantler, S. Marzani, and K. J. Ozeren: 'Higgs production in gluon fusion at next-to-next-to-leading order QCD for finite top mass'. *Eur. Phys. J.* (2010) C66: pp. 359–372. doi: 10.1140/epjc/s10052-010-1258-x. arXiv: 0912.2104 [hep-ph] (cit. on pp. 31, 33, 34, 39, 40, 50, 58).

366. Del Duca, V., W. Kilgore, C. Oleari, C. R. Schmidt, and D. Zeppenfeld: 'Kinematical limits on Higgs boson production via gluon fusion in association with jets'. *Phys. Rev.* (2003) D67: p. 073003. doi: 10.1103/PhysRevD.67.073003. arXiv: hep-ph/0301013 [hep-ph] (cit. on pp. 31, 67).

367. Anastasiou, C., K. Melnikov, and F. Petriello: 'Higgs boson production at hadron colliders: Differential cross sections through next-to-next-to-leading order'. *Phys. Rev. Lett.* (2004) 93: p. 262002. doi: 10.1103/PhysRevLett.93.262002. arXiv: hep-ph/0409088 [hep-ph] (cit. on p. 32).

368. Catani, S. and M. Grazzini: 'HNNLO: A Monte Carlo program to compute Higgs boson production at hadron colliders'. *PoS* (2007) RADCOR2007: p. 046. arXiv: 0802.1410 [hep-ph] (cit. on p. 32).

369. Anastasiou, C., C. Duhr, F. Dulat, F. Herzog, and B. Mistlberger: 'Higgs Boson Gluon-Fusion Production in QCD at Three Loops'. *Phys. Rev. Lett.* (2015) 114.21: p. 212001. doi: 10.1103/PhysRevLett.114.212001. arXiv: 1503.06056 [hep-ph] (cit. on pp. 32, 33).

370. Boughezal, R., F. Caola, K. Melnikov, F. Petriello, and M. Schulze: 'Higgs boson production in association with a jet at next-to-next-to-leading order in perturbative QCD'. *JHEP* (2013) 1306: p. 072. doi: 10.1007/JHEP06(2013)072. arXiv: 1302.6216 [hep-ph] (cit. on p. 33).

371. Chen, X., T. Gehrmann, E. W. N. Glover, and M. Jaquier: 'Precise QCD predictions for the production of Higgs + jet final states'. *Phys. Lett.* (2015) B740: pp. 147–150. doi: 10.1016/j.physletb.2014.11.021. arXiv: 1408.5325 [hep-ph] (cit. on p. 33).

372. Boughezal, R., F. Caola, K. Melnikov, F. Petriello, and M. Schulze: 'Higgs boson production in association with a jet at next-to-next-to-leading order'. (2015). arXiv: 1504.07922 [hep-ph] (cit. on p. 33).

373. Boughezal, R., C. Focke, W. Giele, X. Liu, and F. Petriello: 'Higgs boson production in association with a jet using jettiness subtraction'. (2015). arXiv: 1505.03893 [hep-ph] (cit. on p. 33).

374. Ball, R. D., M. Bonvini, S. Forte, S. Marzani, and G. Ridolfi: 'Higgs production in gluon fusion beyond NNLO'. *Nucl. Phys.* (2013) B874: pp. 746–772. doi: 10.1016/j.nuclphysb.2013.06.012. arXiv: 1303.3590 [hep-ph] (cit. on p. 33).

375. Lo Presti, N. A., A. A. Almasy, and A. Vogt: 'Leading large-x logarithms of the quark–gluon contributions to inclusive Higgs-boson and lepton-pair production'. *Phys. Lett.* (2014) B737: pp. 120–123. doi: 10.1016/j.physletb.2014.08.044. arXiv: 1407.1553 [hep-ph] (cit. on p. 33).

376. Moch, S., J. A. M. Vermaseren, and A. Vogt: 'The Three loop splitting functions in QCD: The Nonsinglet case'. *Nucl. Phys.* (2004) B688: pp. 101–134. doi: 10.1016/j.nuclphysb.2004.03.030. arXiv: hep-ph/0403192 [hep-ph] (cit. on p. 33).

377. Vogt, A., S. Moch, and J. A. M. Vermaseren: 'The Three-loop splitting functions in QCD: The Singlet case'. *Nucl. Phys.* (2004) B691: pp. 129–181. doi: 10.1016/j.nuclphysb.2004.04.024. arXiv: hep-ph/0404111 [hep-ph] (cit. on p. 33).

378. Anastasiou, C., C. Duhr, F. Dulat, and B. Mistlberger: 'Soft triple-real radiation for Higgs production at N3LO'. *JHEP* (2013) 1307: p. 003. doi: 10.1007/JHEP07(2013)003. arXiv: 1302.4379 [hep-ph] (cit. on p. 33).

379. Zhu, H. X.: 'On the calculation of soft phase space integral'. *JHEP* (2015) 1502: p. 155. doi: 10.1007/JHEP02(2015)155. arXiv: 1501.00236 [hep-ph] (cit. on p. 33).

380. Gehrmann, T., M. Jaquier, E. W. N. Glover, and A. Koukoutsakis: 'Two-Loop QCD Corrections to the Helicity Amplitudes for $H \to 3$ partons'. *JHEP* (2012) 1202: p. 056. doi: 10.1007/JHEP02(2012)056. arXiv: 1112.3554 [hep-ph] (cit. on p. 33).

381. Duhr, C. and T. Gehrmann: 'The two-loop soft current in dimensional regularization'. *Phys. Lett.* (2013) B727: pp. 452–455. doi: 10.1016/j.physletb.2013.10.063. arXiv: 1309.4393 [hep-ph] (cit. on p. 33).

382. Li, Y. and H. X. Zhu: 'Single soft gluon emission at two loops'. *JHEP* (2013) 1311: p. 080. doi: 10.1007/JHEP11(2013)080. arXiv: 1309.4391 [hep-ph] (cit. on p. 33).

383. Dulat, F. and B. Mistlberger: 'Real-Virtual-Virtual contributions to the inclusive Higgs cross section at N3LO'. (2014). arXiv: 1411.3586 [hep-ph] (cit. on p. 33).

384. Duhr, C., T. Gehrmann, and M. Jaquier: 'Two-loop splitting amplitudes and the single-real contribution to inclusive Higgs production at N^3LO'. *JHEP* (2015) 1502: p. 077. doi: 10.1007/JHEP02(2015)077. arXiv: 1411.3587 [hep-ph] (cit. on p. 33).

385. Anastasiou, C., C. Duhr, F. Dulat, F. Herzog, and B. Mistlberger: 'Real-virtual contributions to the inclusive Higgs cross-section at N^3LO'. *JHEP* (2013) 1312: p. 088. doi: 10.1007/JHEP12(2013)088. arXiv: 1311.1425 [hep-ph] (cit. on p. 33).

386. Kilgore, W. B.: 'One-loop single-real-emission contributions to $pp \to H + X$ at next-to-next-to-next-to-leading order'. *Phys. Rev.* (2014) D89.7: p. 073008. doi: 10.1103/PhysRevD.89.073008. arXiv: 1312.1296 [hep-ph] (cit. on p. 33).

387. Li, Y., A. von Manteuffel, R. M. Schabinger, and H. X. Zhu: 'N^3LO Higgs boson and Drell-Yan production at threshold: The one-loop two-emission contribution'. *Phys. Rev.* (2014) D90.5: p. 053006. doi: 10.1103/PhysRevD.90.053006. arXiv: 1404.5839 [hep-ph] (cit. on p. 33).

388. Anastasiou, C., C. Duhr, F. Dulat, E. Furlan, F. Herzog, and B. Mistlberger: 'Soft Expansion of Double-Real-Virtual Corrections to Higgs Production at N^3LO'. (2015). arXiv: 1505.04110 [hep-ph] (cit. on p. 33).

389. Baikov, P. A., K. G. Chetyrkin, A. V. Smirnov, V. A. Smirnov, and M. Steinhauser: 'Quark and gluon form factors to three loops'. *Phys. Rev. Lett.* (2009) 102: p. 212002. doi: 10.1103/PhysRevLett.102.212002. arXiv: 0902.3519 [hep-ph] (cit. on p. 33).

390. Lee, R. N., A. V. Smirnov, and V. A. Smirnov: 'Analytic Results for Massless Three-Loop Form Factors'. *JHEP* (2010) 1004: p. 020. doi: 10.1007/JHEP04(2010)020. arXiv: 1001.2887 [hep-ph] (cit. on p. 33).

391. Gehrmann, T., E. W. N. Glover, T. Huber, N. Ikizlerli, and C. Studerus: 'Calculation of the quark and gluon form factors to three loops in QCD'. *JHEP* (2010) 1006: p. 094. doi: 10.1007/JHEP06(2010)094. arXiv: 1004.3653 [hep-ph] (cit. on p. 33).

392. Anastasiou, C., S. Buehler, C. Duhr, and F. Herzog: 'NNLO phase space master integrals for two-to-one inclusive cross sections in dimensional regularization'. *JHEP* (2012) 1211: p. 062. doi: 10.1007/JHEP11(2012)062. arXiv: 1208.3130 [hep-ph] (cit. on p. 33).

393. Höschele, M., J. Hoff, A. Pak, M. Steinhauser, and T. Ueda: 'Higgs boson production at the LHC: NNLO partonic cross sections through order ε and convolutions with splitting functions to N^3LO'. *Phys. Lett.* (2013) B721: pp. 244–251. doi: 10.1016/j.physletb.2013.03.003. arXiv: 1211.6559 [hep-ph] (cit. on p. 33).

394. Tarasov, O. V., A. A. Vladimirov, and A. Y. Zharkov: 'The Gell-Mann-Low Function of QCD in the Three Loop Approximation'. *Phys. Lett.* (1980) B93: pp. 429–432. doi: 10.1016/0370-2693(80)90358-5 (cit. on p. 33).

395. Larin, S. A. and J. A. M. Vermaseren: 'The three-loop QCD β-function and anomalous dimensions'. *Phys. Lett.* (1993) B303: pp. 334–336. doi: 10.1016/0370-2693(93)91441-0. arXiv: hep-ph/9302208 [hep-ph] (cit. on p. 33).

396. Ritbergen, T. van, J. A. M. Vermaseren, and S. A. Larin: 'The four-loop β-function in quantum chromodynamics'. *Phys. Lett.* (1997) B400: pp. 379–384. doi: 10.1016/S0370-2693(97)00370-5. arXiv: hep-ph/9701390 [hep-ph] (cit. on pp. 33, 108).

397. Czakon, M.: 'The four-loop QCD β-function and anomalous dimensions'. *Nucl. Phys.* (2005) B710: pp. 485–498. doi: 10.1016/j.nuclphysb.2005.01.012. arXiv: hep-ph/0411261 [hep-ph] (cit. on pp. 33, 107, 108).

398. Buehler, S. and A. Lazopoulos: 'Scale dependence and collinear subtraction terms for Higgs production in gluon fusion at N3LO'. *JHEP* (2013) 1310: p. 096. doi: 10.1007/JHEP10(2013)096. arXiv: 1306.2223 [hep-ph] (cit. on p. 33).

399. Anastasiou, C., C. Duhr, F. Dulat, E. Furlan, T. Gehrmann, et al.: 'Higgs boson gluon–fusion production at threshold in N^3LO QCD'. *Phys. Lett.* (2014) B737: pp. 325–328. doi: 10.1016/j.physletb.2014.08.067. arXiv: 1403.4616 [hep-ph] (cit. on p. 33).

400. Anastasiou, C., C. Duhr, F. Dulat, E. Furlan, T. Gehrmann, et al.: 'Higgs boson gluon-fusion production beyond threshold in N^3LO QCD'. *JHEP* (2015) 1503: p. 091. doi: 10.1007/JHEP03(2015)091. arXiv: 1411.3584 [hep-ph] (cit. on p. 33).

401. Florian, D. de, J. Mazzitelli, S. Moch, and A. Vogt: 'Approximate N^3LO Higgs-boson production cross section using physical-kernel constraints'. *JHEP* (2014) 1410: p. 176. doi: 10.1007/JHEP10(2014)176. arXiv: 1408.6277 [hep-ph] (cit. on p. 33).

402. Pak, A., M. Rogal, and M. Steinhauser: 'Production of scalar and pseudo-scalar Higgs bosons to next-to-next-to-leading order at hadron colliders'. *JHEP* (2011) 1109: p. 088. doi: 10.1007/JHEP09(2011)088. arXiv: 1107.3391 [hep-ph] (cit. on pp. 34, 40).

403. Cacciari, M., G. P. Salam, and G. Soyez: 'The anti-k_t jet clustering algorithm'. *JHEP* (2008) 0804: p. 063. doi: 10.1088/1126-6708/2008/04/063. arXiv: 0802.1189 [hep-ph] (cit. on pp. 39, 43).

404. Harlander, R. V., S. Liebler, and H. Mantler: 'SusHi: A program for the calculation of Higgs production in gluon fusion and bottom-quark annihilation in the Standard Model and the MSSM'. *Comput. Phys. Commun.* (2013) 184: pp. 1605–1617. doi: 10.1016/j.cpc.2013.02.006. arXiv: 1212.3249 [hep-ph] (cit. on pp. 39, 68).

405. Harlander, R., T. Seidensticker, and M. Steinhauser: 'Corrections of $\mathcal{O}(\alpha\alpha_s)$ to the decay of the Z boson into bottom quarks'. *Phys. Lett.* (1998) B426: pp. 125–132. doi: 10.1016/S0370-2693(98)00220-2. arXiv: hep-ph/9712228 [hep-ph] (cit. on p. 40).

406. Seidensticker, T.: 'Automatic application of successive asymptotic expansions of Feynman diagrams'. (1999). arXiv: hep-ph/9905298 [hep-ph] (cit. on p. 40).

407. Steinhauser, M.: 'MATAD: A Program package for the computation of MAssive TADpoles'. *Comput. Phys. Commun.* (2001) 134: pp. 335–364. doi: 10.1016/S0010-4655(00)00204-6. arXiv: hep-ph/0009029 [hep-ph] (cit. on p. 40).

408. Grazzini, M.: 'NNLO predictions for the Higgs boson signal in the $H \to WW \to l\nu l\nu$ and $H \to ZZ \to 4l$ decay channels'. *JHEP* (2008) 0802: p. 043. doi: 10.1088/1126-6708/2008/02/043. arXiv: 0801.3232 [hep-ph] (cit. on p. 42).

409. Nagy, Z. and Z. Trocsanyi: 'Next-to-leading order calculation of four jet observables in electron positron annihilation'. *Phys. Rev.* (1999) D59: p. 014020. doi: 10.1103/PhysRevD.59.01402010.1103/PhysRevD.62.099902,10.1103/PhysRevD.62.099902,10.1103/PhysRevD.59.014020. arXiv: hep-ph/9806317 [hep-ph] (cit. on p. 42).

410. Nagy, Z.: 'Next-to-leading order calculation of three jet observables in hadron hadron collision'. *Phys. Rev.* (2003) D68: p. 094002. doi: 10.1103/PhysRevD.68.094002. arXiv: hep-ph/0307268 [hep-ph] (cit. on p. 42).

411. Martin, A. D., W. J. Stirling, R. S. Thorne, and G. Watt: 'Parton distributions for the LHC'. *Eur. Phys. J.* (2009) C63: pp. 189–285. doi: 10.1140/epjc/s10052-009-1072-5. arXiv: 0901.0002 [hep-ph] (cit. on p. 43).

412. Aad, G. et al. (The ATLAS collaboration): 'Search for the Higgs boson in the $H \to WW \to lvjj$ decay channel at $\sqrt{s} = 7$ TeV with the ATLAS detector'. *Phys. Lett.* (2012) B718: pp. 391–410. doi: 10.1016/j.physletb.2012.10.066. arXiv: 1206.6074 [hep-ex] (cit. on p. 43).

References for part III

43. Harlander, R. V., T. Neumann, K. J. Ozeren, and M. Wiesemann: 'Top-mass effects in differential Higgs production through gluon fusion at order α_s^4'. *JHEP* (2012) 1208: p. 139. doi: 10.1007/JHEP08(2012)139. arXiv: 1206.0157 [hep-ph] (cit. on pp. 6, 14, 19, 23, 26, 31, 32, 34–37, 39, 40, 42, 53, 57, 70).

58. Aad, G. et al. (The ATLAS collaboration): 'Measurements of the Total and Differential Higgs Boson Production Cross Sections Combining the $H \to \gamma\gamma$ and $H \to ZZ^* \to 4\ell$ Decay Channels at $\sqrt{s} = 8$ TeV with the ATLAS Detector'. (2015). arXiv: 1504.05833 [hep-ex] (cit. on pp. 8, 25, 61).

59. *Measurements of the Higgs boson production and decay rates and coupling strengths using pp collision data at $\sqrt{s} = 7$ and 8 TeV in the ATLAS experiment*. Tech. rep. ATLAS-CONF-2015-007. Geneva: CERN, Mar. 2015 (cit. on pp. 8, 25, 61).

60. Aad, G. et al. (The ATLAS collaboration): 'Study of the spin and parity of the Higgs boson in diboson decays with the ATLAS detector'. (2015). arXiv: 1506.05669 [hep-ex] (cit. on pp. 8, 25, 61).

61. Khachatryan, V. et al. (The CMS collaboration): 'Precise determination of the mass of the Higgs boson and tests of compatibility of its couplings with the standard model predictions using proton collisions at 7 and 8 TeV'. (2014). arXiv: 1412.8662 [hep-ex] (cit. on pp. 8, 25, 61).

62. Giardino, P. P., K. Kannike, I. Masina, M. Raidal, and A. Strumia: 'The universal Higgs fit'. *JHEP* (2014) 1405: p. 046. doi: 10.1007/JHEP05(2014)046. arXiv: 1303.3570 [hep-ph] (cit. on pp. 8, 25, 61).

81. David, A. et al. (The LHC Higgs Cross Section Working Group collaboration): 'LHC HXSWG interim recommendations to explore the coupling structure of a Higgs-like particle'. (2012). arXiv: 1209.0040 [hep-ph] (cit. on pp. 12, 62).

83. Grzadkowski, B., M. Iskrzynski, M. Misiak, and J. Rosiek: 'Dimension-Six Terms in the Standard Model Lagrangian'. *JHEP* (2010) 1010: p. 085. doi: 10.1007/JHEP10(2010)085. arXiv: 1008.4884 [hep-ph] (cit. on pp. 13, 62).

84. Buchmüller, W. and D. Wyler: 'Effective Lagrangian Analysis of New Interactions and Flavor Conservation'. *Nucl. Phys.* (1986) B268: pp. 621–653. doi: 10.1016/0550-3213(86)90262-2 (cit. on pp. 13, 62).

85. Lehman, L.: 'Extending the Standard Model Effective Field Theory with the Complete Set of Dimension-7 Operators'. *Phys. Rev.* (2014) D90.12: p. 125023. doi: 10.1103/PhysRevD.90.125023. arXiv: 1410.4193 [hep-ph] (cit. on pp. 13, 62).

114. Dawson, S., I. M. Lewis, and M. Zeng: 'Usefulness of effective field theory for boosted Higgs production'. *Phys. Rev.* (2015) D91: p. 074012. doi: 10.1103/PhysRevD.91.074012. arXiv: 1501.04103 [hep-ph] (cit. on pp. 14, 79).

115. Neumann, T. and M. Wiesemann: 'Finite top-mass effects in gluon-induced Higgs production with a jet-veto at NNLO'. *JHEP* (2014) 1411: p. 150. doi: 10.1007/JHEP11(2014)150. arXiv: 1408.6836 [hep-ph] (cit. on pp. 14, 19, 23, 26, 32, 37, 45–49, 51–55, 70).

238. Heinemeyer, S. et al. (The LHC Higgs Cross Section Working Group collaboration): 'Handbook of LHC Higgs Cross Sections: 3. Higgs Properties'. (2013). Ed. by Heinemeyer, S. doi: 10.5170/CERN-2013-004. arXiv: 1307.1347 [hep-ph] (cit. on pp. 26, 62).

253. Schröder, Y. and M. Steinhauser: 'Four-loop decoupling relations for the strong coupling'. *JHEP* (2006) 0601: p. 051. doi: 10.1088/1126-6708/2006/01/051. arXiv: hep-ph/0512058 [hep-ph] (cit. on pp. 27, 64, 108).

254. Chetyrkin, K. G., J. H. Kühn, and C. Sturm: 'QCD decoupling at four loops'. *Nucl. Phys.* (2006) B744: pp. 121–135. doi: 10.1016/j.nuclphysb.2006.03.020. arXiv: hep-ph/0512060 [hep-ph] (cit. on pp. 27, 64, 108).

263. Del Duca, V., W. Kilgore, C. Oleari, C. Schmidt, and D. Zeppenfeld: 'Higgs + 2 jets via gluon fusion'. *Phys. Rev. Lett.* (2001) 87: p. 122001. doi: 10.1103/PhysRevLett.87.122001. arXiv: hep-ph/0105129 [hep-ph] (cit. on pp. 28, 31, 67).

264. Del Duca, V., W. Kilgore, C. Oleari, C. Schmidt, and D. Zeppenfeld: 'Gluon fusion contributions to H + 2 jet production'. *Nucl. Phys.* (2001) B616: pp. 367–399. doi: 10.1016/S0550-3213(01)00446-1. arXiv: hep-ph/0108030 [hep-ph] (cit. on pp. 28, 31, 67, 72).

366. Del Duca, V., W. Kilgore, C. Oleari, C. R. Schmidt, and D. Zeppenfeld: 'Kinematical limits on Higgs boson production via gluon fusion in association with jets'. *Phys. Rev.* (2003) D67: p. 073003. doi: 10.1103/PhysRevD.67.073003. arXiv: hep-ph/0301013 [hep-ph] (cit. on pp. 31, 67).

404. Harlander, R. V., S. Liebler, and H. Mantler: 'SusHi: A program for the calculation of Higgs production in gluon fusion and bottom-quark annihilation in the Standard Model and the MSSM'. *Comput. Phys. Commun.* (2013) 184: pp. 1605–1617. doi: 10.1016/j.cpc.2013.02.006. arXiv: 1212.3249 [hep-ph] (cit. on pp. 39, 68).

413. Harlander, R. V. and T. Neumann: 'Probing the nature of the Higgs-gluon coupling'. *Phys. Rev.* (2013) D88: p. 074015. doi: 10.1103/PhysRevD.88.074015. arXiv: 1308.2225 [hep-ph] (cit. on p. 59).

414. Aad, G. et al. (The ATLAS collaboration): 'Search for $H \to \gamma\gamma$ produced in association with top quarks and constraints on the Yukawa coupling between the top quark and the Higgs boson using data taken at 7 TeV and 8 TeV with the ATLAS detector'. *Phys. Lett.* (2015) B740: pp. 222–242. doi: 10.1016/j.physletb.2014.11.049. arXiv: 1409.3122 [hep-ex] (cit. on p. 61).

415. Khachatryan, V. et al. (The CMS collaboration): 'Search for the associated production of the Higgs boson with a top-quark pair'. *JHEP* (2014) 09. [Erratum: JHEP10,106(2014)]: p. 087. doi: 10.1007/JHEP09(2014)087, 10.1007/JHEP10(2014)106. arXiv: 1408.1682 [hep-ex] (cit. on p. 61).

416. Aad, G. et al. (The ATLAS collaboration): 'Search for the Standard Model Higgs boson produced in association with top quarks and decaying into $b\bar{b}$ in pp collisions at $\sqrt{s}$ = 8 TeV with the ATLAS detector'. *Eur. Phys. J.* (2015) C75.7: p. 349. doi: 10.1140/epjc/s10052-015-3543-1. arXiv: 1503.05066 [hep-ex] (cit. on p. 61).

417. Khachatryan, V. et al. (The CMS collaboration): 'Search for a standard model Higgs boson produced in association with a top-quark pair and decaying to bottom quarks using a matrix element method'. *Eur. Phys. J.* (2015) C75.6: p. 251. doi: 10.1140/epjc/s10052-015-3454-1. arXiv: 1502.02485 [hep-ex] (cit. on p. 61).

418. Gracey, J. A.: 'Classification and one loop renormalization of dimension-six and dimension-eight operators in quantum gluodynamics'. *Nucl. Phys.* (2002) B634: pp. 192–208. doi: 10.1016/j.nuclphysb.2004.06.053. arXiv: hep-ph/0204266 [hep-ph]. Erratum ibid. *Nucl. Phys.* (2004) B696 (cit. on pp. 63, 64).

419. Neill, D.: 'Two-Loop Matching onto Dimension Eight Operators in the Higgs-Glue Sector'. (2009). arXiv: 0908.1573 [hep-ph] (cit. on pp. 63, 64).

420. Germer, J.: 'Maximally Helicity Violating amplitudes for Higgs production processes'. MA thesis. Universität Karlsruhe, 2007 (cit. on p. 63).

421. Arzt, C.: 'Reduced effective Lagrangians'. *Phys. Lett.* (1995) B342: pp. 189–195. doi: 10.1016/0370-2693(94)01419-D. arXiv: hep-ph/9304230 [hep-ph] (cit. on p. 64).

422. Georgi, H.: 'On-shell effective field theory'. *Nucl. Phys.* (1991) B361: pp. 339–350. doi: 10.1016/0550-3213(91)90244-R (cit. on p. 64).

423. Politzer, H. D.: 'Power Corrections at Short Distances'. *Nucl. Phys.* (1980) B172: p. 349. doi: 10.1016/0550-3213(80)90172-8 (cit. on p. 64).

424. Semenov, A.: 'LanHEP: A Package for the automatic generation of Feynman rules in field theory. Version 3.0'. *Comput. Phys. Commun.* (2009) 180: pp. 431–454. doi: 10.1016/j.cpc.2008.10.012. arXiv: 0805.0555 [hep-ph] (cit. on p. 65).

425. Christensen, N. D. and C. Duhr: 'FeynRules - Feynman rules made easy'. *Comput. Phys. Commun.* (2009) 180: pp. 1614–1641. doi: 10.1016/j.cpc.2009.02.018. arXiv: 0806.4194 [hep-ph] (cit. on p. 65).

426. Tentyukov, M. and J. Fleischer: 'A Feynman diagram analyzer DIANA'. *Comput. Phys. Commun.* (2000) 132: pp. 124–141. doi: 10.1016/S0010-4655(00)00147-8. arXiv: hep-ph/9904258 [hep-ph] (cit. on p. 65).

427. Nogueira, P.: 'Automatic Feynman graph generation'. *J. Comput. Phys.* (1993) 105: pp. 279–289. doi: 10.1006/jcph.1993.1074 (cit. on p. 65).

428. Vermaseren, J. A. M.: 'New features of FORM'. (2000). arXiv: math-ph/0010025 [math-ph] (cit. on p. 65).

429. Kreckel, R.: *nvegas.c, Implementation of G. P. Lepage's VEGAS-algorithm*. 1996-2000. URL: ftp://muon.physik.uni-mainz.de/pub/pvegas/ (cit. on p. 65).

430. Lepage, G. P.: 'A New Algorithm for Adaptive Multidimensional Integration'. *J. Comput. Phys.* (1978) 27: pp. 192–203. DOI: 10.1016/0021-9991(78)90004-9 (cit. on p. 65).

431. Lepage, G. P.: *VEGAS – An Adaptive Multi-dimensional Integration Program*. Tech. rep. Cornell University, 1980 (cit. on p. 65).

432. Plehn, T., D. L. Rainwater, and D. Zeppenfeld: 'Determining the structure of Higgs couplings at the LHC'. *Phys. Rev. Lett.* (2002) 88: p. 051801. DOI: 10.1103/PhysRevLett.88.051801. arXiv: hep-ph/0105325 [hep-ph] (cit. on p. 67).

433. Hankele, V., G. Klämke, and D. Zeppenfeld: 'Higgs + 2 jets as a probe for CP properties'. (2006). arXiv: hep-ph/0605117 [hep-ph] (cit. on pp. 67, 71, 72).

434. Klämke, G. and D. Zeppenfeld: 'Higgs plus two jet production via gluon fusion as a signal at the CERN LHC'. *JHEP* (2007) 0704: p. 052. DOI: 10.1088/1126-6708/2007/04/052. arXiv: hep-ph/0703202 [HEP-PH] (cit. on p. 67).

435. Hagiwara, K., Q. Li, and K. Mawatari: 'Jet angular correlation in vector-boson fusion processes at hadron colliders'. *JHEP* (2009) 0907: p. 101. DOI: 10.1088/1126-6708/2009/07/101. arXiv: 0905.4314 [hep-ph] (cit. on p. 67).

436. Andersen, J. R., K. Arnold, and D. Zeppenfeld: 'Azimuthal Angle Correlations for Higgs Boson plus Multi-Jet Events'. *JHEP* (2010) 1006: p. 091. DOI: 10.1007/JHEP06(2010)091. arXiv: 1001.3822 [hep-ph] (cit. on p. 67).

437. Campanario, F., M. Kubocz, and D. Zeppenfeld: 'Gluon-fusion contributions to Phi + 2 Jet production'. *Phys. Rev.* (2011) D84: p. 095025. DOI: 10.1103/PhysRevD.84.095025. arXiv: 1011.3819 [hep-ph] (cit. on p. 67).

438. Campanario, F. and M. Kubocz: 'Higgs boson CP-properties of the gluonic contributions in Higgs plus three jet production via gluon fusion at the LHC'. *JHEP* (2014) 1410: p. 173. DOI: 10.1007/JHEP10(2014)173. arXiv: 1402.1154 [hep-ph] (cit. on p. 67).

439. Demartin, F., F. Maltoni, K. Mawatari, B. Page, and M. Zaro: 'Higgs characterisation at NLO in QCD: CP properties of the top-quark Yukawa interaction'. *Eur. Phys. J.* (2014) C74.9: p. 3065. doi: 10.1140/epjc/s10052-014-3065-2. arXiv: 1407.5089 [hep-ph] (cit. on p. 67).

440. Arnold, K., M. Bahr, G. Bozzi, F. Campanario, C. Englert, et al.: 'VBFNLO: A Parton level Monte Carlo for processes with electroweak bosons'. *Comput. Phys. Commun.* (2009) 180: pp. 1661–1670. doi: 10.1016/j.cpc.2009.03.006. arXiv: 0811.4559 [hep-ph] (cit. on p. 71).

441. Arnold, K., J. Bellm, G. Bozzi, M. Brieg, F. Campanario, et al.: 'VBFNLO: A Parton Level Monte Carlo for Processes with Electroweak Bosons – Manual for Version 2.5.0'. (2011). arXiv: 1107.4038 [hep-ph] (cit. on p. 71).

442. Arnold, K., J. Bellm, G. Bozzi, F. Campanario, C. Englert, et al.: 'Release Note – Vbfnlo-2.6.0'. (2012). arXiv: 1207.4975 [hep-ph] (cit. on p. 71).

443. Zimmermann, M.: 'Investigation of the Higgs-gluon Coupling Tensor Structure in the Decay Channel $H \to \gamma\gamma$ with the ATLAS Experiment'. MA thesis. Freiburg University, 2014 (cit. on pp. 79, 80).

References for part IV

130. Olive, K. A. et al. (The Particle Data Group collaboration): 'Review of Particle Physics'. *Chin. Phys* (2014) C38: p. 090001. doi: 10.1088/1674-1137/38/9/090001 (cit. on pp. 16, 43, 108).

151. Lüscher, M., P. Weisz, and U. Wolff: 'A Numerical method to compute the running coupling in asymptotically free theories'. *Nucl. Phys.* (1991) B359: pp. 221–243. doi: 10.1016/0550-3213(91)90298-C (cit. on pp. 17, 112).

154. Lüscher, M.: 'Properties and uses of the Wilson flow in lattice QCD'. *JHEP* (2010) 1008: p. 071. doi: 10.1007/JHEP08(2010)071,10.1007/JHEP03(2014)092. arXiv: 1006.4518 [hep-lat] (cit. on pp. 17, 83–86, 89, 103, 104, 107).

155. Lüscher, M. and P. Weisz: 'Perturbative analysis of the gradient flow in non-abelian gauge theories'. *JHEP* (2011) 1102: p. 051. doi: 10.1007/JHEP02(2011)051. arXiv: 1101.0963 [hep-th] (cit. on pp. 17, 83–87, 103).

156. Lüscher, M.: 'Chiral symmetry and the Yang–Mills gradient flow'. *JHEP* (2013) 1304: p. 123. DOI: 10.1007/JHEP04(2013)123. arXiv: 1302.5246 [hep-lat] (cit. on pp. 17, 85, 115).

157. Borsányi, S., S. Dürr, Z. Fodor, C. Hölbling, S. D. Katz, et al.: 'High-precision scale setting in lattice QCD'. *JHEP* (2012) 1209: p. 010. DOI: 10.1007/JHEP09(2012)010. arXiv: 1203.4469 [hep-lat] (cit. on pp. 17, 83).

159. Fodor, Z., K. Holland, J. Kuti, D. Nogradi, and C. H. Wong: 'The Yang-Mills gradient flow in finite volume'. *JHEP* (2012) 1211: p. 007. DOI: 10.1007/JHEP11(2012)007. arXiv: 1208.1051 [hep-lat] (cit. on pp. 17, 83, 112).

162. Lüscher, M.: 'Step scaling and the Yang-Mills gradient flow'. *JHEP* (2014) 1406: p. 105. DOI: 10.1007/JHEP06(2014)105. arXiv: 1404.5930 [hep-lat] (cit. on pp. 17, 83, 112).

210. Binoth, T. and G. Heinrich: 'Numerical evaluation of multiloop integrals by sector decomposition'. *Nucl. Phys.* (2004) B680: pp. 375–388. DOI: 10.1016/j.nuclphysb.2003.12.023. arXiv: hep-ph/0305234 [hep-ph] (cit. on pp. 19, 20, 30, 84, 100).

216. Smirnov, V. A.: *Analytic tools for Feynman integrals*. Vol. 250. 2012: pp. 1–296. DOI: 10.1007/978-3-642-34886-0 (cit. on pp. 20, 21, 30, 97, 123).

217. Chetyrkin, K. G. and F. V. Tkachov: 'Integration by parts: The algorithm to calculate β-functions in 4 loops'. *Nucl. Phys.* (1981) B192: pp. 159–204. DOI: 10.1016/0550-3213(81)90199-1 (cit. on pp. 20, 30, 95).

220. Smirnov, A. V.: 'FIESTA 3: cluster-parallelizable multiloop numerical calculations in physical regions'. *Comput. Phys. Commun.* (2014) 185: pp. 2090–2100. DOI: 10.1016/j.cpc.2014.03.015. arXiv: 1312.3186 [hep-ph] (cit. on pp. 20, 100, 126).

221. Anastasiou, C., F. Herzog, and A. Lazopoulos: 'On the factorization of overlapping singularities at NNLO'. *JHEP* (2011) 1103: p. 038. DOI: 10.1007/JHEP03(2011)038. arXiv: 1011.4867 [hep-ph] (cit. on pp. 22, 101).

250. Chetyrkin, K. G., B. A. Kniehl, and M. Steinhauser: 'Decoupling relations to $\mathcal{O}(\alpha_s^3)$ and their connection to low-energy theorems'. *Nucl. Phys.* (1998) B510: pp. 61–87. DOI: 10.1016/S0550-3213(97)00649-4. arXiv: hep-ph/9708255 [hep-ph] (cit. on pp. 27, 108).

253. Schröder, Y. and M. Steinhauser: 'Four-loop decoupling relations for the strong coupling'. *JHEP* (2006) 0601: p. 051. doi: 10.1088/1126-6708/2006/01/051. arXiv: hep-ph/0512058 [hep-ph] (cit. on pp. 27, 64, 108).

254. Chetyrkin, K. G., J. H. Kühn, and C. Sturm: 'QCD decoupling at four loops'. *Nucl. Phys.* (2006) B744: pp. 121–135. doi: 10.1016/j.nuclphysb.2006.03.020. arXiv: hep-ph/0512060 [hep-ph] (cit. on pp. 27, 64, 108).

396. Ritbergen, T. van, J. A. M. Vermaseren, and S. A. Larin: 'The four-loop β-function in quantum chromodynamics'. *Phys. Lett.* (1997) B400: pp. 379–384. doi: 10.1016/S0370-2693(97)00370-5. arXiv: hep-ph/9701390 [hep-ph] (cit. on pp. 33, 108).

397. Czakon, M.: 'The four-loop QCD β-function and anomalous dimensions'. *Nucl. Phys.* (2005) B710: pp. 485–498. doi: 10.1016/j.nuclphysb.2005.01.012. arXiv: hep-ph/0411261 [hep-ph] (cit. on pp. 33, 107, 108).

444. Harlander, R. V. and T. Neumann: 'The perturbative QCD gradient flow to three loops'. 2015 (cit. on pp. 81, 110).

445. Lüscher, M.: 'Trivializing maps, the Wilson flow and the HMC algorithm'. *Commun. Math. Phys.* (2010) 293: pp. 899–919. doi: 10.1007/s00220-009-0953-7. arXiv: 0907.5491 [hep-lat] (cit. on p. 83).

446. Lüscher, M.: 'Topology, the Wilson flow and the HMC algorithm'. *PoS* (2010) LATTICE2010: p. 015. arXiv: 1009.5877 [hep-lat] (cit. on p. 83).

447. Fodor, Z., K. Holland, J. Kuti, D. Nogradi, and C. H. Wong: 'The gradient flow running coupling scheme'. *PoS* (2012) LATTICE2012: p. 050. arXiv: 1211.3247 [hep-lat] (cit. on pp. 83, 112).

448. Chetyrkin, K. G., M. Faisst, C. Sturm, and M. Tentyukov: 'epsilon-finite basis of master integrals for the integration-by-parts method'. *Nucl. Phys.* (2006) B742: pp. 208–229. doi: 10.1016/j.nuclphysb.2006.02.030. arXiv: hep-ph/0601165 [hep-ph] (cit. on p. 96).

449. Czakon, M.: 'Automatized analytic continuation of Mellin-Barnes integrals'. *Comput. Phys. Commun.* (2006) 175: pp. 559–571. doi: 10.1016/j.cpc.2006.07.002. arXiv: hep-ph/0511200 [hep-ph] (cit. on p. 98).

450. Smirnov, A. V. and V. A. Smirnov: 'On the Resolution of Singularities of Multiple Mellin-Barnes Integrals'. *Eur. Phys. J.* (2009) C62: pp. 445–449. doi: 10.1140/epjc/s10052-009-1039-6. arXiv: 0901.0386 [hep-ph] (cit. on p. 98).

451. Wolfram Research, Inc.: *Mathematica*. Version 7.0. 2008 (cit. on pp. 99, 117).

452. Mertig, R., M. Bohm, and A. Denner: 'FEYN CALC: Computer algebraic calculation of Feynman amplitudes'. *Comput. Phys. Commun.* (1991) 64: pp. 345–359. doi: 10.1016/0010-4655(91)90130-D (cit. on pp. 99, 121).

453. Sjödahl, M.: 'ColorMath - A package for color summed calculations in SU(N_c)'. *Eur. Phys. J.* (2013) C73.2: p. 2310. doi: 10.1140/epjc/s10052-013-2310-4. arXiv: 1211.2099 [hep-ph] (cit. on pp. 100, 121).

454. Lee, R. N.: 'LiteRed 1.4: a powerful tool for reduction of multiloop integrals'. *J. Phys. Conf. Ser.* (2014) 523: p. 012059. doi: 10.1088/1742-6596/523/1/012059. arXiv: 1310.1145 [hep-ph] (cit. on pp. 100, 123).

455. Genz, A. C. and A. A. Malik: 'An Imbedded Family of Fully Symmetric Numerical Integration Rules'. *SIAM J. Numer. Anal.* (1983) 20.3: pp. 580–588 (cit. on pp. 101, 131).

456. Genz, A. C. and A. A. Malik: 'Remarks on algorithm 006: An adaptive algorithm for numerical integration over an N-dimensional rectangular region'. *J. Comput. Appl. Math.* (1980) 6.4: pp. 295–302. doi: 10.1016/0771-050X(80)90039-X (cit. on pp. 101, 131).

457. Fousse, L., G. Hanrot, V. Lefèvre, P. Pélissier, and P. Zimmermann: 'MPFR: A Multiple-Precision Binary Floating-Point Library with Correct Rounding'. *ACM Trans. Math. Softw.* (2007) 33.2: 13:1–13:15. doi: 10.1145/1236463.1236468 (cit. on pp. 101, 127, 132).

458. Holoborodko, P.: *MPFR C++*. 2008-2012. url: http://www.holoborodko.com/pavel/mpfr/ (cit. on pp. 101, 127, 132).

459. Davis, P. J. and P. Rabinowitz.: *Methods of Numerical Integration*. 2nd ed. Academic Press, 1984 (cit. on p. 102).

460. Iri, M., S. Moriguti, and Y. Takasawa: 'On a certain quadrature formula (in Japanse)'. *Kokyuroku Res. Inst. Math. Sci., Kyoto University* (1970) 91: pp. 82–118. English translation in *J. Comput. Appl. Math.* (1987) 17.1–2 (cit. on pp. 102, 132).

461. Caswell, W. E.: 'Asymptotic Behavior of Nonabelian Gauge Theories to Two Loop Order'. *Phys. Rev. Lett.* (1974) 33: p. 244. doi: 10.1103/PhysRevLett.33.244 (cit. on p. 105).

462. Jones, D. R. T.: 'Two Loop Diagrams in Yang-Mills Theory'. *Nucl. Phys.* (1974) B75: p. 531. doi: 10.1016/0550-3213(74)90093-5 (cit. on p. 105).

463. Tarasov, O. V. and A. A. Vladimirov: 'Two Loop Renormalization of the Yang-Mills Theory in an Arbitrary Gauge'. *Sov. J. Nucl. Phys.* (1977) 25: p. 585 (cit. on p. 105).

464. Egorian, E. and O. V. Tarasov: 'Two Loop Renormalization of the QCD in an Arbitrary Gauge'. *Teor. Mat. Fiz.* (1979) 41: pp. 26–32 (cit. on p. 105).

465. Davydychev, A. I., P. Osland, and O. V. Tarasov: 'Two loop three gluon vertex in zero momentum limit'. *Phys. Rev.* (1998) D58: p. 036007. doi: 10.1103/PhysRevD.58.036007. arXiv: hep-ph/9801380 [hep-ph] (cit. on p. 105).

466. Chetyrkin, K. G.: 'Four-loop renormalization of QCD: Full set of renormalization constants and anomalous dimensions'. *Nucl. Phys.* (2005) B710: pp. 499–510. doi: 10.1016/j.nuclphysb.2005.01.011. arXiv: hep-ph/0405193 [hep-ph] (cit. on p. 107).

467. Chetyrkin, K. G., J. H. Kühn, and M. Steinhauser: 'RunDec: A Mathematica package for running and decoupling of the strong coupling and quark masses'. *Comput. Phys. Commun.* (2000) 133: pp. 43–65. doi: 10.1016/S0010-4655(00)00155-7. arXiv: hep-ph/0004189 [hep-ph] (cit. on p. 108).

468. Schmidt, B. and M. Steinhauser: 'CRunDec: a C++ package for running and decoupling of the strong coupling and quark masses'. *Comput. Phys. Commun.* (2012) 183: pp. 1845–1848. doi: 10.1016/j.cpc.2012.03.023. arXiv: 1201.6149 [hep-ph] (cit. on p. 108).

References for appendix

216. Smirnov, V. A.: *Analytic tools for Feynman integrals*. Vol. 250. 2012: pp. 1–296. doi: 10.1007/978-3-642-34886-0 (cit. on pp. 20, 21, 30, 97, 123).

220. Smirnov, A. V.: 'FIESTA 3: cluster-parallelizable multiloop numerical calculations in physical regions'. *Comput. Phys. Commun.* (2014) 185: pp. 2090–2100. doi: 10.1016/j.cpc.2014.03.015. arXiv: 1312.3186 [hep-ph] (cit. on pp. 20, 100, 126).

451. Wolfram Research, Inc.: *Mathematica*. Version 7.0. 2008 (cit. on pp. 99, 117).

452. Mertig, R., M. Bohm, and A. Denner: 'FEYN CALC: Computer algebraic calculation of Feynman amplitudes'. *Comput. Phys. Commun.* (1991) 64: pp. 345–359. doi: 10.1016/0010-4655(91)90130-D (cit. on pp. 99, 121).

453. Sjödahl, M.: 'ColorMath - A package for color summed calculations in SU(N_c)'. *Eur. Phys. J.* (2013) C73.2: p. 2310. doi: 10.1140/epjc/s10052-013-2310-4. arXiv: 1211.2099 [hep-ph] (cit. on pp. 100, 121).

454. Lee, R. N.: 'LiteRed 1.4: a powerful tool for reduction of multiloop integrals'. *J. Phys. Conf. Ser.* (2014) 523: p. 012059. doi: 10.1088/1742-6596/523/1/012059. arXiv: 1310.1145 [hep-ph] (cit. on pp. 100, 123).

455. Genz, A. C. and A. A. Malik: 'An Imbedded Family of Fully Symmetric Numerical Integration Rules'. *SIAM J. Numer. Anal.* (1983) 20.3: pp. 580–588 (cit. on pp. 101, 131).

456. Genz, A. C. and A. A. Malik: 'Remarks on algorithm 006: An adaptive algorithm for numerical integration over an N-dimensional rectangular region'. *J. Comput. Appl. Math.* (1980) 6.4: pp. 295–302. doi: 10.1016/0771-050X(80)90039-X (cit. on pp. 101, 131).

457. Fousse, L., G. Hanrot, V. Lefèvre, P. Pélissier, and P. Zimmermann: 'MPFR: A Multiple-Precision Binary Floating-Point Library with Correct Rounding'. *ACM Trans. Math. Softw.* (2007) 33.2: 13:1–13:15. doi: 10.1145/1236463.1236468 (cit. on pp. 101, 127, 132).

458. Holoborodko, P.: *MPFR C++*. 2008-2012. url: http://www.holoborodko.com/pavel/mpfr/ (cit. on pp. 101, 127, 132).

460. Iri, M., S. Moriguti, and Y. Takasawa: 'On a certain quadrature formula (in Japanse)'. *Kokyuroku Res. Inst. Math. Sci., Kyoto University* (1970) 91: pp. 82–118. English translation in *J. Comput. Appl. Math.* (1987) 17.1–2 (cit. on pp. 102, 132).

469. Davis, P. J. and P. Rabinowitz: *Methods of numerical integration*. Computer science and applied mathematics. Academic Press, 1984 (cit. on p. 131).

470. Johnson, S. G.: *Cubature*. 2014. url: http://ab-initio.mit.edu/wiki/index.php/Cubature (cit. on p. 131).

471. McNamee, J. and F. Stenger: 'Construction of fully symmetric numerical integration formulas of fully symmetric numerical integration formulas'. English. *Numer. Math.* (1967) 10.4: pp. 327–344. doi: 10.1007/BF02162032 (cit. on p. 131).

Der Wissenschaftler findet seine Belohnung in dem,
was Poincaré die Freude am Verstehen nennt,
nicht in den Anwendungsmöglichkeiten seiner Erfindung.

The scientist finds his reward in what Henri-Poincaré
calls the joy of comprehension, and not in the possibilities
of application to which any discovery of his may lead.

— Albert Einstein[1]

DANKSAGUNG

Mein größter Dank gilt Prof. Dr. Robert Harlander für die Projektideen die in dieser Arbeit verwirklicht wurden und für die kontinuierliche Betreuung während der Arbeit. Er hat das ein oder andere mal dafür gesorgt, dass ich nicht zu sehr das Ziel aus den Augen verloren habe. Zudem darf nicht unerwähnt bleiben, dass Prof. Harlander mir mit dem Korrekturlesen der Arbeit und den zahlreichen kritischen Anmerkungen einen großen Gefallen erwiesen hat.

Bei Prof. Dr. Michał Czakon bedanke ich mich dafür, dass er sich bereit erklärt hat das Zweitgutachten anzufertigen. Bei Prof. Dr. Markus Schumacher, Prof. Dr. Robert Harlander und Dr. Marius Wiesemann möchte ich mich sehr für die Postdoc-Empfehlungsschreiben bedanken, die sie an mehrere Dutzend Kollegen in aller Welt verteilt haben, und mir damit geholfen haben einige Antworten zu erhalten.

Weiterhin möchte ich mich bei den ehemaligen Mitgliedern der Arbeitsgruppe von Prof. Harlander – insbesondere Dr. Marius Wiesemann, Dr. Tom Zirke und Dr. Stefan Liebler sowie Dr. Hendrik Mantler und Dr. Anurag Tripathi – für viele interessante Gespräche und eine gute Arbeitsatmosphäre bedanken. Gleicher Dank gilt Dipl. Phys. Mario Prausa, der sich auch für das Korrekturlesen dieser Arbeit bereiterklärt hat.

1 Aus einer Zusammenfassung eines stenographisch aufzeichneten Gesprächs "A Socratic Dialogue" zwischen Planck, Einstein und Murphy in "Where science is going", Max Planck, 1932. Zurückübersetzt in "Einstein sagt", Alice Calaprice, 1996.

Meine Kommilitonen, mit denen ich das Studium begonnen habe, und die bis dato ebenfalls als Doktoranden in Wuppertal sind, dürfen nicht unerwähnt bleiben: Ich danke Andreas Behrendt, Sebastian Mathys, Sascha Reinecke und Simon Schlesinger für eine äußerst schöne Studienzeit und wüsche ihnen alles Gute für die Zukunft.

Besonders danken möchte ich abschließend meiner Familie für die fortwährende Unterstützung und Geduld während meines Studiums.